

Spatial and temporal regulation of the RhoA GEF Ect2 during cell division

Dissertation der Fakultät für Biologie
der Ludwig-Maximilians-Universität München



Sandra Schneid

München, 2022

Diese Dissertation wurde angefertigt unter der Leitung von Prof. Dr. Esther Zanin im Bereich der Zell- und Entwicklungsbiologie an der Ludwig-Maximilians-Universität München.

Erstgutachterin: Prof. Dr. Esther Zanin

Zweitgutachter: Prof. Dr. Christof Osman

Tag der Abgabe: 18.05.2022

Tag der mündlichen Prüfung: 22.12.2022

Eidesstattliche Erklärung:

Ich versichere hiermit an Eides statt, dass meine Dissertation selbständig und ohne unerlaubte Hilfsmittel angefertigt worden ist.

München, 18.05.2022

Sandra Schneid

Erklärung:

Hiermit erkläre ich, dass die vorliegende Dissertation weder ganz, noch teilweise bei einer anderen Prüfungskommission vorgelegt worden ist und, dass ich mich nicht anderweitig einer Doktorprüfung ohne Erfolg unterzogen habe.

München, den 18.05.2022

Sandra Schneid

Publications originating from this thesis

Schneid, S., Wolff, F., Buchner, K., Bertram, N., Baygün, S., Barbosa, P., Mangal, S., & Zanin, E. (2021). The BRCT domains of ECT2 have distinct functions during cytokinesis. *Cell reports*, 34(9), 108805. <https://doi.org/10.1016/j.celrep.2021.108805>

Schneid, S. and Wolff, F. are co-first authors of this paper.

Contributions

In this thesis, some conclusions built on preceding work (Buchner, 2019) and some experimental work has been conducted by Kristina Buchner (KB), Friederike Wolff (FW), Nils Bertram (NB), and Prof. Dr. Esther Zanin (EZ). Their contributions will be indicated in the figure legends and the text by mentioning their name or initials.

Acknowledgments

First, I would like to thank my supervisor Prof. Dr. Esther Zanin for giving me the opportunity to conduct my Ph.D. in her lab as well as for her support and guidance throughout the time. Thanks Esther, for letting me dive into the fascinating world of cell division!

Moreover, I want to thank my TAC members Prof. Dr. Annette Müller-Taubenberger and Prof. Dr. Claudia Veigl for their valuable input and the fruitful discussions during our annual meetings. I am grateful for your effort and your help! Many thanks also go to Prof. Dr. Christof Osman who kindly agreed on co-reviewing this thesis as well as to Prof. Dr. Heinrich Jung, Prof. Dr. Nicolas Gompel, Dr. Serena Schwenkert, and Prof. Dr. Annette Müller-Taubenberger, for being part of my evaluation board.

I am grateful for being a member of the graduate school Life Science Munich, through which I gained insights into diverse research fields, had the possibility to meet other enthusiastic, young researchers, and could expand my skill outside of the lab. In this context, I also want to thank Nadine Hamze and Korbinian Dischinger for their kind support and assistance. Many thanks to Tatjana, Nadja, and Sylvia for their excellent technical support and for making my daily life in the lab much easier.

Special thanks to you Fritzi, you were a great companion and constant support during my Ph.D. Thank you for accompanying me through ups and downs, the many laughs, and your unconditional help and friendship! There is nobody I would have rather worked on a project than you! Especially, during the time after the Conradt group had moved and Covid-19 had swept away the entire social life in the uni, it sometimes felt like we were the “last women standing”. Thanks to you this time was nevertheless enjoyable and cheerful.

I also want to thank Prof. Dr. Charles N. David who supervised my master thesis for encouraging me to conduct a Ph.D. With your exceptional enthusiasm for science, you are a real inspiration to me and you have shaped my scientific instincts and motivation throughout

the last years. Thanks for the various scientific discussions and nice conversations over the years and the nice dinner nights at your house.

To all the past and present members of the AG Zanin, AG Conradt, AG Mikeladze-Dvali, and AG Wagener: What should I say- it was a blast meeting you all! Thanks for the great and heartwarming welcome, the friendly and cooperative atmosphere in the lab throughout the years, and for sharing your experience, knowledge, and advice with me! Grinning, I will always remember the nice time we had especially our legendary PhDinners and get-togethers, although they were limited in number due to the COVID-19 pandemic. Thanks to the Coffee Group, I not only received my daily dose(s) of caffeine, but also my daily dose(s) of delightful chats and amusement. For that, especially thank you Jenny, Lisa, Fritz, Adi, Elisabeth, Laura, and Sriyash.

Last but not least, I want to share my gratitude with all my friends, especially Anka, Marcel, Vanessa, Judith, and Daniel, my boyfriend Andi, and my family. Thank you for your never-ending support, your advice, your open ears, and your shoulders to lean on! Without you, I would not have mastered this sometimes challenging time. Also thanks a lot to Emilia and Joni, you both just brought so much joy into my life!

Abstract

During cytokinesis, the last step of cell division, the contraction of an actomyosin ring physically splits the mother cell into two daughter cells. In animal cells, the formation of the actomyosin ring requires the activation of the small GTPase RhoA by its guanine nucleotide exchange factor (GEF) Ect2. Despite its important role during cytokinesis, Ect2 regulation is incompletely understood. The current view is that Ect2 activity is prevented by an autoinhibitory interaction between its three N-terminal BRCT domains and the catalytic DH-GEF domain. However, the contributions of the single BRCT domains remain unclear. In addition, recent *in vitro* data suggested that the membrane-binding domain PH and the flexible S-loop, connecting N- and the C-terminus, also participate in Ect2 activity regulation. The relevance of these contributions in living cells remains mainly elusive. Thus, this thesis examined how the individual BRCT domains, the PH domain, and the S-loop contribute to Ect2 function and regulation in human cells.

By the use of structure-function studies and live-cell confocal microscopy, this study revealed that each BRCT domain contributes differently to Ect2 function and regulation. Moreover, first evidence was collected for an involvement of the PH domain and the S-loop in Ect2 regulation in living cells. Consistent with previous data the BRCT1 domain was found to be essential for Ect2 function during cytokinesis. BRCT1 deletion led to cytokinetic failure due to a lack of contractile ring formation and furrow ingression. BRCT0, while not essential for cytokinesis, contributes to its proper timing by helping to release autoinhibition. BRCT0 deletion allowed successful cytokinesis, though furrow ingression was delayed. Neither the BRCT0 nor the BRCT1 domains appear to play a major role in GEF inhibition. In contrast, the BRCT2 domain turned out to be enormously important for GEF inhibition. BRCT2 deletion resulted in the formation of large membrane blebs due to the hyperactivation of RhoA. Moreover, furrow ingression was delayed and an increased number of cells failed cytokinesis. Furthermore, fluorescence analysis and pull-down assays demonstrated that all BRCT domains interact with RacGAP1 and contribute to Ect2 midzone recruitment. Additionally, it was revealed that Plk1 binds to all BRCT domains and specifically phosphorylates the BRCT0 domain. A point mutation in the PH domain and a phospho-mimetic S-loop led to the formation of large membrane blebs during cytokinesis.

In summary, the presented work gives detailed mechanistic insights into the regulation of Ect2 activity and how this regulation cooperates with other mechanisms to ensure faithful cytokinesis. It appears that three structural domains contribute to Ect2 autoinhibition: the BRCT2 domain, the PH domain, and the S-loop. Moreover, the essential role of the BRCT1 domain for Ect2 activation was confirmed. Although BRCT0 seems to have a minor role, it supports Ect2 activation. This demonstrates that Ect2 regulation is more complex than initially assumed and that current models have to be revised to fit the new findings. Mis-regulated Ect2 is tightly linked to cancer development which is why the knowledge gained here could in the long run contribute to the development of new therapeutic strategies in the fight against cancer.

Zusammenfassung

In der letzten Phase der Zellteilung der Zytokinese kommt es durch das Zusammenziehen eines kontraktiven Aktin-Myosin-Rings zur Teilung der Mutterzelle in zwei Tochterzellen. In tierischen Zellen muss für die Bildung des Aktin-Myosin-Rings die kleine GTPase RhoA durch seinen Guaninnukleotid-Austauschfaktor (GEF) Ect2 aktiviert werden. Obwohl Ect2 folglich eine wichtige Rolle während der Zytokinese spielt, ist die Regulierung seiner Aktivität nicht vollends verstanden. Das aktuelle Regulationsmodell geht davon aus, dass die drei N-terminalen BRCT-Domänen mit der katalytischen DH-GEF-Domäne eine autoinhibitorische Interaktion eingehen, wodurch die GEF-Aktivität von Ect2 verhindert wird. Wie die einzelnen BRCT-Domänen jedoch zur Autoinhibierung beitragen, ist nicht bekannt. Zusätzlich lieferten neueste *in vitro*-Daten Hinweise darauf, dass die Membranbindedomäne PH und die flexible S-Schleife, die den N- und C-Terminus verbindet, ebenfalls an der Ect2-Regulierung beteiligt sind. Ob jedoch die PH-Domäne und die S-Schleife relevante Beiträge zur Ect2-Regulierung in lebenden Zellen beisteuern, ist weitgehend unverständlich. Deshalb wurde in dieser Doktorarbeit untersucht, wie die einzelnen BRCT-Domänen, die PH-Domäne und die S-Schleife zur Funktion und Regulierung von Ect2 in Humanzellen beitragen.

Mit Hilfe von Struktur-Funktionsstudien und konfokaler Lebendzellmikroskopie konnte in dieser Arbeit gezeigt werden, dass jede BRCT-Domäne auf unterschiedliche Art und Weise zur Funktion und der Regulierung von Ect2 beiträgt. Ebenfalls wurden erste Hinweise darauf gefunden, dass die PH-Domäne und die S-Schleife an der Regulierung der Ect2-Aktivität in lebenden Zellen beteiligt sind. Im Einklang mit früheren Ergebnissen wurde gezeigt, dass die BRCT1-Domäne für die Funktion von Ect2 während der Zytokinese unerlässlich ist. So führte das Entfernen von BRCT1 zu einer hohen Fehlerrate bei der Zytokinese, da weder ein kontraktiver Ring noch eine Teilungsfurche gebildet werden konnte. BRCT0 erwies sich zwar nicht als essenziell für die Zytokinese, hilft aber dabei, die Autoinhibition zu lösen und trägt somit zum korrekten zeitlichen Ablauf der Zytokinese bei. Zwar konnten sich in der Abwesenheit von BRCT0 Zellen erfolgreich teilen, jedoch kam es zu einer Verzögerung beim Einziehen der Spaltungsfurche. Bei der GEF-Regulierung scheinen weder die BRCT0 noch die BRCT1-Domäne eine große Rolle zu spielen. Im Gegensatz dazu stellte sich die BRCT2-Domäne als enorm wichtig für diese heraus. Charakteristisch für das Entfernen der BRCT2-Domäne war

die Bildung von großen Membranblasen, die da herrührten, dass RhoA durch fehlreguliertes Ect2 übermäßig aktiviert wurde. Ebenso war das Voranschreiten der Spaltungsfurche beeinträchtigt und Zellen scheiterten vermehrt an der Teilung. Fluoreszenzanalysen und Pull-Down Assays zeigten zudem, dass jede einzelne BRCT Domänen mit RacGAP1 interagieren kann und dazu beiträgt, Ect2 zur Mittelzone zu rekrutieren. Auch wurde gezeigt, dass Plk1 alle BRCT Domänen bindet und BRCT0 spezifisch phosphoryliert. Außerdem führten eine Punktmutation in der PH Domäne und eine phosphomimetische S-Schleife zur Bildung großer Membranblasen während der Zytokinese.

Zusammenfassend kann gesagt werden, dass die vorliegende Arbeit detaillierte Einblicke in die Mechanismen der Aktivitätsregulierung von Ect2 liefert und aufzeigt, wie diese mit weiteren regulatorischen Maßnahmen kooperieren, um eine erfolgreiche Zytokinese zu gewährleisten. Demnach scheinen drei strukturelle Komponenten an der Ect2 Autoinhibierung beteiligt zu sind: BRCT2, PH und die S-Schleife. Außerdem konnte die essenzielle Rolle von BRCT1 für die Ect2 Aktivierung bestätigt werden. Obwohl die BRCT0 Domäne eine untergeordnete Rolle zu spielen scheint, ist sie dennoch wichtig für die Aktivierung von Ect2. All das zeigt, dass die Ect2 Regulierung eine größere Komplexität aufweist als ursprünglich angenommen. Derzeitigen Modelle müssen deshalb überarbeitet werden, um den neuen Erkenntnissen gerecht zu werden. Die Fehlregulierung von Ect2 ist eng mit der Krebsentstehung verknüpft, weshalb die hier gewonnenen Erkenntnisse langfristig zur Entwicklung neuer therapeutischer Strategien in der Krebsbekämpfung beitragen könnten.

Table of contents

Acknowledgments	I
Abstract	III
Zusammenfassung	V
List of figures	XI
List of tables	XV
Abbreviations	XVI
Gene and protein abbreviations	XIX
1 Introduction	1
1.1 A brief overview of the cell cycle and its regulation in animal cells	1
1.2 Cytokinesis in animal cells	5
1.3 Central spindle assembly.....	7
1.4 The mitotic spindle positions the contractile ring.....	9
1.5 The small GTPase RhoA triggers the assembly of the contractile ring.....	12
1.6 The actomyosin ring drives cleavage furrow ingression	14
1.7 Abscission is the last step of cytokinesis	15
1.8 Precise control of RhoA signaling	17
1.9 Epithelial cell transforming 2 (Ect2) protein	18
1.9.1 The GEF Ect2 is essential for cytokinesis	18
1.9.2 Ect2 structural domains and their function.....	21
1.9.3 Ect2 regulation during mitosis	24
1.9.3.1 Regulation by mitotic kinases	24
1.9.3.2 Ect2 autoinhibition.....	27
1.9.3.3 Release of Ect2 autoinhibition	28
1.9.4 Understanding Ect2 regulation during cytokinesis benefits the understanding of Ect2 during tumorigenesis	29
1.10 Aim of my thesis	30
2 Materials and methods	32
2.1 Plasmid generation for stable cell lines and protein purification	32
2.1.1 DNA-amplification by Polymerase Chain Reaction (PCR)	32
2.1.2 Site-directed mutagenesis	33

2.1.3	Gibson assembly	34
2.1.4	XhoI restriction digest and ligation.....	34
2.1.5	Plasmid transformation of chemically competent <i>E. coli</i> DH5 α and BL21.....	35
2.1.6	Isolation and sequencing of bacterial plasmid DNA.....	35
2.2	Protein expression and purification	36
2.2.1	GST-tagged proteins	36
2.2.2	MPB-tagged proteins.....	36
2.3	<i>In vitro</i> pull-down assays with GST-RacGAP1 and GST-PBD.....	37
2.4	<i>In vitro</i> Kinase-assays.....	37
2.5	Cell culture techniques	38
2.5.1	Cell culture maintenance and freezing of HeLa cell lines.....	38
2.5.2	siRNA transfection and drug treatment	38
2.5.3	Generation of stable cell lines and induction of transgene expression	39
2.5.4	Preparation of cell lysates, western blotting, and blot quantification.....	40
2.6	Immunofluorescence microscopy	41
2.7	Life-cell imaging.....	41
2.8	Image analysis and quantifications	42
2.8.1	Live-cell imaging.....	42
2.8.1.1	Analysis of bleb formation and characterization of blebs	42
2.8.1.2	Analysis of NG-Ect2 localization.....	43
2.8.1.3	Analysis of cleavage furrow ingression	44
2.8.2	Counting nuclei for multinucleation assay in fixed samples	44
2.9	Statistical analysis.....	44
3	Results.....	57
3.1	Preamble.....	57
3.2	A genetic replacement system for Ect2 in HeLa cells.....	58
3.3	Ect2 mutant variants are expressed at similar levels as endogenous Ect2, which can be efficiently knocked down by RNAi.....	61
3.4	Ect2 ^{WT} rescues phenotypes elicited by depletion of endogenous Ect2	62
3.4.1	Ect2 ^{WT} rescues cytokinetic failure after endogenous Ect2 depletion by RNAi.....	63
3.4.2	Ect2 ^{WT} rescues the defect in cleavage furrow formation and ingression after depletion of endogenous Ect2 by RNAi	65

3.4.3	Ect2 ^{WT} shows similar regulation and activity as endogenous Ect2 during cell division	66
3.4.4	Ect2 ^{WT} shows similar localization as endogenous Ect2 during cell division	69
3.4.5	Conclusion.....	70
3.5	Analyzing the contributions of each BRCT domain to Ect2 function and regulation...	70
3.5.1	The BRCT domains of Ect2 are essential for cytokinesis and inhibit GEF activity ...	71
3.5.2	The BRCT0 domain is not essential for cytokinesis but supports robust furrow ingression.....	76
3.5.3	The BRCT1 domain is required for furrow ingression and successful cytokinesis ..	79
3.5.4	The BRCT2 domain inhibits Ect2 activity and is required for successful cytokinesis	83
3.5.5	Characterization of unrestrained Ect2 cortical contractility	88
3.5.5.1	Elevated membrane blebbing does not delay furrow ingression in cells lacking BRCT2-mediated inhibition	88
3.5.5.2	Large blebs grow significantly longer and take longer to retract than small blebs	89
3.5.5.3	Increased intracellular pressure in blebbing Ect2 ^{ΔBRCT0-2} , Ect2 ^{ΔBRCT2} , and Ect2 ^{W307A} cells often results in cell shape oscillations.....	92
3.5.6	Analysis of Ect2 localization.....	94
3.5.6.1	All BRCT domains are needed for midzone localization	94
3.5.6.2	Each BRCT domain binds RacGAP1 <i>in vitro</i>	100
3.6	Analysis of Plk1 function in releasing Ect2 autoinhibition	102
3.6.1	Plk1 acts upstream of BRCT2-mediated inhibition.....	103
3.6.2	Plk1 binds to all BRCT domains via its PBD.....	105
3.6.3	Plk1 phosphorylates BRCT0 <i>in vitro</i>	106
3.7	BRCT2-mediated inhibition acts in parallel to astral microtubules.....	108
3.8	Analyzing the contributions of the S-loop and the PH-domain to Ect2 function and regulation	115
3.8.1	The S-loop of Ect2 contributes to the negative regulation of Ect2 GEF activity during mitosis	116
3.8.2	The PH-domain negatively regulates Ect2 GEF activity during mitosis.....	121

3.8.3	Increased intracellular pressure in strongly blebbing cells often results in cell shape oscillations and cytokinetic failure	125
3.8.4	Analysis of the Ect2 localization in S-loop and PH-mutants	126
3.8.4.1	Rendering the S-loop phospho-deficient and mutation C765K in the PH domain result in premature localization to the metaphase membrane	127
3.8.4.2	Rendering the S-loop phospho-mimetic and the C765K mutation in the PH domain increase Ect2 localization to the equatorial membrane and the midzone during anaphase	129
4	Discussion.....	134
4.1	Overview and model of Ect2 regulation.....	134
4.2	RacGAP1 interaction with BRCT1 activates Ect2 in anaphase	137
4.3	Mechanisms of Ect2 autoinhibition.....	139
4.4	RacGAP1 exerts spatial control upon active Ect2.....	143
4.5	Autoinhibition keeps part of Ect2 pool inactive during anaphase	144
4.6	BRCT2-mediated inhibition vs PH-mediated inhibition- which one is released first?	145
4.7	The role of BRCT0 and Plk1 in releasing Ect2 autoinhibition	149
4.8	RhoA zone formation in Ect2 missing the BRCT domains	150
4.9	Closing remarks and future perspective	153
	Bibliography	154
	Curriculum vitae	173

List of figures

Figure 1: Schematic overview of the different cell cycle phases in animal cells.	2
Figure 2: Mitotic stages in animal cells.	3
Figure 3: Schematic overview of cytokinesis in animal cells.....	5
Figure 4: The mitotic spindle in meta-and anaphase.....	8
Figure 5: Models showing how the mitotic spindle positions the cytokinetic furrow.	11
Figure 6: RhoA signaling during human cytokinesis leads to the assembly of the contractile ring.....	14
Figure 7: The structure of the GEF Ect2 in humans.	19
Figure 8: Ribbon representation of the canonical BRCT domain-fold on the example of human XRCC1.	22
Figure 9: Model of Ect2 activation during cytokinesis in animal cells.	29
Figure 10: Flp-FRT mediated single-copy integration of transgenes using the Flp-In T-Rex™ system to generate stable transgenic HeLa cell lines.	59
Figure 11: Schematic overview of stable transgenic HeLa cell lines that were used in this thesis.	60
Figure 12: The NG-Ect2 ^{WT} transgene is expressed similarly to endogenous Ect2 after Ect2 depletion by RNAi.....	61
Figure 13: Depletion of Ect2 leads to bi- and multinucleated cells.	63
Figure 14: Expression of Ect2 ^{WT} rescues cytokinetic failure after the depletion of endogenous Ect2.....	64
Figure 15: Expression of Ect2 ^{WT} rescues the defect in furrow formation and ingression after the depletion of endogenous Ect2 by RNAi.	66
Figure 16: Ect2 ^{WT} shows similar regulation and activity as endogenous Ect2 during cell division.	68
Figure 17: Localization of NG-Ect2 ^{WT} during mitosis.....	69
Figure 18: The BRCT domains in Ect2 are essential for cytokinesis.	73
Figure 19: Deletion of the BRCT domains delays furrow ingression and increases Ect2 activity.	74

Figure 20: Large bleb formation in Ect2 ^{ΔBRCT0-2} is efficiently blocked by the inhibition of RhoA activity.	75
Figure 21: BRCT0 is not essential for cytokinesis.	77
Figure 22: Deletion of BRCT0 slightly delays furrow ingression and slightly increases Ect2 activity.	78
Figure 23: BRCT1 is essential for cytokinesis.	81
Figure 24: Deletion of BRCT1 strongly impairs furrow formation and ingression, whereas mutation T153A+K195M in BRCT1 shows wild-type-like ingression.	82
Figure 25: BRCT2 is partially required for cytokinesis.	84
Figure 26: Deletion of BRCT2 and mutation W307A in the BRCT2 domain result in delayed furrow ingression and the formation of large membrane blebs.	86
Figure 27: Large bleb formation in Ect2 ^{ΔBRCT2} is efficiently blocked by the inhibition of RhoA activity.	87
Figure 28: Formation of large blebs is not the reason for delayed furrow ingression in Ect2 ^{ΔBRCT2} and Ect2 ^{W307A}	88
Figure 29: Formation and retraction of small blebs during anaphase in control and Ect2 ^{WT} . ..	90
Figure 30: Formation and retraction of large membrane blebs during meta- and anaphase in Ect2 ^{ΔBRCT0-2} and Ect2 ^{ΔBRCT2}	91
Figure 31: Large blebs grow significantly longer and take longer to retract than small blebs.	92
Figure 32: Hyperactive Ect2 ^{ΔBRCT0-2} , Ect2 ^{ΔBRCT2} , and Ect2 ^{W307A} trigger cell shape oscillations during anaphase, which often result in cytokinesis failure.	94
Figure 33: NG-Ect2 localization of the different BRCT mutants during meta- and anaphase. ..	96
Figure 34 Scheme of NG-Ect2 intensity measurements 9 min after anaphase onset.	97
Figure 35: Deletion of each BRCT domain decreases and mutation W307A in the BRCT2 domain increases Ect2 localization to the equatorial region.	99
Figure 36: Overview of MBP-tagged N-terminal Ect2 fragments used for <i>in vitro</i> studies. ..	101
Figure 37: Each BRCT domain can interact with RacGAP1 <i>in vitro</i>	102
Figure 38: The role of Plk1 in releasing Ect2 autoinhibition.	103
Figure 39: Plk1 inhibition blocks Ect2 ^{WT} midzone recruitment and furrow ingression and cytokinesis in control cells.	104
Figure 40: Plk1 inhibition does not affect large bleb formation in BRCT2 lacking cells.	105

Figure 41: Plk1 binds to all BRCT domains via its PBD.	106
Figure 42: BRCT0 is phosphorylated by Plk1 <i>in vitro</i>	107
Figure 43: Stabilization of astral microtubules by depleting MCAK does not affect cytokinetic success in cells lacking BRCT2-mediated inhibition.	109
Figure 44: Stabilization of astral microtubules by depleting MCAK triggers the formation of medium blebs and does not influence the formation of large blebs and furrow ingression in cells lacking BRCT2-mediated inhibition.	112
Figure 45: Stabilization of astral microtubules by depleting MCAK has no influence on Ect2 localization in cells lacking BRCT2-mediated inhibition.	114
Figure 46: The S-loop encompasses about twice as many possible phosphorylation sites than the entire Ect2 protein.	117
Figure 47: NG-Ect2 ^{S-loopAA} and NG-Ect2 ^{S-loopSTDE} proteins are expressed at endogenous levels and are functional during cytokinesis.	118
Figure 48: Phospho-deficient S-loop mutations slightly speed up furrow ingression and phospho-mimetic S-loop mutations slightly delay furrow ingression and elicit the formation of large membrane blebs.	119
Figure 49: The PH domain folds back onto the DH-GEF domain and binds to the catalytic center.	122
Figure 50: NG-Ect2 ^{P703D} and NG-Ect2 ^{C765K} proteins are expressed at endogenous levels and are functional during cytokinesis.	123
Figure 51: C765K mutation in the PH-domain slightly delays furrow ingression and triggers the formation of large membrane blebs, whereas mutation P703D shows none of these effects.....	124
Figure 52: Hyperactive Ect2 ^{S-loopSTDE} and Ect2 ^{C765K} trigger cell shape oscillations during anaphase, which often result in cytokinesis failure.....	126
Figure 53: NG-Ect2 localization of different Ect2 mutants during metaphase.....	127
Figure 54: C765K mutation in the PH domain and phospho-deficient mutations in the S-loop result in premature Ect2 localization to the metaphase membrane.....	128
Figure 55: NG-Ect2 localization of different PH and S-loop mutants during meta- and anaphase.	130
Figure 56: Mutations in the PH domain and the S-loop show different effects on Ect2 localization.	133

Figure 57: Schematic model of the 2-step activation of Ect2.	136
Figure 58: Models of releasing autoinhibition in <i>C. elegans</i> and human cells.	146

List of tables

Table 1: Reaction setup for standard PCR.....	33
Table 2: Thermocycling conditions for standard PCR	33
Table 3: Reaction setup for site-directed mutagenesis	33
Table 4: Thermocycling conditions for site-directed mutagenesis	34
Table 5: Reaction setup Xho I restriction digest	35
Table 6: Reaction setup for DNA ligation	35
Table 7: Primary, secondary, and antibodies and dyes.	45
Table 8: HeLa cell lines.	46
Table 9: Software used throughout the thesis.....	48
Table 10 Commercial kits	48
Table 11: siRNAs for knockdown of gene expression	48
Table 12: Bacterial strains	48
Table 13: Materials and reagents.....	49
Table 14: Primers used for plasmid generation	50
Table 15: General and obtained plasmids.....	51
Table 16: Generated plasmids.....	52
Table 17: Buffers and solutions.....	53
Table 18: Microscopes.....	55
Table 19: All transgenic Ect2 mutant proteins are expressed to endogenous levels after the depletion of endogenous Ect2 by RNAi.....	62
Table 20: Summary of the results obtained by Friederike Wolff from analyzing the RhoA membrane localization during anaphase in Ect2 mutant cell lines (Schneid et al., 2021). ...	137

Abbreviations

6xHis	hexahistidine
aa	aminoacid
AHD	anillin homology domain
Ala	alanine
AOS	anaphase onset
APC/C	Anaphase promoting complex/cylosome
Asp	aspartic acid
BRCT	BRCA-1 C-terminal
BSA	bovine serum albumin
<i>C. elegans</i>	<i>Caenorhabditis elegans</i>
carb	Carbenicillin
CPC	chromosomal passenger complex
C-terminus	carboxy terminus
<i>D. melanogaster</i>	<i>Drosophila melanogaster</i>
ddH ₂ O	double-distilled water
DH	Dbl homology
DMEM	Dulbecco's modified eagle medium
DMSO	dimethyl sulfoxide
DNA	deoxyribonucleic acid
dNTPs	deoxynucleotide triphosphates
DTT	Dithiothreitol
<i>E. coli</i>	<i>Escherichia coli</i>
Ect2	epithelial cell transforming 2
EDTA	ethylenediaminetetraacetic acid
ESCRT III	Endosomal Sorting Complex Required for Transport III
EtOH	ethanol
FACS	fluorescence-activated cell sorting

F-actin	filamentous actin
FBS	fetal bovine serum
Flp	flippase
FRT	flippase recognition target
GAP	GTPase activating protein
GAP	GTPase activating protein
GDI	guanosine dissociation inhibitor
GDP	guanosine diphosphate
GEF	guanine nucleotide exchange factor
Glu	glutamic acid
GST	glutathione-S-transferase
GTP	guanosine triphosphate
<i>H. sapiens</i>	<i>Homo sapiens</i>
HEPES	4-(2-hydroxyethyl)-1-piperazineethanesulfonic acid
kDa	kilo Dalton
LB	lysogeny broth
M	molar
<i>M. musculus</i>	<i>Mus musculus</i>
MBP	maltose binding protein
MeOH	methanol
MT	microtubule
NG	mNeonGreen
N-terminus	amino terminus
o/n	over night
P/S	penicillin/streptomycin
PAGE	polyacrylamide gel electrophoresis
PBD	Polo-box domain
PBS	phosphate-buffered saline
PBS	polybasic sequence
PCR	polymerase chain reaction

PH	pleckstrin homology
PIP2	phosphatidylinositol 4,5-bisphosphate
Pro	proline
PT	phenotype
PVDF	polyvinylidene fluoride
RNA	ribonucleic acid
RNAi	RNA interference
rpm	revolutions per minute
RT	room temperature
SAC	spindle assembly checkpoint
SB	sample buffer
SDS	sodium dodecylsulfate
Ser	serine
siRNA	short interfering RNA
TBS	Tris buffered saline
TBS-T	Tris buffered saline with Tween20
TE	Tris- EDTA
tet	tetracycline
Thr	threonine
WT	wild-type
<i>X. laevis</i>	<i>Xenopus laevis</i>

Gene and protein abbreviations

Gene symbols	Gene name	Species
<i>BRCA1</i>	Breast cancer type 1 susceptibility protein	<i>H. sapiens</i>
<i>CDK1</i>	Cyclin dependent kinase 1	<i>H. sapiens</i>
<i>CENPE</i>	Centromere protein E	<i>H. sapiens</i>
<i>ECT2</i>	Epithelial cell transforming 2	<i>H. sapiens</i>
<i>FOXM1</i>	Forkhead box protein M1	<i>M. musculus</i>
<i>INCENP</i>	Inner centromere protein	<i>H. sapiens</i>
<i>KIF4</i>	Kinesin family member 4	<i>H. sapiens</i>
<i>MCAK</i>	Mitotic centromere-associated kinesin	<i>H. sapiens</i>
<i>MDC1</i>	Mediator of DNA damage checkpoint protein 1	<i>H. sapiens</i>
<i>MKLP1</i>	Mitotic kinesin-like protein 1	<i>H. sapiens</i>
<i>MKLP2</i>	Mitotic kinesin-like protein 2	<i>H. sapiens</i>
<i>MLCP</i>	Myosin light chain phosphatase	<i>H. sapiens</i>
<i>MP-GAP</i>	Mitotic phase GTP activating protein	<i>H. sapiens</i>
<i>PRC1</i>	Protein regulator of cytokinesis 1	<i>H. sapiens</i>
<i>RACGAP1</i>	Rac GTPase activating protein 1	<i>H. sapiens</i>
<i>RAD9</i>	DNA repair protein Rad9	<i>H. sapiens</i>
<i>RHOA</i>	Ras homology family member A	<i>H. sapiens</i>
<i>ROCK</i>	Rho associated kinase	<i>H. sapiens</i>
<i>TOPBP1</i>	DNA topoisomerase 2-binding protein 1	<i>H. sapiens</i>

1 Introduction

Although living organisms can diverge extremely, they share the same basic building block, the cell. This theory was first postulated by Theodore Schwann and Matthias Jacob Schleiden in the 19th century and is known as the “cell theory”. Rudolf Virchow extended this theory by stating that all cells arise from pre-existing cells through division (Mazzarello, 1999). Throughout their lifetime cells repeatedly pass through a series of well-defined stages, which is called the cell cycle, in which they first duplicate their cell content and then distribute it among two newly forming daughter cells. This not only allows the reproduction of unicellular organisms, but also the development of complex organisms from a single fertilized egg cell. Moreover, it enables multicellular organisms to sustain their physiological fitness by healing wounds or rejuvenating tissues. It is of fundamental importance that this process occurs error-free as mistakes can have detrimental effects on animate beings and are linked to various diseases such as cancer. Therefore, nature has evolved a cell-cycle control system that ensures that events take place in the right order at the right time.

1.1 A brief overview of the cell cycle and its regulation in animal cells

In animals, the cell cycle can be divided into four phases. The S-phase (synthesis phase) and the M-phase (mitotic phase) represent the two main phases, which are temporally separated by two gap phases (G1 and G2) (Morgan, 2006) (Figure 1).

Cells enter G1 after they have successfully divided. Here they can either exit the cell cycle and enter the resting phase G0 or prepare themselves for another round of cell division. This depends on internal and external signals, which consider for example nutrient availability or cell fate. When proliferation is favorable cells grow until a point where they are ready to enter S-phase. During the S-phase cells duplicate their genome and the centrosome, which will build the spindle apparatus in mitosis, and then pass on into G2. Here they have further time to grow and synthesize proteins necessary to enter the mitotic phase. These preparatory phases are also summarized as interphase, as it is the period in between two division events (Morgan, 2006).

During the mitotic phase cells have to accomplish nuclear division (mitosis) and cytoplasmic division (cytokinesis). Therefore, the nuclear envelope breaks down and the DNA condenses into compact chromosomes (prophase-prometaphase). These consist of two identical sister chromatids, held together by proteinaceous cohesion rings. Moreover, microtubules emanating from opposing centrosomes build up the mitotic spindle and bind to attachment sites, the kinetochores, on the sister chromatids. Once all chromatids are connected to the mitotic spindle and aligned at the center (metaphase), the cohesion rings are enzymatically dissolved and the shortening of microtubules pulls both sister chromatids apart towards the cell poles (onset of anaphase). Simultaneously a contractile actomyosin ring forms between the segregating chromosomes at the cell equator, which ingresses and pinches off the two daughter cells (anaphase-telophase) (Morgan, 2006) (Figure 1 and Figure 2).

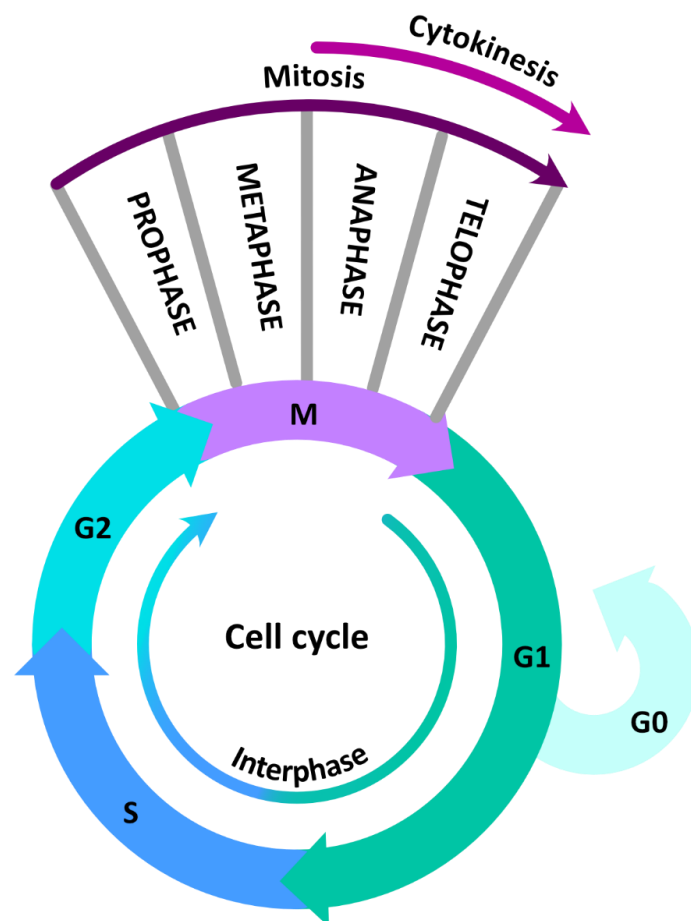


Figure 1: Schematic overview of the different cell cycle phases in animal cells. The cell cycle contains two major phases: the synthesis phase (S-phase) and the mitotic phase (M-phase), which are time-wise separated by two gap phases (G1 and G2). Together S-phase, G1, and G2 are called the interphase as they depict the time in between two division events, in which the cell duplicates its genome and prepares for another round of cell division. M-phase can be divided into four phases: prophase, metaphase, anaphase, and telophase during which the

cell undergoes mitosis (genomic division) and cytokinesis (cytoplasmic division). When cells should not undergo another round of division, they can exit the cell cycle by entering the resting phase G₀. (adapted from Morgan, 2006)

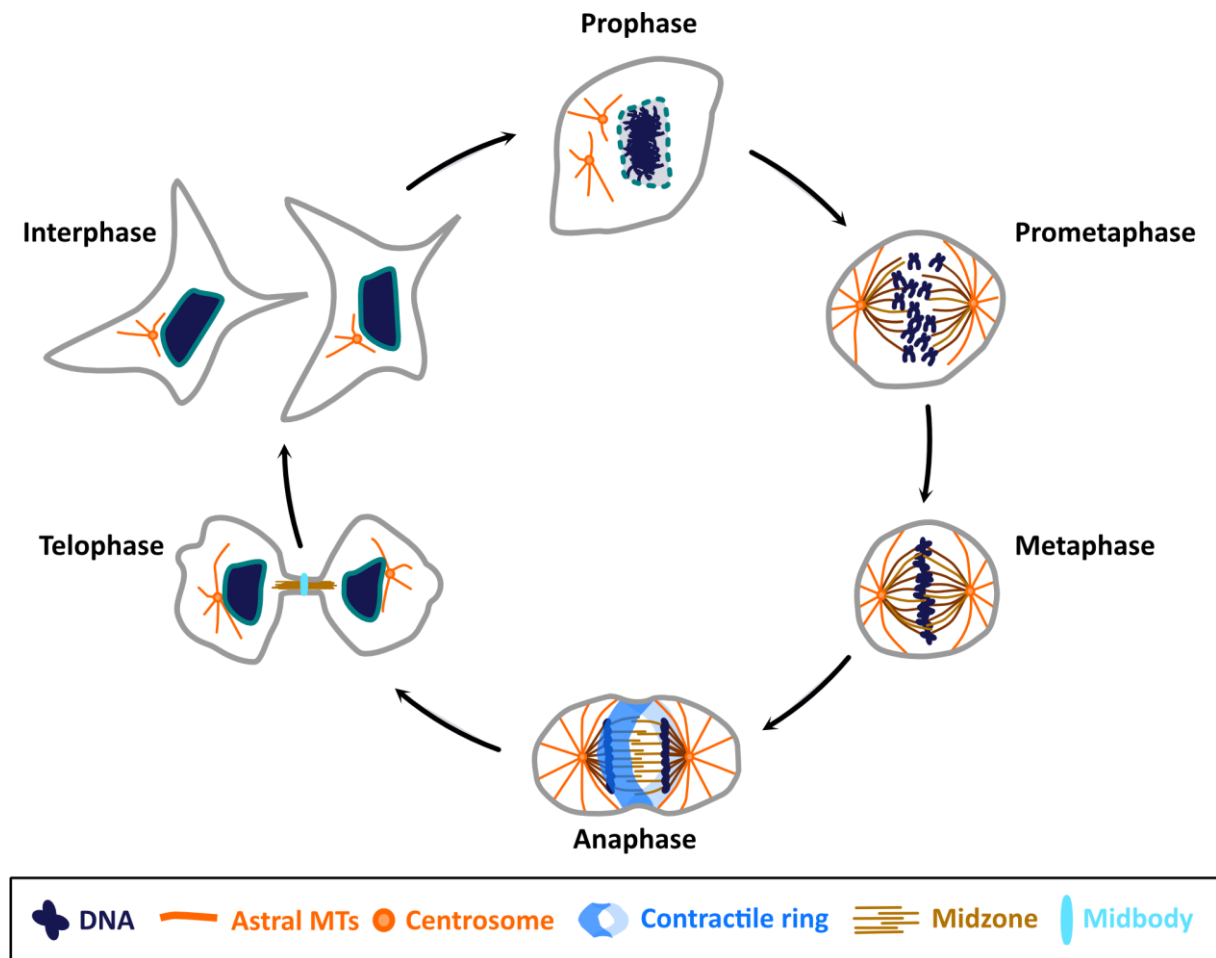


Figure 2: Mitotic stages in animal cells. As animal cells enter the mitotic phase, the nuclear envelope breaks down and the chromosomes (sister-chromatids) start to condensate (prophase). Moreover, both centrosomes move apart to opposite sides of the cell and nucleate microtubules, which form the mitotic spindle and attach to the kinetochores of the sister chromatids (prometaphase). As soon as all chromatids are tethered to spindle microtubules and are aligned at the center of the cell (metaphase), the cohesion rings of the sister chromatids are dissolved and the chromatids are pulled towards the opposite cell poles (onset of anaphase). At the same time, a contractile ring assembles and subsequently contracts between the separating chromosomes, which leads to the formation of two daughter cells (anaphase and telophase). (adapted from Morgan, 2006)

As the cell cycle is a fundamental process to ensure the organism's welfare it has to be tightly regulated. For this, a sophisticated control system has evolved, which ensures that the cell cycle steps occur in a certain order. The system relies on the activity of members of the protein kinase family cyclin-dependent kinases (Cdks). Cdks get activated through binding to regulatory proteins called cyclins. In each cell cycle, cyclins undergo a cycle of synthesis and degradation, which results in an increase and decrease in Cdk activities at certain times. This

oscillation of Cdk activities again leads to periodic changes in the phosphorylation of components of the cell cycle machinery. Through binding to stage-specific cyclins, Cdks can target different proteins and thereby trigger the initiation of different cell cycle events (Morgan, 2006).

Furthermore, the cell cycle control system comprises surveillance points, where it integrates feedback from the cell cycle machinery. The so-called checkpoints guarantee that preceding stage-specific processes are completed before the cell moves on to the next cell cycle phase. When defects are recognized the cell cycle is temporally halted, providing time to fix the problem. Once the prerequisites are met, the cell can pass on to the next step (Morgan, 2006).

The first checkpoint is the so-called restriction checkpoint in G1/S-phase. Here cells decide whether to enter another round of mitosis based on incoming growth factor signaling. When the signals are strong enough, G1/S-phase cyclins are expressed, Cdks get activated and the transcription of genes that are necessary to enter the S-phase is stimulated. Additionally, to prevent the replication of defective DNA, DNA damage triggers a signaling cascade that pauses the cell cycle and allows DNA repair (Poon, 2016).

The next checkpoint is the replication checkpoint in S-phase, which ensures that the entire genome is replicated once before cell division occurs. It gets activated when replication comes to a halt for example due to a lack of nucleotides or DNA damages and prevents the progression to the mitotic phase. Cells then have the time to reactivate the stalled replication fork or restart replication (Poon, 2016).

During G2, right before cells enter the mitotic phase, a DNA damage checkpoint similar to the one in G1 makes sure that DNA is intact (Poon, 2016).

Lastly, the spindle assembly checkpoint (SAC) at the metaphase-to-anaphase transition ensures that each daughter cell receives a complete set of chromosomes during cell division. Both sister kinetochores have to be bound by spindle microtubules of opposing poles to allow the distribution of the sister chromatids among both daughter cells. Free kinetochores are bound by SAC protein complexes, which block the activation of the anaphase-promoting complex/cyclosome (APC/C). APC/C activity is needed to release the cohesion connection of sister chromatids and trigger mitotic exit (Lara-Gonzalez et al., 2012).

1.2 Cytokinesis in animal cells

Cytokinesis is the last step of the mitotic phase in which the mother cell gets physically split into two separated daughter cells. In animal cells, it starts at the onset of anaphase and involves the invagination of the plasma membrane between the segregating chromosomes. The mechanical force for the membrane invagination is provided by a contractile actomyosin ring formed at the equatorial cell cortex in response to signals from the anaphase spindle. Gradual ring contraction pulls the attached membrane inwards generating a cleavage furrow, which eventually pinches off two cells. After ingression is completed, the cells stay connected by a thin intercellular bridge, which gets eventually cleaved in a final step called abscission (D'Avino et al., 2015; Green et al., 2012) (Figure 3).

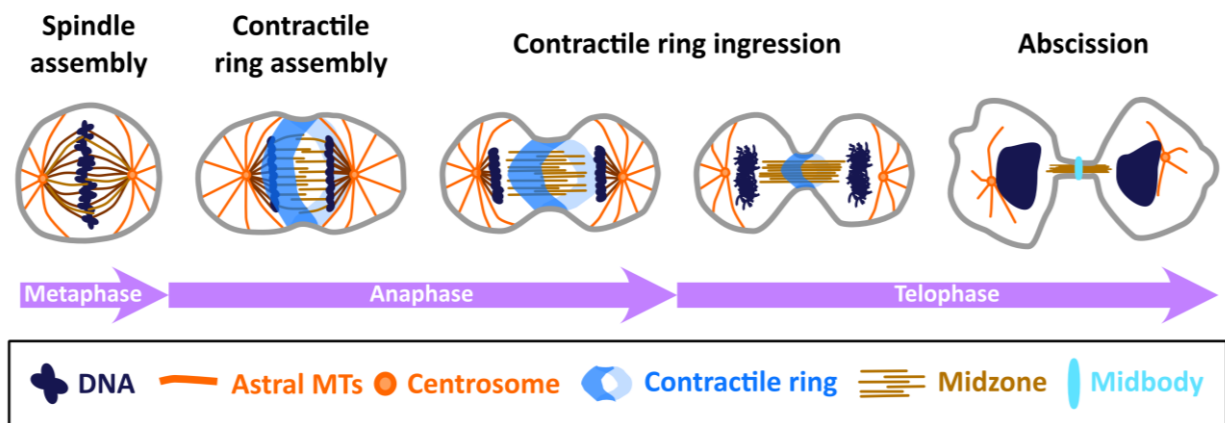


Figure 3: Schematic overview of cytokinesis in animal cells. Animal cytokinesis starts with anaphase onset with the formation of the spindle midzone and the assembly of a contractile ring underneath the equatorial plasma membrane between the segregating chromosomes. Subsequent constriction of the contractile ring leads to the formation of a cleavage furrow that pinches off two separate cells. Once the ring has fully constricted the cells stay connected by an intercellular bridge, which is eventually cleaved during abscission. (adapted from Fededa & Gerlich, 2012)

One major challenge of cytokinesis is to equally divide the content of the mother cell between two newly formed cells. The most important thing here is that each daughter cell inherits a full diploid set of chromosomes and one centrosome. This not only ensures the integrity of individual cells but also the welfare of multicellular organisms. In order to achieve this aim, contractile ring assembly must occur in coordination with genomic division and only at the cell equator between the separated chromosomes. Therefore, precise spatial and temporal regulation of cytokinesis is extremely important. It is known that in animal cells, active

signaling between the mitotic spindle and the cell cortex ensures correct spatial and temporal placement of the contractile ring (Eggert et al., 2006; Green et al., 2012; Verma et al., 2019). Further regulation is provided by the action of two mitotic kinases, Cdk1 and polo like kinase 1 (Plk1), and two regulatory complexes, the chromosomal passenger complex (CPC) and the APC/C (Eggert et al., 2006; Green et al., 2012; Verma et al., 2019). The temporal coordination of genomic and cytoplasmic division is achieved by the fact that both processes are initiated by the same molecular trigger. After the SAC is satisfied, the transition from metaphase to anaphase is triggered by the activity of the APC/C, which initiates both the separation of the sister chromatids and the formation of the cleavage furrow (Pines, 2011). Functioning as a ubiquitin ligase, the APC/C targets the inhibitor of the protease separase, which is responsible for the cleavage of the cohesion rings. At the same time, the activator of the Cdk1 kinase cyclin B is targeted for degradation (Pines, 2011). A decline in Cdk1 activity results in the removal of inhibiting phosphorylations in proteins required for cytokinesis by counteracting phosphatases (Holder et al., 2019).

At the onset of anaphase, the mitotic spindle reorganizes to form an array of interdigitating microtubules, called central spindle or midzone, between the separating chromosome masses. Together, midzone microtubules and astral microtubules emanating from the two centrosomes, specify the site of cleavage furrow formation at the cell equator. Studies in several animal model systems have established the small GTPase RhoA as the master regulator of contractile ring assembly (Drechsel et al., 1997; Jantsch-Plunger et al., 2000; Kishi et al., 1993; Loria et al., 2012; Mabuchi et al., 1993; Prokopenko et al., 1999; Yüce et al., 2005). Signals from the anaphase spindle lead to RhoA activation by its guanine nucleotide exchange factor (GEF) Epithelial cell transforming 2 (Ect2) in a restricted equatorial zone. Subsequently, active RhoA recruits and activates downstream effectors, which build up the contractile ring and drive its contraction (D'Avino et al., 2015; Eggert et al., 2006; Green et al., 2012).

Given the role of cytokinesis, it does not surprise, that various diseases exist which are associated with defective cytokinesis. Failed cytokinesis, may it be due to failed contractile ring formation or incomplete furrow ingression, for example, gives rise to tetraploid cells. These cells are genomically unstable and often trigger the formation of tumors (Lacroix & Maddox, 2012; Lens & Medema, 2019; Lim & Ganem, 2014). Moreover, mal-coordination of genomic division and contractile ring ingression can result in the miss-segregation of

chromosomes. The resulting aneuploidy is also often found in cancer cells (Lacroix & Maddox, 2012; Storchova & Kuffer, 2008). Numerical aberrations of centrosomes can also cause aneuploidy. During disturbed cytokinesis, both centrosomes may end up in one cell. As a consequence, instead of a bipolar spindle, a multipolar spindle is formed during the next cell division, which subsequently miss-segregates the chromosomes (Bettencourt-Dias et al., 2011). Additionally, several other diseases such as the Lowe syndrome, anemia, the Wiskott-Aldrich syndrome, and female infertility were linked to defective cytokinesis (Lacroix & Maddox, 2012; Lens & Medema, 2019). All this underlines how important it is that cytokinesis occurs undisturbed, as without successful cytokinesis all other preceding cell cycle events are nullified.

The following sections discuss important steps of cytokinesis such as central spindle assembly, furrow positioning, and formation as well as the final cut, also known as abscission, in more detail. Moreover, the role of the GTPase RhoA and its activator Ect2 during cytokinesis will be described.

1.3 Central spindle assembly

The mitotic spindle is not only the molecular machinery that drives the separation of the sister-chromatids, but it also positions the cleavage furrow during cytokinesis. This requires drastic remodeling of the metaphase spindle at the onset of anaphase. Three major classes of microtubules compose the metaphase spindle: kinetochore microtubules, which tether the chromosomes to the spindle apparatus, astral microtubules, which emanate from both centrosomes towards the cell cortex, and non-kinetochore microtubules, which extend from both sites of the spindle towards the midplane where they overlap (Gadde & Heald, 2004; McIntosh et al., 2012; Pavin & Tolic, 2021) (Figure 4). As the sister chromatids are pulled towards the cell poles during anaphase, arrays of overlapping antiparallel microtubules build up the central spindle or so-called spindle midzone in the space between the separating chromatids (Mastronarde et al., 1993; McDonald et al., 1979; McIntosh et al., 1979) (Figure 4).

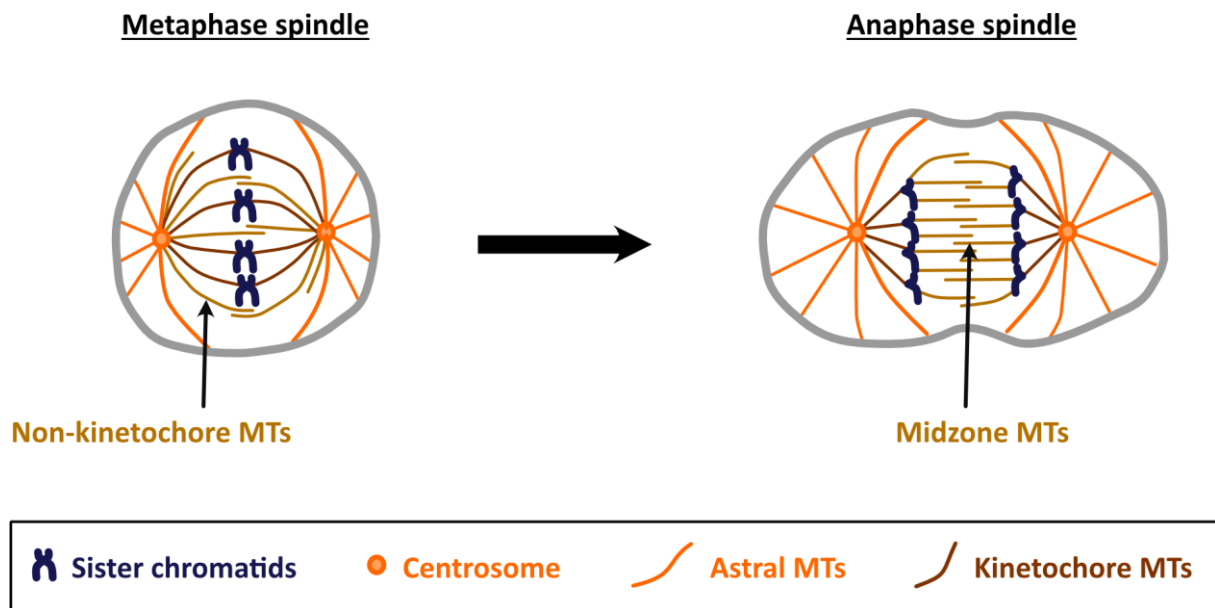


Figure 4: The mitotic spindle in meta-and anaphase. The metaphase spindle is comprised of three major classes of microtubules (MTs): the kinetochore MTs, by which the sister chromatids are attached to the spindle, astral MTs, which radiate from both centrosomes towards the cell cortex, and non-kinetochore MTs, which extend from both sites of the spindle towards the midplane where they overlap. Upon entry into anaphase, the spindle gets remodeled to form the anaphase spindle, which central feature is the spindle midzone. The midzone is formed by bundles of antiparallel MTs in the space between the separating sister chromatids. (adapted from Nazockdast & Redemann, 2020)

In part, it is formed by existing non-kinetochore microtubules, but microtubules also assemble *de novo* through a process that is independent of centrosomes (Kamasaki et al., 2013; Uehara & Goshima, 2010; Uehara et al., 2009). The central spindle is important for cytokinesis as it serves as a structural platform from which many sub-processes, such as contractile ring assembly and abscission, are controlled (Fededa & Gerlich, 2012; Glotzer, 2009; Wadsworth, 2021). Thus, proper assembly is mandatory. This is ensured by various proteins that stabilize and organize the microtubule bundles within the central spindle. Important factors are the microtubule crosslinker protein regulator of cytokinesis 1 (PRC1), the CPC, and the centralspindlin complex (Fededa & Gerlich, 2012; Glotzer, 2009; Wadsworth, 2021). PRC1 dimers bundle antiparallel microtubules and additionally recruit the mitotic kinase Plk1 to the midzone (Neef et al., 2007; Subramanian et al., 2010). The CPC contains, amongst others, the Aurora B kinase, which regulates midzone formation by phosphorylating several of its components (Carmena & Earnshaw, 2003). Centralspindlin is an evolutionary conserved tetrameric complex formed by two molecules of each, the kinesin mitotic kinesin-like protein 1 (MKLP1) and the GTPase activating protein (GAP) Rac GTPase-activating protein 1 (RacGAP1)

(Mishima et al., 2002). It not only helps to structurally shape the central spindle but also holds a special role in cleavage furrow positioning (see later chapter 1.4). Before anaphase, high Cdk1 activity prevents central spindle formation by blocking the function of many proteins involved (Holder et al., 2019).

1.4 The mitotic spindle positions the contractile ring

The contractile ring has to be precisely positioned in the middle of the cell between the segregating sister chromatids to ensure the equal distribution of the cell content among the nascent daughter cells. Pioneer work in echinoderm eggs demonstrated almost 40 years ago that the displacement of the anaphase spindle directly after the cleavage furrow had already appeared, promoted the formation of a new furrow according to the new spindle position while the old furrow regressed (Rappaport, 1985). Nowadays, it is generally accepted that signals arising from the mitotic spindle specify the position of the cleavage plane (D'Avino et al., 2015; Green et al., 2012; Mishima, 2016). However, how the spindle directs correct cleavage site specification, is highly debated as studies in different model organisms have obtained different results. Over the years different models for cleavage site specification have been proposed, which are based on different signals from astral and midzone microtubules (Mishima, 2016) (Figure 5). These may diverge in the origin of the inductive signal, but all of them share the same outcome, which is the accumulation and activation of the small GTPase RhoA in a narrow equatorial zone at the membrane. As aforementioned RhoA activation is required for contractile ring assembly and cytokinesis (Bement et al., 2005; Jordan & Canman, 2012; Piekny et al., 2005). In the following, the mentioned models are discussed in more detail.

The widely accepted midzone stimulation model assumes that signals emitted from the midzone or so-called central spindle promote contractile ring formation at the overlying equatorial cortex (Mishima, 2016) (Figure 5 A). The model was initially postulated after micromanipulation experiments in grasshopper neuroblasts have shown that furrow ingression always coincides with the midzone of the spindle (Kawamura, 1977). Conversely, spatial separation of the midzone and the overlying cortex, by the insertion of a glass needle, prevented furrow ingression in cultured human cells (Cao & Wang, 1996). Since then, it was demonstrated in several other studies that the midzone is the major signaling site for furrow induction (Adams et al., 1998; Bonaccorsi et al., 1998; Bringmann & Hyman, 2005; Giansanti

et al., 2001; van Oostende Triplet et al., 2014b; Yüce et al., 2005). Several studies also provided insights into the molecular nature of the emitted signal. It was suggested that the RhoA GEF Ect2 takes over the central role. Early during vertebrate cytokinesis, Ect2 gets recruited to the midzone via the centralspindlin component RacGAP1. Ect2-RacGAP1 interaction is assumed to stimulate Ect2 GEF activity by releasing Ect2 autoinhibition. Active Ect2 then translocates to the equatorial membrane, where it stimulates the nucleotide exchange in RhoA, thereby inducing the signaling cascade of furrow formation (Basant & Glotzer, 2018; D'Avino et al., 2015; Green et al., 2012). As this topic is rather complex it will be discussed in more detail in separate chapters (see chapters 1.5 and 1.9.3.3).

Likewise, the model of astral stimulation claims that a subset of long astral microtubules, which extend to the equatorial cortex contributes positive signals for furrow formation at the center of the cell (Mishima, 2016) (Figure 5 B). Experiments in several model systems have shown that astral microtubules alone can promote furrowing (Baruni et al., 2008; Bringmann & Hyman, 2005; Canman et al., 2003; Rappaport, 1961). Later it was suggested that they do so by allowing the transport of important regulators, such as RacGAP1, to the membrane at the division site (Breznau et al., 2017; Verma & Maresca, 2019). At the membrane RacGAP1 then initiates contractile ring assembly via the Ect2-RhoA pathway similar to what is described in the previous paragraph.

Contrary to that, the model of astral relaxation suggests that astral microtubules, which radiate from the centrosomes and contact the cell cortex, prevent cortical contractility at the cell poles. In relation to the poles, the equator would then exhibit stronger contractility which induces local furrow formation (Mishima, 2016) (Figure 5 C). The concept of astral microtubules negatively regulating the accumulation of contractile ring components and contractility is supported by various studies in different model organisms, where they either misplaced the spindle or selectively destroyed astral microtubules by laser ablation or drug treatment (Bement et al., 2005; Chen et al., 2008; Foe & von Dassow, 2008; Murthy & Wadsworth, 2008; van Oostende Triplet et al., 2014b; Werner et al., 2007). In contrast to the aforementioned furrow-inducing signals at the cell equator, the molecular nature of the inhibitory signals is still poorly understood. However, recent studies have succeeded in providing some insights into the principles of these signals. As so Mangal et al. (2018) identified an active clearance mechanism of contractile ring components at the cell poles in

C. elegans, which depends on Aurora A kinase activation by its aster-based activator TPXL-1. Whether a similar mechanism exists in other model systems remains elusive up to this point, but recent evidence demonstrated that astral microtubules negatively regulate the polar cell cortex in human cells (Chen et al., 2021). The authors showed that formins get inactivated specifically at the cell poles by an aster-mediated mechanism which results in the depletion of the actin cortex and the reduction of cortical stiffness.

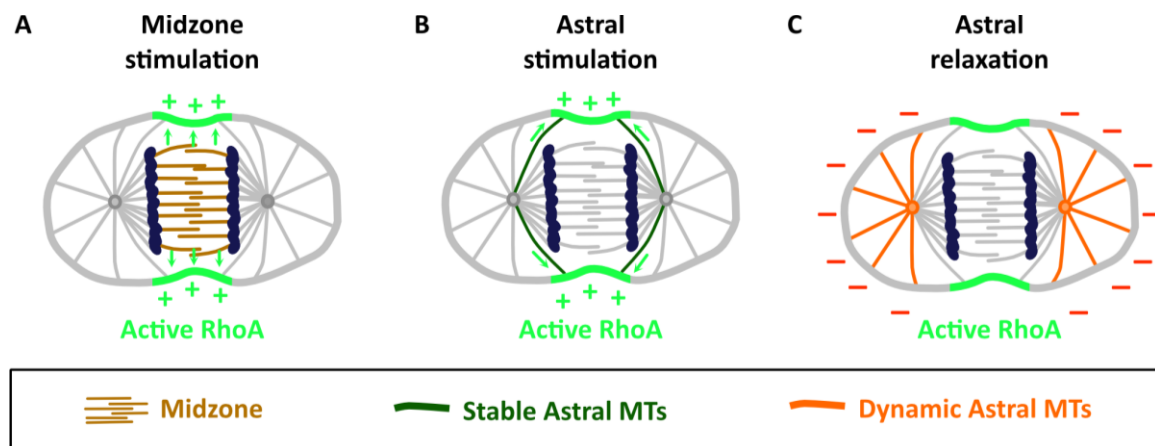


Figure 5: Models showing how the mitotic spindle positions the cytokinetic furrow. (A) The midzone stimulation model predicts that signals from the spindle midzone stimulate the activation of RhoA at the equatorial membrane. (B) The astral stimulation model assumes that a subset of stable astral microtubules reaches the equatorial membrane and stimulates the activation of RhoA in a narrow equatorial zone. (C) In the astral relaxation model, inhibitory signals from astral microtubules prevent the activation of RhoA at the cell poles, thereby helping to restrict contractile ring formation to the equator. (adapted from Mishima, 2016)

The fact that none of the above models can explain all the different findings led to the consensus that they are not mutually exclusive but rather work hand in hand to ensure proper furrow positioning (D'Avino et al., 2015; Eggert et al., 2006; Mishima, 2016). Indeed, the co-existence of aster- and midzone-derived signals could be shown in *C. elegans* as asters and midzone separated by a laser were both able to trigger furrow formation (Bringmann & Hyman, 2005). Likewise, both impaired midzone formation and altered astral microtubule stability influenced RhoA zone formation in cultured human cells (van Oostende Triplet et al., 2014b). This principle of several partially redundant mechanisms, coexisting in a cell, makes the process of division site specification robust to perturbations and ensures the faithful division of the mother cell into two daughter cells. The notion is that the contributions of different microtubule populations vary depending on cell size and morphology. So, it seems that the midzone signal is more important for smaller epithelial cells than for large embryonic

cells, in which the equatorial membrane is far away from central spindle microtubules. Even though the anaphase spindle provides the dominant cues for cleavage site specification, additional spindle-independent cues exist. During asymmetric cell division of *Drosophila* neuroblasts (Cabernard et al., 2010) or the *C. elegans* zygote (Jordan et al., 2016), for example, the positioning of the contractile ring is also influenced by polarity proteins. Further, cues coming from the segregating chromosomes induce local softening of the polar cortex by loosening the connection of the actin network with the plasma membrane in *Drosophila* and human cells (Rodrigues et al., 2015).

1.5 The small GTPase RhoA triggers the assembly of the contractile ring

RhoA belongs to the Rho family of GTPases, which is highly conserved in many organisms and, among others, includes Rac1 and Cdc42 (Haga & Ridley, 2016; Piekny et al., 2005). Rho GTPases are important regulators of the cytoskeleton and are involved in various cellular processes such as cell motility, cell polarization, cell adhesion, and cytokinesis (Etienne-Manneville & Hall, 2002; Haga & Ridley, 2016; Heasman & Ridley, 2008; Jordan & Canman, 2012). During cytokinesis, the reorganization of the actomyosin network results in the assembly of the contractile ring at the cell equator. In most animal cells this is controlled by the small GTPase RhoA (Drechsel et al., 1997; Jantsch-Plunger et al., 2000; Kishi et al., 1993; Loria et al., 2012; Mabuchi et al., 1993; Prokopenko et al., 1999; Yüce et al., 2005), which localizes in its active form to the future division site during anaphase (Takaishi et al., 1995; Yonemura et al., 2004). Loss of RhoA activity, either by C3 exoenzyme treatment, a Rho inhibitor, depletion, or dominant-negative mutations, was shown to prevent the formation of the contractile ring and thus the physical division of cells in cell culture and in many different organisms including flies, frogs, and nematodes (Drechsel et al., 1997; Jantsch-Plunger et al., 2000; Kishi et al., 1993; Lai et al., 2005; Melendez et al., 2011; Moorman et al., 1996; Prokopenko et al., 1999).

Like all GTPases, RhoA acts as a molecular switch, cycling between an inactive GDP-bound and an active GTP-bound state with the help of regulatory proteins. GEFs accelerate the release of GDP and allow the rebinding of GTP, thereby helping to activate RhoA, while GTPase activating proteins (GAPs) help to deactivate RhoA by stimulating its intrinsically low hydrolase activity.

Additionally, guanine-nucleotide dissociation inhibitors (GDIs) bind inactive Rho GTPases and keep them cytoplasmic (Garcia-Mata et al., 2011). During human cytokinesis, Ect2 and M-phase GAP (MP-GAP) act as major GEF and GAP for RhoA, respectively (Tatsumoto et al., 1999; Zanin et al., 2013) (Figure 6).

At the onset of anaphase, RhoA gets activated by Ect2 and binds the membrane in a narrow region at the center of the cell. Once activated RhoA recruits and activates downstream effectors, which are required for the assembly and the constriction of the contractile ring (Piekny et al., 2005, Jordan & Canman, 2012) (Figure 6). By activating diaphanous-related formins RhoA stimulates the assembly of long actin filaments, which form the structural framework of the ring (Castrillon & Wasserman, 1994; Evangelista et al., 2002; Watanabe et al., 2008). Additionally, profilins help to rapidly assemble actin filaments. They bind to actin monomers and stimulate the exchange of GDP to GTP, thereby converting them into an active state from which they can be easily polymerized by formins (Goldschmidt-Clermont et al., 1992). In parallel to filamentous actin formation, RhoA activates the RhoA-associated kinase (ROCK) which promotes myosin II motor activity in two ways. First, ROCK directly activates myosin II motor activity by phosphorylating its regulatory light chain, and second, it prevents myosin II dephosphorylation by inhibiting the antagonizing myosin light chain phosphatase (MLCP). Activated myosin II then interacts with the actin scaffold and is responsible for its constriction. Additionally, the contractile ring contains crosslinkers such as anillin and septins. Anillin is a scaffold protein that can bind to RhoA (Piekny & Glotzer, 2008), actin, myosin (Straight et al., 2005), Ect2 (Frenette et al., 2012), and septins (Field et al., 2005). Thereby it links the cortical ring to the plasma membrane and provides stability to the ingressing furrow (Liu et al., 2012; Piekny & Glotzer, 2008). Septins themselves form higher-ordered structures and were reported to stabilize the cleavage furrow by facilitating full activation of myosin II (Joo et al., 2007).

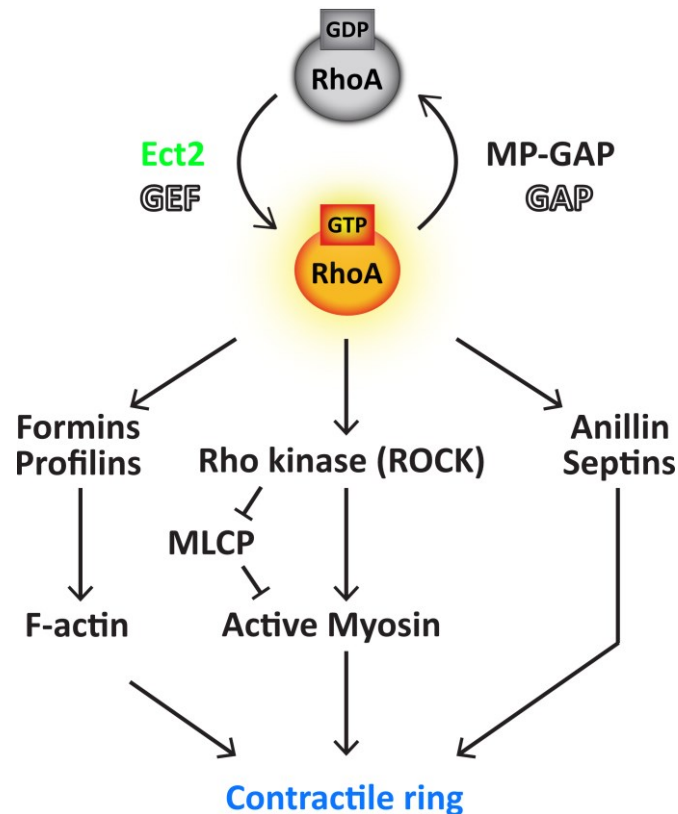


Figure 6: RhoA signaling during human cytokinesis leads to the assembly of the contractile ring. RhoA is a molecular switch, which cycles between an active GTP-bound and an inactive GDP-bound state with the help of its GEF Ect2 and its GAP MP-GAP. During anaphase, active RhoA recruits and activates several downstream effectors. It stimulates the formation of F-actin through formins and profilins and the activation of myosin II by Rho kinase (ROCK). Actin and myosin form the basic structure of the contractile ring. Furthermore, RhoA recruits crosslinkers such as anillin and septins. (adapted from Piekny et al., 2005)

1.6 The actomyosin ring drives cleavage furrow ingression

The actomyosin ring assembles as a thin structure (0.1-0.2 μm) of interlinked filaments underneath the plasma membrane and can range in width from less than a micron to 20 μm between species (Schroeder, 1990, O'Shaughnessy & Thiyagarajan, 2018). It was suggested that this occurs in a stepwise process in which first a broad actomyosin band is formed at the cell equator, which eventually gets remodeled into a thinner equatorial ring (Hu et al., 2011; Lewellyn et al., 2011; Mabuchi, 1994; Szafer-Glusman et al., 2011). Actin and myosin can either be assembled *de novo* or brought to the equator by cortical flow (Sugioka, 2021). Since the contractile ring is attached to the equatorial membrane via anillin and septins, its contraction pulls in the overlying membrane and the furrow starts to show. The ingression is accompanied by the continuous disassembly of actomyosin filaments, which keeps the density in the ring

constant and allows the shrinkage of the ring at a relatively constant rate (Calvert et al., 2011; Carvalho et al., 2009; Mabuchi, 1994; Murrell et al., 2015; O'Shaughnessy & Thiyagarajan, 2018; Schroeder, 1990).

How the actomyosin filaments exactly align and how the constrictive force is generated, remains poorly understood (Eggert et al., 2006; Fededa & Gerlich, 2012; Green et al., 2012). Early findings suggested that the force for ring contraction is generated by myosin filaments sliding along actin filaments similar to the mechanism found in muscles (Schroeder Schroeder, 1968, 1972); However, a sarcomere-like arrangement of myosin and actin could not be reliably shown (Green et al., 2012; O'Shaughnessy & Thiyagarajan, 2018). Recent work by Spira et al. (2017) demonstrated that a randomly oriented actomyosin network initiates furrow ingression and, as ingression proceeds, aligns along the equator in a myosin II-dependent fashion.

Efficient furrow ingression not only requires the formation and contraction of the actomyosin ring at the center of the cell, but also the softening of the polar cortex. The tension generated by the polar cortex counteracts the contractile force at the cell equator and therefore influences the rate of furrow ingression (Turlier et al., 2014). Consistently, forced polar relaxation by light-induced inactivation of myosin II at both cell poles was shown to speed up furrow ingression in cultured cells (Yamamoto et al., 2021). More and more evidence accumulates showing that actin, myosin, and their crosslinkers are actively removed from the cortex to reduce polar tension and allow efficient furrow ingression (Chapa et al., 2020; Chen et al., 2021; Mangal et al., 2018; Ramkumar et al., 2021; Rodrigues et al., 2015). Furthermore, polar relaxation ensures a stable cell shape while the cell ingresses, as it limits cortex contractions at the poles, which can lead to shape oscillations and the failure of cytokinesis (Sedzinski et al., 2011).

1.7 Abscission is the last step of cytokinesis

At the end of cytokinesis, the furrow reaches a point where it cannot constrict any further and the two daughter cells stay connected by an intercellular bridge, formed by compacted antiparallel midzone microtubules (Mierzwa & Gerlich, 2014). In the middle of the intercellular bridge microtubule ends overlap and form, together with associated proteins, an electron-dense structure, called the midbody. The midbody was first described by Walther Flemming

in the 19th century and is therefore also referred to as the Flemming body. It is an important regulatory structure administering the final step of cytokinesis called abscission, in which the daughter cells are ultimately split in two.

In order to form both, the intercellular bridge and the midbody, the midzone must be rearranged and this includes the disassembly of actomyosin filaments and the re-localization of both midzone and contractile ring components to three distinct midbody substructures (D'Avino & Capalbo, 2016; Mierzwa & Gerlich, 2014). The kinesin superfamily protein member 4 (KIF4), a kinesin, and the microtubules bundling protein PRC1 remain at the central overlap site called the midbody core (Hu et al., 2012). The midbody core is surrounded by the midbody ring, which is formed by former contractile ring components such as anillin, RhoA, Ect2, RacGAP1, septins, and the citron kinase (Gai et al., 2011; Hu et al., 2012; Kechad et al., 2012) and flanked by the midbody arms, which accumulate the two motor proteins centromere protein E (CENP-E) and mitotic kinesin-like protein 2 (MKLP2) and Aurora B kinase (Gruneberg et al., 2004; Hu et al., 2012; Yen et al., 1991).

After the disassembly of the actomyosin ring, the midbody anchors the plasma membrane to the intercellular bridge and prevents the reopening of the cleavage furrow. Findings of several groups have revealed various ways by which several midbody ring components including anillin, septins, and centralspindlin, contribute to this process (Kechad et al., 2012; Lekomtsev et al., 2012; Makyio et al., 2012).

Along with this, the intercellular bridge continues to narrow on both sites of the midbody, which is mediated by regulatory factors delivered by endosomal vesicles (Schiel & Prekeris, 2013). This specifies the future sites for abscission and stimulates the recruitment of the endosomal sorting complex required for transport III (ESCRT-III) complex, which is involved in many membrane-scission events (Vietri et al., 2020). ESCRT-III polymerizes into helical filaments, which attach to the plasma membrane and lead to their constriction. Together with simultaneous removal of microtubules, this terminates with the physical separation of both daughter cells (Vietri et al., 2020). To ensure that abscission occurs at the right time, the assembly of the abscission machinery is tightly controlled by the CPC and the mitotic kinase Plk1 (D'Avino & Capalbo, 2016).

1.8 Precise control of RhoA signaling

As described in detail in 1.4, signaling between the anaphase spindle and the cell cortex establishes the activation of RhoA by its GEF Ect2 at the cell equator. However, it is not enough to simply activate RhoA. Instead, efficient cytokinesis requires a well-defined amount of active RhoA. Experiments in *C. elegans* have shown that progressively reducing RhoA levels by RNAi progressively slows down furrow ingression (Loria et al., 2012) and similar results were predicted by biophysical modeling of furrow constriction (Turlier et al., 2014). Likewise, increasing the amount of active RhoA, by expressing a constitutively active RhoA mutant or by depleting its negative regulator MP-GAP, led to slower furrow ingression and the formation of large blebs (Miller & Bement, 2009; Zanin et al., 2013). During anaphase, cells release pressure in form of small membrane blebs at the poles, thereby stabilizing cell shape (Hickson et al., 2006; Sedzinski et al., 2011; Tokumitsu & Maramorosch, 1967). Increased RhoA activity leads to an increase in cortical contractility, which in turn leads to higher intracellular pressure and causes the otherwise small membrane blebs to grow bigger (Tinevez et al., 2009). During the retraction of large blebs, the generated cytoplasmic flow can introduce cell shape oscillations, which often entail failed cytokinesis (Sedzinski et al., 2011; Taneja et al., 2020). All these observations demonstrate how important it is to keep the levels of active and inactive RhoA precisely balanced to ensure reliable cytokinesis. One way of achieving this is by tightly controlling the activity of Ect2, which will be discussed in more detail in chapter 1.9.3.

Active RhoA associates with the plasma membrane via two lipid anchors (Michaelson et al., 2001). Therefore, RhoA is thought to move freely within the membrane and diffuse away from the site of activation over time (Bement et al., 2006). Nevertheless, active RhoA accumulates in a restricted equatorial zone. For this, astral microtubules in particular play an important role and several experiments, in which astral microtubules were modified, have demonstrated that they control the dimensions of the RhoA zone at the membrane with high precision. As so lengthening of astral microtubules by depleting the kinesin mitotic centromere-associated kinesin (MCAK), implicated in the negative regulation of microtubule length (Desai et al., 1999; Hedrick et al., 2008; Rankin & Wordeman, 2010a), could narrow the zone of active RhoA at the equator (van Oostende Triplet et al., 2014b; Zanin et al., 2013). Conversely, specifically depleting astral microtubules by low doses of nocodazole or trichostatin A led to a broader equatorial RhoA zone (Bement et al., 2005; Murthy & Wadsworth, 2008; van Oostende Triplet

et al., 2014b; von Dassow et al., 2009; Zanin et al., 2013). Although this clearly shows that astral microtubules negatively regulate RhoA zone dimensions, the fact that RhoA zones could still form in the absence of astral microtubules implies that additional mechanisms help to spatially restrict active RhoA. RhoA inactivation by its GAP has been suggested to prevent the spreading of active RhoA within the membrane (Bement et al., 2006; Miller & Bement, 2009). However, this theory is controversial as MP-GAP depletion in human cells did not result in a broadened RhoA zone (Zanin et al., 2013). Additionally, corralling mechanisms could help to retain RhoA at the cell equator. It has been shown recently, that GTP-RhoA is intrinsically prone to rapidly dissociate from the plasma membrane (Budnar et al., 2019). In the same study, GTP-RhoA membrane residence time was positively influenced by binding to the phospholipid phosphatidylinositol 4,5-bisphosphate (PIP2) and anillin. PIP2 is specifically enriched at the cleavage furrow in animal cells (Emoto et al., 2005; Field et al., 2005) and could thereby contribute to the formation of a narrow RhoA zone. Alternatively, the dense actin network below the plasma membrane could inhibit the diffusion of RhoA within the membrane. It is known that by forming a physical barrier the actin cytoskeleton drastically reduces the mobility of membrane-bound proteins (Kusumi et al., 2012).

But why is keeping a narrow RhoA zone so important? RhoA is the master regulator of contractile ring assembly and with its localization at the membrane, it defines the area where contractile ring components accumulate. Thus, RhoA localizing to a broader equatorial zone simultaneously results in a broader contractile ring, which has been shown to negatively influence furrow ingression. Depending on the degree of widening, furrow ingression was either slowed down (Miller & Bement, 2009) or completely abolished (Bement et al., 2005; Yüce et al., 2005) in the presence of a broad RhoA zone.

1.9 Epithelial cell transforming 2 (Ect2) protein

1.9.1 The GEF Ect2 is essential for cytokinesis

Epithelial cell transforming 2 (Ect2) is a GEF, which is highly conserved within the animal kingdom and orthologues exist in many species such as *H. sapiens* (Ect2), *D. melanogaster* (Pebble), *C. elegans* (ECT-2), and *X. laevis* (Ect2). It belongs to the Dbl family of GEFs, which specifically activates Rho GTPases and is involved in various signaling events (Zheng, 2001).

Human Ect2 comprises 883 amino acids and has several functional domains as shown in Figure 7. The N-terminal part of the protein contains three BRCT domains and the C-terminal part harbors the catalytic Dbl homology (DH)-GEF domain, a pleckstrin-homology (PH), and a polybasic sequence (PBS). N- and C-terminus are connected by a linker called S-loop. Additionally, it contains two nuclear localization signals (NLS). (Figure 7)

The structure and function of the individual domains will be the topic of the following chapter (chapter 1.9.2).

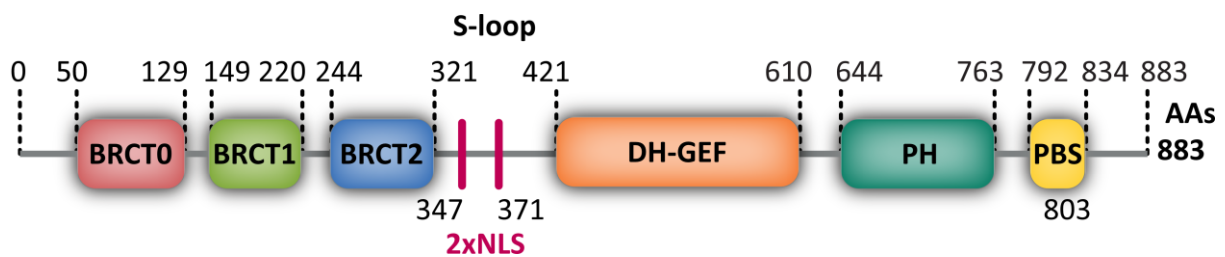


Figure 7: The structure of the GEF Ect2 in humans. Ect2 comprises 883 amino acids. The N-terminus contains three BRCT domains, called BRCT0, BRCT1, and BRCT2, and the C-terminus harbors the catalytic DH-GEF domain, a PH, and a PBS domain. Moreover, Ect2 comprises two NLS sequences. The exact location of the individual domains and the NLSs are indicated above and below, respectively.

Ect2 is best known for its function in cytokinesis, during which it activates the major contractile ring activator RhoA. Consistent with the critical role of the contractile ring, Ect2 has been found essential for cleavage furrow formation in *Drosophila*, *C. elegans*, and human cultured cells, and loss of its functions results in cytokinetic failure (Dechant & Glotzer, 2003; Kim et al., 2005; Prokopenko et al., 1999; Tatsumoto et al., 1999; Yüce et al., 2005). However, Ect2 also holds functions outside of cytokinesis. One example is its requirement for cell rounding in metaphase, where the cell cortex gets massively remodeled in response to RhoA signaling (Matthews et al., 2012). An example of a RhoA-independent role is its involvement in the DNA damage response, where Ect2 helps to activate DNA-dependent cell cycle checkpoints in S- and G2/M-phase and to induce DNA-damage associated cell death (He et al., 2016).

The cytokinetic function of Ect2 was first described in *Drosophila*, where Pebble mutants resulted in the absence of contractile ring function and the formation of multinucleated cells after cellularization (Hime & Saint, 1992; Lehner, 1992). Both, genetic interaction studies and yeast-two-hybrid assays, later revealed that it functions as a GEF for Rho1 (the *Drosophila* orthologue of RhoA) (Prokopenko et al., 1999). Mammalian Ect2 was initially described as a

transforming protein, which was identified in a mitogenic screen (Miki et al., 1991). Only later Ect2 was shown to have similarities with regulators of Rho GTPases, to directly interact with RhoA, RhoC, and Rac1 and to catalyze the nucleotide exchange in RhoA, Rac1, and Cdc42 *in vitro* (Miki et al., 1991; Miki et al., 1993; Tatsumoto et al., 1999). Finally, a conserved function of Ect2 in mammalian cytokinesis was demonstrated by injection of an Ect2 antibody and overexpression of an N-terminal fragment, what both prevented cytokinesis (Tatsumoto et al., 1999).

As has already been briefly mentioned above, Ect2 activity is required for cell rounding in metaphase (Matthews et al., 2012), nevertheless, the bulk of the protein is expected to be activated during anaphase (Basant & Glotzer, 2018; D'Avino et al., 2015; Green et al., 2012). Before anaphase, an intramolecular interaction between the N- and C-terminus of Ect2 prevents GEF activity. With the onset of anaphase, this autoinhibition is then released by the interaction with RacGAP1 (Basant & Glotzer, 2018; D'Avino et al., 2015; Green et al., 2012). Recent data further suggest an additional inhibitory interaction of the PH domain with the catalytic domain (Chen et al., 2020). Details will be discussed in chapter 1.9.3.2.

Ect2 function is thought to be tightly connected with its localization. During cytokinesis, Ect2 localizes to the midzone and the equatorial membrane in human cells (Chalamalasetty et al., 2006; Liu et al., 2004; Tatsumoto et al., 1999; Zhao & Fang, 2005). Both localizations were suggested to be required for cleavage furrow formation and ingression in human cells (Kotýnková et al., 2016; Su et al., 2011; Wolfe et al., 2009). Interestingly, Ect2 midzone localization is absent in *D. melanogaster* and *C. elegans* (Motegi et al., 2006; Prokopenko et al., 1999). This brought up different views of how and especially where Ect2 is activated (see chapter 1.9.3.3).

Considering the essential role of Ect2 during cytokinesis, its activity must be tightly regulated in space and time to avoid abnormal RhoA activation, which could completely sabotage cytokinesis. This is achieved by autoinhibition (chapter 1.9.3.2) and its localized resolution (chapter 1.9.3.3) in cooperation with the actions of mitotic kinases (chapter 1.9.3.1).

1.9.2 Ect2 structural domains and their function

As a member of the family of Dbl-homology (DH) GEFs, Ect2 has a characteristic catalytic domain that specifically activates Rho GTPases by facilitating the exchange of GDP to GTP (Rossman et al., 2005; Zheng, 2001). Ect2 has been shown to target Cdc42, Rac1, and RhoA *in vitro* (Tatsumoto et al., 1999), but during cytokinesis, the main *in vivo* target is RhoA (D'Avino et al., 2015; Green et al., 2012; Piekny et al., 2005). Mutation of four highly conserved residues in the DH domain (PVQR → AAAA, 565-568) mimicked the loss of Ect2 by RNAi demonstrating the requirement of DH functionality for Ect2 functioning during cytokinesis and transformation (Saito et al., 2004; Su et al., 2011).

Typically, DH domains are paired with a C-terminally located pleckstrin homology (PH) domain and this is also the case in Ect2 (Figure 7). PH domains comprise around 100 amino acids and were first described for the protein Pleckstrin found in platelets (Tyers et al., 1988). From then on, many proteins involved in cell signaling or cytoskeleton function were identified to feature PH domains. Even though they can greatly differ in primary sequence, all PH domains adopt a highly conserved fold (Blomberg & Nilges, 1997). PH domains can interact with phosphoinositides and thereby recruit proteins to the plasma membrane but were also shown to mediate protein-protein interactions (Lemmon, 2007, 2008; Lenoir et al., 2015; Scheffzek & Welte, 2012). In Ect2 the PH domain, together with the PBS, was shown to be required for plasma membrane localization during anaphase (Chalamalasetty et al., 2006; Su et al., 2011). This cooperative targeting mechanism is strongly conserved, except in *C. elegans*, where ECT-2 lacks the PBS (Su et al., 2011). It has also been shown that in human cells the PH domain can interact with the crosslinker anillin, which is thought to tether astral microtubules to the plasma membrane positioning the contractile ring at the cell equator (Frenette et al., 2012). More recently, crystal structure analysis revealed that the PH domain of Ect2 directly interacts with the catalytic DH-GEF domain (Chen et al., 2020). In the same study, disrupting this interaction led to increased GEF activity *in vitro*, which implicates the PH domain in Ect2 negative regulation. The role of the PH domain in Ect2 autoinhibition will be discussed further in chapter 1.9.3. However, the exact functioning of the PH domain in Ect2 remains unclear.

At the N-terminus, Ect2 contains three BRCA1 C-terminal (BRCT) domains: BRCT0, BRCT1, and BRCT2 (Zou et al., 2014). BRCT domains are specialized interaction domains, which can specifically recognize and bind phosphorylated peptides, DNA, and poly(ADP-ribose) (Leung & Glover, 2011). Single units and multiple copy arrays exist, which all share a highly conserved structure, in which variances are predominantly found in the connecting loops. The canonical BRCT topology comprises a 4-stranded β -sheet, which is flanked by two α -helices on the one and one α -helix on the other side (Figure 8).

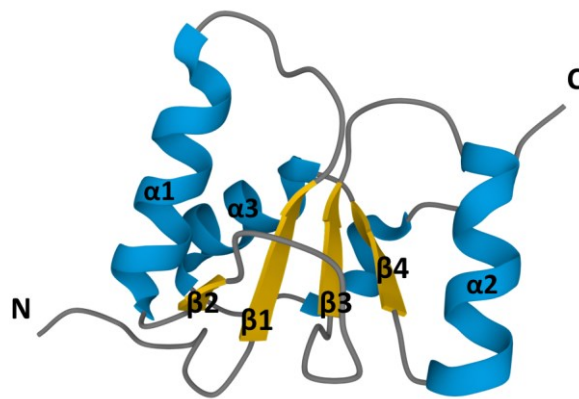


Figure 8: Ribbon representation of the canonical BRCT domain-fold on the example of human XRCC1. The canonical BRCT domain fold comprises a 4-stranded- β -sheet, which is flanked by two α -helices on one side and one α -helix on the other. (structure retrieved and adapted from rcsb.org, Berman et al., 2000; Hammel et al., 2021; Pourfarjam, 2020; Sehnal et al., 2021).

Long time it had been assumed that Ect2 features only two BRCT domains (BRCT1 and BRCT2), which form a so-called tandem BRCT repeat (Kim et al., 2005; Tatsumoto et al., 1999). The typical packing of both BRCTs in this repeat establishes two binding pockets which allow not only the interaction with the phosphopeptide but also provide specificity (Leung & Glover, 2011). The phosphate-binding pocket is formed by the N-terminal BRCT domain (which would be BRCT1 in Ect2) and the specificity pocket is formed by both BRCT domains (Leung & Glover, 2011). The BRCT domains in Ect2, therefore, were thought to function as a unit. By solving the crystal structure of Ect2, Zou et al. (2014) showed that BRCT1 and BRCT2 in Ect2 adopt a perpendicular orientation instead of a parallel conformation, which is characteristically found in canonical tandem-BRCT domains. Moreover, crystallization demonstrated the presence of an additional BRCT domain, which was defined as BRCT0. It is located at the very N-terminal end and is the least conserved of all BRCT domains in Ect2. Both findings contradict the

canonical view of Ect2 having a tandem BRCT repeat and rather indicate that the BRCT domains in Ect2 feature a different mode of operation than initially assumed. So far, the only other protein comprising an array of three BRCT domains identified to date is DNA topoisomerase 2-binding protein 1 (TopBP1). TopBP1 is involved in the maintenance of genome integrity and serves as a scaffold in processes such as DNA replication, DNA repair, and DNA damage checkpoint response (Bagge et al., 2021). Structural analysis of TopBP1 revealed that BRCT1 and BRCT2 each exhibit a phosphopeptide binding site, while BRCT0 lacks a classical interactions site. Additional functional analysis demonstrated that these binding sites function independently, as binding to DNA repair protein Rad9 (Rad9) is compromised by mutations in BRCT1 but not in BRCT2 (Rappas et al., 2011). Although the BRCT domains in Ect2 and TopBP1 in principle share a similar structure and BRCT1 in both proteins establishes protein interactions, the BRCT0 domain in Ect2 is oriented very differently, and the BRCT2 domain lacks an important helix, which normally contributes to phosphopeptide binding (Rappas et al., 2011; Zou et al., 2014). Thus, even though similarities exist, the binding mode of both proteins could be different. Functionally, the BRCT domains in Ect2 are thought to inhibit Ect2 activity as they can bind to the catalytic DH-GEF domain (see below chapter 1.9.3) (Kim et al., 2005; Saito et al., 2004). However, the BRCT domains are also essential for normal Ect2 function during cytokinesis. As so the structural disruption of the BRCT2 domain (Kim et al., 2005) or deletion of all BRCT domains (Matthews et al., 2012) rendered Ect2 incapable of rescuing cytokinetic failure in Ect2-depleted cells. The reason for this is their requirement for Ect2 activation (see chapter 1.9.3).

The BRCT domains and the DH-GEF domain are connected by a linker region, called S-loop, which does not adopt any specific conformation during crystallization and thus probably allows great conformational changes (Chen et al., 2020). It harbors both nuclear localization signal (NLS) sequences of Ect2 and has many putative phosphorylation sites. Phosphorylation of some of the sites was suggested to be important for Ect2 activity and/or influence the binding of interaction partners. Nevertheless, the role of the S-loop remains poorly understood and insights on its function, aside from being a linker and harboring the NLSs, just start to emerge (more see chapter 1.9.3).

1.9.3 Ect2 regulation during mitosis

As Ect2 is the key activator for the RhoA-dependent formation of the contractile ring, its activity is tightly regulated throughout mitosis. Intense research over the last decades has revealed that control strategies on several levels ensure that Ect2 is active at the right time and the right place.

Ect2 protein levels fluctuate throughout the cell cycle (Liot et al., 2011). Ect2 expression gets activated in S-phase and peaks during mitosis (Seguin et al., 2009). At the mitotic exit, when Ect2 activity is no longer needed, the APC/C sends the majority of Ect2 for degradation at the proteasome, while the rest gets reimported into the nucleus (Liot et al., 2011). Thus, coupling Ect2 protein levels to the time where it functions, depicts one way of preventing unwanted Ect2 activity.

1.9.3.1 Regulation by mitotic kinases

Reversible phosphorylation represents one of the major regulatory tools by which protein functions and signaling pathways are controlled within the cell. Throughout mitosis, Ect2 is heavily phosphorylated (Kimura et al., 2000; Matthews et al., 2012; Niiya et al., 2006; Niiya et al., 2005; Tatsumoto et al., 1999; Yüce et al., 2005) and phosphatase treatment of immunoprecipitated Ect2 resulted in reduced GEF activity *in vitro* (Tatsumoto et al., 1999), suggesting that phosphorylation regulates Ect2 activity. The two mitotic kinases Cdk1 and Plk1 were suggested to be responsible for Ect2 phosphorylation during mitosis. Both were shown to target Ect2 *in vitro* and in living cells (Hara et al., 2006; Niiya et al., 2006; Suzuki et al., 2015; Yüce et al., 2005).

Cdk1 is directed to proline and preferentially phosphorylates proline-threonine and proline-serine sites (Malumbres, 2014; Rhind & Russell, 2012; Salaun et al., 2008). It is active from the G2 phase onwards until metaphase, where it regulates the entry into the mitotic phase. Examples of mitotic processes regulated by Cdk1 are nuclear envelope breakdown, chromosome condensation, centrosomes separation, and bipolar spindle assembly. As mentioned earlier the activity of Cdks depends on the interaction with co-activating cyclins. For Cdk1 activity during mitosis, this is cyclin B (Malumbres, 2014; Rhind & Russell, 2012; Salaun et al., 2008).

Plk1 is a highly conserved serine-threonine kinase and its activity peaks in mitosis (Colicino & Hehnly, 2018; Combes et al., 2017; Petronczki et al., 2008; Schmucker & Sumara, 2014). In mammals five paralogues exist, each characterized by a unique function. Via its polo box domain (PBD) Plk1 recognizes preferentially Cdk1-primed consensus sites (Ser-pSer/pThr-Pro/X), allowing direct binding of target proteins (Elia, Cantley, et al., 2003; Elia, Rellos, et al., 2003). Plk1 function is essential as it controls mitotic entry, centrosome separation, and cytokinesis, to name but a few. During cytokinesis, Plk1 localizes to the central spindle and the midbody and from there it regulates contractile ring assembly, as it facilitates RhoA activation, and abscission, as it regulates the assembly of the abscission machinery (Colicino & Hehnly, 2018; Combes et al., 2017; Petronczki et al., 2008; Schmucker & Sumara, 2014).

As aforementioned Ect2 localization is closely associated with its function. Thus, it depicts another way of regulation and was shown to be influenced by Cdk1 and Plk1 activity. Ect2 comprises two nuclear localization signals (NLS), both located in the S-loop (Tatsumoto et al., 1999). Thus, Ect2 localizes to the nucleus in interphase (Chalamalasetty et al., 2006; Matthews et al., 2012; Tatsumoto et al., 1999). It has been suggested that the ability of Ect2 to interact with β -importins, which recognize the NLSs and shuttle Ect2 into the nucleus, is negatively regulated by Cdk1-mediated phosphorylation (Suzuki et al., 2015). The authors reported that wildtype Ect2 interacts with β -importins in interphase, but not in metaphase. Further, they showed that the interaction depends on two sites next to the NLSs (T342 and S345), which are targeted by Cdk1. The phospho-mimetic mutant of these sites prevented the interaction with β -importins in interphase, while the phospho-deficient mutant allowed it in metaphase. This probably helps to prevent the activation of RhoA in the cytoplasm before mitosis. Indeed, it was shown that premature cytoplasmic localization due to mutations in the NLS, leads to increased transforming activity of Ect2 and premature Ect2-dependent cell rounding (Matthews et al., 2012; Saito et al., 2004).

During anaphase, Ect2 gets recruited to the midzone through its interaction with the centralspindlin component RacGAP1 (Nishimura & Yonemura, 2006; Somers & Saint, 2003; Yüce et al., 2005; Zhao & Fang, 2005). The interaction requires the preceding phosphorylation of RacGAP1 by Plk1 (Burkard et al., 2009; Petronczki et al., 2007; Yüce et al., 2005) and the removal of one inhibitory Cdk1 phosphorylation in the S-loop of Ect2 (T342) (Yüce et al., 2005). Ect2 midzone localization can be prevented by depleting RacGAP1 or its binding partner

MKLP1 (both interfere with correct midzone assembly) and Plk1 inhibition, which was reported to result in a homogenous Ect2 localization all around the cell periphery. This is why RacGAP1 binding has been proposed to spatially restrict Ect2 to the cell equator (Su et al., 2011). Moreover, RacGAP1 interaction is thought to release Ect2 autoinhibition, which will be discussed in chapter 1.9.3.3.

Additionally, translocation to the plasma membrane is thought to be a key step of Ect2 functioning during cytokinesis (Su et al., 2011). Ect2 membrane association was shown to be prevented by Cdk1-dependent phosphorylation in its PBS membrane-binding domain (T815) (Su et al., 2011). As Cdk1 activity is high throughout early mitosis and drops with the onset of anaphase due to the degradation of its activator cyclin B and counteracting phosphatases (Holder et al., 2019), Ect2 membrane association is restricted to anaphase.

Aside from the role in regulating Ect2 nuclear localization, Cdk1-mediated phosphorylation of T342 has been suggested to stimulate Ect2 activity (Hara et al., 2006). Phospho-mimetic T341D (= T342D in our Ect2 isoform) enhanced the ability of Ect2 to interact with another N-terminal Ect2 fragment, which led to the idea that the phosphorylation of T341 induces an open conformation of Ect2, which supports its activation. This idea stands in contradiction to the findings of Yüce et al. (2005), who showed that phosphorylation of T342 blocks the interaction between Ect2 and RacGAP1 and thus prevents the release of Ect2 autoinhibition before anaphase (Burkard et al., 2007; Somers & Saint, 2003; Wolfe et al., 2009). Furthermore, overexpression of phosphorylation deficient T341 Ect2 mutants was shown to rescue Ect2 RNAi induced multinucleation as efficient as Ect2 WT overexpression, suggesting that the phosphorylation is not essential for cytokinesis (Hara et al., 2006).

Ect2 can directly interact with Plk1 in a phospho-dependent manner (Niiya et al., 2006). As mentioned above, Plk1 binding often requires a priming phosphorylation by Cdk1 (Elia, Cantley, et al., 2003; Elia, Rellos, et al., 2003). T412 in the S-loop was identified as a Cdk1 target and its phosphorylation is critical for the interaction of Ect2 and Plk1 since phospho-deficient T412A strongly reduced the interaction with Plk1 (Niiya et al., 2006). Furthermore, Ect2T412A reduced the levels of active GTP-RhoA in the cells, and unlike Ect2 WT, its overexpression did not cause hypercontractility in cells (Niiya et al., 2006). This indicates a phosphorylation-dependent role of T412 in Ect2 activity regulation.

1.9.3.2 Ect2 autoinhibition

A common regulatory mode among GEF proteins is the inhibitory interaction of the N-terminus with the catalytically active C-terminus (Rossman et al., 2005; Zheng, 2001). Various studies have demonstrated that such an autoinhibitory regulation also exists in Ect2. Tatsumoto et al. (1999) first described that the expression of an N-terminal Ect2 fragment, containing the BRCT domains, had a dominant-negative effect on cytokinesis and resulted in the formation of multinucleated cells. Later interaction studies showed that the N-terminus can directly associate with the DH-GEF domain (Kim et al., 2005; Saito et al., 2004) and this was recently supported by crystal structure analysis (Chen et al., 2020). Moreover, the BRCT domains could block the transforming activity elicited by unregulated C-terminal Ect2 in living cells (Saito et al., 2004) as well as the GDP to GTP exchange in RhoA *in vitro* (Zou et al., 2014). Two groups further supported the idea of the BRCT domains being involved in the autoinhibition of Ect2 activity, by showing increased *in vitro* GEF activity after either the structural disruption of BRCT2 (Kim et al., 2005) or the deletion of all BRCT domains (Chen et al., 2020). Likewise, artificial membrane targeting of an N-terminal Ect2 truncation led to increased cortical contractility in living cells (Kotýnková et al., 2016). (Figure 9)

During the course of my study, structural data and results from *in vitro* GEF assays were published which suggest that the S-loop and the PH domain are implicated in Ect2 autoinhibition. An Ect2 N-terminal truncation including the S-loop showed elevated GEF-activity and higher binding affinity to RhoA *in vitro* (Chen et al., 2020), which let the authors suggest that the S-loop prevents Ect2 activity by interfering with RhoA binding. In the same study, it was demonstrated that the PH domain directly interacts with the DH-GEF domain and that two specific residues in the PH domain, P703, and C765, are key for this. Mutation of either of these residues increased Ect2 GEF activity *in vitro*, implying that the PH domain not only regulates Ect2 localization but also takes part in the negative regulation of its activity. That the PH domain regulates the activity of the adjacent DH domain is commonly found in DH-GEFs (Zheng, 2001), but has so far never been proposed to regulate GEF activity in Ect2. One reason for this could be that many studies removed the entire PH domain and as PH is also required for Ect2 membrane localization this probably masks its role in Ect2 negative regulation. (Figure 9)

1.9.3.3 Release of Ect2 autoinhibition

As aforementioned, Ect2 interacts with midzone-based RacGAP1 during anaphase, and several studies suggested that this interaction is required for cleavage furrow positioning and ingression (Burkard et al., 2009; Burkard et al., 2007; Petronczki et al., 2007; Su et al., 2011; Wolfe et al., 2009; Yüce et al., 2005). Based on these studies the canonical model of Ect2 activation during anaphase was postulated, which assumes that the binding to RacGAP1 releases the autoinhibitory interaction in Ect2. As these studies were all conducted in human cells and the Ect2 orthologues do not localize to the midzone (Motegei et al., 2006; Prokopenko et al., 1999), it was seen critical whether RacGAP1 has a similar function in *C. elegans* and *D. melanogaster*. Mutating two residues (T153A and K195M) in the BRCT1 domain abrogated efficient midzone recruitment (Kotýnková et al., 2016; Wolfe et al., 2009) and RacGAP1 interaction *in vitro* (Wolfe et al., 2009; Zou et al., 2014). T153 and K195 were chosen because they are analogous to the residues responsible for phosphopeptide binding in two other BRCT domain-containing proteins (Wolfe et al., 2009). Altogether these observations led to the view that the mentioned residues are essential for Ect2 to interact with RacGAP1 and to become active. Findings by Kotýnková et al. (2016), showing that mutating these residues allows normal cytokinesis, questioned the relevance of the canonical model and especially the role of RacGAP1 in Ect2 activation. This reopened the question of how Ect2 gets activated at the onset of anaphase. During the course of this study, the identification of another surface patch in the BRCT1 domain, required for RacGAP1 binding and successful cytokinesis (Gomez-Cavazos et al., 2020), has restored the essential role of RacGAP1 binding in Ect2 activation. This study furthermore shows that this is also true in *C. elegans*. Moreover, they demonstrate that in principle ECT-2 and Cyk4 (worm orthologue of RacGAP1) can interact at the midzone in *C. elegans*. However, autoinhibition seems to be stronger than in humans, which prevents this interaction *in vivo*. Additionally, RacGAP1 was suggested to contribute to Ect2 activation in another way. The C-termini of Ect2 and RacGAP1 interact *in vitro* and this was proposed to fully release Ect2 inhibition and promote RhoA activation (Zhang & Glotzer, 2015). (Figure 9)

Based on *in vitro* GEF activity measurements, the PH-mediated inhibition has been proposed as the predominant one of both autoinhibitory interactions found in Ect2 (Chen et al., 2020). The authors further suggested an autocatalytic activation mechanism in which GTP-RhoA binding to the PH domain triggers its unbinding from the DH-GEF domain. Subsequently, the

unrestrained DH-GEF would bind to GDP-RhoA and catalyze its nucleotide exchange. Thus, RhoA would trigger its own activation. (Figure 9)

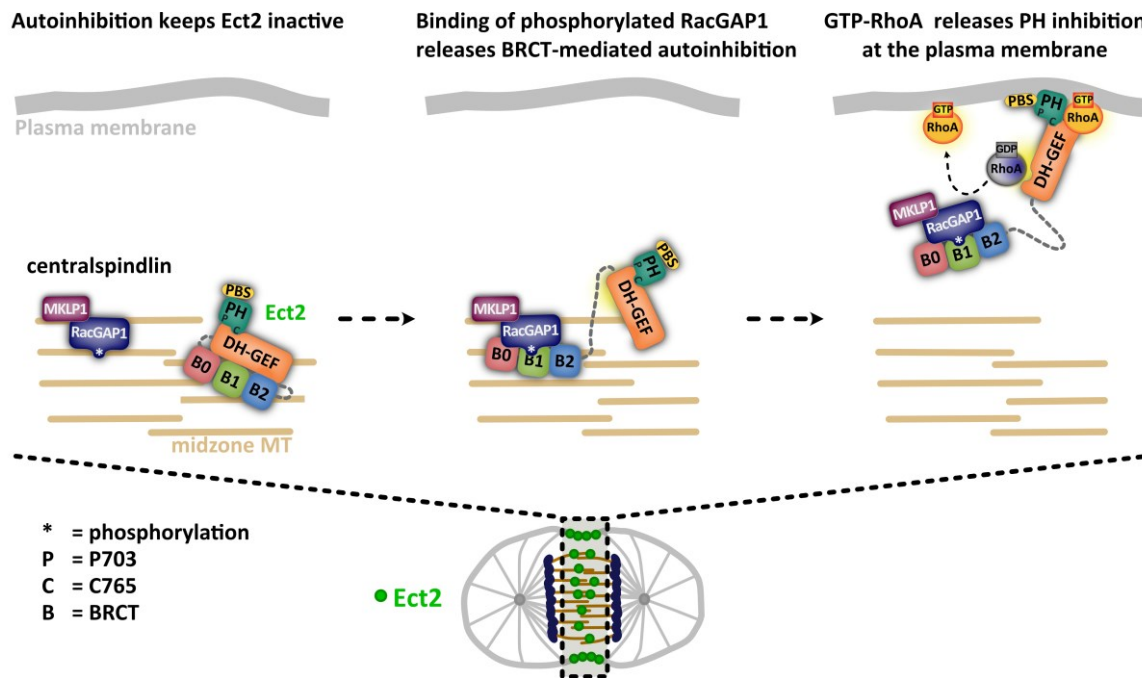


Figure 9: Model of Ect2 activation during cytokinesis in animal cells. Ect2 activity is prevented in metaphase by an autoinhibitory interaction of its N-terminal BRCT domains with the catalytic DH-GEF domain (Kim et al., 2005; Saito et al., 2003; Tatsumoto et al., 1999). Additionally, the PH domain restrains Ect2 activity by binding to the catalytic center (Chen et al., 2020). Upon anaphase onset midzone-based RacGAP1 is phosphorylated by Plk1 and can interact with the BRCT1 domain of Ect2, which releases the BRCT-dependent inhibition (Burkard et al., 2009; Burkard et al., 2007; Gomez-Cavazos et al., 2020; Petronczki et al., 2007; Su et al., 2011; Wolfe et al., 2009; Yüce et al., 2005). Ect2 then translocates to the plasma membrane where it gets fully active due to the binding GTP-RhoA, which releases PH-mediated inhibition (Chen et al., 2020).

1.9.4 Understanding Ect2 regulation during cytokinesis benefits the understanding of Ect2 during tumorigenesis

Ect2 is an oncogene in many cancer types including brain, lung, and pancreatic tumors. Although, cancer cells often show aberrant localization and upregulated expression of Ect2, its role in tumorigenesis was suggested to be distinct from its physiological role during cytokinesis and rather be a consequence of *ECT2* gene amplifications (Fields & Justilien, 2010). However specific point mutations in the Ect2 sequence are also found in various cancers (Chen et al., 2020). Recently, a few of those point mutations, lying in the DH-PH domain, have been analyzed concerning their effect on Ect2 functionality during cytokinesis (Chen et al., 2020).

Not surprisingly, two mutations located at the catalytic center abrogated Ect2 function and led to binucleated cells. As mentioned at the beginning of this introduction, polyploid cells are often genomically unstable and implicated in tumor formation (Lacroix & Maddox, 2012; Lens & Medema, 2019; Lim & Ganem, 2014). Two other mutations affected the interaction between the DH GEF domain with the BRCT and the PH domain, respectively. Both led to increased *in vitro* GEF activity and the PH mutation led to a slight increase in multinucleation, yet, for the most part, supported successful cytokinesis. Ensuing experiments revealed that it leads to faster proliferation *in vitro*, transformation, and bigger tumors when compared to Ect2 WT. Transforming activity had already been described before after the removal of the S-loop (Saito et al., 2004) and the phosphorylation of T328 in the S-loop (Justilien et al., 2011). Moreover, it has been recently demonstrated that the transcription factor forkhead box protein M1 (FoxM1) suppresses chromosomal instability and thus tumor development by preventing Ect2-dependent F-actin polymerization in a non-transcriptional manner (Limzerwala et al., 2020). The authors could show, that FoxM1 directly interacts with BRCT1+BRCT2 and the very C-terminal part of Ect2 and thereby prevents its activity. Collectively, this demonstrates that understanding Ect2 function and regulation during cytokinesis also benefits the understanding of Ect2 function during tumorigenesis. This especially applies to the functioning of individual structural domains.

1.10 Aim of my thesis

Cytokinesis, the final step in cell division, ensures that the duplicated genome is physically distributed between two daughter cells, thereby maintaining correct ploidy. The key step of cytokinesis is the activation of the small GTPase RhoA in a narrow equatorial zone at the membrane in anaphase, which subsequently promotes the assembly and constriction of a contractile ring in the center of the cell. Given its importance for genomic integrity, this process must be tightly regulated. Ect2, as the activator of RhoA, holds a central position in the regulation of cytokinesis. Despite years of research, Ect2 functioning and regulation are still incompletely understood. It is widely accepted that the N-terminal BRCT domains are the main regulatory domains, which not only inhibit GEF activity but also facilitate the activation of Ect2 by binding to RacGAP1. However, many of the studies were based on the assumption that Ect2 features a canonical tandem BRCT domain, in which both BRCT domains together

facilitate the binding of interaction partners. The fact that Ect2 has three BRCT domains, which are also very differently oriented towards each other (Zou et al., 2014), suggests a different way how interactions are established and opens up the possibility that each BRCT domain functions differently during cytokinesis. While BRCT1 is associated with the activatory interaction with RacGAP1, the roles of BRCT0 and BRCT2 remain elusive. Thus, the first aim of my thesis was to scrutinize how the single BRCT domains contribute to Ect2 activation and to the spatial and temporal regulation of Ect2 activity, which has so far never been addressed in detail. Moreover, recent data from Chen et al. (2020) have proposed that, different than previously assumed, Ect2 autoinhibition is not solely established by the BRCT domains, but that the membrane-binding domain PH and the connective S-loop also participate. The phosphorylation of the S-loop has been proposed earlier to regulate Ect2 activity (Hara et al., 2006). Since the roles of the PH and the S-loop are poorly understood and most of the data were obtained *in vitro*, the second aim was to analyze whether the PH domain and the phosphorylation status of the S-loop regulate Ect2 activity in living cells. Understanding Ect2 regulation is not only crucial for the field of cytokinesis, but also for medical research, as defects have been shown to be involved in tumorigenesis.

Toward these goals, the strategy was either to delete entire domains or to insert specific domain mutations in Ect2 and to analyze the resulting consequences on its function and regulation. Here, the focus lay on the spatial and temporal aspects, which is why live-cell imaging was chosen as the major technique. Conclusions based on the analysis of living cells, furthermore, more likely reflect the physiological situation than conclusions based on *in vitro* analyses. Nevertheless, some *in vitro* experiments were employed to elucidate how the binding of interaction partners is achieved and whether certain domains are phosphorylated. Moreover, the use of a genetic replacement system for Ect2 in HeLa cells established earlier in the laboratory, allowed the analysis of Ect2 mutant proteins at WT levels and in the absence of endogenous Ect2. This represents a major advantage over earlier studies, which often transiently overexpressed Ect2 variants and/or had endogenous Ect2 in the background, which may lead to unwanted side effects.

2 Materials and methods

2.1 Plasmid generation for stable cell lines and protein purification

For the generation of plasmids used to establish stable NG-Ect2 mutant cell lines (see 2.5.3), Ect2 fragments were amplified from pEZ197 (Ect2^{WT}) and pExA128 (for Ect2^{S-loopSTDE}), respectively, and inserted into the pcDNA5/FRT/TO expression vector via Gibson assembly (see 2.1.3). pEZ197 was previously generated by Dr. Kristina Buchner (Buchner, 2019). Ect2 point mutations were inserted by amplifying pEZ197 with primers comprising the respective mutation(s) (site-directed mutagenesis see 2.1.2, Table 14).

To be able to overexpress (in bacteria) and purify different Ect2 proteins and RacGAP1 (1-288aa) (see 2.2) for *in vitro* pull-down and kinase assays (see 2.3 and 2.4), several expression plasmids were generated by Nils Bertram and Prof. Dr. Esther Zanin. For this, respective Ect2 fragments were amplified by PCR (see 2.1.1) from pEZ197 with primers containing Xho I restriction sites. This allowed their insertion into the pMBP/6xHis expression vector following Xho I digestion (see 2.1.4). For RacGAP1 (1-288aa) the respective fragment was amplified from pEZ75 and inserted into pGEX-4T via Gibson assembly (see 2.1.3, done by Prof. Dr. Esther Zanin).

2.1.1 DNA-amplification by Polymerase Chain Reaction (PCR)

DNA sequences used for the generation of plasmids were amplified by PCR. Table 1 shows the composition of each PCR reaction and Table 2 shows the used cycling parameters. All reactions were done with Phusion polymerase and the primers used can be found in Table 14. Subsequently, PCR products were separated on a 0.8 % agarose gel at 120 V for about 1 h. For visualization, UVView was used (1 µl UVView/6 µl sample (3 µl PCR product + 3 µl ddH₂O)). After digesting the template DNA with DpnI restriction enzyme (1 µl DpnI/50 µl PCR) for 1 h at 37 °C, the PCR samples were purified using the NucleoSpin Gel and PCR Clean-up kit according to the manufacturer's instructions. DNA was eluted in 20 µl ddH₂O or elution buffer.

Table 1: Reaction setup for standard PCR

	Volume (50 μ l reaction)
5x HF buffer	10 μ l
DNA template (1:100 diluted)	1 μ l
dNTPs (10 mM)	1 μ l
Phusion Polymerase	0.5 μ l
Forward Primer (100 pmol/ μ l)	0.25 μ l
Reverse Primer (100 pmol/ μ l)	0.25 μ l
H ₂ O	37 μ l

Table 2: Thermocycling conditions for standard PCR

	Temperature	Duration	
Initial denaturation	98 °C	30 s	
Denaturation	98	10 s	29x repeats
Annealing	According to primer	30 s	
Elongation	72 °C	30 s for 1 kb	
Final elongation	72 °C	3 min	
Cooldown	12 °C	10 min	

2.1.2 Site-directed mutagenesis

To change single nucleotides, primers harboring the respective point mutation(s) were designed. The DNA was then amplified with these primers with the following reaction setup and temperature cycling conditions (Table 3, Table 4). Subsequently, template DNA was digested by DpnI and samples purified with the NucleoSpin Gel and PCR Clean-up kit.

Table 3: Reaction setup for site-directed mutagenesis

	Volume (50 μ l reaction)
5x HF buffer	10 μ l
DNA template (~20 ng/ μ l)	1 μ l
dNTPs (10 mM, 1:5 diluted)	6.25 μ l

Phusion Polymerase	1 μ l
Forward Primer (100 pmol/ μ l, 1:10 diluted)	1.25 μ l
Reverse Primer (100 pmol/ μ l, 1:10 diluted)	1.25 μ l
H ₂ O	29.25 μ l

Table 4: Thermocycling conditions for site-directed mutagenesis

	Temperature	Duration	
Initial denaturation	98 °C	30 s	
Denaturation	98	10 s	16x repeats
Annealing	55 °	1 min	
Elongation	72 °C	30 s for 1 kb	
Final elongation	72 °C	10 min	
Cooldown	12 °C	10 min	

2.1.3 Gibson assembly

Appropriate amounts of the received PCR products (equal molarities for all fragments up to 0.5 pmol total in 7.5 μ l) were mixed with 2x Gibson Assembly master-mix (7.5 μ l) according to the manufacturer's instructions and incubated at 50 °C for 1 h.

2.1.4 XhoI restriction digest and ligation

For the generation of expression plasmids to overexpress different MBP-tagged Ect2 proteins in bacteria (see 2.2), the pMBP/6xHis vector and the Ect2 PCR products, containing the Xho I restriction site, were digested with Xho I (see Table 5) for 1 h at 37 °C. To prevent re-ligation, the vector was dephosphorylated by rSAP treatment for 1 h at 37 °C. After heat inactivation for 20 min at 65 °C, the cut vector and the Ect2 fragments were cleaned using the NucleoSpin Gel and PCR Clean-up kit. For the ligation by default an insert:vector ratio of 1:3 was used. When problems occurred, different ratios were tested. The ligation reaction was carried out in 20 μ l (Table 6) at RT for at least 2 h or at 16 °C over night (o/n). Subsequently, the samples were heated up to 65 °C for 20 min to inactivate the enzyme.

Table 5: Reaction setup Xho I restriction digest

	Volume (50 µl reaction)
DNA	1 µg
Cut Smart (10 x)	5 µl
Xho I	1 µl
H ₂ O	39 µl

Table 6: Reaction setup for DNA ligation

	Volume (20 µl reaction)
Vector DNA	~50 ng
Insert DNA	Depending on insert and insert:vector ratio
T4 DNA Ligase Buffer (10 X)	2 µl
T4 Ligase	1 µl
H ₂ O	X µl

2.1.5 Plasmid transformation of chemically competent *E. coli* DH5α and BL21

DH5α/BL21 (50 µl) cells were thawed on ice, 5 µl Gibson assembly mix/ligation mix were added and everything was incubated on ice for 20 min. Following a 45 s heat-shock at 42 °C, cells rested for 2 min on ice and recovered in 1 ml LB medium at 37 °C for 1 h. To select positive clones, cells were plated on LB plates containing the appropriate antibiotic and grown at 37 °C o/n.

2.1.6 Isolation and sequencing of bacterial plasmid DNA

Bacterial colonies were picked from selection LB-plates and grown in 4 ml LB medium, supplemented with the adequate antibiotic, at 37 °C o/n. The next day, bacterial cells were harvested at 6000 rpm for 5 min. The plasmid DNA was extracted either with the NucleoSpin Plasmid DNA Mini kit or the Qiagen plasmid mini kit (for the generation of stable cell lines) according to the manufacturer's instructions. The resulting pellet was dissolved in 20-30 µl TE buffer or filtered ddH₂O and stored at -20 °C.

The purified DNA was checked for sequence correctness by DNA sequencing, which was performed at the internal Genomics Service Unit of the Faculty of Biology at the LMU according to their instructions.

2.2 Protein expression and purification

To overexpress MBP- and GST-tagged proteins, plasmids shown in Table 16 were transformed into competent *E. coli* BL21 and glycerol stocks were frozen at -20 °C. One day before protein expression was started, 20 ml LB + Carbenicillin (carb, 100 µg/ml) were inoculated with the respective glycerol stock and incubated at 37 °C and 200 rpm o/n. The next morning 1 l LB carb (for MBP-constructs LB + 0.02 % glucose + carb) was inoculated with 10 ml of the overnight culture ($OD_{600} \sim 0.05$). When the bacteria had grown to an OD_{600} of 0.4-0.8 at 37 °C, protein expression was induced with IPTG (1 M stock). All steps after harvesting were performed at 4 °C.

2.2.1 GST-tagged proteins

Protein expression was induced with 1 mM IPTG for 3 h at 37 °C for pGEX-4T (GST) and pGEX-6P-1 PBD (GST-PBD) and with 0.1 mM IPTG for 5 h at 25 °C for pGST-RACGAP1 (GST-RacGAP1). Bacteria were harvested at 6000 rpm for 15 min and subsequently the pellet was washed once with cold 1 xPBS (50 ml) and snap-frozen in liquid N₂. Per protein 100 µl GST-Sepharose beads were washed three times with 1 ml lysis buffer (10 mM Tris pH 8, 150 mM NaCl, 1 mM EDTA, 0.05 % NP-40) and pelleted at 500 g for 5 min. The bacteria pellet was thawed on ice and resuspended in 7.5 ml lysis buffer supplemented with 5 mM DTT and 1 mM PMSF and cComplete protease inhibitor cocktail. After 15 min on ice cells were sonicated for 3 min (amplitude 50 %, 10 s ON 10 s OFF). After centrifugation (15 min, 10000 rpm), the supernatant and the equilibrated beads were incubated for 1.5 h on a rotating wheel. Beads were washed 3 x for 5 min with lysis buffer and resuspended in 200 µl lysis buffer and stored at 4 °C for up to one week. Protein concentrations were determined by SDS-PAGE. 1 µg and 2 µg of BSA were run in parallel with the samples and served as mass reference.

2.2.2 MPB-tagged proteins

For pMBP/6xHis and all pMBP/6xHis-Ect2 fragments protein expression was induced with 0.3 mM IPTG for 3 h at 25 °C. Bacteria were pelleted at 6000 rpm, washed once with cold 1 xPBS, resuspended in 20 ml MBP- buffer (20 mM Tris pH 7.4, 200 mM NaCl, 1 mM EDTA) and snap-frozen in liquid N₂ and stored at -80 °C. Bacteria suspensions were thawed on ice and

supplemented with 5 mM DTT, 1 mM PMSF, and cOmplete protease inhibitor cocktail. After sonication (3 min, amplitude 50 %, 10 s ON, 10 s OFF), 1 % Triton X-100 was added to the lysates and everything was rotated for 20 min. Cell debris was pelleted (20 min, 10000 rpm) and the supernatants (5 ml each) were added to amylose resin columns. After 15 min of incubation, columns were washed with 5 ml washing buffer (20 mM Tris pH 7.4, 800 mM NaCl, 1mM EDTA). Proteins were eluted in elution buffer (20 mM Tris pH 7.4, 200 mM NaCl, 1 mM EDTA, 20 mM Maltose) and collected in 1 ml aliquots, which were snap-frozen in liquid N₂ and stored at -80 °C. Protein concentrations were determined by SDS-PAGE. 1 µg and 2 µg of BSA were run in parallel with the samples and served as mass reference.

2.3 *In vitro* pull-down assays with GST-RacGAP1 and GST-PBD

To study the interaction of N-terminal Ect2 mutant proteins with RacGAP1 and the PBD domain of Plk1, purified GST-RACGAP1 or GST-PBD beads and eluted MBP/6xHis-Ect2 fragments were mixed (done by Prof. Dr. Esther Zanin). The reaction volume was 300 µl binding buffer (20 mM HEPES pH 7.2, 150 mM NaCl, 5 mM MgCl₂, 0.1 % Triton X-100, 1 mM DTT), which contained a final concentration of ~2 mM for each protein. After samples were rotated for 1 h at 4 °C, beads were washed three times for 5 min in binding buffer. Samples were resuspended in 2 x sample buffer and heated up to 95 °C for 5 min. Proteins were separated by SDS-PAGE and stained with Coomassie blue. MBP/6xHis-Ect2 proteins exhibiting a similar molecular weight as GST-RacGAP1 or GST-PBD were detected with an anti-6xHis antibody on immunoblots.

2.4 *In vitro* Kinase-assays

In vitro Plk1 kinase assays were performed in a total volume of 20 µl for 30 min at 30 °C. To assay kinase activity, 300 ng purified MBP/6xHis-Ect2 protein were incubated with 200 ng of recombinant Plk1 kinase in the presence of 1 µCi of [gamma-P³²] ATP and 0.2 mM rATP in kinase buffer (25 mM HEPES pH 7.5, 50 mM NaCl, 10 mM MgCl₂, 0.1 % Triton X-100 and 1 mM DTT). Kinase reactions were stopped by the addition of 2x sample buffer and heating for 5 min at 95 °C. Subsequently, samples were separated by 10 % SDS-PAGE, stained with Coomassie blue, and dried prior to autoradiography. An erased storage phosphor screen was exposed to

the dried gel o/n in an exposure cassette and scanned on the next day using a Typhoon Trio Imager (GE Healthcare). MBP-Ect2 BRCT0-S-loop served as positive control.

2.5 Cell culture techniques

2.5.1 Cell culture maintenance and freezing of HeLa cell lines

All HeLa cell lines (Table 8) were grown in T25 and T75 flasks, respectively, at 37 °C and 5 % ambient CO₂ in Dulbecco's modified eagle medium (DMEM), which was supplemented with 10 % fetal bovine serum (FBS) and 1 % Penicillin/Streptomycin (P/S). At the time of seeding, transgene expression was induced by adding the appropriate amount of tetracycline (Table 8). For freezing, HeLa cells were grown in two T75 flasks to about 90 % confluency. Cells were collected by trypsinization, resuspended in fresh medium, and pelleted at 1000 rpm for 5 min. Subsequently, the cell pellet was resuspended in 10 ml 1x freezing medium and distributed to 10 cryotubes (1 ml each). Aliquots were frozen at -80 °C and in liquid nitrogen tanks, respectively.

2.5.2 siRNA transfection and drug treatment

To deplete endogenous proteins RNA interference (RNAi) was used. For this, HeLa cells were transfected with a final concentration of 30 nM siRNA using LipofectamineTM RNAiMAX. For one well of a 12-well plate, 3 µl of transfection reagent and 1.5 µl siRNA (20µM) were mixed with 200 µl reduced-serum Opti-Mem I and incubated for 15 min at RT. The medium in the well was exchanged by 800 µl fresh medium and the transfection mixture was added (1 ml/well final). For 6-well plates, the volumes were doubled (2 ml/well final). In the experiments where MCAK and Ect2 were depleted, MCAK/control RNAi was performed 3 h prior to Ect2 RNAi. The Ect2 RNAi mixture was later directly added to the medium already containing the MCAK siRNA. In all experiments, controls were treated equivalently with 30 nM of non-targeting siRNA.

To get a homogenous cell population, in all experiments the cell cycle was synchronized with a single thymidine block. Around 21 h after the transfection, cells were treated with 0.5 mM thymidine for 24 h. Cells were released from the thymidine block by three consecutive 5 min

washing steps with fresh medium (1 ml/well for 12-well plate, 2 ml/well for 6-well plate, 800 μ l/well for 4-well chamber, and 300 μ l/well for 8-well chamber).

To prevent bleb formation, RhoA kinase activity was inhibited at least 1 h prior to the start of live-cell imaging by the addition of 10 μ M Y27632 (10 mM stock in DMSO). Controls were treated with the appropriate amounts of DMSO.

To prevent Plk1 activity specifically during anaphase, 100 nM of the Plk1 inhibitor BI2536 (100 mM stock in DMSO) was added to synchronized cells in metaphase directly before filming. Cells that went into anaphase around 15 min after BI2536 addition were analyzed. Cells that were exposed to BI2536 longer than \sim 25 min were arrested in metaphase. Controls were treated with an appropriate amount of DMSO.

To show that bleb formation is dependent on RhoA, RhoA activity was inhibited in cells by incubating them with pure DMEM containing 0.5 μ g/ml C3 transferase (100 μ M stock in water) for 6 h. Control cells were incubated in pure DMEM.

2.5.3 Generation of stable cell lines and induction of transgene expression

For the generation of isogenic Ect2 mutant cell lines, the Flp-In T-REx system was used (see Figure 10). This system allows the Flp/FRT-mediated stable integration of a gene of interest. To trigger the integration into the genome, vectors carrying the Flp recombinase (pOG44 vector) and the gene of interest (pcDNA5/FRT/TO vector), have to be co-transfected into the HeLa host cell line (Flp-In T-REx). Flp-In T-REx cells were seeded into 6-well plates one day before transfection. Per well 300 ng pcDNA5 and 900 ng pOG44 were co-transfected with XtremeGene9 according to the manufacturer's protocol. As the pcDNA5/FRT/TO vector also provides a hygromycin resistance gene, after five days positively transfected cells could be selected over a period of two weeks by adding 0.2 mg/ml hygromycin to the medium. Then, cells that had survived were pooled and could be used for experiments.

2.5.4 Preparation of cell lysates, western blotting, and blot quantification

To examine the expression levels of endogenous and exogenous Ect2, cell lysates were prepared for each cell line. For this, cells were seeded in 6-well plates in DMEM-FBS-tet and transfected the next day with a final siRNA concentration of 30 nM. The day after, the cells were synchronized with thymidine (0.5 mM) and released from the block 24 h later by washing 3 x for 5 min with DMEM-FBS-tet. After 8-9 h, cells were once washed with 1x PBS and harvested in anaphase by adding adequate amounts of 1x sample buffer (Table 17). Subsequently, samples were heated up to 95 °C for 5 min and sonicated in a water bath sonicator for 20 min. Cell lysates were stored at -20°C.

Equal amounts of cell lysates were loaded on a 10 % SDS-gel and run in 1 x running buffer (stacking gel 80 V, resolving gel 120 V). The proteins were transferred onto an Immobilon-P PVDF membrane for 2 h at 4 °C by wet-blotting in transfer buffer containing 20 % ethanol with constant 300 mA. Subsequently, the membrane was blocked in 5 % milk in TBS-T for 1 h at RT. The incubation with the respective primary antibody (Table 7) in 5 % milk in TBS-T followed. Ect2 antibody was incubated o/n at 4 °C and α -tubulin antibody was incubated 1 h at RT. After washing three times for 5 min with TBS-T the membrane was incubated with the secondary antibody (HRP anti-mouse, Table 7) in 5 % milk in TBS-T for 1 h at RT. After the membrane was washed three times with TBS-T and once with TBS for 5 min, the protein signals were detected with the ChemiDoc XRS+ system (Bio-Rad). SuperSignal™ West Femto and ECL™ Prime Western Blotting/ECL™ Western Blotting Reagents were used as substrates for Ect2 and α -tubulin, respectively.

Protein levels were quantified using the Image Lab software. Expression levels of endogenous Ect2, transgenic Ect2, and tubulin were determined by measuring the intensities of their respective bands. Then endogenous and transgenic Ect2 levels were normalized to α -tubulin and subsequently, the amount of transgenic Ect2 proteins was calculated relative to endogenous Ect2.

2.6 Immunofluorescence microscopy

For multinucleation assays, HeLa cells were seeded onto poly-L-lysine-coated 18 mm glass coverslips in DMEM-FBS-tet at a confluency of around 30 % one day before transfection. For coating, coverslips were incubated in 1 M HCl at 50-60 °C for 5 h and subsequently washed thoroughly with distilled H₂O in five consecutive washing steps. After rinsing them with 100 % EtOH, evenly spread coverslips were dried between Whatman papers. The clean coverslips were then incubated in 15 ml poly-L-lysine solution (1 mg/ml) in a 50 ml tube for 1 h on a rotating wheel. After that, coverslips were intensively washed five times with distilled H₂O and once with 100 % EtOH and dried between Whatman paper under a sterile hood. Before seeding, individual coverslips were again rinsed once with 70 % EtOH and once 100 % EtOH and dried under the sterile hood. One day after releasing them from the thymidine block interphase cells were washed once with ice-cold 1x PBS and subsequently fixed with ice-cold methanol for 5 min. After washing with 1x PBS the fixed cells were incubated in 0.1 % Triton X-100 in 1x PBS (PBS-T) for 2 min and blocked in 4 % BSA-PBS-T for 1 h at RT or o/n at 4 °C. The appropriate primary antibodies were diluted in 4 % BSA-PBS-T according to Table 7 and coverslips incubated for 1-2 h at RT. After washing 3 x for 5 min with PBS-T, the coverslips were incubated with suitable secondary antibodies and Hoechst (dilution in 4 % BSA-PBS-T see Table 7) for 1 h at RT. Prior to mounting coverslips were washed 3 x with PBS-T and 1 x PBS for 5 min. Coverslips were mounted in mounting medium on glass slides, sealed with nail polish, and stored at -20 °C. Immunofluorescence microscopy was performed on a Leica TCS SP5 microscope and a Nikon eclipse Ti spinning disk confocal microscope (details see Table 18). For assessing multinucleation, 5-7 optical sections (63 x, á 1 µm apart) were acquired along the z-axis.

2.7 Life-cell imaging

To analyze Ect2 domain function in living cells, cells were seeded in 12-well plates in DMEM-FBS-tet at a confluency of around 30 %. One day after the transfection, cells were split into ibidiTreat 2-/4-/8-well imaging chambers together with 0.5 mM thymidine. The day after the thymidine block was released and 8-9 h later cells were imaged in ibidiTreat 2-/4-/8-well imaging chambers without ambient CO₂ at 37 °C in a heated chamber. Therefore, the medium

was exchanged with a CO₂-independent medium supplemented with 10 % FBS, 0.1 Pen-Strep, 2 nM L-glutamine and tetracycline before imaging. To visualize the DNA during imaging, SiR-DNA stock solution was diluted at 1:10000 in imaging medium and added to the cells 1 h before filming. Imaging was performed at a Nikon eclipse Ti spinning disk confocal microscope. To analyze furrow formation, blebbing, and Ect2 localization cells were imaged every 3 min for 5 h (Plk1 experiments were stopped after around 2 h). Three-channel images (DIC, 488 nm, 638 nm) were acquired at 60x magnification on 5 planes, which were each 4 μm apart. For bleb characterization, 60x -DIC images were taken on 15 planes (1.2 μm apart) every 30 s for 1.5 h.

2.8 Image analysis and quantifications

To study whether specific domains are required for different aspects of Ect2 function during cytokinesis, live-cell time-lapse images and images of fixed samples were used. All images were analyzed and processed in ImageJ. Graphs were plotted in Prism and graphics were created with Affinity Designer (Table 9):

2.8.1 Live-cell imaging

2.8.1.1 Analysis of bleb formation and characterization of blebs

To assess whether Ect2 activity is elevated in our Ect2 mutant cell lines, the number of blebs that emerged from each cell in meta- and anaphase was counted manually on time-lapse images. Cells were categorized into the following groups: 0 blebs, 1-2 blebs, 3-5 blebs, and ≥ 5 blebs. Graphs depict the mean of experiments. Standard deviation was determined for the percentage of all blebbing cells (0 %-100% blebs).

To differentiate large blebs from small blebs, the length of blebs was measured at the time of its maximal extension and the width was measured in the middle of the blebs (~ at half of the maximal length). The lifetime of blebs was defined as the time between its first emergence and its full reabsorption. Graphs each show the mean of all analyzed cells.

2.8.1.2 Analysis of NG-Ect2 localization

Endogenous Ect2 is absent from the metaphase membrane but at the onset of anaphase, it localizes to the equatorial membrane and the midzone. To check whether our Ect2 mutants show aberrant localization during meta- and anaphase, we analyzed their NG-fluorescence signals in different regions in confocal time-lapse images.

Ect2 membrane localization during metaphase

To assess the localization to the metaphase membrane NG-fluorescence intensity was measured along two 10-pixel wide lines, which were drawn horizontally and vertically over the metaphase plate (see Figure 54 A). An exemplary intensity plot is shown in Figure 54 B. Both membrane peaks of a linescan were aligned and averaged, resulting in an intensity value for the future polar region (horizontal linescan) and an intensity value for the future equatorial region (vertical linescan). The mean background intensity outside the cell was measured in a box (10-30 μm^2) and subtracted from both values. The cytoplasmic level was calculated as the average of the fifth to the eighth value following the peak from both linescans (8 values in total). Then, both peak values were divided by the cytoplasmic value to identify enrichments exceeding the cytoplasmic level. Each analysis was done on the last metaphase frame (0 min). Graphs depict the mean of all analyzed cells.

Ect2 localization to the equatorial membrane and the midzone during anaphase

In anaphase, Ect2 localization was analyzed for the polar and equatorial membrane and the midzone. Calculations were done 6 min and 9 min after anaphase onset (second and third anaphase frame, respectively). The average background intensity was measured in a box outside the cell at the respective time. The cytoplasmic value was calculated as the average of the fifth to the eighth value following the polar peak (4 values). All graphs display the mean of all analyzed cells.

To examine polar membrane localization, NG-fluorescence intensity was measured along two 10-pixel wide lines, which were drawn from the inside out across both polar membranes (see Figure 34 A top). An exemplary intensity plot is shown in Figure 34 B and C. Both membrane peaks were aligned and averaged. After background subtraction, polar values were divided by the cytoplasmic value.

To measure the localization to the equatorial membrane as well as to the midzone a 10-pixel wide line was drawn vertically across the cell equator and fluorescence intensity was measured (see Figure 34 A bottom). After background subtraction, the signals of both membrane peaks were averaged and normalized to the cytoplasmic background. To exclude signals arising from the membrane, the midzone intensity was determined 6 pixels away from the membrane by averaging the 10 highest values. Lastly, the midzone value was divided by the cytoplasmic value.

2.8.1.3 Analysis of cleavage furrow ingression

To quantitatively compare the ability of the different Ect2 mutant cell lines to ingress the cleavage furrow, the equatorial cell width of each cell was measured 12 min after anaphase onset (third anaphase frame) on live-cell time-lapse images. Graphs depict the mean of experiments.

2.8.2 Counting nuclei for multinucleation assay in fixed samples

To determine whether cells expressing transgenic Ect2 mutants can successfully divide, confocal images of fixed and stained interphase cells (see Figure 13) were analyzed. The number of nuclei per cell was determined and cells were classified as mono-, bi and multinucleated. Graphs depict the mean of experiments.

2.9 Statistical analysis

All statistical analyses were done in R (R Core Team, 2021). Normal distribution of data was checked by the Shapiro-Wilk test and equality of variances by Levene test. Based on normality and variance analysis, the statistical significance of differences between two samples was determined by student's t-test or Kruskal-Wallis Rank sum test. To compare data from more than two samples, generalized linear models (GLM) were fitted, followed by an analysis of variance (ANOVA). P-values were obtained by multiple comparison tests after Tukey according to the method by Westfall (Bretz et al., 2011). Friederike Wolff developed the R code used to compare multiple samples. The test used for a specific data set is indicated in the corresponding figure legend.

Table 7: Primary, secondary, and antibodies and dyes.

Antibody	Host	Western Blot	Immuno-fluorescence	Live-cell imaging	Manufacturer	Fixation
Ect2	Mouse	1:250	-	-	Santa Cruz, sc-514750	-
α - tubulin	Mouse	1:10000	1:500	-	Sigma-Aldrich, T6199	Methanol
6x-His	Mouse				Thermo Fisher Scientific, MA1-135	
Alexa Fluor™ 488 anti- mouse	Goat	-	1:500	-	Life Technologies, A32723	
Alexa Fluor™ 635 anti- mouse	Goat	-	1:500	-	Life Technologies, 816 A31574	-
Hoechst 33258	-	-	1:1000 (stock 1mg/ml)	-	Sigma-Aldrich, 861405	-
Mouse HRP	Goat	1:20000 (α -tubulin) 1:3000 (Ect2)	-		Bio-Rad, 170-6516	-
SiR-DNA	-	-	-	1:10000	Spirochrome, SC007	

Table 8: HeLa cell lines.

Cell line	Background		Amount of tetracycline used for induction	Amino acid sequence	Generated by	Reference
HeLa Flp- In TRex	HeLa	No transgene	-			Tighe et al. (2004)
EZ69	HeLa Flp- In TRex	Expression of NG-Ect2 ^{WT} , RNAi resistant pEZ197	0.2 µg/ml	1-883	Seren Baygun	Buchner (2019)
EZ70	HeLa Flp- In TRex	Expression of NG- Ect2 ^{ΔBRCT0} , RNAi resistant pEZ227	0.2 µg/ml	139-883	Seren Baygun	Buchner (2019)
EZ72	HeLa Flp- In TRex	Expression of NG-Ect2 ^{ΔBRCT0-2} , RNAi resistant pEZ204	0.2 µg/ml	328-883	Seren Baygun	Buchner (2019)
EZ74	HeLa Flp- In TRex	Expression of NG-Ect2 ^{ΔBRCT2} , RNAi resistant pEZ232	0.2 µg/ml	1-237, 328-883	Kristina Buchner	Buchner (2019)
EZ76	HeLa Flp- In TRex	Expression of NG-Ect2 ^{ΔBRCT1} , RNAi resistant pEZ242	0.2 µg/ml	1-138, 238-883	Kristina Buchner	Buchner (2019)
EZ80	HeLa Flp- In TRex	Expression of NG- Ect2 ^{T153A+K195M} , RNAi resistant pEZ247	0.2 µg/ml	1-883, T153A + K195M	Kristina Buchner	Buchner (2019)

EZ83	HeLa Flp- In TRex	Expression of Ect2 ^{S-loop^{AA}} , RNAi resistant pEZ265	0.01 µg/ml	1-883, between 328-421 all Ser/Thr => Ala	Kristina Buchner	Buchner (2019)
EZ104	HeLa Flp- In TRex	FACS sorted EZ76 NG-Ect2 ^{ΔBRCT1}	0.2 µg/ml		Sandra Schneid	Schneid et al. (2021)
EZ107	HeLa Flp- In TRex	FACS sorted EZ76 NG-Ect2 ^{ΔBRCT1}	0.2 µg/ml		Sandra Schneid	Schneid et al. (2021)
EZ111	HeLa Flp- In TRex	Expression of NG-Ect2 ^{S-loop^{STDE}} , RNAi resistant pEZ310	0.01 µg/ml	1-883, between 328-421 all Ser/Thr => Asp/Glu	Nils Bertram	This study
EZ117	HeLa Flp- In TRex	Expression of NG-Ect2 ^{P703D} , RNAi resistant pEZ314	0.02 µg/ml	1-883, P703D	Nils Bertram	This study
EZ118	HeLa Flp- In TRex	Expression of NG-Ect2 ^{C765K} , RNAi resistant pEZ315	0.2 µg/ml	1-883, C765K	Nils Bertram	This study
EZ119	HeLa Flp-In TRex	Expression of NG-Ect2 ^{W307A} , RNAi resistant pEZ313	0.2 µ/ml	1-883, W307A	Nils Bertram	Schneid et al. (2021)

Table 9: Software used throughout the thesis

Software		
ImageJ	NIH	https://imagej.nih.gov
Prism	GraphPad	https://www.graphpad.com
Affinity Designer	Serif	https://affinity.serif.com/de/designer/
RStudio	R Development Core Team, 2015	https://www.rstudio.com/
Image Lab v. 5.2.1. build 11	Bio-Rad	https://www.bio-rad.com

Table 10 Commercial kits

Kits	Manufacturer
NulceoSpin Gel and PCR Clean-up kit	Macherey-Nagel, 740609.50
Qiagen Plasmid Mini Kit	Qiagen, 12125
NucleoSpin Plasmid, Mini kit for plasmid DNA	Macherey-Nagel, 740588.50

Table 11: siRNAs for knockdown of gene expression

Gene	Sequence	Transfection reagent	Final concentration	Company / Catalog Number
Non-targeting	Unknown sequence	Lipofectamine™ RNAiMAX	30 nm	Dharmacon, D-001810-01-20
Ect2	GGCGGAAUGAACAGGAU UU	Lipofectamine™ RNAiMAX	30 nm	Dharmacon
MCAK	GCAGGCUAGCAGACAAA UAUU	Lipofectamine™ RNAiMAX	30 nm	Dharmacon

Table 12: Bacterial strains

Bacterial strain	Usage
DH5α	DNA transformation
BL21	Recombinant protein expression

Table 13: Materials and reagents

Reagent	Source	Identifier
18 mm glass coverslips	Roth	P233.1
μ -Slide (2-well, 4-well, 8-well)	ibidi	80286 80426 80826
Cell culture flasks (T25, T75) 6-well and 12-well plates	Greiner Bio One	690175 658175 657160 665180
FBS	Thermo Scientific	10270106
P/S	PAN Biotech	A2213
DMEM GlutaMAX™	Thermo Scientific	11584516
CO ₂ -independent medium	Thermo Fisher	18045054
Thymidine	Sigma	T1895
Plk1 inhibitor BI2536	Selleckchem	S1109
RhoA kinase inhibitor Y27632	VWR	CAYM10005583-1
C3 transferase	tebu-bio	CT04-A
Tetracycline	Sigma-Aldrich	T7660
Hygromycin	Sigma-Aldrich	H3274
poly-L-lysine	Sigma-Aldrich	P1524
DpnI	NEB	R0176L
XhoI	NEB	R0146
Gibson mix	NEB	E2611
Phusion polymerase + Phusion buffers	NEB	M0530L
T4 DNA ligase	NEB	M0202
L-glutamine	Thermo Fisher Scientific	25030149
PMSF	Sigma-Aldrich	P7626-G1

DTT	Roth	6908.3
Amylose resin	NEB	E8021S
Glutathione Sepharose	Sigma-Aldrich	GE17-0756-01
cOmplete Protease inhibitor cocktail	Roche	11836153001
ECL™ Prime Western Blotting	GE Healthcare	RPN22236
ECL™ Western Blotting Reagents	GE Healthcare	RPN2106
SuperSignal™ West Femto Maximum Sensitivity	Thermo Fisher Scientific	34094
Lipofectamine™ RNAiMAX	Thermo Fisher Scientific	13778075
X-tremeGene9	Sigma-Aldrich	8079398949
[gamma-P32]ATP, 800 Ci/mmol, 10mCi/ml	Hartmann Analytic	SRP-801
PLK1 Recombinant Human Protein	Thermo Fisher Scientific	PV3501
rATP	Metabion	N10015
UView™	Bio-Rad	1665112

Table 14: Primers used for plasmid generation

Primer	Sequence (5' to 3')	Used for plasmid
EZ1277+EZ1278 EZ1276+EZ1279	TCATTTGCCTTTTCATATAAATACATAGTTTCTCC ACAAGCAGGAGGCAAGGTGGCAAGTTGCAAAAG ATTTATATGAAAAGGCAAATGAGCCTGAGC TGCCACCTTGCCCTCTGCTTGTGTCAGGAACTG	pEZ310
EZ1282 EZ1283	TCAAGCAAGAGTGGTTCGCGGGAAGCATTCAAATGG CCATTTGAATGCTTCCCGCGAACCCTTGCTTGA	pEZ313
EZ1284 EZ1285	CTCTTAAGCATATTCACCTAATGGATCTTCTCAGATTAAGAAGG CCTTCTTAATCTGAGAAAGATCCATTAGGTGAATATGCTTAAGAG	pEZ314
EZ1286 EZ1287	GACATGTAGCTAACACCATTAAGAAAGCAGATGCTGAGAATC GATTCTCAGCATCTGCTTTCTTAATGGTGTGTTAGCTACATGTC	pEZ315

EZ1346	ATCATAGTATCCGGGAATCCGGGGATCCAC	pEZ336
EZ1347	CGGAATCCCGGATACTATGATGCTGAATGTG	
EZ1348	ATCGTCAGTCAGGGCCCGCCATCATTGGGA	
EZ1349	ATGGCGGGCCCTGACTGACGATCTGCCTCGC	
EZ1335	AAACTCGAGATGGCTGAAAATAGTGTATTAAC	pEZ330
EZ1336	TCCTCGAGTGCTGACTGCTTTGAAGGAAGTGG	
EZ1338	AAACTCGAGATGTGTGCGCCGTTGTATTGTAC	pEZ331
EZ1337	TCCTCGAGTTCATATAAATACATAGTTTCTCCAGC	
EZ1338	AAACTCGAGATGTGTGCGCCGTTGTATTGTAC	pEZ332
EZ1339	TCCTCGAGAACTTTAAATTCATTTCTAAAGTCATC	
EZ1340	AAACTCGAGATGCCTCCATTTCAAGATTGTATTTAAG	pEZ334
EZ1337	TCCTCGAGTTCATATAAATACATAGTTTCTCCAGC	
EZ1335	AAACTCGAGATGGCTGAAAATAGTGTATTAAC	pEZ335
EZ1337	TCCTCGAGTTCATATAAATACATAGTTTCTCCAGC	
EZ1346	ATCATAGTATCCGGGAATCCGGGGATCCAC	pEZ336
EZ1347	CGGAATCCCGGATACTATGATGCTGAATGTG	
EZ1348	CGGAATCCCGGATACTATGATGCTGAATGTG	
EZ1349	ATGGCGGGCCCTGACTGACGATCTGCCTCGC	
EZ1335	AAACTCGAGATGGCTGAAAATAGTGTATTAAC	pEZ338
EZ1339	TCCTCGAGAACTTTAAATTCATTTCTAAAGTCATC	
EZ1335	AAACTCGAGATGGCTGAAAATAGTGTATTAAC	pEZ340
EZ1350	TCCTCGAGTGAAAATGGCAAAGGCTCTCC	

Table 15: General and obtained plasmids.

Plasmid name	Backbone	Information
pOG44	-	Encodes Flp recombinase Invitrogen, V600520
pGEX-6P-1 GST-PLK-1 PBD	-	For protein purification Gift of I. Sumara Martino et al. (2017)
MBP/6xHis	-	For protein purification Hofweber et al. (2018)
pGEX-4T	-	GE Healthcare, GE28-9545-49
pExA128	-	Customized Gene sequence Eurofins
pEZ75	pcDNA5/FRT/TO	RacGAP1 used as template (generated by Esther Zanin)

pEZ197	pcDNA5/FRT/TO	NG-Ect2 ^{WT} used as template (generated by Pedro Barbosa)
--------	---------------	---

Table 16: Generated plasmids.

Plasmid name	Backbone	Primers used	Method	Generated by	Information
pEZ310	pcDNA5/FRT/TO	EZ1277 EZ1278 EZ1276 EZ1279	Gibson cloning	Esther Zanin/ Nils Bertram	To generate NG-Ect2 ^{S-loopSTDE}
pEZ313	pcDNA5/FRT/TO	EZ1282 EZ1283	Gibson cloning	Esther Zanin/ Maysoon Noureddine	To generate NG-Ect2 ^{W307A}
pEZ314	pcDNA5/FRT/TO	EZ1284 EZ1285	Gibson cloning	Esther Zanin/ Maysoon Noureddine	To generate NG-Ect2 ^{P703D}
pEZ315	pcDNA5/FRT/TO	EZ1286 EZ1287	Gibson cloning	Esther Zanin/ Maysoon Noureddine	To generate NG-Ect2 ^{C765K}
pEZ330	pMal-Flag-His	EZ1335 EZ1336	Restriction cloning	Nils Bertram	For protein purification MPB-Ect2-B0-S-sloop (AA 1-421)
pEZ331	pMBP/6xHis	EZ1338 EZ1337	Restriction cloning	Nils Bertram	For protein purification MPB-Ect2-B1+2 (AA 137-324)
pEZ332	pMBP/6xHis	EZ1338 EZ1339	Restriction cloning	Nils Bertram	For protein purification MPB-Ect2-B1 (AA 137-237)

pEZ334	pMBP/6xHis	EZ1340 EZ1337	Restriction cloning	Nils Bertram	For protein purification MPB-Ect2-B2 (AA 238-324)
pEZ335	pMBP/6xHis	EZ1335 EZ1337	Restriction cloning	Nils Bertram	For protein purification MBP-Ect2 0-2 (AA 1-324)
pEZ336	pGEX-4T	EZ1346 EZ1347 EZ1348 EZ1349	Gibson cloning	Esther Zanin	For protein purification GST-RacGAP1 (AA 1-288)
pEZ338	pMBP/6xHis	EZ1335 EZ1339	Restriction cloning	Esther Zanin	For protein purification MBP-Ect2 B0+1 (AA 1-237)
pEZ340	pMBP/6xHis	EZ1335 EZ1350	Restriction cloning	Esther Zanin	For protein purification MBP-Ect2 B0 (AA 1-137)

Table 17: Buffers and solutions.

Buffer/Solution	Composition
Mounting medium	4 % n-Propyl-Gallate 90 % Glycerol in 1x PBS
sample buffer (2 x)	2 ml stacking buffer 4 ml 10 % SDS 140 μ l β -Mercaptoethanol 4 ml 50 % Glycerol 100 μ l saturated Bromphenol blue solution

Coomassie staining solution	100 ml 100 % MeOH 50 ml glacial acetic acid 0.5 g brilliant blue Adjust to 500 ml with ddH ₂ O
Coomassie destaining solution	250 ml 100 % EtOH 50 ml glacial acetic acid Adjust to 500 ml with ddH ₂ O
Running buffer (10 x)	30.3 g Tris 144 g Glycine Adjust to 1 l with ddH ₂ O
Transfer buffer (1x)	200 ml 100 % EtOH 100 ml Running buffer Adjust to 1 l with ddH ₂ O
Resolving buffer (4 x)	18.17 g Tris 24 ml 1 M HCl 0.4 g SDS Adjust pH to 8.8 with HCl Adjust to 100 ml with ddH ₂ O
Stacking buffer (4 x)	6 g Tris 38.5 ml 1 M HCl 0.4 g SDS Adjust pH to 6.8 with HCl Adjust to 100 ml with ddH ₂ O
PBS (10 x)	25.6 g Na ₂ HPO ₄ x 7H ₂ O 80 g NaCl 2 g KCl 2 g KH ₂ PO ₄ Adjust to 1l with ddH ₂ O
PBS-T	PBS (1 x) 0.1 % Triton X-100

TBS (10 x)	2 KCL 80 g NaCl 30 g Tris-base Adjust pH to 7.4 with HCl Adjust to 1l with ddH ₂ O
TBS-T (1x)	TBS (1x) 0.1 % Tween
Freezing solution (1 x)	10 % DMSO 65% DMEM medium 25% FBS
LB broth	10 g Tryptone 5 g yeast extract 10 g NaCl 800 ml MilliQ H ₂ O
TE buffer	10 mM Tris-HCl 1 mM EDTA Adjust pH to 8.0 with HCl Adjust volume to 1 l with ddH ₂ O

Table 18: Microscopes

Microscope	Equipment	Manufacturer
Nikon eclipse Ti spinning disk confocal microscope	<u>Lasers:</u> Andor laser line combiner Diode 405 nm Diode 488 nm Diode 561 nm Diode 638 nm <u>Objectives:</u> CFI Apochromat TIRF 60x oil/ 1.49/* CFI P-Apo 100x Lambda oil/ 1.45* *DIC available <u>Camera:</u> ANDOR iXon DU-888U3-CS0-BV EMCCD camera 1024 x 1024 pixel	Nikon

	Pixel size 13 x 13 μm <u>Software:</u> NIS Elements	
Leica TCS SP5 microscope	<u>Lasers:</u> Diode laser 405 nm kpl Coherent (25 mW) Argon Laser (458 nm, 476 nm, 488 nm, 514 nm), 5mW DPSS Laser kpl 561 nm MG (10 mW) HeNe Laser 594 nm, Uniphase (2.5 mW) HeNe Laser 633 nm, Uniphase (10 mW) <u>Objectives:</u> HCX PL APO Lambda Blue 63x 1.4 oil <u>Software:</u> Leica Application Suite Software	Leica

3 Results

Part of the presented data in this chapter has already been published in Cell Reports. See the following reference:

Schneid, S., Wolff, F., Buchner, K., Bertram, N., Baygün, S., Barbosa, P., Mangal, S., & Zanin, E. (2021). The BRCT domains of ECT2 have distinct functions during cytokinesis. *Cell reports*, 34(9), 108805. <https://doi.org/10.1016/j.celrep.2021.108805>

Schneid, S. and Wolff, F. are co-first authors of this paper.

Several figures have been reproduced or modified in compliance with the author's rights, which are stated here: <https://www.elsevier.com/about/policies/copyright#Author-rights>

Following Figures and Tables contain data from Schneid et al. (2021):

Figure 12, Figure 13, Figure 14 B and C, Figure 15, Figure 16 B and C, Figure 18 B and C, Figure 19, Figure 20, Figure 21 B and C, Figure 22, Figure 23 B and C, Figure 24, Figure 25 B and C, Figure 26, Figure 27, Figure 28, Figure 29, Figure 30, Figure 31, Figure 32, Figure 33, Figure 34, Figure 35, Figure 37, Figure 39, Figure 40, Figure 41, Figure 42, Figure 43, Figure 44, Figure 45, Table 19 and Table 20.

3.1 Preamble

The project to elucidate the contributions of the three BRCT domains to Ect2 function and regulation in human cells had been started by Dr. Kristina Buchner. Together with Seren Baygun and Pedro Barbosa she had established a genetic replacement system for Ect2 in HeLa cells. This replacement system allows the assessment of the function of specifically engineered Ect2 variants after depleting endogenous Ect2 by RNAi. For the system to work, the engineered Ect2 mutant variants must be similarly expressed as endogenous Ect2 after endogenous Ect2 had been depleted by RNAi.

Dr. Kristina Buchner had tested the function of several engineered Ect2 mutant variants after the depletion of endogenous Ect2 using a multinucleation assay (Buchner, 2019). She had found, that the BRCT1 domain but not the BRCT0 domain is required for cell division. For the BRCT2 deletion mutant, she had observed an intermediate phenotype suggesting that the BRCT2 domain is partially required for cell division. Subsequently, she had also assayed, for some of the cell lines, large bleb formation, NG-Ect2 localization, and anillin recruitment. However, all those studies had been performed in the presence of endogenous Ect2 (Buchner, 2019), which might compete with Ect2 mutant variants. Therefore, her results do not allow to make conclusions on the functionality of the Ect2 mutant variants during cytokinesis.

As it was mandatory to express Ect2 variants at endogenous levels and to deplete endogenous Ect2 to reveal the function of the individual BRCT domains during cytokinesis, first of all the optimal conditions for expression induction and Ect2 RNAi were established. Subsequently, my focus lay on the analysis of live-cell recordings, while my colleague Friederike Wolff analyzed RhoA and anillin patterns in fixed cells. On the way, the methods used for analyzing large bleb formation and Ect2 localization were revised and adjusted to receive more meaningful results.

3.2 A genetic replacement system for Ect2 in HeLa cells

To study the different domain contributions to Ect2 regulation, a genetic replacement system for Ect2 in HeLa cells was established by Dr. Kristina Buchner (Buchner, 2019) (see chapter 2.5.3). In this replacement system, single copies of Ect2 transgenes can be stably integrated into the T-REXTM HeLa host cell line, which carries flippase recognition target (FRT) sites at a specific genomic locus. By co-expressing flippase, transgenes get integrated into the genome by homologous recombination at this site (O'Gorman et al., 1991). The expression of the transgenes is inducible as it is controlled by a system based on the tet-operon. In the absence of tetracycline, two tetracycline repressors (tetR) bind to two tandem tet operator 2 (tetO2) sequences and thereby block expression. The addition of tetracycline to the cell medium releases tetR from tetO2 and transgenes can be expressed. (Hillen & Berens, 1994; Hillen et al., 1983; Yao et al., 1998) (Figure 10).

To allow the analysis of mutant Ect2 proteins without endogenous Ect2 in the background, the Ect2 transgenes harbor four silent mutations in the BRCT1 domain, which render them

resistant to RNAi knockdown (highlighted for Ect2^{WT} in Figure 10). Additionally, they feature an N-terminal neongreen-tag, which allows easy analysis of their protein localization during the different cell cycle phases.

Figure 11 shows an overview of the stable cell lines used in this thesis and the cell lines which were previously generated and described by Buchner (2019) are underlined. The cell lines harbor Ect2 transgenes in which either BRCT0 (NG-Ect2^{ΔBRCT0}), BRCT1 (NG-Ect2^{ΔBRCT1}), BRCT2 (NG-Ect2^{ΔBRCT2}), or all three BRCT domains (NG-Ect2^{ΔBRCT0-2}) were deleted. Additionally, several cell lines with point mutations in BRCT1 (NG-Ect2^{T153A+K195M}), BRCT2 (NG-Ect2^{W307A}), the S-loop (NG-Ect2^{S-loopAA}, NG-Ect2^{S-loopSTDE}), and the PH-domain (NG-Ect2^{P703D}, NG-Ect2^{C765K}) were analyzed. NG-Ect2^{WT} served as proof of principle and allowed comparison of mutant with wild-type behavior/phenotype.

For the sake of clarity, in the following the prefix "NG-" will only be used in a few places, mainly in figures concerning protein amounts and protein localization, and otherwise omitted.

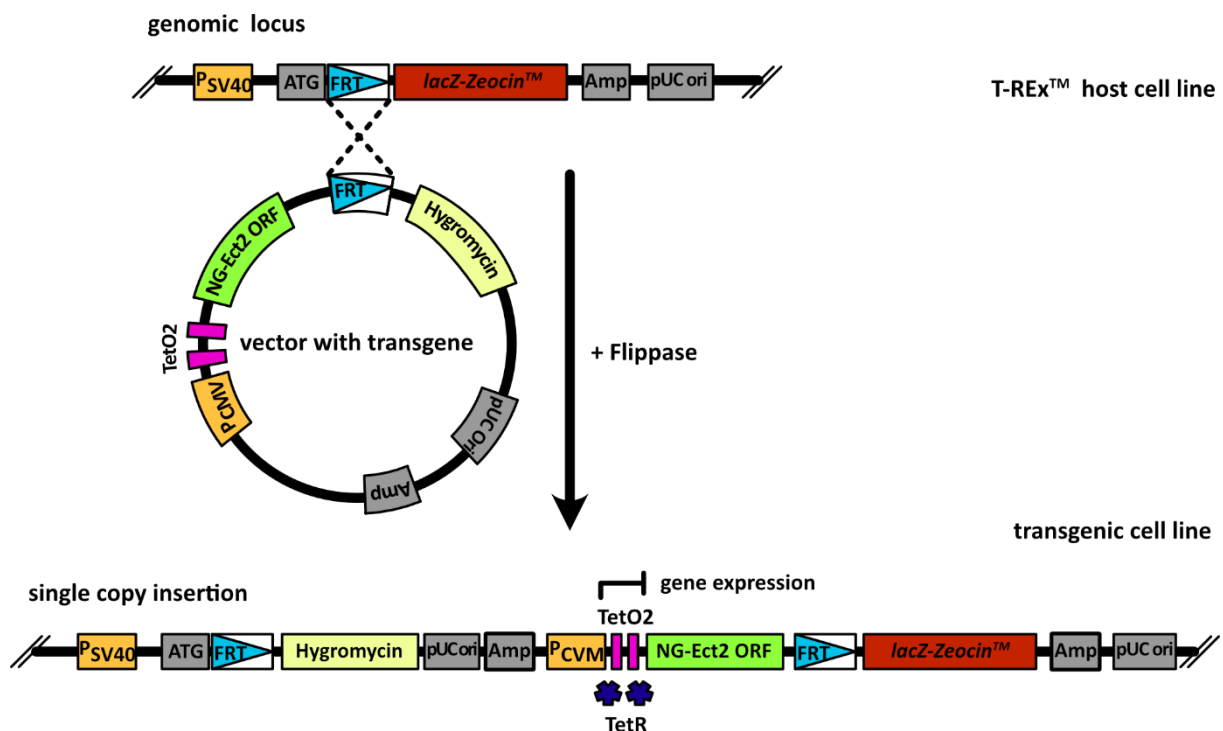


Figure 10: Flp-FRT mediated single-copy integration of transgenes using the Flp-In T-Rex™ system to generate stable transgenic HeLa cell lines. NG-tagged transgenes were cloned into the pcDNA5/FRT/TO expression vector, which contains FRT sites. Co-transfection with an Flp-recombinase encoding vector allowed the FRT/Flp-mediated, stable integration of the transgenes into a specific locus in the Flp-In TRex HeLa cell line. Transgene expression in the stable cell lines is controlled by a system based on the tet-operon. That is why tetracycline has to be added to the medium to release both TetR repressors, which block gene expression by

binding to TetO2 sequences located anterior of the transgenes. The figure was created based on Life Technologies Corporation, 2012.

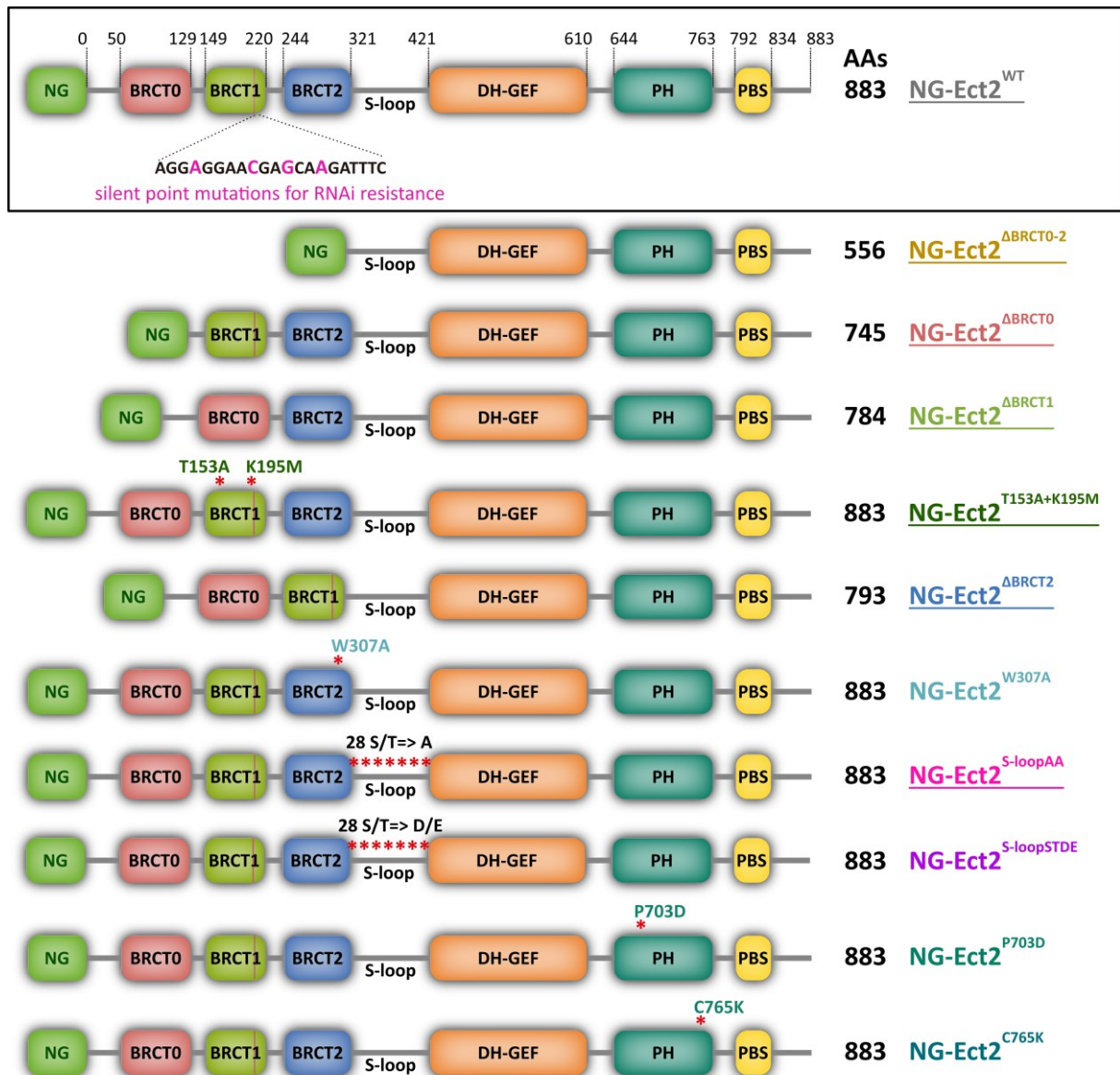


Figure 11: Schematic overview of stable transgenic HeLa cell lines that were used in this thesis. The cell lines carry mutant versions of Ect2, that either have BRCT domains deleted or one and more point mutations in specific domains (marked with asterisks), respectively. All transgenic Ect2 proteins were rendered RNAi resistant by the introduction of four silent point mutations in the BRCT1 domain (see NG-Ect2^{WT}) and have an NG-tag. Their expression was induced by the addition of tetracycline. Cell lines previously generated by Dr. Kristina Buchner are underlined.

3.3 Ect2 mutant variants are expressed at similar levels as endogenous Ect2, which can be efficiently knocked down by RNAi

Before the analysis of a novel Ect2 cell line was started, it was tested whether the respective transgene is expressed to similar levels as endogenous Ect2 via western blot analysis. Thereby we could rule out unspecific phenotypes caused by increased or decreased transgene expression. To analyze the effects of Ect2 variants on cytokinesis in the absence of endogenous Ect2 in the background, we further checked whether endogenous Ect2 can be efficiently depleted by our RNAi protocol. After Ect2 RNAi no residual endogenous Ect2 was detected by immunoblotting- even after prolonged exposure (Figure 12, first two lanes). Mutant protein expression was still present after the depletion of endogenous Ect2, as can be seen for Ect2^{WT} in Figure 12. This was the case for all examined cell lines and exemplary immunoblots of all other cell lines will be presented in the corresponding paragraphs below. Apart from visually assessing transgene expression, we quantitatively measured their signal intensity on immunoblots in the absence of endogenous Ect2. Normalization to the endogenous protein level revealed that all transgenes show similar expression levels, which were not significantly different in comparison to endogenous Ect2 (Table 19). For details of the western blot quantification see chapter 2.5.4.

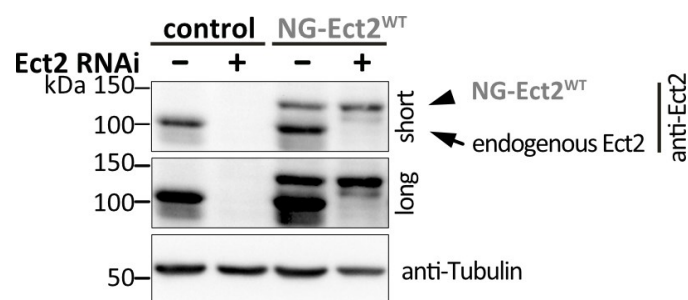


Figure 12: The NG-Ect2^{WT} transgene is expressed similarly to endogenous Ect2 after Ect2 depletion by RNAi. Western blot analysis of lysates from control and NG-Ect2^{WT} cells treated with and without Ect2 RNAi to knock down endogenous Ect2. Blots were probed with anti-Ect2 and anti- α -tubulin (as loading control). Endogenous Ect2 has a molecular weight of 100.1 kDa and NG-Ect2^{WT} of 127.0 kDa.

Table 19: All transgenic Ect2 mutant proteins are expressed to endogenous levels after the depletion of endogenous Ect2 by RNAi. Shown are mean±SD expression levels relative to endogenous Ect2. Signal intensities of Ect2 protein bands were measured for 2-3 independent cell lysates on immunoblots. Ect2 band intensities were normalized to respective tubulin loading controls and quantified relative to the control (endogenous Ect2). Kruskal Wallis test detected no significant difference in expression levels for all mutant Ect2 proteins compared to Ect2^{WT}. Data acquired by SS and FW.

cell line	% mean NG-Ect2 levels to endogenous Ect2	Kruskal-Wallis- test
Ect2 ^{WT}	102 (+/- 48)	/
Ect2 ^{ΔBRCT0-2}	97 (+/- 65)	n.s.
Ect2 ^{ΔBRCT0}	107 (+/- 60)	n.s.
Ect2 ^{ΔBRCT1 clone 1}	83 (+/- 24)	n.s.
Ect2 ^{ΔBRCT1 clone 2}	79 (+/- 18)	n.s.
Ect2 ^{T153A+K195M}	111 (+/- 18)	n.s.
Ect2 ^{ΔBRCT2}	102 (+/- 35)	n.s.
Ect2 ^{W307A}	123 (+/- 59)	n.s.
Ect2 ^{S-loopAA}	88 (+/- 22)	n.s.
Ect2 ^{S-loopSTDE}	101 (+/- 66)	n.s.
Ect2 ^{P703D}	84 (+/- 21)	n.s.
Ect2 ^{C765K}	146 (+/- 68)	n.s.

3.4 Ect2^{WT} rescues phenotypes elicited by depletion of endogenous Ect2

Before it could be analyzed how the function and regulation of Ect2 during cytokinesis is affected by different structural modifications, it had to be ensured, that the established replacement system works. Therefore, it was tested whether the expression of Ect2^{WT} can compensate for the loss of endogenous Ect2 and whether Ect2^{WT} activity is similarly regulated to endogenous Ect2. As Ect2 localization is closely linked to its function, we also analyzed whether Ect2^{WT} localizes normally during cell division.

3.4.1 Ect2^{WT} rescues cytokinetic failure after endogenous Ect2 depletion by RNAi

First, multinucleation assays were conducted in the presence and absence of endogenous Ect2. Under normal conditions, HeLa cells have a single nucleus and are considered mononucleated (Figure 13, example labeled with “1”). In the absence of Ect2 activity, a contractile ring cannot form, the two sets of chromosomes cannot be spatially separated and therefore remain in one binucleated cell (Figure 13, example labeled with “2”). When cytokinesis fails repeatedly, this results in multinucleated cells (Kim et al., 2005; Tatsumoto et al., 1999) (Figure 13, example labeled with “3”). Thus, mono-, bi-, and multinucleation was quantified in control, Ect2-depleted control, and Ect2-depleted Ect2^{WT} cells to determine whether Ect2^{WT} supports cytokinesis when endogenous Ect2 is absent. We also analyzed Ect2^{WT} with endogenous Ect2 present and detected no effect on cytokinetic success thereby excluding synergistic effects triggered by transgene expression.

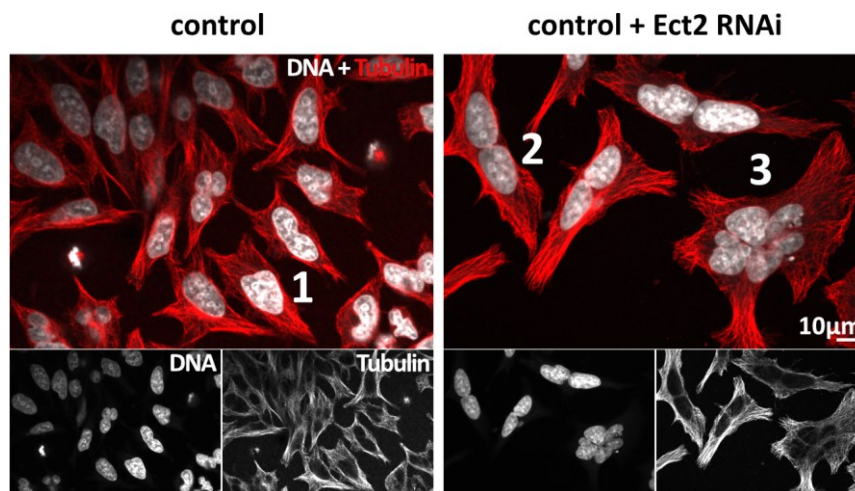


Figure 13: Depletion of Ect2 leads to bi- and multinucleated cells. Immunofluorescence images of control and Ect2-depleted control cells in interphase stained with anti- α -tubulin and Hoechst. (1) marks a cell with one nucleus (mononucleated), (2) marks a cell with two nuclei (binucleated), and (3) marks a cell with three nuclei (multinucleated).

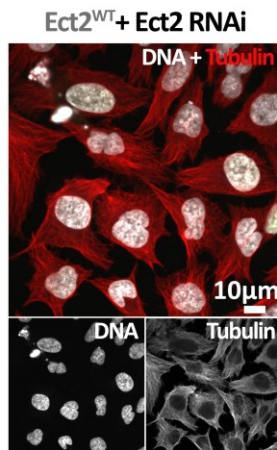
As expected, more than 95% of control cells were mononucleated, whereas control cells depleted of Ect2 exhibited primarily bi- and multinucleation (~80%) (Figure 14 C) (% mononucleation $p < 0.001$, determined by Tukey's test). The expression of Ect2^{WT} could restore mononucleation to control levels (~96%) in the absence of endogenous Ect2 (% mononucleation not significant compared to control, determined by Tukey's test) (Figure

14 B and C). This was even the case when Ect2^{WT} expression was induced with a 20-fold lower concentration of tetracycline than normal (0.01 µg/ml instead of 0.2 µg/ml) (Figure 14 C Ect2^{WT low ind}) (% mononucleation not significant compared to control, determined by Tukey's test). Assuming that this leads to strongly reduced Ect2^{WT low ind} protein levels, the result suggests that reduced levels of functional Ect2^{WT} are sufficient to support proper cytokinesis. However, to allow reliable conclusions about this, protein levels would need to be quantitated by western blot analysis. All in all, these results indicated that Ect2^{WT} is functional during cytokinesis and can replace endogenous Ect2.

A



B



C

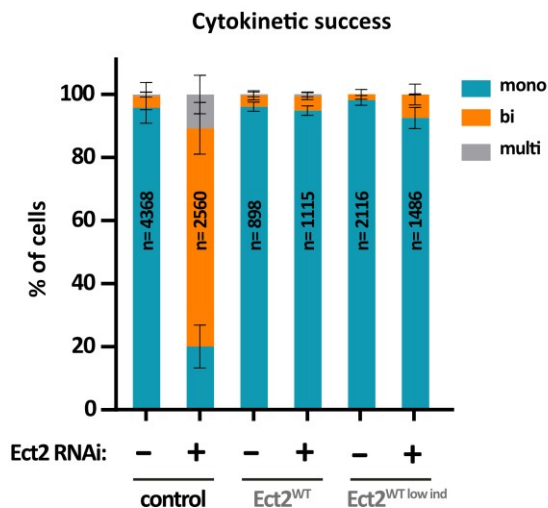


Figure 14: Expression of Ect2^{WT} rescues cytokinetic failure after the depletion of endogenous Ect2. (A) Schematic representation showing the domain organization of the NG-tagged Ect2^{WT} protein. (B) Immunofluorescence images of Ect2^{WT} cells depleted of endogenous Ect2 in interphase stained with anti- α -tubulin and Hoechst. Images kindly provided by Prof. Dr. Esther Zanin. (C) Percentages of mono-, bi- and multinucleated cells in control and Ect2^{WT} cells treated with or without Ect2 RNAi to deplete endogenous Ect2. Ect2^{WT low ind} was induced with a 20-fold reduced amount of tetracycline (0.01 µg/ml). (n=number of cells, data from ≥ 4 independent experiments presented as mean \pm SD, data acquired by SS, KB, FW, EZ).

3.4.2 Ect2^{WT} rescues the defect in cleavage furrow formation and ingression after depletion of endogenous Ect2 by RNAi

Formation and ingression of the cytokinetic ring is the crucial feature of cytokinesis, so next, dividing control, control+Ect2 RNAi, and Ect2^{WT}+Ect2 RNAi cells were filmed to see whether they form a cleavage furrow. Representative image sequences can be seen in Figure 15 A. Control cells rounded up from prometaphase on and the chromosomes came together at the metaphase plate at the time of metaphase (0 min). Anaphase started with the separation of the sister chromatids by the mitotic spindle. Furrow ingression was visible at 6-9 min after anaphase onset and was completed within 12-15 min. Since Ect2 is essential for furrow formation and ingression (Chalamalasetty et al., 2006; Yüce et al., 2005), control cells depleted of Ect2 failed to ingress and divide. Ect2^{WT} expression in Ect2-depleted cells restored the ability of cells to ingress and divide. (Figure 15 A)

To quantitatively compare cleavage furrow ingression, the equatorial cell width 12 min after anaphase onset was measured in control, control+Ect2 RNAi, and Ect2^{WT}+Ect2 RNAi cells. At this time, the cytokinetic ring is just about fully constricted in control cells. As expected, 12 min after anaphase onset, Ect2-depleted cells had a significantly bigger equatorial cell width of 16.7 μm compared to 4.7 μm in control cells. This ingression failure could be fully rescued by the expression of Ect2^{WT}, which resulted in an equatorial cell width of 4.4 μm . These results, further confirmed that the established replacement system for Ect2 is working and can be used to investigate the functions of the different Ect2 domains. (Figure 15 B)

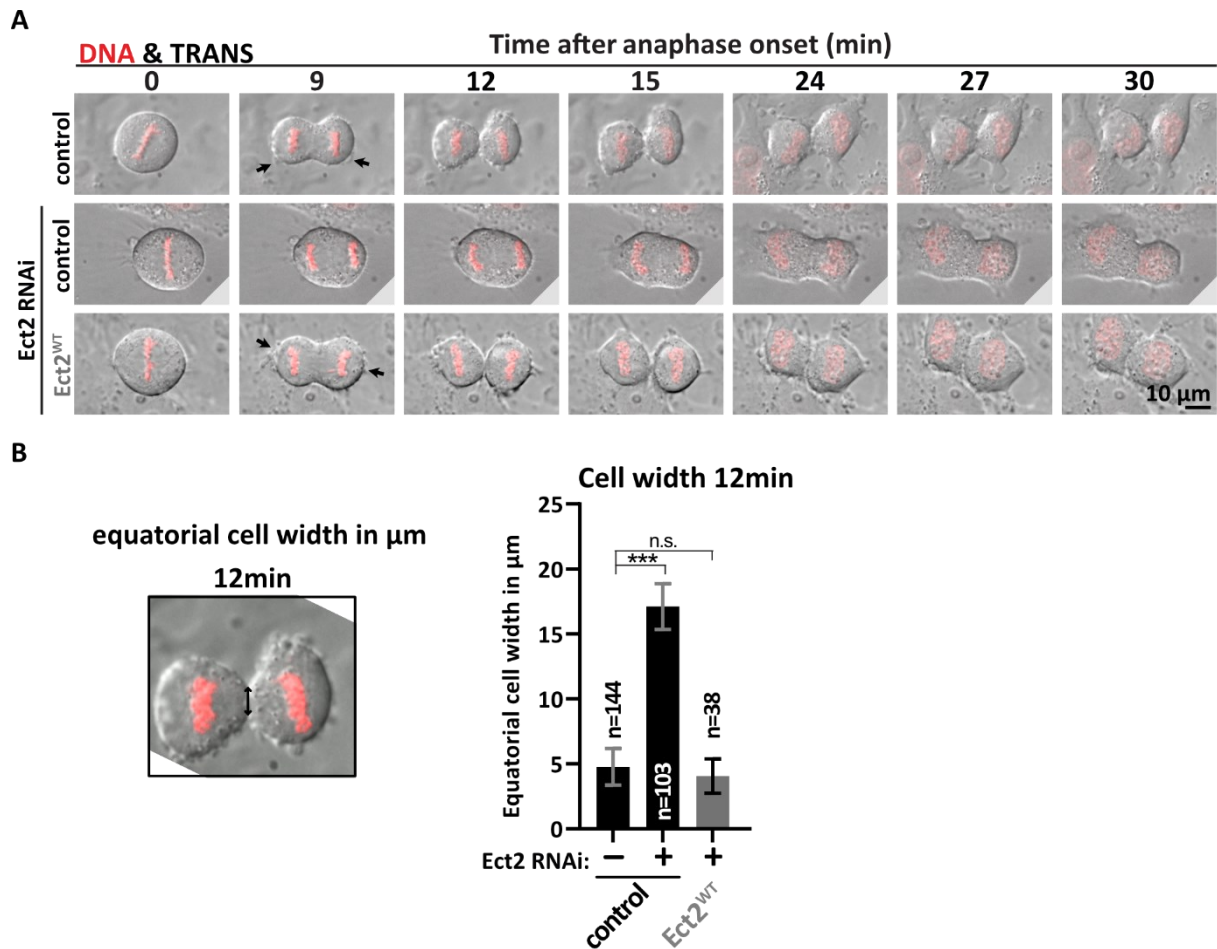


Figure 15: Expression of Ect2^{WT} rescues the defect in furrow formation and ingression after the depletion of endogenous Ect2 by RNAi. (A) Representative live-cell image sequences of dividing control, Ect2-depleted control, and Ect2^{WT} cells. Endogenous Ect2 was depleted by RNAi as indicated. DNA was probed with SiR-DNA. Time in minutes after anaphase onset. Small blebs are indicated by black arrows. (B) Equatorial cell width in μ m measured 12 min after anaphase onset for controls and Ect2^{WT} cells. Endogenous Ect2 was depleted by RNAi as indicated. (n=number of cells, data from ≥ 5 independent experiments presented as mean \pm SD, *** $p < 0.001$ and n.s.=not significant determined by Tukey's test).

3.4.3 Ect2^{WT} shows similar regulation and activity as endogenous Ect2 during cell division

Next, we wanted to test, whether Ect2^{WT} is normally regulated during cytokinesis. During the drastic morphological changes in anaphase, cells release internal pressure in form of small blebs at their polar membrane to stabilize cell shape (Hickson et al., 2006; Sedzinski et al., 2011; Tokumitsu & Maramorosch, 1967). However, bigger blebs are unusual and were shown to be triggered by elevated RhoA activity (Zanin et al., 2013). Since Ect2 activates RhoA, membrane blebbing can also be an indicator for increased Ect2 activity and we used large bleb

formation as a readout for hyperactive Ect2. The schematic in Figure 16 A portrays a non-blebbing cell, which forms no blebs in metaphase and a few small blebs in anaphase, respectively (indicated by black arrows). Moreover, a strongly blebbing cell is depicted, which features several large membrane blebs in meta- and anaphase (indicated by pink arrowhead). A membrane bleb had to grow to a size of at least 1/3 of the cell length to be considered a large bleb in our analysis. Example images for control, Ect2^{WT}+Ect2 RNAi and blebbing Ect2^{ΔBRCT2}+Ect2 RNAi cells in meta- and anaphase are presented in Figure 16 B. To detect defects in Ect2 regulation, blebbing was quantified during meta- and anaphase in time-lapse videos, and the number of large blebs, formed by each cell for control and Ect2^{WT}+Ect2 RNAi cells, was counted. For comparison cells exhibiting 1-2, 3-4, or more than 5 blebs were grouped. Large blebs were formed in 6.6 % and 16.3 % of Ect2^{WT}+Ect2 RNAi cells in meta- and anaphase, respectively. Compared to control, percentages were slightly increased (0.5 % in metaphase and 3.1 % in anaphase Figure 16 B and C). However, only 1-2 blebs were counted in blebbing Ect2^{WT}+Ect2 RNAi cells (4% and 14.7 % of total cells). Thus, Ect2^{WT} shows activity similar to endogenous Ect2 and can be used for comparison.

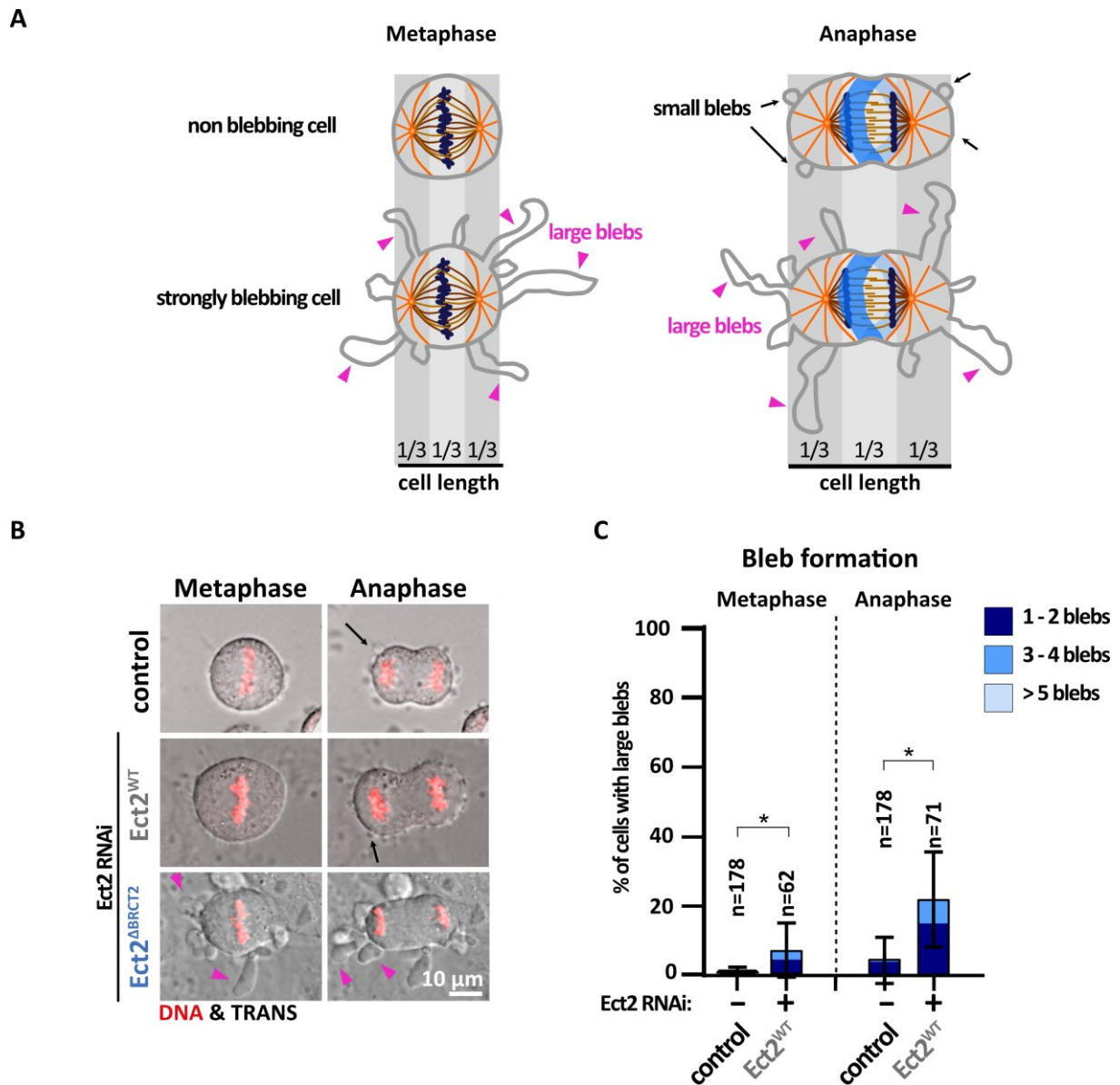


Figure 16: Ect2^{WT} shows similar regulation and activity as endogenous Ect2 during cell division. (A) Schematic illustration of a non-blebbing and strongly blebbing cell in meta- and anaphase. Pink arrowheads indicate large membrane blebs, which have to be at least 1/3 of the cell diameter, and black arrows indicate small membrane blebs. Bleb formation was quantified by counting the number of large blebs formed by a cell. For better comparison cells forming 1-2, 3-4, or >5 blebs were grouped. (B) Live-cell images of control, Ect2^{WT}, and Ect2^{ΔBRCT2} cells in meta- and anaphase treated with Ect2 RNAi as indicated. Small membrane blebs are indicated by black arrows and large blebs with pink arrowheads. DNA was probed with SiR-DNA. (C) Percentages of control and Ect2^{WT} cells, which formed 1-2, 3-4, and >5 large blebs during meta- and anaphase. Endogenous Ect2 was depleted by RNAi as indicated. (n=number of cells, data from ≥5 independent experiments presented as mean, SD for total blebbing, *p<0.05 determined by Kruskal Wallis test, data acquired by SS and EZ).

3.4.4 Ect2^{WT} shows similar localization as endogenous Ect2 during cell division

Lastly, the localization of NG-Ect2^{WT} was examined during cell division after depletion of endogenous Ect2. During interphase endogenous Ect2 resides in the nucleus. In prometaphase, after nuclear envelope breakdown, Ect2 localizes cytoplasmic and at the beginning of anaphase, Ect2 starts to accumulate at the equatorial membrane as well as on the tips of overlapping midzone microtubules, the so-called midzone. Following furrow ingression, Ect2 is found at the midbody (Chalamalasetty et al., 2006; Liu et al., 2004; Tatsumoto et al., 1999). Ect2 localization to the midzone and equatorial membrane was suggested to be required for cleavage furrow formation and ingression (Kotýnková et al., 2016; Su et al., 2011; Wolfe et al., 2009).

To examine whether Ect2 localization is altered, Ect2^{WT}+Ect2 RNAi cells were filmed during cell division and its NG-fluorescence signal was visually inspected. In Figure 17 Ect2^{WT} localization is shown over time, starting at the last metaphase frame (0 min). As previously, published Ect2^{WT} (Chalamalasetty et al., 2006; Liu et al., 2004; Tatsumoto et al., 1999) was absent from the metaphase membrane and started to accumulate at the equatorial membrane and the midzone at anaphase onset (3 min onwards). After furrow ingression was completed (12-15 min) NG-Ect2 was present at the midbody (Figure 17). Again, this result affirmed that Ect2^{WT} behaves similarly to endogenous Ect2.

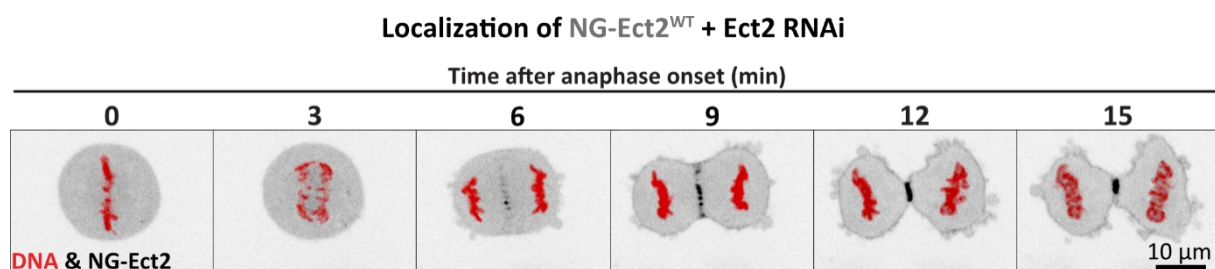


Figure 17: Localization of NG-Ect2^{WT} during mitosis. Representative fluorescence image sequence showing the localization (grey) of NG-Ect2^{WT} at consecutive timepoints during cell division starting at the last metaphase frame (0 min) until furrow ingression is completed (12-15 min). NG-fluorescence signal is shown in grey and SiR-DNA signal (DNA) in red. Time in minutes (min) after anaphase onset. Endogenous Ect2 was depleted by RNAi.

3.4.5 Conclusion

We wanted to analyze the effect of different structural modifications on the function and regulation of Ect2. Therefore a genetic replacement system was established in HeLa cells (Buchner, 2019). To validate its functionality, it was first tested whether the integration of a wild-type transgene can compensate for the loss of endogenous Ect2 and shows similar regulation and localization.

In summary, it could be shown that the expression of Ect2^{WT} can fully rescue the cytokinetic failure evoked by Ect2 knockdown by RNAi. It can also restore normal furrow formation and ingression and showed only slightly increased Ect2 activity in meta- and anaphase. Moreover, Ect2^{WT} shows normal localization during meta- and anaphase. While it is absent from the membrane in metaphase, at anaphase onset Ect2^{WT} accumulates at the equatorial membrane and at the tips of overlapping midzone microtubules and resides at the midbody after the membrane had fully ingressed.

All these results demonstrated that the Ect2 replacement system in HeLa cells works and thus the analysis of the different domain contributions to Ect2 function and regulation in the absence of endogenous Ect2 was started. Except for the multinucleation assays, all analyses in the transgenic cell lines were exclusively done in the absence of endogenous Ect2. **In the following, Ect2 RNAi will not be mentioned each time in the text.**

3.5 Analyzing the contributions of each BRCT domain to Ect2 function and regulation

The canonical model of Ect2 regulation during cell division predicts that Ect2 activity is autoinhibited by an interaction of the N-terminal BRCT domains with the catalytic DH-PH domain. By binding of the BRCT domains to the phosphorylated centralspindlin component RacGAP1, this interaction is supposed to be released and Ect2 gets active (D'Avino et al., 2015; Green et al., 2012).

BRCT domains are specialized interaction domains, which can specifically recognize and bind phosphorylated peptides, DNA, and poly(ADP-ribose) (Leung & Glover, 2011). Ect2 had long been assumed to contain two BRCT domains (BRCT1 and BRCT2) that together form a so-called

tandem BRCT repeat (Kim et al., 2005; Tatsumoto et al., 1999). Tandem BRCT repeats exhibit a typical packing of both BRCT domains, which allows the cooperative binding of phosphorylated targets (Leung & Glover, 2011). BRCT1 and BRCT2 in Ect2, therefore, were thought to function as a unit to facilitate the binding of phosphorylated RacGAP1 and thereby the activation of Ect2. By solving the crystal structure of the N-terminus of Ect2, Zou et al. (2014) showed that BRCT1 and BRCT2 in Ect2 adopt a perpendicular orientation instead of a parallel conformation, which is characteristically found in canonical tandem-BRCT domains. Moreover, crystallization demonstrated the presence of an additional BRCT domain, BRCT0, at the very N-terminal end. Both findings contradict the canonical view of a tandem BRCT repeat in Ect2 and rather indicate that the BRCT domains in Ect2 feature a different mode of operation than initially assumed.

Due to the erroneous assumption that Ect2 contains a tandem BRCT repeat, little is known about the roles of the individual BRCT domains. Therefore, this study aimed to elucidate how each BRCT domain contributes to Ect2 function and regulation during cell division. The strategy was to modify the BRCT domains of Ect2 and to analyze how those modifications affect cytokinesis. For this purpose, several stable transgenic cell lines were used, most of which had been generated previously in the laboratory (Buchner, 2019). Those cell lines stably express Ect2 variants that either lack all or single BRCT domains or carry specific point mutations in BRCT domains, which have been previously reported to affect the functioning of the respective domain. Details will be explained in the respective chapters below.

3.5.1 The BRCT domains of Ect2 are essential for cytokinesis and inhibit GEF activity

Previous binding studies and structural data have shown that the N-terminal BRCT domains of Ect2 directly bind to the DH-GEF domain (Chen et al., 2020; Kim et al., 2005; Saito et al., 2004). It was suggested that the BRCT domains thereby inhibit Ect2 GEF activity, as the removal and the structural disruption of the BRCT domains resulted in increased GEF activity *in vitro* (Chen et al., 2020; Kim et al., 2005; Zou et al., 2014). Further support for Ect2 autoinhibition by the BRCT domains comes from experiments that artificially targeted the GEF domain to the membrane (Kotýnková et al., 2016) and overexpression studies of C- and N-terminal Ect2 fragments (Bement et al., 2015; Chan & Nance, 2013; Kim et al., 2005; Matthews et al., 2012;

Saito et al., 2004; Su et al., 2014; Su et al., 2011; Tatsumoto et al., 1999). However, apart from the role in Ect2 activity inhibition, the BRCT domains are also important for Ect2 function during cytokinesis. In previous studies, both, disrupting the BRCT2 domain (Kim et al., 2005) and deleting all BRCT domains (Matthews et al., 2012) rendered Ect2 incapable of rescuing cytokinetic failure in Ect2-depleted cells.

Although, these experiments provided valuable hints towards the function of the BRCT domains, in many of them Ect2 variants were overexpressed, which might lead to defects itself or might sequester binding partners, or were expressed in the presence of endogenous Ect2, which might compete with the Ect2 mutants and thus falsify the conclusions. In addition, *in vitro* experiments might not reflect the actual situation in cells and using an artificial membrane tether could introduce synergistic effects with the deletion of the BRCT domains. In contrast to that, our replacement system allows the analysis of Ect2 mutants, that are expressed at endogenous levels, after endogenous Ect2 was depleted by RNAi. This represents a major advantage over previous studies. Moreover, by using the replacement system it is possible to investigate the spatial and temporal aspects of Ect2 function throughout cell division in living cells.

Thus, the analysis was started by assessing the role of all BRCT domains in Ect2 function and regulation during cytokinesis in our replacement system. For this, a previously established Ect2 mutant cell line was used, in which all three BRCT domains (Ect2^{ΔBRCT0-2}) (Buchner, 2019) were deleted and the effects on cytokinetic success, furrow formation, and Ect2 activity regulation were examined.

Western blot analysis and subsequent signal quantification demonstrated that the expression levels of Ect2^{ΔBRCT0-2} do not differ from endogenous Ect2 levels (Table 19 and Figure 18 B). Thus, it was analyzed whether Ect2^{ΔBRCT0-2} supports successful cytokinesis after the depletion of endogenous Ect2 in multinucleation assays. Consistent with previous reports (Buchner, 2019) more than 65 % of Ect2^{ΔBRCT0-2} expressing cells failed cytokinesis and exhibited two or more nuclei (Figure 18) (% mononucleation p<0.001 compared to control and Ect2^{WT}, determined by Tukey's test). Although this phenotype resembled that of control cells depleted of endogenous Ect2, the latter showed a significantly stronger phenotype with 80 % of the cells failing cytokinesis (% mononucleation p<0.001 compared to Ect2^{ΔBRCT0-2}, determined by Tukey's test). For comparison, less than 5 % of the cells failed division in control cells. As

expected, Ect2 lacking all BRCT domains (Ect2^{ΔBRCT0-2}) appeared to be non-functional during cytokinesis and triggered the formation of bi- and multinucleated cells.

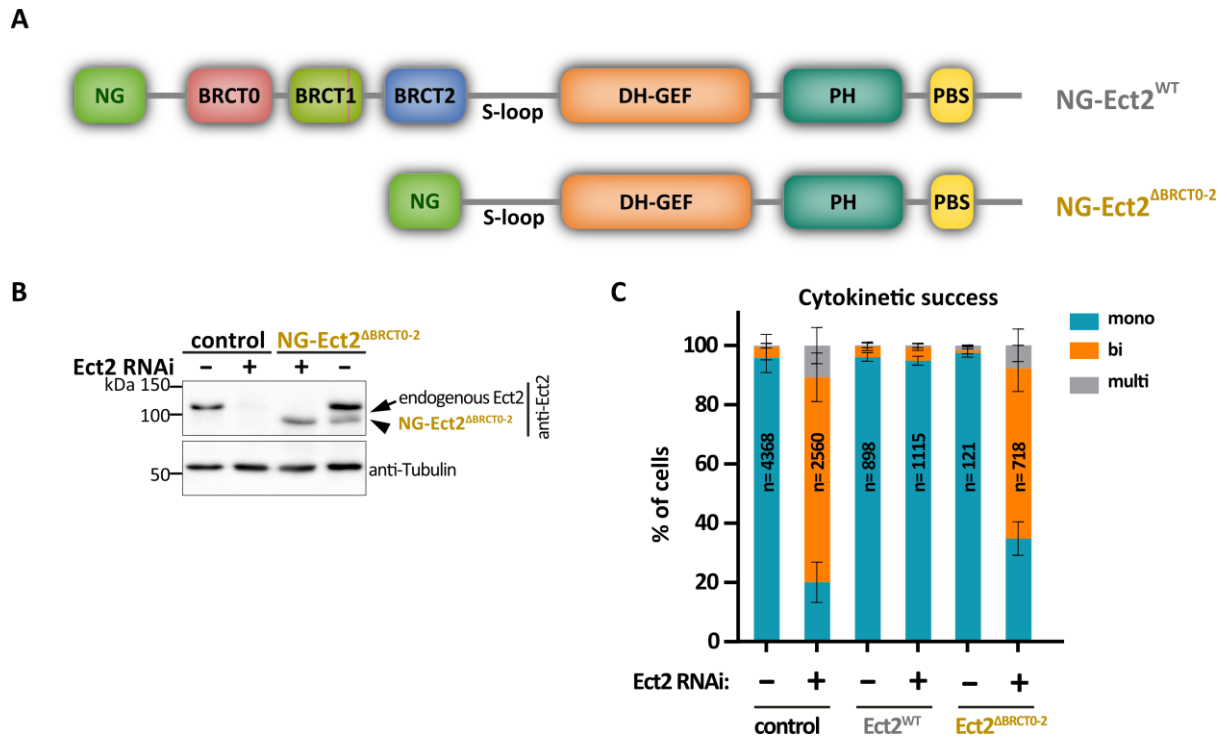


Figure 18: The BRCT domains in Ect2 are essential for cytokinesis. (A) Schematic representation showing the domain organization of the NG-tagged Ect2^{WT} and NG-Ect2^{ΔBRCT0-2} proteins. (B) Western blot analysis of lysates from control and NG-Ect2^{ΔBRCT0-2} cells treated with and without Ect2 RNAi to knock down endogenous Ect2. Blots were probed with anti-Ect2 and anti- α -tubulin (as loading control). Endogenous Ect2 has a molecular weight of 100.1 kDa and NG-Ect2^{ΔBRCT0-2} of 89.6 kDa. Image kindly provided by Friederike Wolff. (C) Percentages of mono-, bi- and multinucleated cells in control, Ect2^{WT}, and Ect2^{ΔBRCT0-2} cells treated with or without Ect2 RNAi to deplete endogenous Ect2. (n=number of cells, data from ≥ 2 independent experiments presented as mean \pm SD, data acquired by SS, KB, FW, EZ).

The high numbers of bi- and multinucleated Ect2^{ΔBRCT0-2} cells suggested problems in either furrow ingression or abscission. So next, it was examined whether Ect2^{ΔBRCT0-2} can form and ingress a cleavage furrow. Therefore, time-lapse movies of dividing cells were analyzed. As portrayed in Figure 19 A, Ect2^{ΔBRCT0-2} cells had difficulties to ingress the membrane. Given the equatorial cell width 12 min after AOS of 12.2 μ m, they were significantly slower than control and Ect2^{WT} cells (4.7 μ m and 4.4 μ m, respectively) (Figure 19 B). However, the defect in furrow ingression seen in Ect2^{ΔBRCT0-2} cells was milder than that of Ect2-depleted control cells (16.7 μ m). Even though cleavage furrow ingression occurred in Ect2^{ΔBRCT0-2} cells, the furrow often regressed later on, which gave rise to binucleated cells. Moreover, probably due to the slower furrow ingression, in some ingressing cells, one nucleus could slip into the opposite

half of the cell, which again led to binucleated cells (data not shown). This phenomenon was afterwards often accompanied by regression of the cleavage furrow. These observations explained why we saw such a high percentage of cytokinetic failure in the multinucleation assay, even though the cells could partially ingress. All in all, these results showed that the BRCT domains are needed for proper furrow formation and ingression and successful cytokinesis.

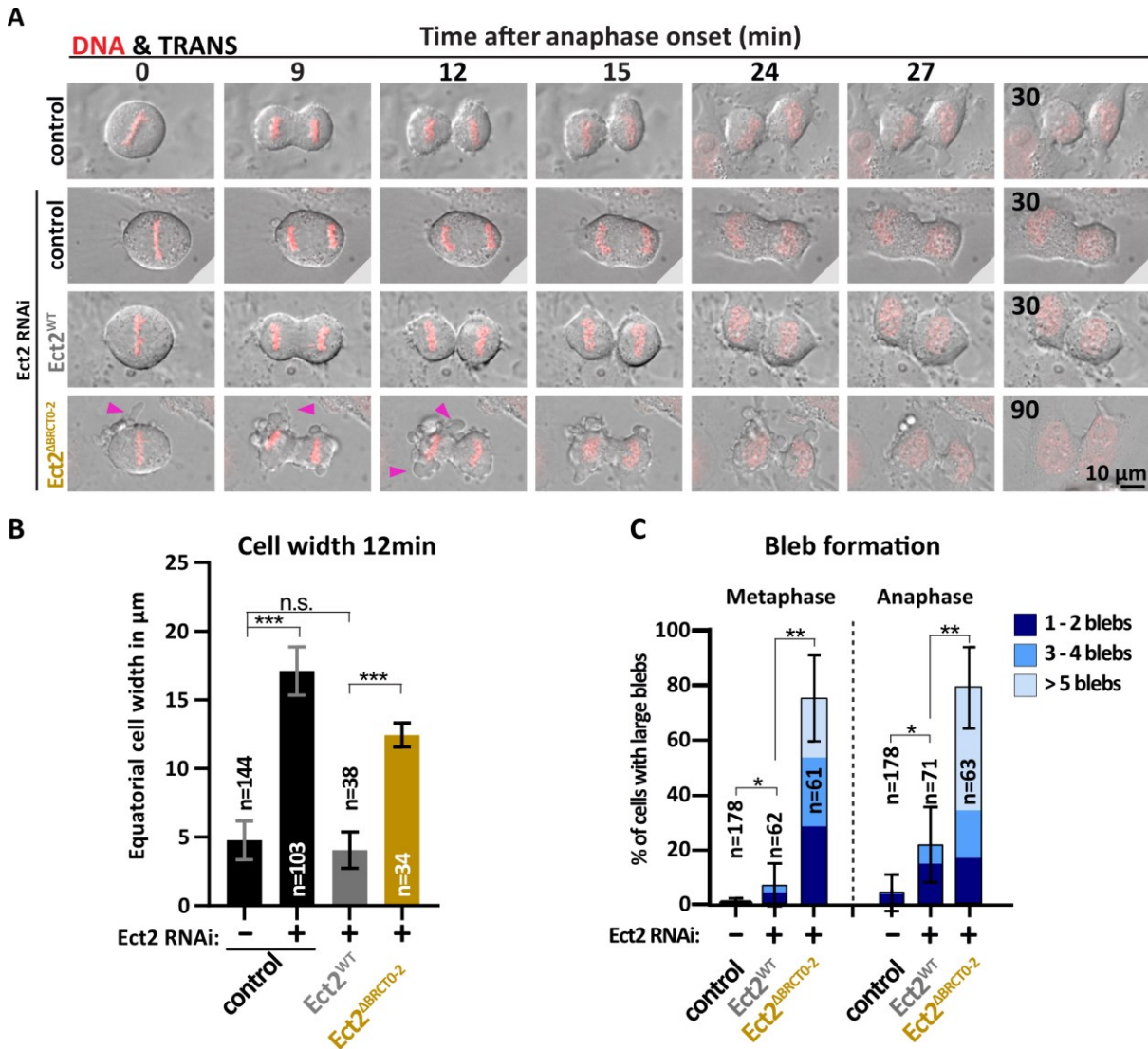


Figure 19: Deletion of the BRCT domains delays furrow ingression and increases Ect2 activity. (A) Representative live-cell image sequences of dividing control, Ect2-depleted control, Ect2^{WT}, and Ect2^{ΔBRCT0-2} cells. Endogenous Ect2 was depleted by RNAi as indicated. DNA was probed with SiR-DNA. Time in minutes after anaphase onset. Large blebs are indicated by pink arrowheads. (B) Equatorial cell width in μm measured 12 min after anaphase onset for controls, Ect2^{WT}, and Ect2^{ΔBRCT0-2} cells. Endogenous Ect2 was depleted by RNAi as indicated (n=number of cells, data from ≥2 independent experiments presented as mean ± SD, ***p<0.001 and n.s.=not significant determined by Tukey's test). (C) Percentages of control, Ect2^{WT}, and Ect2^{ΔBRCT0-2} cells, which formed 1-2, 3-4, and >5 large blebs during meta- and

anaphase. Endogenous Ect2 was depleted by RNAi as indicated. (n=number of cells, data from ≥ 3 independent experiments presented as mean, SD for total blebbing, * $p < 0.05$ and ** $p < 0.01$ determined by Kruskal Wallis test for control and Ect2^{WT} and student's t-test for Ect2^{WT} and Ect2 ^{Δ BRCT0-2}, data acquired by SS).

Strikingly, during live-cell imaging most Ect2 ^{Δ BRCT0-2} cells exhibited large membrane blebs in meta- (74.7 %) and anaphase (78.4 %), which strongly differs from Ect2^{WT} (6.6 % and 16.3 %) (Figure 19 C). In Figure 19 A large membrane blebs are indicated by pink arrowheads. Counting the number of blebs formed by each cell, revealed that over 70 % of blebbing cells exhibited three or more blebs in meta- and anaphase (Figure 19 C). Consistent with previous *in vitro* experiments (Chen et al., 2020) and artificial membrane targeting (Kotýnková et al., 2016), we found that the loss of all three BRCT domains leads to the hyperactivation of Ect2.

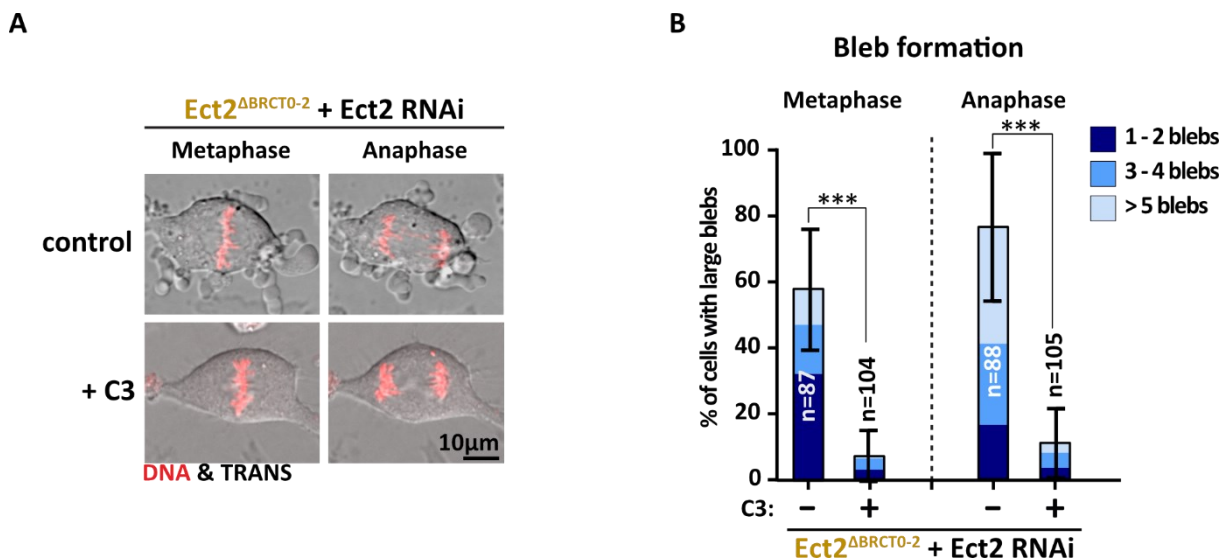


Figure 20: Large bleb formation in Ect2 ^{Δ BRCT0-2} is efficiently blocked by the inhibition of RhoA activity. (A) Live-cell images of control and exoenzyme C3-treated Ect2 ^{Δ BRCT0-2} cells depleted of endogenous Ect2 in meta- and anaphase. DNA was probed with SiR-DNA. (B) Percentages of control and exoenzyme C3-treated Ect2 ^{Δ BRCT0-2} cells, which formed 1-2, 3-4, and >5 large blebs during meta- and anaphase. Endogenous Ect2 was depleted by RNAi. (n=number of cells, data from 3 independent experiments presented as mean, \pm SD for total blebbing, *** $p < 0.001$ determined by Tukey's test).

Increased RhoA activity can be a consequence of hyperactive Ect2 and was shown to elicit large bleb formation (Zanin et al., 2013). Thus, the RhoA inhibitor exoenzyme C3 was added to Ect2 ^{Δ BRCT0-2} cells to test whether membrane blebbing is prevented. Indeed, after the treatment with exoenzyme C3, significantly fewer Ect2 ^{Δ BRCT0-2} cells formed membrane blebs during meta- (6.9 % instead of 57.5 %) and anaphase (11.3 % instead of 76.8 %), and in general, cells treated with exoenzyme C3 exhibited fewer blebs (Figure 20). This result

showed, that when the inhibiting BRCT domains are missing ($Ect2^{\Delta BRCT0-2}$), increased RhoA activation triggers the excessive formation of large blebs.

In summary, the deletion of the BRCT domains led to high levels of multinucleation. Time-lapse imaging revealed delayed ingression of the furrow, which eventually regressed and left cells binucleated. Moreover, it elicited the formation of large membrane blebs that were triggered by the hyperactivation of RhoA by Ect2 missing the BRCT domains. Consistent with the literature, our data indicate that the BRCT domains exercise two functions: (I) they negatively regulate Ect2 activity, and (II) they promote the completion of cytokinesis. So next we tried to decipher, which specific BRCT domain is required for each function.

3.5.2 The BRCT0 domain is not essential for cytokinesis but supports robust furrow ingression

Using database search, in 2011 Ect2 has already been predicted to have a third BRCT domain, which is located before the BRCT1 domain at the N-terminus of Ect2 (Sheng et al., 2011). Then, some years later, crystallization and subsequent structural analysis of the Ect2 N-terminus confirmed the presence of a third BRCT domain (Zou et al., 2014). It turns out that the BRCT0 domain has the least typical sequence of all three BRCT domains in Ect2 and also exhibits a broader variability between species from an evolutionary perspective (Zou et al., 2014). This would explain why it had been identified so late. So far, the role of the BRCT0 domain for Ect2 function and regulation has not been investigated and this prompted us to examine the effects of BRCT0 deletion on cytokinesis.

For this, the previously established cell line expressing $Ect2^{\Delta BRCT0}$ was used (Buchner, 2019). Western blot analysis and subsequent quantification revealed that $Ect2^{\Delta BRCT0}$ was expressed similarly to endogenous Ect2 (Table 19 and Figure 21 B) and hence it was tested whether cells can successfully divide without the BRCT0 domain. Cells that lacked BRCT0 did not show a high failure rate during cytokinesis given that 86.1 % of cells were mononucleated in the multinucleation assay (Figure 21) (also shown by Buchner, 2019) (% mononucleation $p < 0.001$ compared to control and $p < 0.01$ compared to $Ect2^{WT}$, determined by Tukey's test). Hence, $Ect2^{\Delta BRCT0}$ was able to rescue the cytokinetic failure phenotype triggered by the depletion of endogenous Ect2 by RNAi (80 % bi- and multinucleation). Given that $Ect2^{\Delta BRCT0}$ can rescue the

depletion of endogenous Ect2, the BRCT0 domain seems dispensable for Ect2 functioning during cytokinesis.

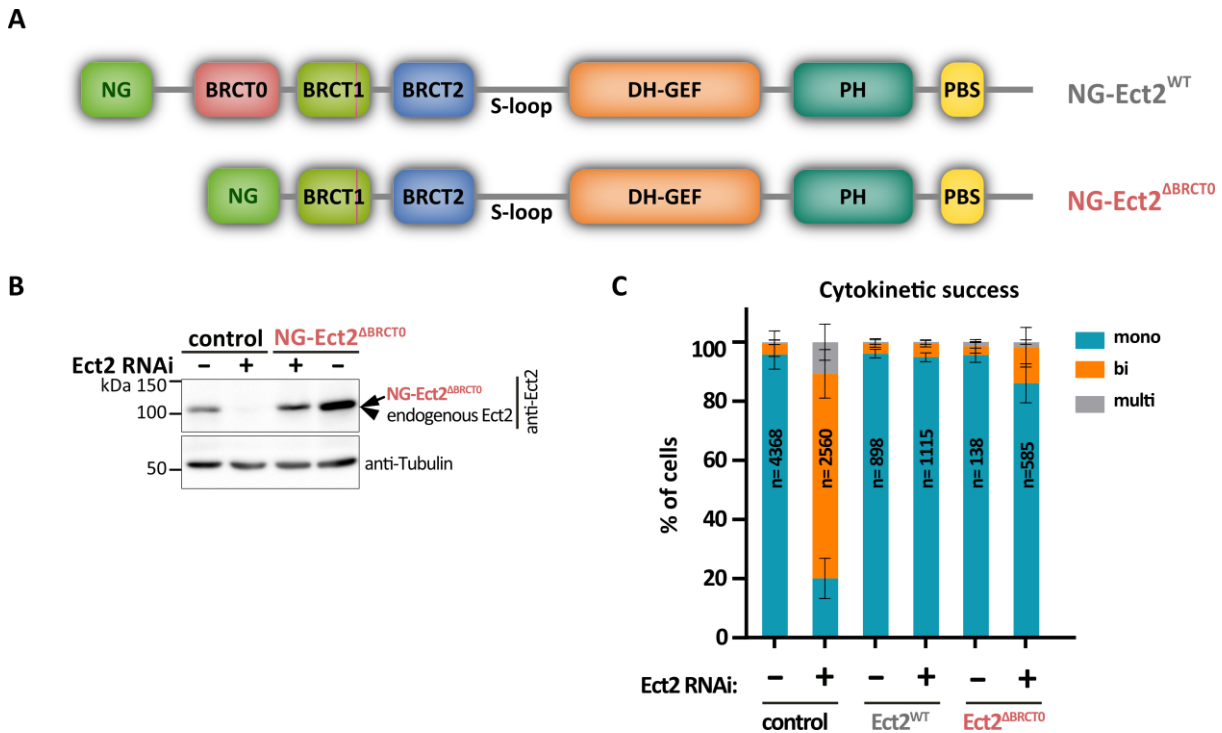


Figure 21: BRCT0 is not essential for cytokinesis. (A) Schematic representation showing the domain organization of the NG-tagged Ect2^{WT} and NG-Ect2^{ΔBRCT0} proteins. (B) Western blot analysis of lysates from control and NG-Ect2^{ΔBRCT0} cells treated with and without Ect2 RNAi to knock down endogenous Ect2. Blots were probed with anti-Ect2 and anti- α -tubulin (as loading control). Endogenous Ect2 has a molecular weight of 100.1 kDa and NG-Ect2^{ΔBRCT0} of 111.7 kDa. Image kindly provided by Friederike Wolff. (C) Percentages of mono-, bi- and multinucleated cells in control, Ect2^{WT}, and Ect2^{ΔBRCT0} cells treated with or without Ect2 RNAi to deplete endogenous Ect2. (n=number of cells, data from ≥ 2 independent experiments presented as mean \pm SD, data acquired by SS, KB, FW, EZ).

According to the results from the multinucleation assay, Ect2^{ΔBRCT0} cells managed cell division successfully. Thus, it was predicted that cells lacking BRCT0 can form a cleavage furrow, but whether the furrow ingresses as efficiently as it does in control and Ect2^{WT} cells was not known. So next cleavage furrow ingression in living Ect2^{ΔBRCT0} cells was analyzed by time-lapse imaging. As can be seen in Figure 22 A, Ect2^{ΔBRCT0} cells appeared to ingress slower than control and Ect2^{WT} cells. Measuring the equatorial cell width 12 min after anaphase onset confirmed that Ect2^{ΔBRCT0} (7.8 μ m) cells show a slight delay in furrow ingression as compared to control and Ect2^{WT} cells, which exhibited a width of 4.7 μ m and 4.4 μ m, respectively (Figure 22 B). Even though, the BRCT0 domain is not critical for cytokinesis it appears to support timely cleavage furrow formation and ingression.

During live-cell imaging it got apparent, that a few $Ect2^{ABRCTO}$ cells exhibited large membrane blebs. Counting the membrane blebs formed by each cell revealed that in the absence of BRCTO ($Ect2^{ABRCTO}$) 21.4 % and 36.0 % of cells showed membrane blebbing in meta- and anaphase, respectively, as compared to 6.6 % and 16.3 % in $Ect2^{WT}$ (Figure 22 C). Worth mentioning is that blebbing cells in meta- and anaphase mainly formed 1-2 blebs (14.6 % and 22.8 % of total cells). Even though $Ect2^{ABRCTO}$ showed higher blebbing rates compared to $Ect2^{WT}$, the difference was statically not significant.

Taken together, the results let us conclude that BRCTO is not essential for cytokinesis but helps to timely form and ingress the furrow. Moreover, given the low levels of membrane blebbing in $Ect2^{ABRCTO}$, the inhibiting action exerted by the N-terminal BRCT domains must primarily rely on domains other than BRCTO.

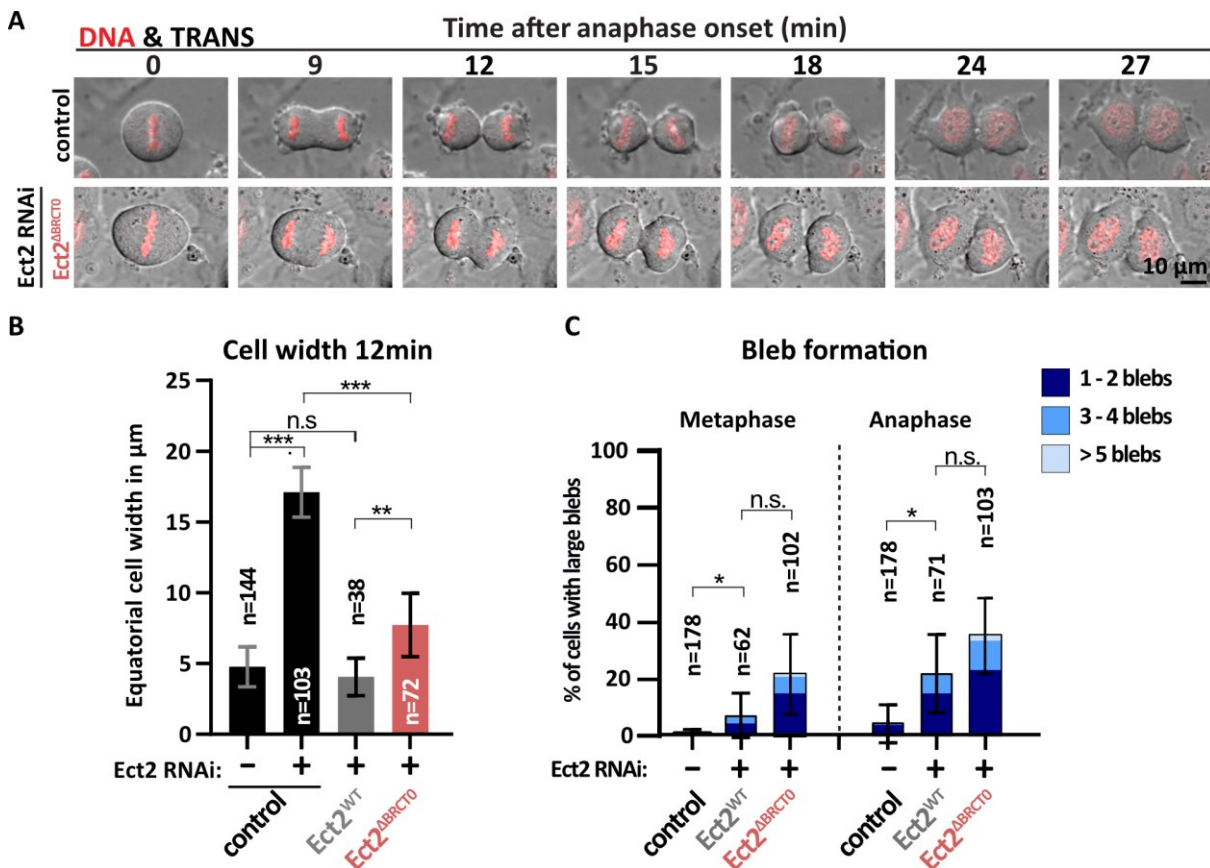


Figure 22: Deletion of BRCTO slightly delays furrow ingression and slightly increases $Ect2$ activity. (A) Representative live-cell image sequences of dividing control and $Ect2^{ABRCTO}$ cells. Endogenous $Ect2$ was depleted by RNAi as indicated. DNA was probed with SiR-DNA. Time in minutes after anaphase onset. (B) Equatorial cell width in μm measured 12 min after anaphase onset for controls, $Ect2^{WT}$ and $Ect2^{ABRCTO}$ cells. Endogenous $Ect2$ was depleted by RNAi as indicated. (n=number of cells, data from ≥ 4 independent experiments presented as mean \pm SD, *** $p < 0.001$, ** $p < 0.01$ and n.s.=not significant determined by Tukey's test) (C)

Percentages of control, Ect2^{WT} and Ect2^{ΔBRCT0} cells, which formed 1-2, 3-4, and >5 large blebs during meta- and anaphase. Endogenous Ect2 was depleted by RNAi as indicated. (n=number of cells, data from ≥4 independent experiments presented as mean, SD for total blebbing, *p<0.05, n.s.=not significant determined by Kruskal Wallis test for control and Ect2^{WT} and by Kruskal Wallis and student's t-test in meta- and anaphase, respectively, for Ect2^{WT} and Ect2^{ΔBRCT0}, data acquired by SS).

3.5.3 The BRCT1 domain is required for furrow ingression and successful cytokinesis

At the onset of anaphase, Ect2 is recruited to the central spindle by binding to the centralspindlin component RacGAP1 (Somers & Saint, 2003; Yüce et al., 2005). This interaction depends on Plk1-mediated phosphorylation of RacGAP1 at the N-terminus (Burkard et al., 2009; Petronczki et al., 2007; Yüce et al., 2005). Phosphorylated RacGAP1 binds to the N-terminal BRCT domains of Ect2 and two residues (T153 and K195) located in the BRCT1 domain have been reported to be crucial for this interaction (Wolfe et al., 2009; Zou et al., 2014). Mutating these residues (T153A and K195M) strongly impaired the interaction of RacGAP1 with N-terminal Ect2 in binding studies (Wolfe et al., 2009; Zou et al., 2014) and abolished the recruitment of transiently expressed N-terminal Ect2 (Wolfe et al., 2009) or full-length Ect2 (Kotýnková et al., 2016) to the midzone. Furthermore, several studies have suggested that the Ect2-RacGAP1 interaction is required for cleavage furrow positioning and ingression (Burkard et al., 2009; Petronczki et al., 2007; Su et al., 2011; Wolfe et al., 2009; Yüce et al., 2005). This has placed the BRCT1 domain at the center of the canonical model of Ect2 activation, which assumes that the interaction of phosphorylated RacGAP1 with the BRCT1 domain releases Ect2 autoinhibition. This canonical model has been challenged by the findings of Kotýnková et al. (2016). They have demonstrated that cells, in which Ect2-RacGAP1 interaction is abolished (Ect2^{T153A + K195M}) can successfully divide. This finding suggested that Ect2 is activated by a different mechanism than BRCT1-RacGAP1 binding.

As the importance of the BRCT1 domain for Ect2 function and regulation has been controversial throughout the years, two Ect2 mutant cell lines had previously been generated (Buchner, 2019), one where the entire BRCT1 domain was deleted (Ect2^{ΔBRCT1}) and one where two point mutations were introduced into the BRCT1 domain (Ect2^{T153A + K195M}) shown to block RacGAP1 binding (Wolfe et al., 2009). Cells of the initial Ect2^{ΔBRCT1} cell line exhibited lower expression levels compared to endogenous Ect2, which is why Dr. Kristina Buchner had

identified wild-type-like expressing cells by fluorescence-activated cell sorting (FACS) and partially analyzed one of the resulting monoclonal cell lines. Unfortunately, the FACS sorted cell lines were not deposited to the lab database, and thus FACS sorting had to be conducted once again to obtain monoclonal Ect2^{ΔBRCT1} cell lines with good transgene expression levels (performed together with Dr. Lisa Richter at CFFlowCyt). Several monoclonal cell lines could be established and two of them were newly analyzed in parallel.

Quantification of immunoblots confirmed that all three cell lines (Ect2^{ΔBRCT1} clone 1 + clone 2 and Ect2^{T153A + K195M}) express the mutant Ect2 transgenes similarly to endogenous Ect2 (Table 19 and Figure 23 B). As clones 1 and 2 showed similar results in all experiments their data were pooled and will be presented as one in the following.

In the multinucleation assays mutating the residues T153 and K195, consistent with previous reports (Buchner, 2019; Kotýnková et al., 2016), did not have a strong impact on the success of cytokinesis (81.4 % mononucleation) (% mononucleation $p < 0,001$ compared to control and $p < 0.01$ compared to Ect2^{WT}, determined by Tukey's test) (Figure 23). Contrary to that deleting the entire BRCT1 domain (both FACS-sorted cell lines) resulted in a strong cytokinetic defect comparable to the loss of Ect2 in control cells, leaving 78.2 % of cells multinucleated (consistent with Buchner, 2019) (% mononucleation $p < 0,001$ compared to control and Ect2^{WT} and not significant compared to control+Ect2 RNAi, determined by Tukey's test). We found that while the BRCT1-RacGAP1 interaction does not seem to be required for successful cytokinesis, the BRCT1 domain itself is essential for cells to divide.

The high numbers of multinucleated cells after the loss of BRCT1 suggested defects either during the formation and/or ingression of the cleavage furrow or during abscission. Time-lapse imaging revealed that Ect2^{ΔBRCT1} cells neither could form a furrow nor showed furrow ingression (Figure 24 A), which led to an equatorial cell width 12 min after anaphase of 15.7 μm as compared to 4.7 μm and 4.4 μm in control and Ect2^{WT}, respectively (Figure 24 B). Comparison with the width measured in control cells depleted of Ect2 (16.7 μm), revealed that loss of BRCT1 has a similarly strong effect on furrow ingression. As the results obtained in the multinucleation assay had suggested, furrow ingression of Ect2^{T153A + K195M} cells looked similar to that of control cells (Figure 24 A). Measuring the equatorial cell width 12 min after anaphase onset further confirmed that Ect2^{T153A + K195M} (5.8 μm) cells do not ingress significantly slower than control (4.7 μm) and Ect2^{WT} (4.4 μm) cells (Figure 24 B). These results

again supported the idea that the BRCT1-RacGAP1 interaction is not critical for normal Ect2 function, whereas the BRCT1 domain itself is indispensable.

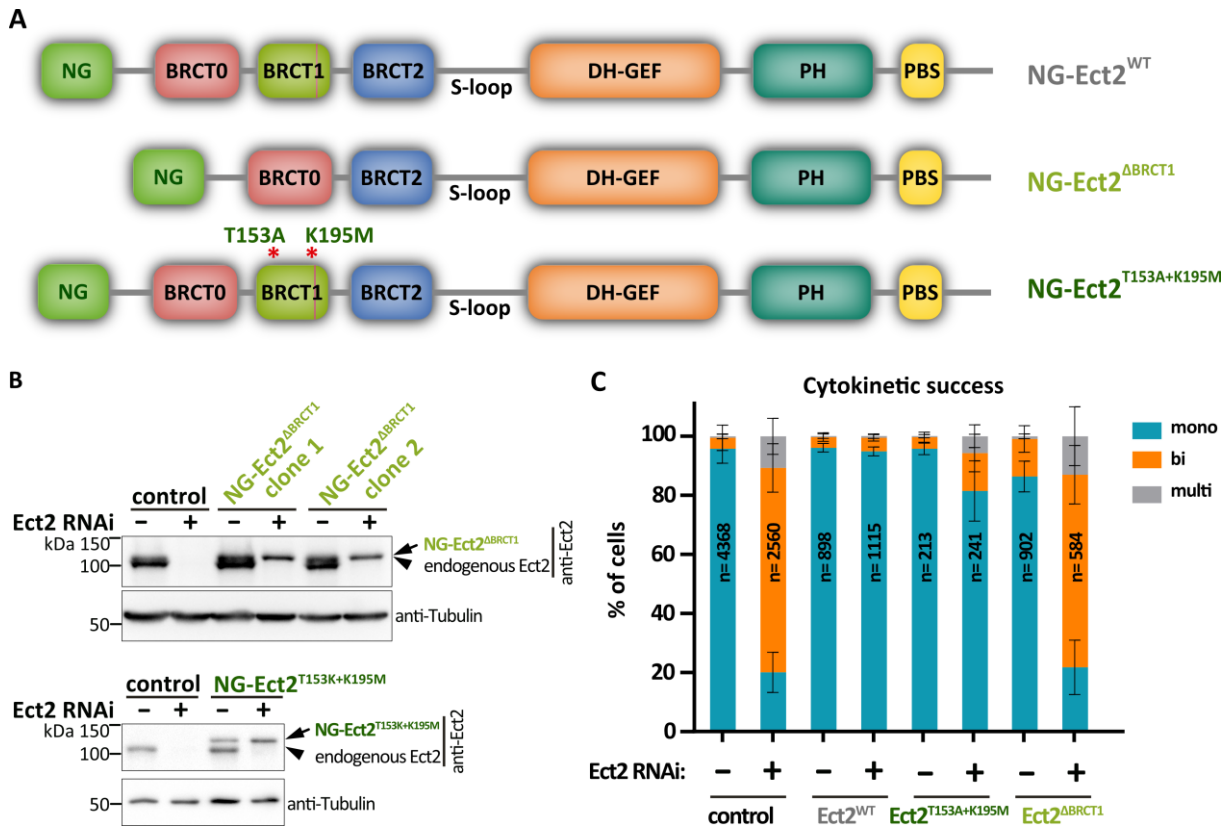


Figure 23: BRCT1 is essential for cytokinesis. (A) Schematic representation showing the domain organization of the NG-tagged Ect2^{WT}, NG-Ect2^{ΔBRCT1}, and NG-Ect2^{T153A+K195M} proteins. Point mutations are indicated by asterisks. (B) Western blot analysis of lysates from control, NG-Ect2^{ΔBRCT1}, and NG-Ect2^{T153A+K195M} cells treated with and without Ect2 RNAi to knock down endogenous Ect2. For NG-Ect2^{ΔBRCT1} two monoclonal cell lines (clone 1 and clone 2) were analyzed. Blots were probed with anti-Ect2 and anti- α -tubulin (as loading control). Endogenous Ect2 has a molecular weight of 100.1 kDa, NG-Ect2^{ΔBRCT1} of 115.2 kDa, and NG-Ect2^{T153A+K195M} of 127.0 kDa. NG-Ect2^{T153A+K195M} kindly provided by Friederike Wolff. (C) Percentages of mono-, bi- and multinucleated cells in control, Ect2^{WT}, Ect2^{ΔBRCT1}, and Ect2^{T153A+K195M} cells treated with or without Ect2 RNAi to deplete endogenous Ect2. Ect2^{ΔBRCT1} represents pooled data of clone 1 and clone 2. (n=number of cells, data from ≥ 3 independent experiments presented as mean \pm SD, data acquired by SS, KB, FW, EZ).

As expected, live-cell imaging revealed that neither the deletion of the BRCT1 domain nor the introduction of the point mutations triggers Ect2 hyperactivation (Figure 24 A and C). In meta- and anaphase, the percentages of cells that formed large membrane blebs in Ect2^{ΔBRCT1} (1.6 % and 23.1 %) and Ect2^{T153A + K195M} (1.5 % and 10.5 %) were comparable to Ect2^{WT} (6.6 % and 16.3 %). Moreover, the cells which formed blebs primarily exhibited less than 5 blebs.

anaphase onset. Control was reproduced from Figure 22 A (B) Equatorial cell width in μm measured 12 min after anaphase onset for controls, Ect2^{WT}, Ect2 ^{Δ BRCT1}, and Ect2^{T153A+K195M} cells. Endogenous Ect2 was depleted by RNAi as indicated. (n=number of cells, data from ≥ 3 independent experiments presented as mean \pm SD, ***p<0.001, n.s.=not significant determined by Tukey's test) (C) Percentages of control, Ect2^{WT}, Ect2 ^{Δ BRCT1}, and Ect2^{T153A+K195M} cells, which formed 1-2, 3-4, and >5 large blebs during meta- and anaphase. Endogenous Ect2 was depleted by RNAi as indicated. (n=number of cells, data from ≥ 3 independent experiments presented as mean, SD for total blebbing, *p<0.05, n.s.=not significant determined by Kruskal Wallis test for control and Ect2^{WT}, for Ect2^{WT} and Ect2 ^{Δ BRCT1} and Ect2^{T153A+K195M} by Kruskal Wallis and student's t-test in meta- and anaphase, respectively, data acquired by SS).

3.5.4 The BRCT2 domain inhibits Ect2 activity and is required for successful cytokinesis

For a long time, the BRCT2 domain has been believed to form a canonical tandem BRCT-repeat with the N-terminally located BRCT1 domain. The BRCT domains of a tandem BRCT-pair are considered to function as a unit and the central role in peptide binding is ascribed to the N-terminally located domain (which would be BRCT1) (Leung & Glover, 2011). That is why research focused on investigating the functionality of either both BRCT domains together or the BRCT1 domain. With the solving of the crystal structure of Ect2 in 2014 by Zou et al., it became obvious that Ect2 features three instead of two BRCT domains and that the conformational set-up of the BRCT1 and the BRCT2 domain is very different from that exhibited by tandem BRCT domains (Zou et al., 2014). Therefore, the view on how the BRCT domains work to regulate and trigger Ect2 activity had to be reconsidered. As a consequence, an Ect2 mutant cell line missing the BRCT2 domain (Ect2 ^{Δ BRCT2}) had been previously generated in our laboratory (Buchner, 2019). During the course of the here presented study, novel structural data (Chen et al., 2020) revealed that the BRCT2 domain is in direct contact with the catalytic DH-PH domain and that this interaction can be disrupted by mutating residue W307 in the BRCT2 domain to alanine. That is why another BRCT2 mutant was generated comprising the W307A mutation (Ect2^{W307A}).

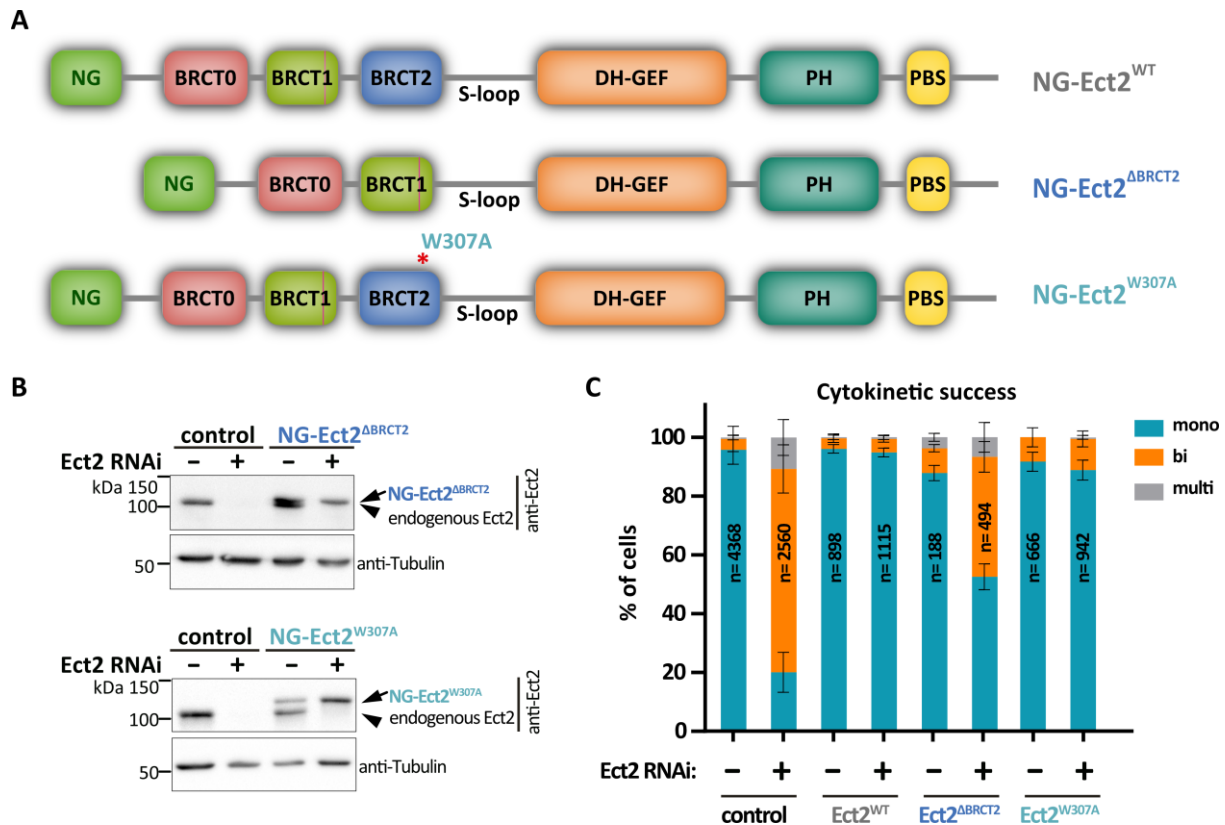


Figure 25: BRCT2 is partially required for cytokinesis. (A) Schematic representation showing the domain organization of the NG-tagged Ect2^{WT}, NG-Ect2^{ΔBRCT2}, and NG-Ect2^{W307A} proteins. The point-mutation is indicated by an asterisk. (B) Western blot analysis of lysates from control, NG-Ect2^{ΔBRCT2}, and NG-Ect2^{W307A} cells treated with and without Ect2 RNAi to knock down endogenous Ect2. Blots were probed with anti-Ect2 and anti- α -tubulin (as loading control). Endogenous Ect2 has a molecular weight of 100.1 kDa, NG-Ect2^{ΔBRCT2} of 116.5 kDa, and NG-Ect2^{W307A} of 127.0 kDa. Images kindly provided by Friederike Wolff. (C) Percentages of mono-, bi- and multinucleated cells in control, Ect2^{WT}, Ect2^{ΔBRCT2}, and Ect2^{W307A} cells treated with or without Ect2 RNAi to deplete endogenous Ect2. (n=number of cells, data from ≥ 2 independent experiments presented as mean \pm SD, data acquired by SS, KB, FW, EZ).

The function of the BRCT2 domain during cytokinesis was determined by analyzing Ect2^{ΔBRCT2} and Ect2^{W307A} cells. Quantification of immunoblots showed that both transgenic proteins are expressed to endogenous levels (Table 19 and Figure 25 B).

Consistent with a previous report from our laboratory (Buchner, 2019), deletion of the BRCT2 domain resulted in a partial rescue phenotype in the multinucleation assay. 52.5 % of the cells were mononucleated and 47.5 % were bi- and multinucleated (% mononucleation $p < 0.001$ compared to control and Ect2^{WT}, determined by Tukey's test). Ect2^{W307A} cells showed no increase in multinucleation and the percentage of mononucleated cells (88.9 %) was comparable to control and Ect2^{WT} cells (% mononucleation not significant compared to control

and Ect2^{WT}, determined by Tukey's test) (Figure 25). Thus, Ect2^{ΔBRCT2} is considered partially and Ect2^{W307A} fully functional during cytokinesis.

Next, furrow ingression was analyzed in these cell lines. During time-lapse imaging, Ect2^{ΔBRCT2} and Ect2^{W307A} cells had problems to ingress on time and most of them formed several large membrane blebs. Exemplary image sequences are shown in Figure 26 A and large membrane blebs are indicated by pink arrowheads. Measuring the equatorial width 12 min after anaphase onset confirmed that Ect2^{ΔBRCT2} and Ect2^{W307A} cells both were delayed in furrow ingression compared to control (4.7 μm) and Ect2^{WT} (4.4 μm), respectively (Figure 26 B). With a width of 12.5 μm, Ect2^{ΔBRCT2} cells were significantly slower than Ect2^{W307A} cells, which exhibited a width of 8.6 μm. However, in comparison to control cells depleted of Ect2 (16.7 μm), both cell lines were able to ingress faster (Figure 26 B).

Quantification of membrane blebbing revealed that in metaphase 67.5 % and anaphase 87.5 % of Ect2^{ΔBRCT2} cells formed large membrane blebs. Moreover, most of the blebbing cells exhibited three or more blebs (more than 70 % of blebbing cells). Similar results were obtained for Ect2^{W307A}, where 56.9 % and 73.3 % of cells in meta- and anaphase, respectively, formed large membrane blebs. Again, most cells showed more than three blebs (more than 75 % of blebbing cells). When compared to the low blebbing levels seen in Ect2^{WT} (6.6 % metaphase and 16.3 % anaphase), these results clearly showed that deletion of BRCT2 and mutation W307A lead to the hyperactivation of Ect2. Moreover, the blebbing phenotype of Ect2^{ΔBRCT2} and Ect2^{W307A} was similar to the one found in Ect2^{ΔBRCT0-2}. Thus, we concluded that the BRCT2 domain inhibits Ect2 GEF activity during mitosis by binding the catalytic center with its W307 residue.

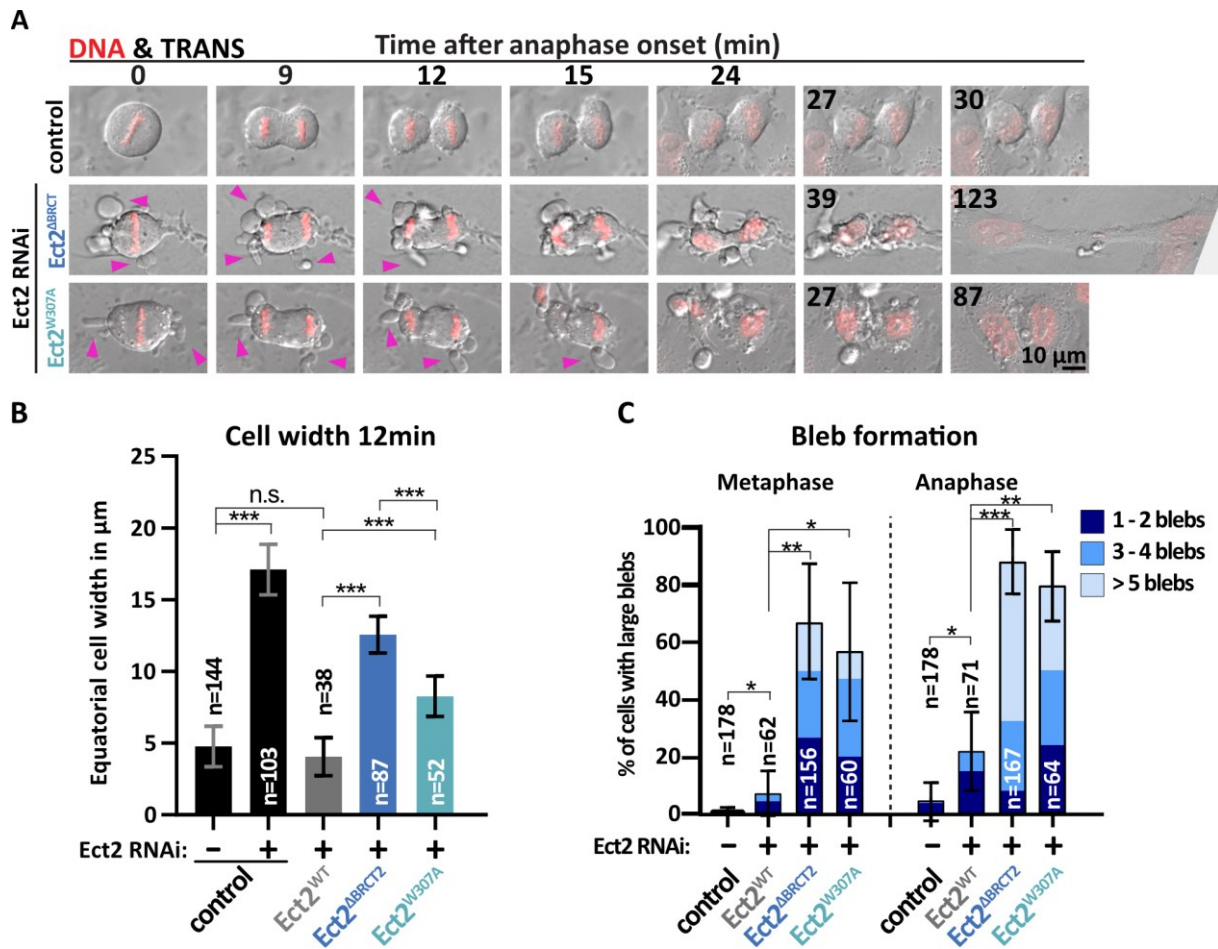


Figure 26: Deletion of BRCT2 and mutation W307A in the BRCT2 domain result in delayed furrow ingression and the formation of large membrane blebs. (A) Representative live-cell image sequences of dividing control, Ect2^{ΔBRCT2}, and Ect2^{W307A} cells. Endogenous Ect2 was depleted by RNAi as indicated. Large blebs are indicated with pink arrow heads. DNA was probed with SiR-DNA. Time in minutes after anaphase onset. (B) Equatorial cell width in μm measured 12 min after anaphase onset for controls, Ect2^{WT}, Ect2^{ΔBRCT2}, and Ect2^{W307A} cells. Endogenous Ect2 was depleted by RNAi as indicated. (n=number of cells, data from ≥3 independent experiments presented as mean ± SD, ***p<0.001, n.s.=not significant determined by Tukey's test) (C) Percentages of control, Ect2^{WT}, Ect2^{ΔBRCT2}, and Ect2^{W307A} cells, which formed 1-2, 3-4, and >5 large blebs during meta- and anaphase. Endogenous Ect2 was depleted by RNAi as indicated. (n=number of cells, data from ≥3 independent experiments presented as mean, SD for total blebbing, ***p<0.001, **p<0.01, *p<0.05, determined by Kruskal Wallis test for control and Ect2^{WT} and with student's t-test for the rest, data acquired by SS).

Increased RhoA activity was shown to be the cause of large bleb formation during mitosis (Zanin et al., 2013). To show once again that excessive membrane blebbing is caused by insufficient regulation of Ect2 activity, bleb formation in Ect2^{ΔBRCT2} expressing cells was suppressed by adding the RhoA inhibitor exoenzyme C3. As above shown for the deletion of all BRCT domains (Ect2^{ΔBRCT0-2}) (Figure 20), exoenzyme C3 efficiently reduced membrane

blebbing in $Ect2^{\Delta BRCT2}$ cells from 64.1 % to 9.9 % in metaphase and from 83.3 % to 17.4 % in anaphase, respectively (Figure 27). However, the proportions of cells forming 1-2, 3-4, and >5 blebs, respectively, stayed similar with and without exoenzyme C3 (Figure 27 B). These results demonstrated that excessive membrane blebbing is elicited by hyperactive RhoA as a consequence of mis-regulated GEF activity in $Ect2^{\Delta BRCT2}$.

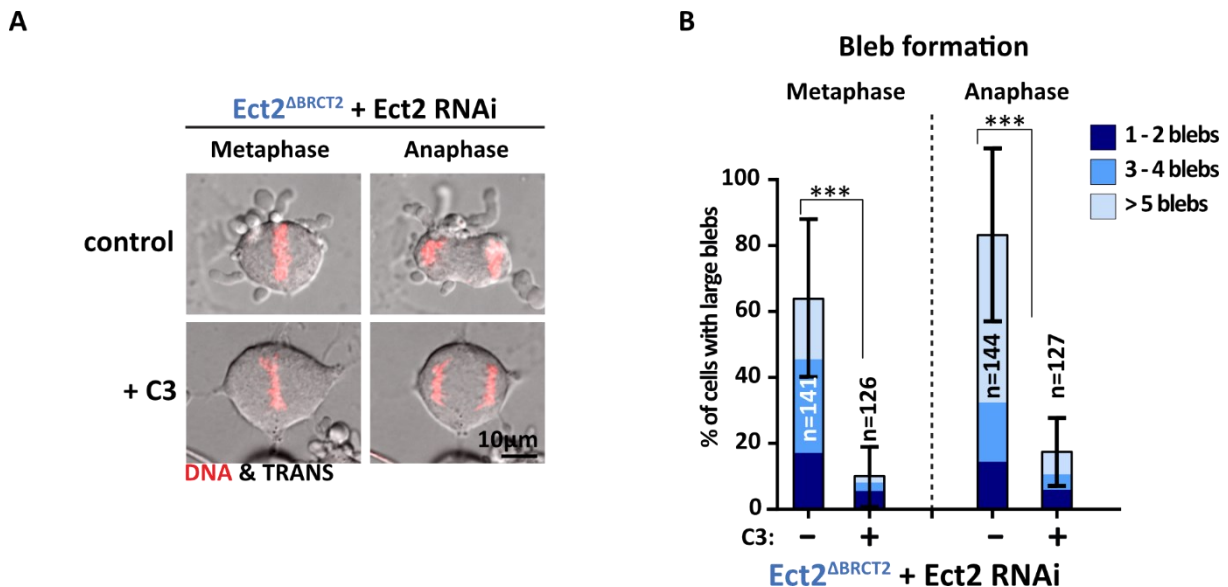


Figure 27: Large bleb formation in $Ect2^{\Delta BRCT2}$ is efficiently blocked by the inhibition of RhoA activity. (A) Live-cell images of control and exoenzyme C3-treated $Ect2^{\Delta BRCT2}$ cells depleted of endogenous Ect2 in meta- and anaphase. DNA was probed with SiR-DNA (B) Percentages of control and exoenzyme C3-treated $Ect2^{\Delta BRCT2}$ cells, which formed 1-2, 3-4, and >5 large blebs during meta- and anaphase. Endogenous Ect2 was depleted by RNAi. (n=number of cells, data from 3 independent experiments presented as mean, \pm SD for total blebbing, *** $p < 0.001$ determined by Tukey's test).

To summarize, we found that deleting the entire BRCT2 domain led to increased multinucleation, impaired furrow formation, and excessive membrane blebbing in meta- and anaphase. Mutating residue W307 to alanine elicited a similarly strong blebbing phenotype, however, furrow ingression was faster than in $Ect2^{\Delta BRCT2}$ but still slower compared to control. Most importantly, it did not result in multinucleation. This led to two conclusions: (I) the BRCT2 domain blocks Ect2 GEF activity and for this W307 residue is critical, and (II) the BRCT2 domain holds a second, yet unknown function, which is required for cytokinesis to occur normally.

3.5.5 Characterization of unrestrained Ect2 cortical contractility

3.5.5.1 Elevated membrane blebbing does not delay furrow ingression in cells lacking BRCT2-mediated inhibition

Compared to control and Ect2^{WT} cells, furrow ingression was significantly slower in Ect2^{ΔBRCT2} and, to a lesser extent, in Ect2^{W307A} cells (see chapter 3.5.4). Both cell lines frequently formed large membrane blebs during meta- and anaphase, which could interfere with timely furrow ingression. To test this hypothesis, contractility was inhibited with the inhibitor Y27632 (Uehata et al., 1997), which prevents Rho-kinase (ROCK) activity and subsequent activation of myosin II. Bleb formation is efficiently blocked by Y27632, but furrow ingression can occur, albeit slightly delayed (Kosako et al., 2000, Zanin et al., 2013).

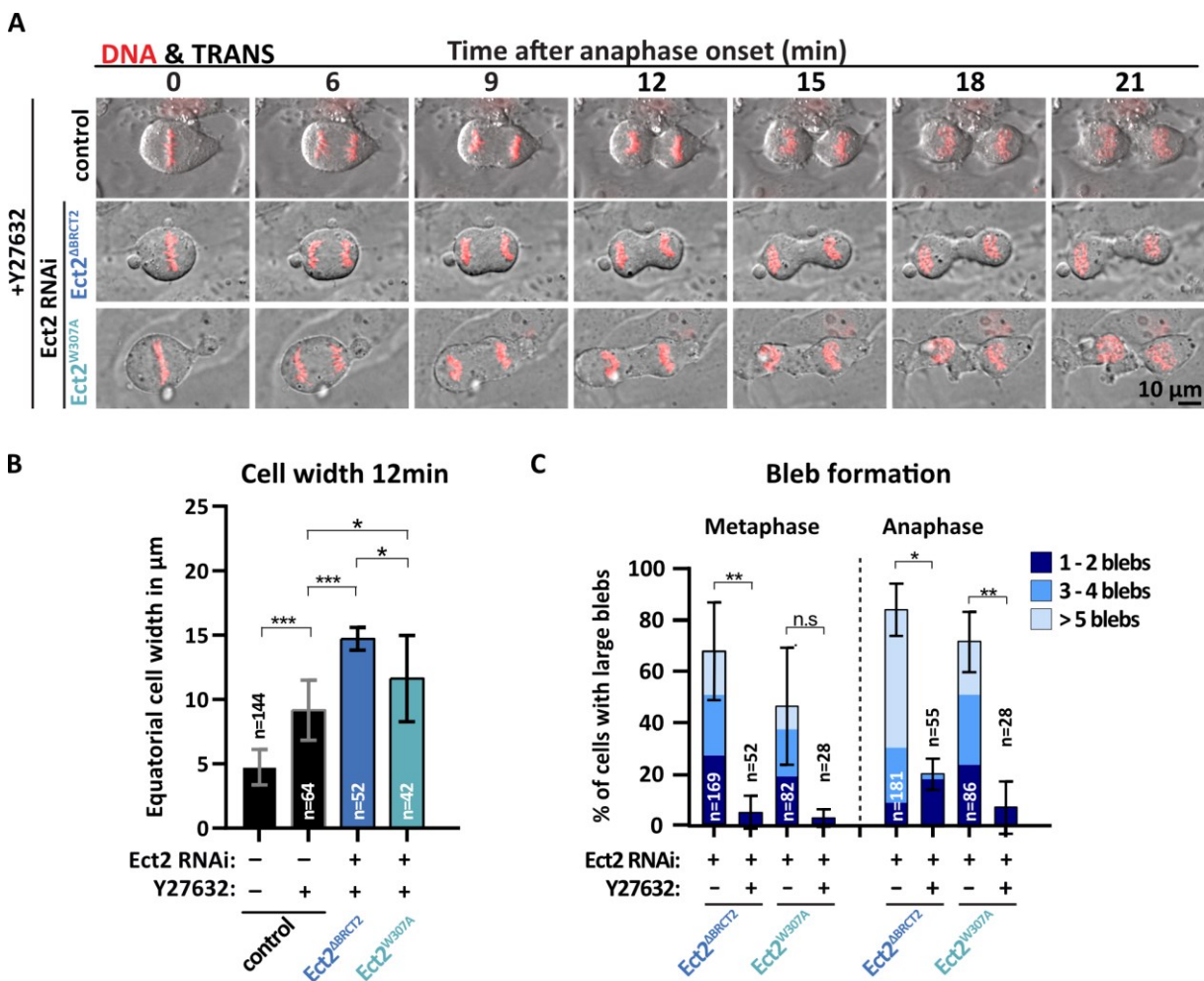


Figure 28: Formation of large blebs is not the reason for delayed furrow ingression in Ect2^{ΔBRCT2} and Ect2^{W307A}. (A) Representative live-cell image sequences of dividing control, Ect2^{ΔBRCT2}, and Ect2^{W307A} cells treated with the ROCK inhibitor Y27632. Endogenous Ect2 was

depleted by RNAi as indicated. DNA was probed with SiR-DNA. Time in minutes after anaphase onset. (B) Equatorial cell width in μm measured 12 min after anaphase onset for control and Y27632-treated control, Ect2 ^{Δ BRCT2} and Ect2^{W307A} cells. Endogenous Ect2 was depleted by RNAi as indicated. (n=number of cells, data from ≥ 2 independent experiments presented as mean \pm SD, ***p<0.001, **p<0.01, *p<0.05, n.s.=not significant determined by Tukey's test) (C) Percentages of control and Y27632-treated control, Ect2 ^{Δ BRCT2} and Ect2^{W307A} cells, which formed 1-2, 3-4, and >5 large blebs during meta- and anaphase. Endogenous Ect2 was depleted by RNAi. (n=number of cells, data from 2 independent experiments presented as mean, SD for total blebbing, **p<0.01, *p<0.05, n.s.=not significant determined by Kruskal Wallis test for Ect2 ^{Δ BRCT2} \pm Y27632 and student's t-test for the rest).

As shown in Figure 28 A, treatment with Y27632 effectively prevented the formation of large blebs in Ect2 ^{Δ BRCT2} and Ect2^{W307A} cells during mitosis and cells were still able to divide. Quantification revealed that Y27632 reduced blebbing in Ect2 ^{Δ BRCT2} from 67.5 % to 4.8 % in meta- and from 87.5 % to 25.0 % in anaphase (Figure 28 C). Similarly, Y27632-treated Ect2^{W307A} cells showed 2.5 % and 7.5 % blebbing, instead of 56.9 % and 73.3 % in meta- and anaphase, respectively (Figure 28 C).

As expected, furrow ingression was slower in control cells treated with Y27632 in comparison to untreated control cells (equatorial cell width 12 min 9.2 μm versus 4.7 μm) (Figure 28 B). Although bleb formation was efficiently inhibited by Y27632, furrow ingression in Ect2 ^{Δ BRCT2} and Ect2^{W307A} cells was still significantly slower than in Y27632-treated control cells (14.7 μm and 11.6 μm versus 9.2 μm in control cells) (Figure 28 B). These results led to the conclusion, that blebbing is not the primary cause of delayed furrow ingression seen in Ect2 ^{Δ BRCT2} and Ect2^{W307A} cells.

3.5.5.2 Large blebs grow significantly longer and take longer to retract than small blebs

It is normal that small membrane blebs are formed at the cell poles during anaphase to balance internal pressure difference (Hickson et al., 2006; Sedzinski et al., 2011; Tokumitsu & Maramorosch, 1967). Contrary to that, the formation of large membrane blebs is highly unusual. As presented in previous chapters (chapter 3.5.1 and 3.5.4) the deletion of all BRCT domains (Ect2 ^{Δ BRCT0-2}) and solely that of the BRCT2 domain (Ect2 ^{Δ BRCT2}), as well as the introduction of the W307A point mutation (Ect2^{W307A}), elicit the frequent formation of large membrane blebs in meta- and anaphase. These membrane blebs are dependent on RhoA activity and represent a direct consequence of hyperactive Ect2.

By eye large membrane blebs can be easily distinguished from small membrane blebs, which in comparison are very dynamic and characterized by short size and lifetime (Charras et al., 2008). In the following section, the difference between small and large membrane blebs will be illustrated by comparing their dimensions and dynamics in a quantitative manner. For this purpose, the maximal length and width, as well as the duration of small and big blebs during mitosis, were measured on time-lapse images (each 30 s apart). For analysis details see chapter 2.8.1.1.

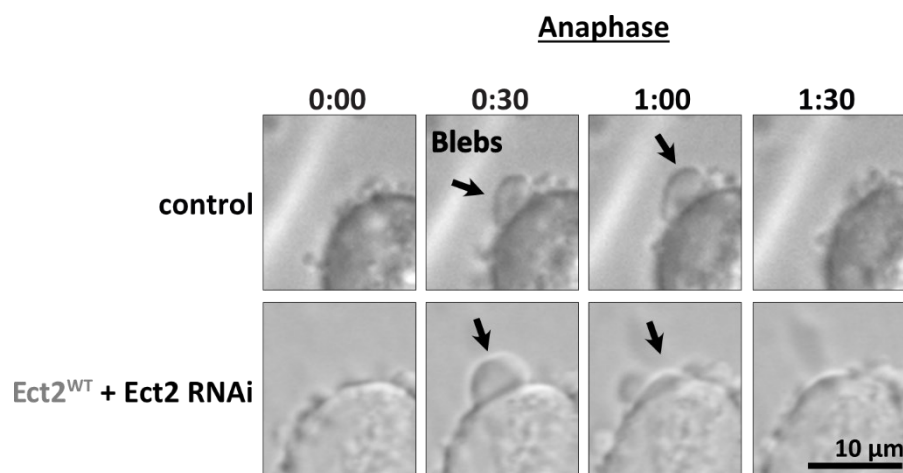


Figure 29: Formation and retraction of small blebs during anaphase in control and Ect2^{WT}. Shown are cutouts of transmission time-lapse images following the formation and retraction of small anaphase blebs in control and Ect2^{WT} cells. Time is indicated in minutes:seconds above the images. Black arrows tag small blebs. Endogenous Ect2 was depleted by RNAi as indicated.

Small blebs were formed and retracted exclusively during anaphase as shown in Figure 29 for a control and Ect2^{WT} cell (indicated by black arrows). The small blebs displayed a mean maximal length of 4.6 μm and a mean width of 6.4 μm in control cells (Figure 31 A and B). The time from their first appearance to full retraction was on average one minute (Figure 31 C). Blebs in Ect2^{WT} had a mean maximal length of 5.4 μm and a mean width of 4.6 μm. Timewise blebs in Ect2^{WT} were visible for around 2.5 minutes. Worth mentioning, Ect2^{WT} occasionally formed large membrane blebs and the shown numbers depict the average for all blebs, which explains the small differences seen. However, the size of small blebs is not significantly different in control and Ect2^{WT}.

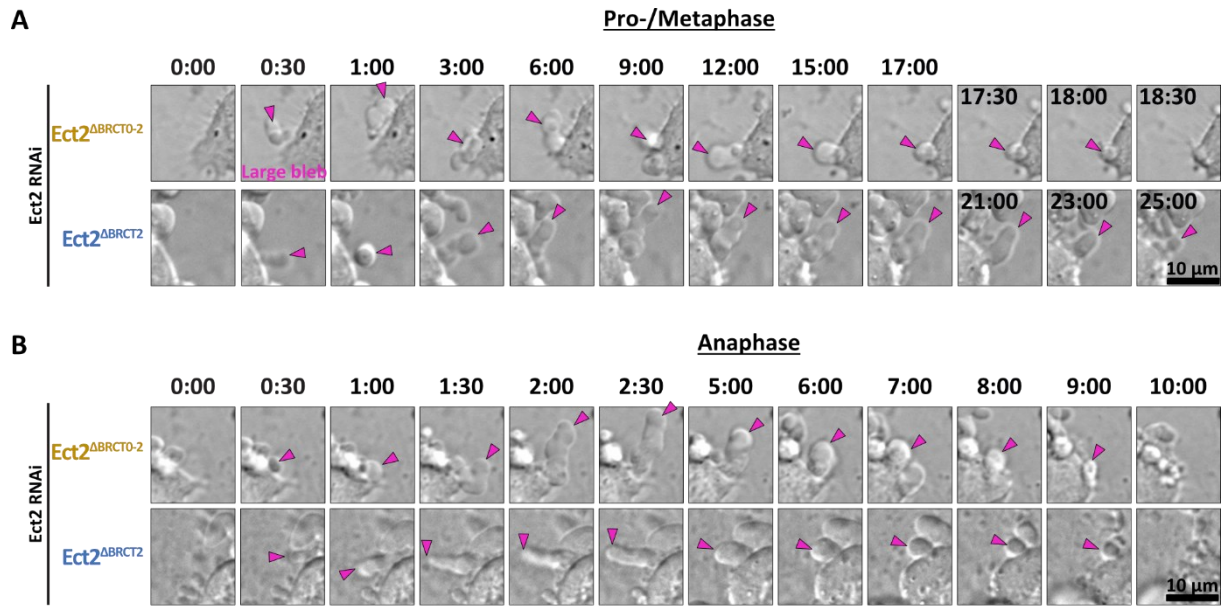


Figure 30: Formation and retraction of large membrane blebs during meta- and anaphase in Ect2^{ΔBRCT0-2} and Ect2^{ΔBRCT2}. Shown are cutouts of transmission time-lapse images following the formation of large membrane blebs in Ect2^{ΔBRCT0-2} and Ect2^{ΔBRCT2} during meta-(A) and anaphase (B). The time is indicated in minutes above the images, and pink arrowheads mark the tip of emerging/retracting blebs. Time is indicated in minutes:seconds.

In contrast to that, Ect2^{ΔBRCT0-2} and Ect2^{ΔBRCT2} cells featured large blebs during meta- and anaphase. Formation and retraction of representative large blebs can be seen in Figure 30, which are indicated by pink arrowheads. These had on average a length of at least 13 μm and a width of 3.5-4.1 μm (Figure 31 A and B). Large metaphase blebs tended to be a little shorter and slimmer compared to large anaphase blebs. Strikingly, the average bleb duration was twice as long in metaphase (19.6 min in Ect2^{ΔBRCT0-2} and 20.0 min in Ect2^{ΔBRCT2}) than in anaphase (9.7 min in Ect2^{ΔBRCT0-2} and 9.5 min in Ect2^{ΔBRCT2}) (Figure 31 C).

Overall, these results emphasize how much small and large blebs differ in respect to size and lifetime. Large blebs are significantly bigger than small blebs and it takes much more time to retract them, which renders them less dynamic.

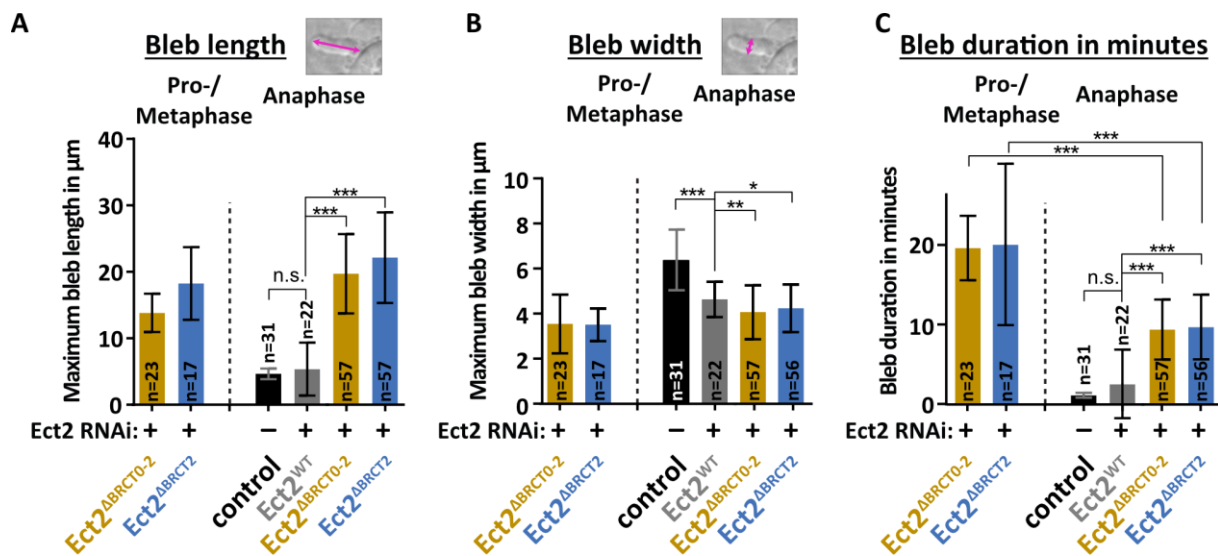


Figure 31: Large blebs grow significantly longer and take longer to retract than small blebs. (A) Maximum length (μm) of blebs in control, Ect2^{WT}, Ect2^{ΔBRCT0-2} and Ect2^{ΔBRCT2} cell during pro-/metaphase and anaphase. (n=number of blebs, *** $p < 0.001$ and n.s.=not significant $p > 0.05$ determined by Tukey's test) (B) Maximum width (μm) of blebs in control, Ect2^{WT}, Ect2^{ΔBRCT0-2} and Ect2^{ΔBRCT2} cell during pro-/metaphase and anaphase. (n=number of blebs, *** $p < 0.001$, ** $p < 0.01$, * $p < 0.05$ determined by Tukey's test) (C) Duration of blebs in minutes in control, Ect2^{WT}, Ect2^{ΔBRCT0-2} and Ect2^{ΔBRCT2} cell during pro-/metaphase and anaphase. (n=number of blebs, *** $p < 0.001$ and n.s.=not significant $p > 0.05$ determined by Tukey's test).

3.5.5.3 Increased intracellular pressure in blebbing Ect2^{ΔBRCT0-2}, Ect2^{ΔBRCT2}, and Ect2^{W307A} cells often results in cell shape oscillations

During anaphase, small blebs form at both cell poles to equalize intracellular pressure differences. This stabilizes cell shape and ensures correct positioning of the furrow at the cell equator (Sedzinski et al., 2011; Tinevez et al., 2009; Tokumitsu & Maramorosch, 1967). In the process of bleb formation, the contractile actomyosin cortex plays a central role. Cortical forces built up intracellular pressure, which can be released at sites of cortical weakness in the form of blebs. The bigger the forces are, the bigger the blebs can grow (Tinevez et al., 2009) and increased cortical contractility induced by hyperactive RhoA was shown to result in big blebs (Tinevez et al., 2009; Zanin et al., 2013). Although the idea of bleb formation is to buffer cortical imbalances to stabilize cell shape, the formation of very big blebs can also create such imbalances and lead to shape oscillations (Sedzinski et al., 2011). Shape oscillations are characterized by alternating contractions of both poles, which push the cytoplasm including the chromosomes from one side to the other. Since it has been demonstrated above (see chapters 3.5.1 and 3.5.4) that increased cortical contractility induced by hyperactive RhoA is

the reason for excessive bleb formation in Ect2^{ΔBRCT0-2}, Ect2^{ΔBRCT2}, and Ect2^{W307A} cells, we were interested whether these cells also exhibit cell shape oscillations.

During time-lapse imaging cells with large blebs more frequently underwent shape oscillations compared to Ect2^{WT} (1.3 %, n=78) (Figure 32). In anaphase, strong membrane blebbing (>70 %) was accompanied by cell shape oscillation in 15.8 % of Ect2^{ΔBRCT0-2}, 12.2 % of Ect2^{ΔBRCT2}, and 15.6 % of Ect2^{W307A} cells, while non-blebbing/slightly blebbing cell lines exhibited either very few (3.5% Ect2^{T153A + K195M}, n=58) or no oscillation events (Ect2^{ΔBRCT0} n=85, Ect2^{ΔBRCT1} n=45). So it seems that the more intense blebbing is, the higher is the percentage of cells that oscillate. As chromosomes in oscillating cells often get mis-segregated and leave the cells binucleate (Sedzinski et al., 2011; Taneja et al., 2020), it was counted how many oscillating cells fail to divide. After shape oscillations, both nuclei ended up in one cell in 66.7 % of Ect2^{ΔBRCT0-2}, 57.1 % of Ect2^{ΔBRCT2}, and 90.0 % of Ect2^{W307A} (Figure 32 B). These observations further supported that GEF activity is increased in Ect2^{ΔBRCT0-2}, Ect2^{ΔBRCT2} and Ect2^{W307A}-expressing cells and results in cell division defects.

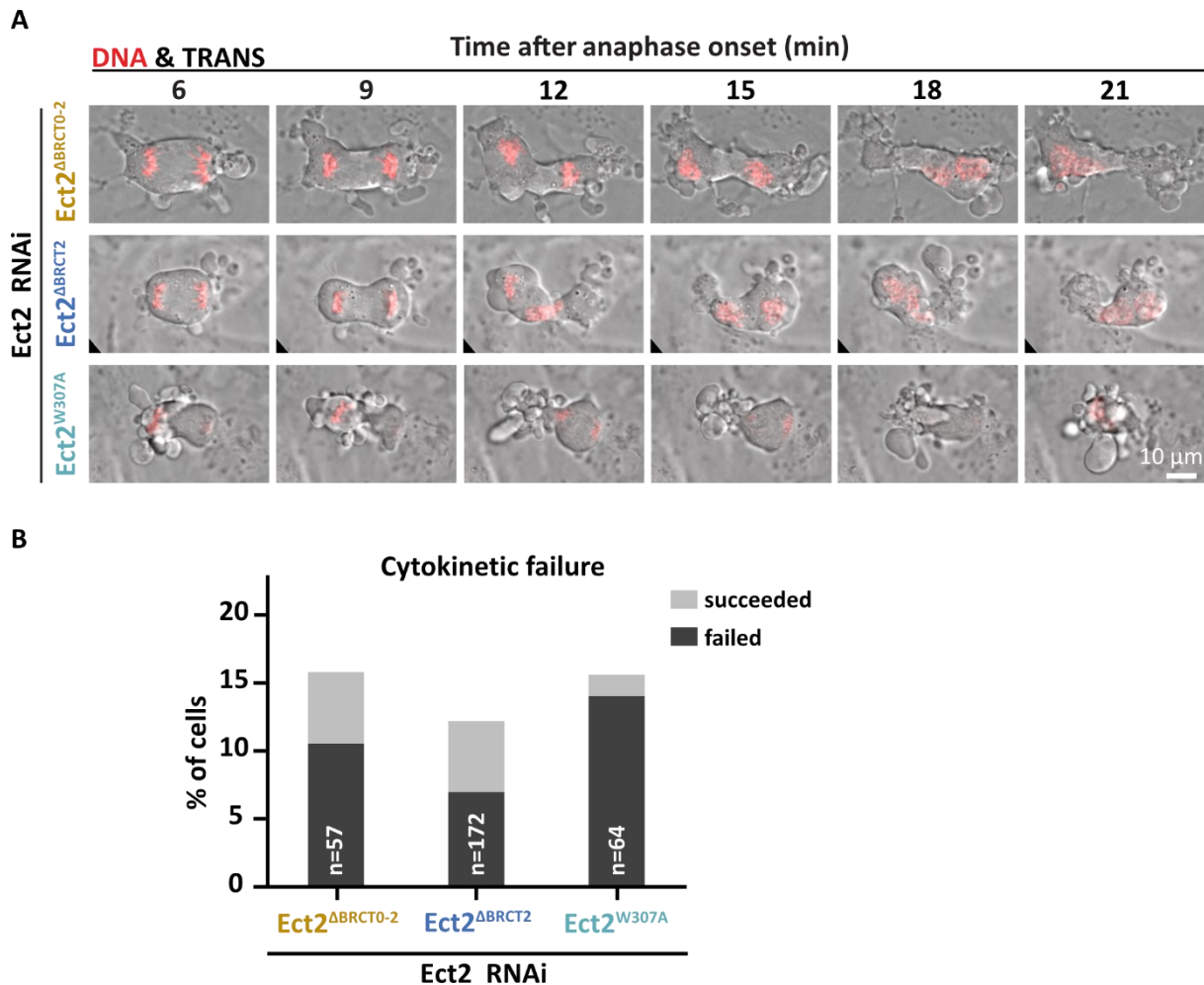


Figure 32: Hyperactive Ect2^{ΔBRCT0-2}, Ect2^{ΔBRCT2}, and Ect2^{W307A} trigger cell shape oscillations during anaphase, which often result in cytokinesis failure. (A) Representative live-cell image sequences of dividing Ect2^{ΔBRCT0-2}, Ect2^{ΔBRCT2}, and Ect2^{W307A} cells, which exhibit cell shape oscillations. Endogenous Ect2 was depleted by RNAi. DNA was probed with SiR-DNA. Time in minutes after anaphase onset. (B) Percentages of Ect2^{ΔBRCT0-2}, Ect2^{ΔBRCT2}, and Ect2^{W307A} cells, which oscillated and managed to divide successfully (light grey) and failed cytokinesis (dark grey), respectively. Endogenous Ect2 was depleted by RNAi. (n=number of cells, data from ≥4 independent experiments presented as mean, data acquired by SS)

3.5.6 Analysis of Ect2 localization

3.5.6.1 All BRCT domains are needed for midzone localization

As described in chapter 3.4.4, Ect2 specifically enriches at the equatorial membrane and on overlapping midzone microtubules at anaphase onset (Chalamalasetty et al., 2006; Su et al., 2011; Tatsumoto et al., 1999). While midzone localization depends on Ect2 binding to RacGAP1 (Nishimura & Yonemura, 2006; Somers & Saint, 2003; Yüce et al., 2005; Zhao & Fang, 2005), plasma membrane localization depends on the PH and PBS domains (Chalamalasetty

et al., 2006; Su et al., 2011). Accumulation in both regions is required for Ect2 to promote robust RhoA signaling at the equatorial cell cortex (Su et al., 2011; Wolfe et al., 2009). Thus, time-lapse imaging of dividing BRCT mutant cells was performed and checked whether they exhibit aberrant protein localization based on their NG-fluorescence signal.

In Figure 33 localization for all BRCT mutants as well as for Ect2^{WT} is shown over time, starting at the last metaphase frame (0 min). For a better illustration of the prevalence of each phenotype, several midzone regions are shown behind each image sequence.

Already by visual inspection of their NG-fluorescence signal, it was apparent that all mutant proteins localize abnormally (Figure 33). Loss of all BRCT domains (Ect2^{ΔBRCT0-2}) completely abolished Ect2 enrichment at the midzone. Although, Ect2^{ΔBRCT0-2} could still localize to the membrane an enrichment at the equator was not observed. Likewise, deletion of the BRCT1 domain (Ect2^{ΔBRCT1}), prevented Ect2 enrichment at the equatorial region, despite allowing Ect2 membrane binding. A membrane signal was also present in Ect2^{ΔBRCT0} and Ect2^{ΔBRCT2}, but the accumulation at the midzone and the equatorial membrane was strongly reduced given the faint signal visible. The same was recognized for Ect2^{T153K+K195M} which is consistent with a previous study, reporting a strong but not full reduction of midzone and equatorial membrane localization of this Ect2 mutant (Kotýnková et al., 2016). The midzone signal being reduced but still visible, indicates that the interaction of Ect2 with RacGAP1 is not fully abrogated by the two mutations in BRCT1. This could account for Ect2^{T153K+K195M} supporting successful cytokinesis demonstrated in chapter 3.5.3 (this issue will be discussed in detail in chapter 4.2). In strong contrast to that, Ect2^{W307A} was characterized by an increased signal at the equatorial membrane and the midzone. (Figure 33)

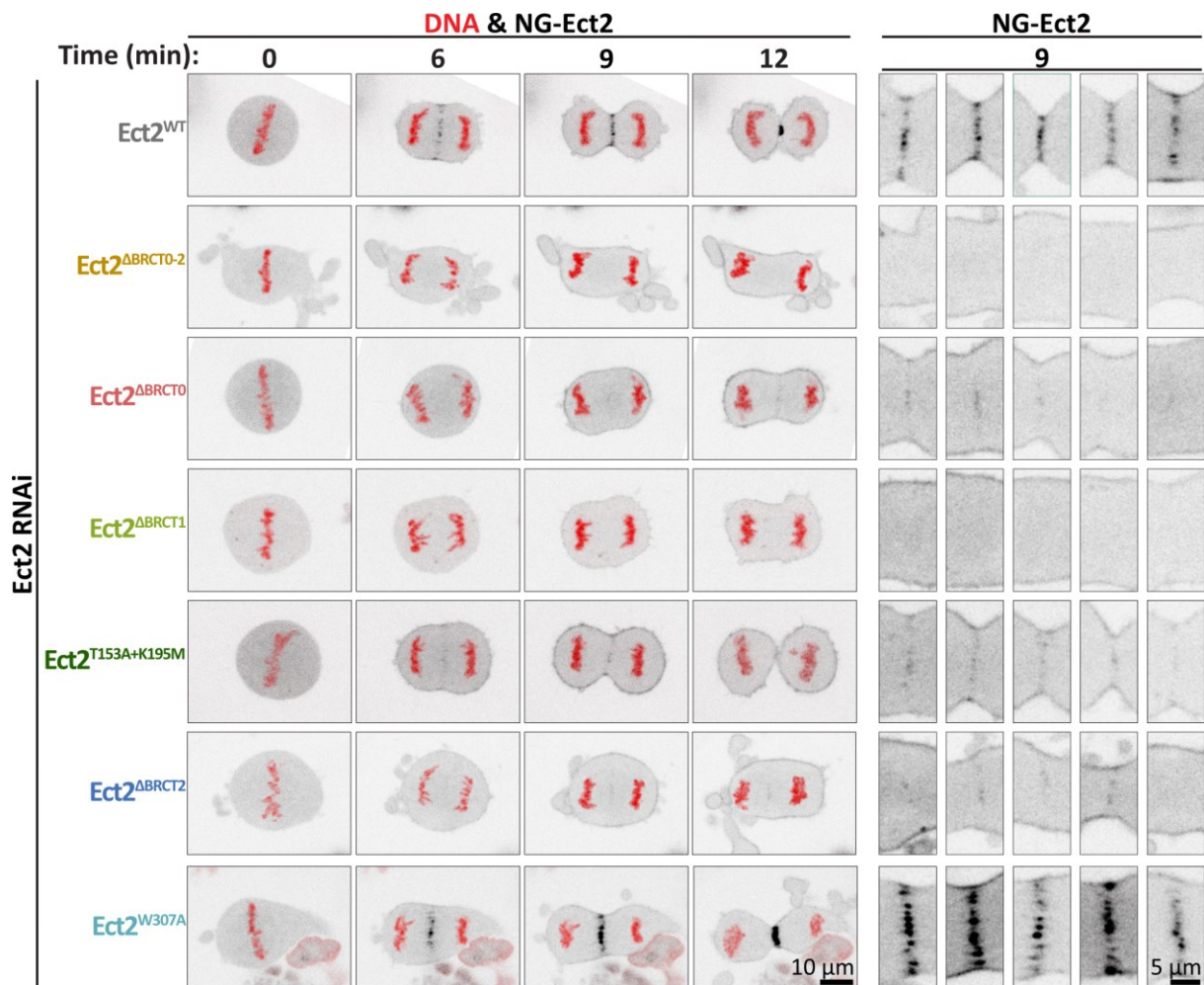


Figure 33: NG-Ect2 localization of the different BRCT mutants during meta- and anaphase. Representative fluorescence image sequences showing the localization (grey) of NG-Ect2^{WT}, NG-Ect2^{ΔBRCT0-2}, NG-Ect2^{ΔBRCT0}, NG-Ect2^{ΔBRCT1}, NG-Ect2^{T153A+K195M}, NG-Ect2^{ΔBRCT2}, and NG-Ect2^{W307A} at consecutive timepoints during cell division. Several cutouts showing the NG-Ect2 localization to the equatorial region 9 min after anaphase onset are presented behind each sequence. Endogenous Ect2 was depleted by RNAi and DNA was probed with SiR-DNA. Time in minutes after anaphase onset.

For better differentiation of the effects elicited by the different BRCT mutants, Ect2 accumulation was also quantitatively analyzed by measuring NG-fluorescence intensity 9 min after anaphase onset. Here, one linescan was drawn across each polar membrane and one across the equator, which captured the signal at the membrane and the midzone (Figure 34 A). Representative intensity plots used for the analysis are depicted in Figure 34 B and C. Details of the measuring method and the subsequent analysis can be found in chapter 2.8.1.2.

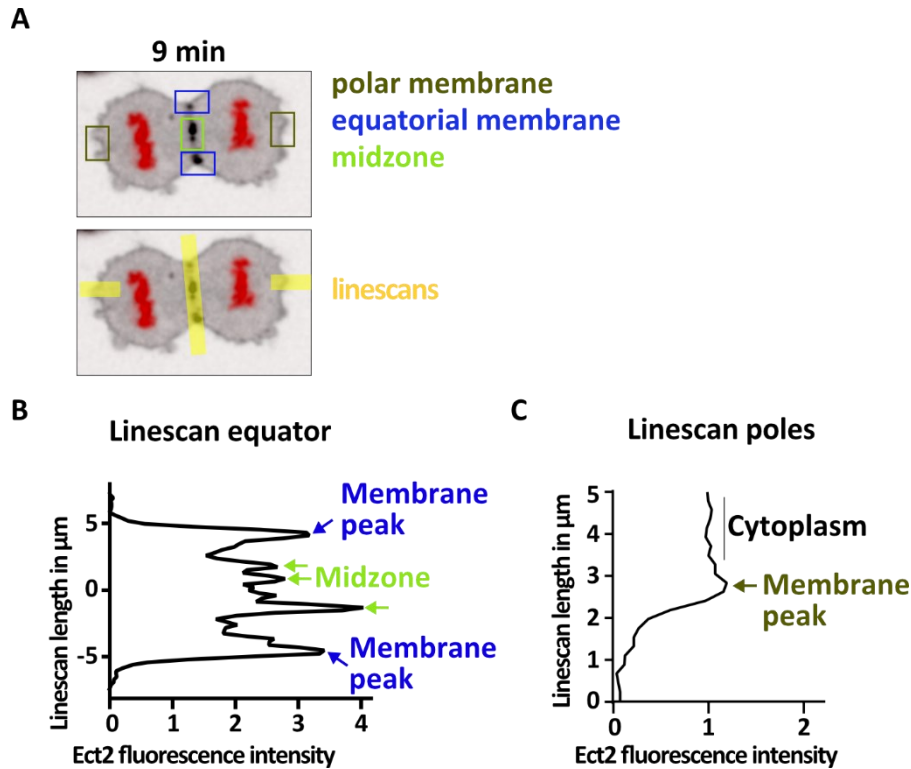


Figure 34 Scheme of NG-Ect2 intensity measurements 9 min after anaphase onset. (A) Representative NG-fluorescence images showing the localization of Ect2^{WT} in an anaphase cell. Polar (khaki) and equatorial (blue) membrane and midzone regions (neongreen) are marked in the top panel and linescans (yellow) used to measure NG-fluorescence intensity in these regions are depicted in the bottom panel. Exemplary intensity plots for the equatorial linescan (B) and the polar linescans (C) for an Ect2^{WT} cell are depicted and the equivalent peaks for each region are marked.

Quantitative analysis revealed that Ect2^{WT} is 2.72 -fold enriched at the equatorial membrane and 3.39 -fold enriched at the midzone in relation to the cytoplasm (Figure 35 B). Intensity at the polar membrane was 1.27-fold of the cytoplasmic level. Therefore 2.16-times more Ect2^{WT} was accumulated at the equatorial membrane in comparison to the polar membrane. (Figure 35)

As seen by visual inspection, all BRCT mutants, except Ect2^{W307A}, showed strongly reduced intensity levels at the equatorial membrane and the midzone region (Figure 35 A). Moreover, they localized slightly more to the polar membrane (Figure 35 A). In respect to midzone localization Ect2^{ΔBRCT0-2} and Ect2^{ΔBRCT1}, which by eye were not detectable at the midzone, displayed the lowest intensities, which were close to the cytoplasmic intensity (Figure 35 B). In comparison, Ect2^{ΔBRCT0}, Ect2^{ΔBRCT2}, and Ect2^{T153A+K195M}, which all presented a faint signal at the midzone, had significantly higher intensity values. Ect2^{T153A+K195M} turned out to have the highest midzone signal. In regards to membrane enrichment, all mutants (Ect2^{ΔBRCT0-2},

Ect2^{ΔBRCT0}, Ect2^{ΔBRCT1}, Ect2^{ΔBRCT2}, and Ect2^{T153A+K195M}) had significant problems to specifically accumulate at the equator (Figure 35 C). While Ect2^{W307A} was strongly increased at the equatorial region, fluorescence intensity at the poles was similar to Ect2^{WT} (Figure 35 A). With a 4.66-fold and 6.36-fold enrichment at the equatorial membrane and the midzone (Figure 35 A and B), respectively, almost twice as much Ect2^{W307A} accumulated at the equator compared to Ect2^{WT}. Moreover, comparing equatorial and polar membrane intensities, revealed that Ect2^{W307A} was 3.86-fold enriched at the equator. (Figure 35)

Taken together the results indicated that all BRCT domains are needed for the recruitment to the equatorial membrane and the midzone. While BRCT1 is essential for Ect2 accumulation at the midzone, BRCT0 and BRCT2 help to recruit typical amounts of Ect2. Further, the results suggested that only a part of the Ect2 molecules present in a cell is being activated at anaphase onset, as releasing Ect2 autoinhibition by W307A mutation strongly increased accumulation at the cell equator. As the midzone localization of Ect2 depends on the interaction with RacGAP1 (Nishimura & Yonemura, 2006; Somers & Saint, 2003; Yüce et al., 2005; Zhao & Fang, 2005), the results further suggested that the BRCT1 domain is essential for RacGAP1 interaction, while BRCT0 and BRCT2 contribute to it. In the case of missing autoinhibition (Ect2^{W307A}), Ect2 RacGAP1 interaction appears to be enhanced.

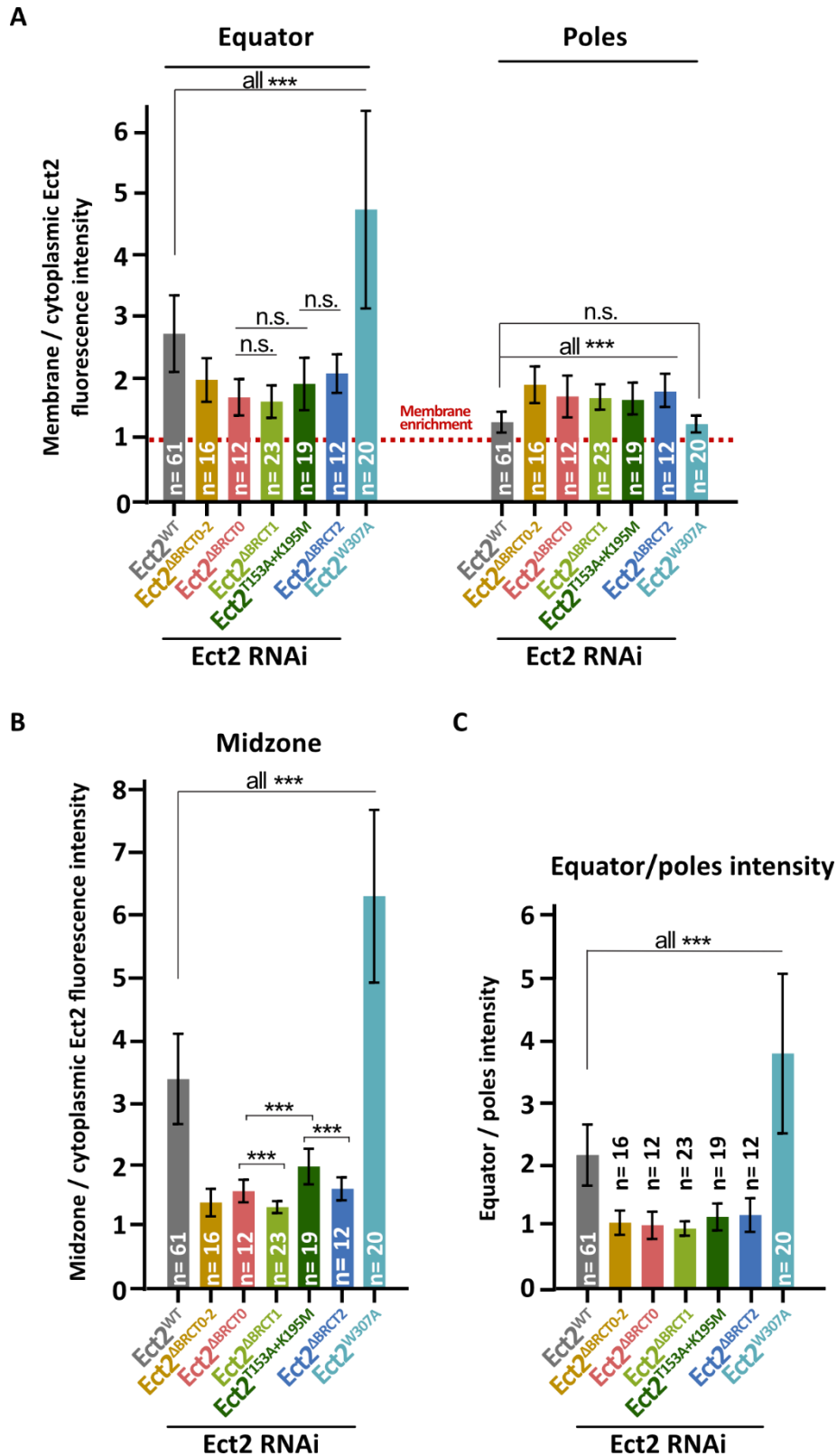


Figure 35: Deletion of each BRCT domain decreases and mutation W307A in the BRCT2 domain increases Ect2 localization to the equatorial region. (A) Fluorescence intensities of NG-Ect2^{WT}, NG-Ect2^{ΔBRCT0-2}, NG-Ect2^{ΔBRCT0}, NG-Ect2^{ΔBRCT1}, NG-Ect2^{ΔBRCT2}, and NG-Ect2^{W307A} at the equatorial and polar membrane 9 min after anaphase onset relative to cytoplasmic levels in cells depleted of endogenous Ect2 by RNAi. (n= number of cells, data from ≥2 independent experiments presented as mean±SD, ***p<0.001 and n.s.= not significant p>0.05 determined

by Kruskal Wallis test and student's t-test according to normality). (B) Fluorescence intensities of NG-Ect2^{WT}, NG-Ect2^{ΔBRCT0-2}, NG-Ect2^{ΔBRCT0}, NG-Ect2^{ΔBRCT1}, NG-Ect2^{ΔBRCT2}, and NG-Ect2^{W307A} at the midzone relative to cytoplasmic levels in cells depleted of endogenous Ect2 by RNAi. (n= number of cells, data from ≥2 independent experiments presented as mean±SD, ***p<0.001 and n.s.= not significant p>0.05 determined by Kruskal Wallis test and student's t-test according to normality). (C) The intensity ratio of the equatorial and the polar membrane for NG-Ect2^{WT}, NG-Ect2^{ΔBRCT0-2}, NG-Ect2^{ΔBRCT0}, NG-Ect2^{ΔBRCT1}, NG-Ect2^{ΔBRCT2}, and NG-Ect2^{W307A}. (n= number of cells, data from ≥2 independent experiments presented as mean±SD, ***p< 0.001 determined by Kruskal Wallis test and student's t-test according to normality).

3.5.6.2 Each BRCT domain binds RacGAP1 *in vitro*

According to the results obtained by analyzing the NG-Ect2 fluorescence signal (see previous chapter 3.5.6.1), all BRCT domains contribute to robust Ect2 localization to the equatorial membrane and the midzone. Since binding of Ect2 to RacGAP1 is essential for midzone localization (Somers & Saint, 2003; Yüce et al., 2005), we wanted to test whether all BRCT domains can interact with RacGAP1. Therefore, we expressed and purified a GST-tagged N-terminal fragment of RacGAP1 (1-288aa) encompassing the Ect2 binding site (Burkard et al., 2009; Wolfe et al., 2009; Zou et al., 2014) along with several MBP-tagged N-terminal fragments of Ect2 containing either BRCT0, BRCT1, BRCT0+1, BRCT1+2 or all BRCT domain (BRCT0-2) (Figure 36).

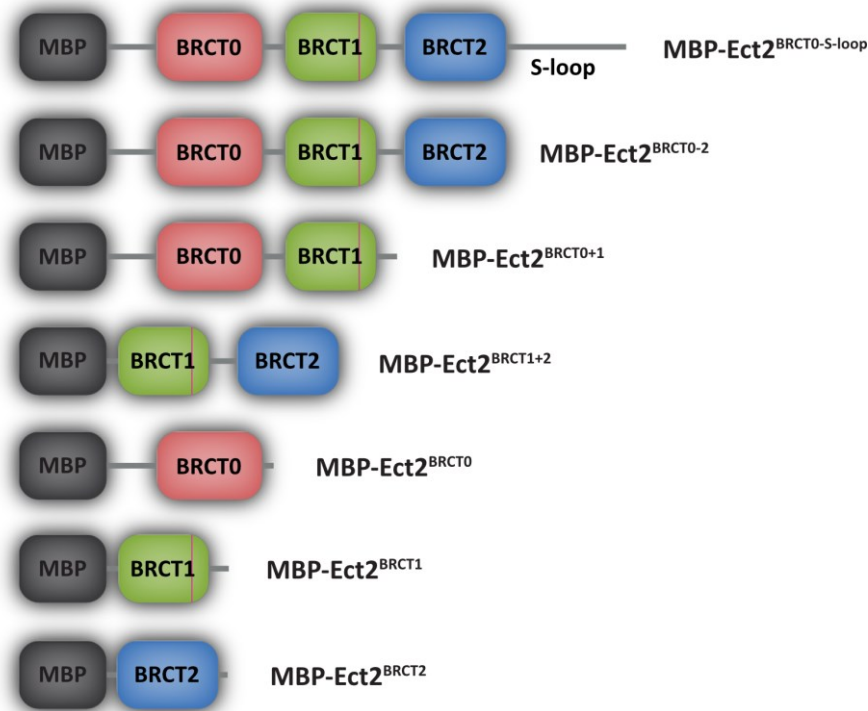


Figure 36: Overview of MBP-tagged N-terminal Ect2 fragments used for *in vitro* studies. MBP-tagged Ect2 proteins were expressed in bacteria and subsequently isolated via amylose affinity chromatography. (For details see chapter 2.2.2)

GST-tagged RacGAP1, bound to glutathione beads, was incubated with different purified N-terminal Ect2 variants and subsequently precipitated by centrifugation. Ect2 variants that could interact with RacGAP1 were subsequently identified via SDS-PAGE and immunoblot analysis (Figure 37) (performed by Prof. Dr. Esther Zanin). We found that while MBP alone did not interact with GST-tagged RacGAP1, MBP-tagged N-terminal Ect2 variants successfully bound to GST-tagged RacGAP1, regardless of whether they included single or more BRCT domains. Even though all BRCT domains bound to RacGAP1, the strongest interaction was found for BRCT1. The results further supported that all BRCT domains interact with RacGAP1 to guarantee efficient midzone recruitment, yet, BRCT1 is the main interactor.

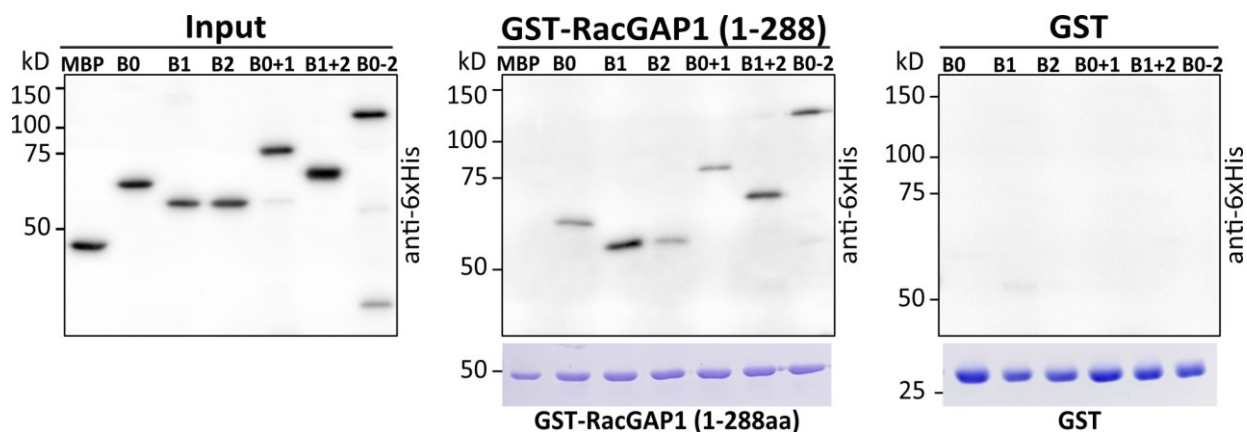


Figure 37: Each BRCT domain can interact with RacGAP1 *in vitro*. Immunoblot analysis of a GST-RacGAP1 pull-down assay. Purified GST-RacGAP1 was incubated with different purified N-terminal fragments of Ect2 (see Figure 36). After pulling down GST-RacGAP1, associated proteins were identified via SDS-PAGE and subsequent immunoblot analysis. Since MBP-Ect2 variants also contained a 6xHis-tag, the immunoblot membrane was probed with antibodies against 6xHis. RacGAP1 could interact with all BRCT domains *in vitro*, however, the strongest interaction was detected with BRCT1. B= BRCT. Pull-down assays were performed by Prof. Dr. Esther Zanin.

3.6 Analysis of Plk1 function in releasing Ect2 autoinhibition

Plk1 is a major mitotic kinase, which is implicated in processes such as spindle assembly, mitotic entry, chromosome segregation, and cytokinesis (Petronczki et al., 2008). In anaphase, Plk1 activity is needed for normal RhoA accumulation at the equatorial membrane and subsequent recruitment of contractile ring components, furrow formation, and successful cytokinesis (Brennan et al., 2007, Petronczki et al., 2007; Santamaria et al., 2007). The centralspindlin component, RacGAP1 was shown to be phosphorylated by Plk1 during mitosis and this is required for its interaction with Ect2 and Ect2 recruitment to the midzone (Kim et al., 2014; Petronczki et al., 2007; Wolfe et al., 2009; Yüce et al., 2005). Further, the binding of RacGAP1 to Ect2 was assumed to be sufficient to stimulate Ect2 GEF activity. However, only in the presence of Plk1 activity, phospho-mimetic Plk1 target sites in RacGAP1 (RacGAP1-4D) could compensate depletion of endogenous RacGAP1 (Wolfe et al., 2009). Together with the fact that in the absence of Plk1 activity only a N-terminal fragment, but not full length Ect2, was recruited to the midzone (Wolfe et al., 2009), this suggests that the release of Ect2 autoinhibition requires additional Plk1-dependent steps. (Figure 38)

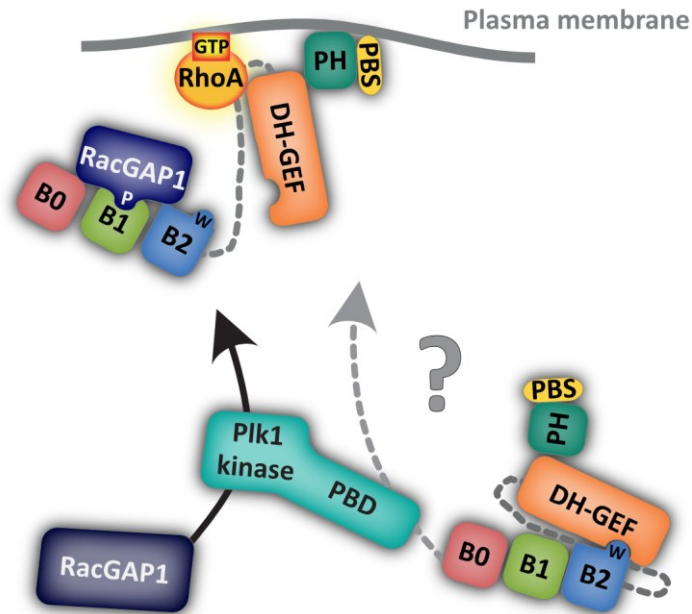


Figure 38: The role of Plk1 in releasing Ect2 autoinhibition. Plk1 phosphorylates RacGAP1 during mitosis, which can subsequently bind to Ect2 via BRCT1 (Burkard et al., 2009; Petronczki et al., 2007; Somers & Saint, 2003; Wolfe et al., 2009; Yüce et al., 2005; Zou et al., 2014). This interaction is thought to release Ect2 autoinhibition and activate Ect2 (Yüce et al., 2005). Apart from this well-established role of Plk1, Ect2 activation seems to require additional, yet unknown, Plk1-dependent steps. B=BRCT, W=W307.

3.6.1 Plk1 acts upstream of BRCT2-mediated inhibition

As described in chapter 3.5.4, deletion of BRCT2 interferes with the autoinhibition of Ect2 activity and results in the excessive formation of large membrane blebs in meta- and anaphase (Figure 26). To test whether Plk1 activity is required for abnormal Ect2 activation seen in Ect2^{ΔBRCT2}, Plk1 was inhibited with the Plk1 inhibitor BI2536 (Petronczki et al., 2007; Steegmaier et al., 2007). If Plk1 acts downstream of BRCT2-mediated inhibition, we would expect, that adding BI2536, suppresses the observed blebbing phenotype in Ect2^{ΔBRCT2} cells. Contrary, if Plk1 acts upstream of BRCT2, blebbing levels should be the same as in untreated Ect2^{ΔBRCT2} cells. As Ect2 activation normally occurs during anaphase and Plk1 inhibition before anaphase results in a prometaphase arrest due to its function in spindle assembly (Lane & Nigg, 1996; Sumara et al., 2004), Plk1 activity was specifically blocked during anaphase.

As previously described (Petronczki et al., 2007), the addition of BI2536 efficiently inhibited Ect2^{WT} midzone recruitment (fluorescence intensity of 3.39 in Ect2^{WT} vs. 1.50 in Ect2^{WT}+BI2536 relative to cytoplasmic levels) (Figure 39 A+B) and Ect2 activation in control cells, which

prevented furrow formation (12 min equatorial cell width 3.4 μm in control vs. 17.7 μm in control+BI2536) (Figure 39 C) and cytokinesis (2 % failure in control vs. 81 % in control+BI2536, Figure 39 D). Thus, Plk1 activity was effectively blocked by adding BI2536.

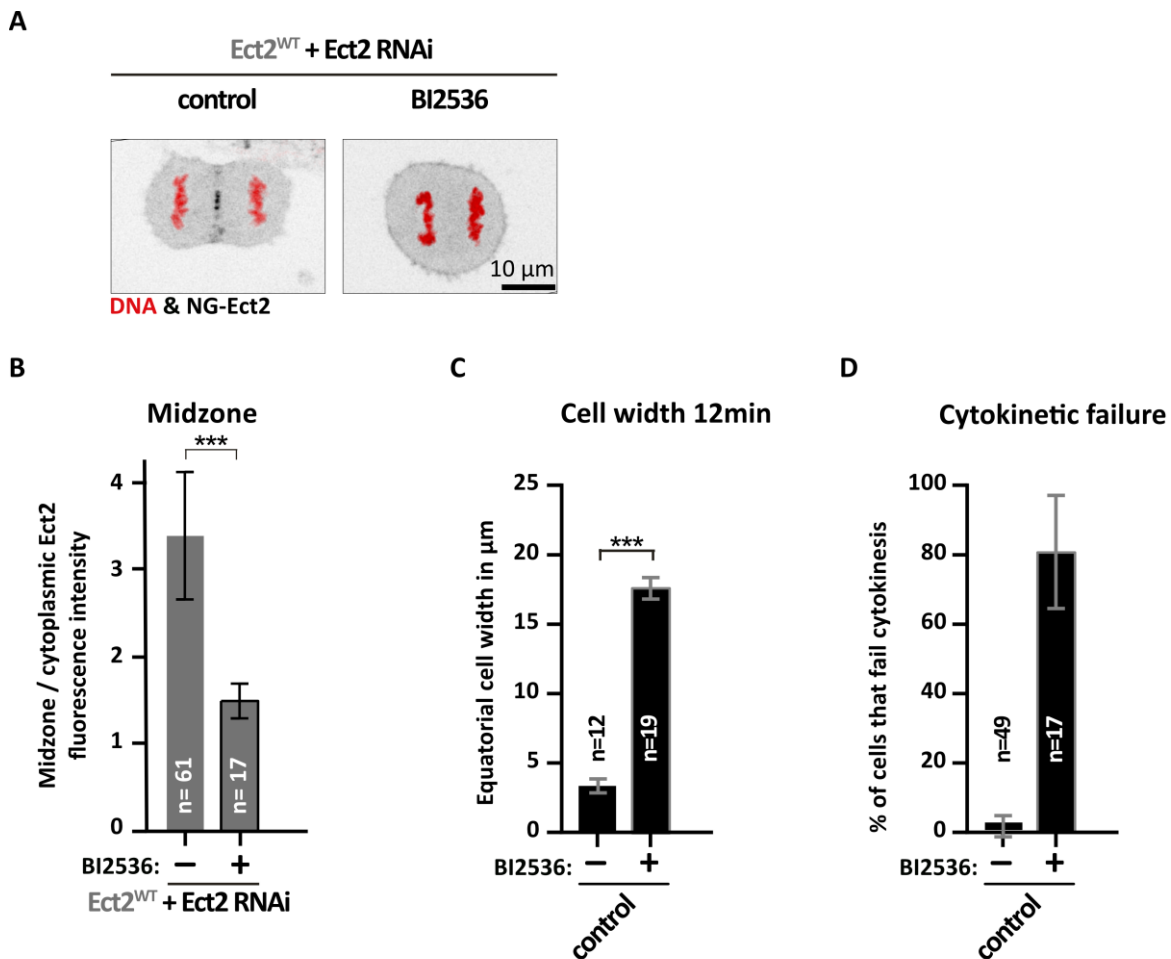


Figure 39: Plk1 inhibition blocks Ect2^{WT} midzone recruitment and furrow ingression and cytokinesis in control cells. (A) Fluorescence live-cell images showing the localization of NG-Ect2^{WT} in anaphase cells treated with and without the Plk1 inhibitor BI2536. Endogenous Ect2 was depleted by RNAi. DNA was probed with SiR-DNA. (B) Fluorescence intensities at the midzone of Ect2^{WT} cells treated with and without BI2536 relative to cytoplasmic levels. (n= number of cells, data from 9 independent experiments presented as mean \pm SD, ***p<0.001 determined by student's t-test). (C) Equatorial cell width in μm measured 12 min after anaphase onset for control cells treated with and without BI2536. (n=number of cells, data from \geq 2 independent experiments presented as mean \pm SD, ***p<0.001 determined by Tukey's test, data acquired by EZ). (D) Percentage of control cells treated with and without BI2536, which failed cytokinesis. (n=number of cells, data from 4 independent experiments presented as mean \pm SD).

Interestingly, Ect2^{ΔBRCT2} cells treated with BI2536 retained the same excessive blebbing phenotype as untreated Ect2^{ΔBRCT2} cells (82 % versus 83 % in anaphase), where most cells formed more than 3 blebs (Figure 40). Thus, the release of the BRCT2-mediated inhibition is

independent of Plk1 activity, which seems to be required upstream for an additional, yet unknown, task besides RacGAP1 phosphorylation. Taken together, we could show that Plk1 activity is required upstream of BRCT2-mediated inhibition to activate Ect2.

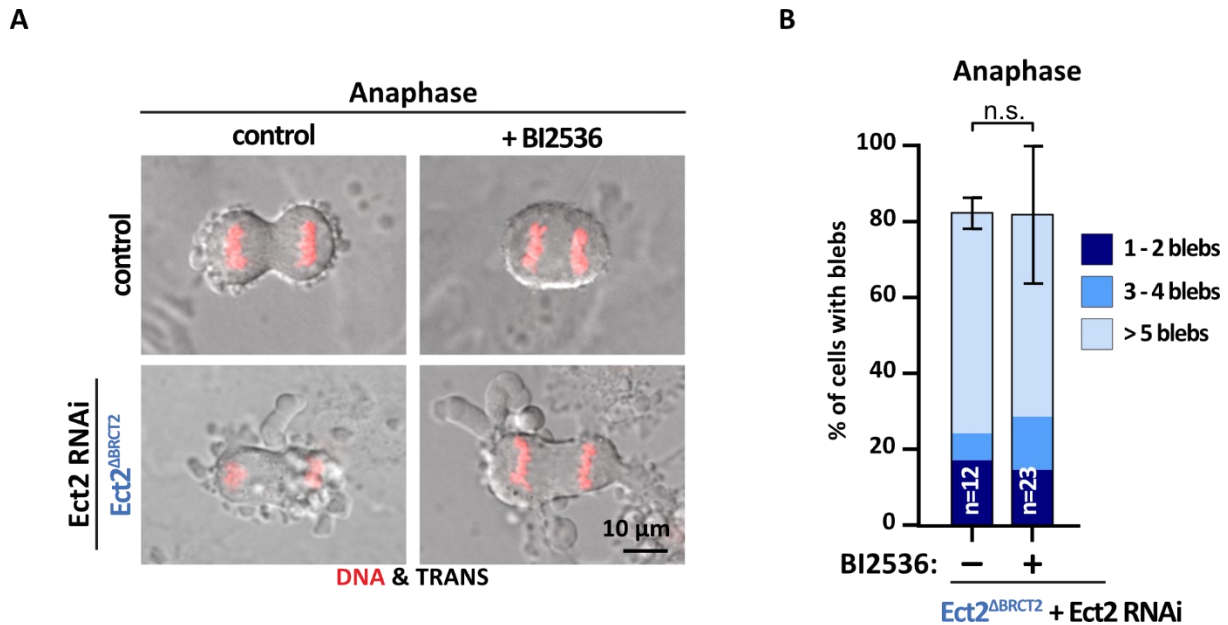


Figure 40: Plk1 inhibition does not affect large bleb formation in BRCT2 lacking cells. (A) Live-cell images of control and Ect2^{ΔBRCT2} cells treated with and without the Plk1 inhibitor BI2536 in anaphase. Endogenous Ect2 was depleted as indicated. DNA was probed with SiR-DNA. (B) Percentages of control and BI2536-treated Ect2^{ΔBRCT2} cells, which formed 1-2, 3-4, and >5 large blebs during anaphase. Endogenous Ect2 was depleted by RNAi. (n=number of cells, data from ≥2 independent experiments presented as mean, ±SD for total blebbing, n.s.= not significant p> 0.05 determined by Tukey's test). Experiments and analyses were performed by Prof. Dr. Esther Zanin.

3.6.2 Plk1 binds to all BRCT domains via its PBD

Plk1 and Ect2 both localize to the midzone during anaphase and directly interact in cells (Golsteyn et al., 1995; Niiya et al., 2006; Tatsumoto et al., 1999). This interaction was shown to be mediated by the polo-box domain (PBD) of Plk1 (Niiya et al., 2006). To clarify to which Ect2 domain(s) Plk1 binds, several truncated MBP-tagged variants of N-terminal Ect2 were expressed and purified (Figure 36). These included fragments containing all BRCT domains plus the S-loop (MBP-Ect2^{BRCT0-S-loop}), BRCT0 (MBP-Ect2^{BRCT0}), BRCT0+1 (MBP-Ect2^{BRCT0+1}), and BRCT1+2 (MBP-Ect2^{BRCT1+2}). Prof. Dr. Esther Zanin conducted pull-down assays (similarly to chapter 3.5.6.2) with purified GST and GST-PBD and found that all MBP-Ect2 truncations were precipitated exclusively by GST-PBD (Figure 41 A). BRCT1 (MBP-Ect2^{BRCT1}) and BRCT2 (MBP-

Ect2^{BRCT2}) alone were successfully pulled down by GST-PBD, however, the interaction was weaker as that seen with BRCT0 (Figure 41 B).

These *in vitro* results indicated that Plk1 interacts with Ect2 by binding to all three BRCT domains, where the strongest binding occurs with BRCT0.

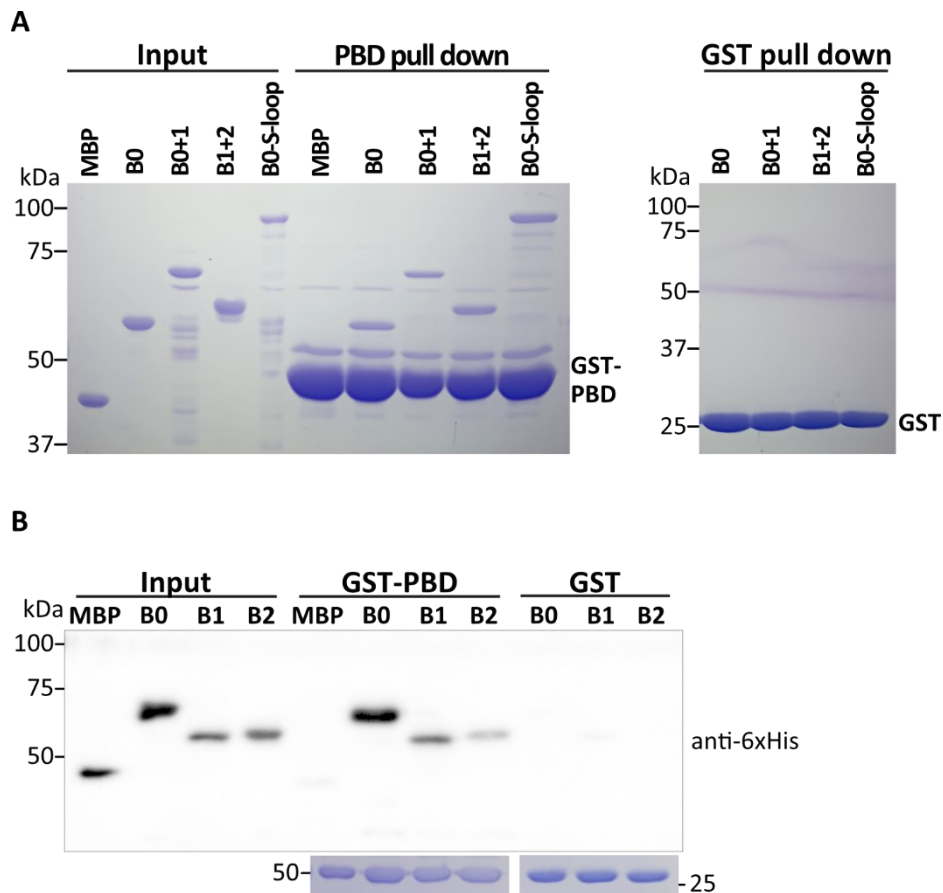


Figure 41: Plk1 binds to all BRCT domains via its PBD. SDS-PAGE analysis of a GST-PBD pull-down assay. Purified GST-PBD was incubated with different purified N-terminal fragments of Ect2 (see Figure 36). After pulling down GST-PBD, associated proteins were identified via SDS-PAGE (A) and or via SDS-PAGE and subsequent immunoblot analysis (B). The SDS-gel was stained with Coomassie blue and since MBP-Ect2 variants also contained a 6x His-tag, the immunoblot membrane was probed with antibodies against His to detect interacting proteins. PBD could interact with all BRCT domains *in vitro*, however, the strongest interaction was detected with BRCT0. B= BRCT. Pull-down assays were performed by Prof. Dr. Esther Zanin.

3.6.3 Plk1 phosphorylates BRCT0 *in vitro*

We found that Plk1 interacts with all three BRCT domains of Ect2 via its PBD *in vitro* (Figure 41) and Niiya et al. (2006) published that Plk1 can phosphorylate an N-terminal fragment of Ect2, which includes all BRCT domains and the S-loop, *in vitro*. As the S-loop contains many putative phosphorylation sites, it was speculated to be the site of phosphorylation. To further

dissect which exact part Plk1 targets, we used recombinant, N-terminal Ect2 proteins (Figure 36) in *in vitro* Plk1 kinase assays (details see chapter 2.4). As N-terminal fragments with and without the S-loop (MBP-Ect2^{BRCT0-S-loop} and MBP-Ect2^{BRCT0-2}) were both successfully phosphorylated (Figure 42 A), the phosphorylation must occur in the part containing the BRCT domains. Therefore, we analyzed *in vitro* phosphorylation of MBP-Ect2^{BRCT0+1}, MBP-Ect2^{BRCT1+2} and MBP-Ect2^{BRCT0}. Plk1 was only able to phosphorylate proteins containing the BRCT0 domain (MBP-Ect2^{BRCT0} and MBP-Ect2^{BRCT0+1}) (Figure 42 B). This demonstrated that the residues targeted by Plk1 must lie in the BRCT0 domain of Ect2.

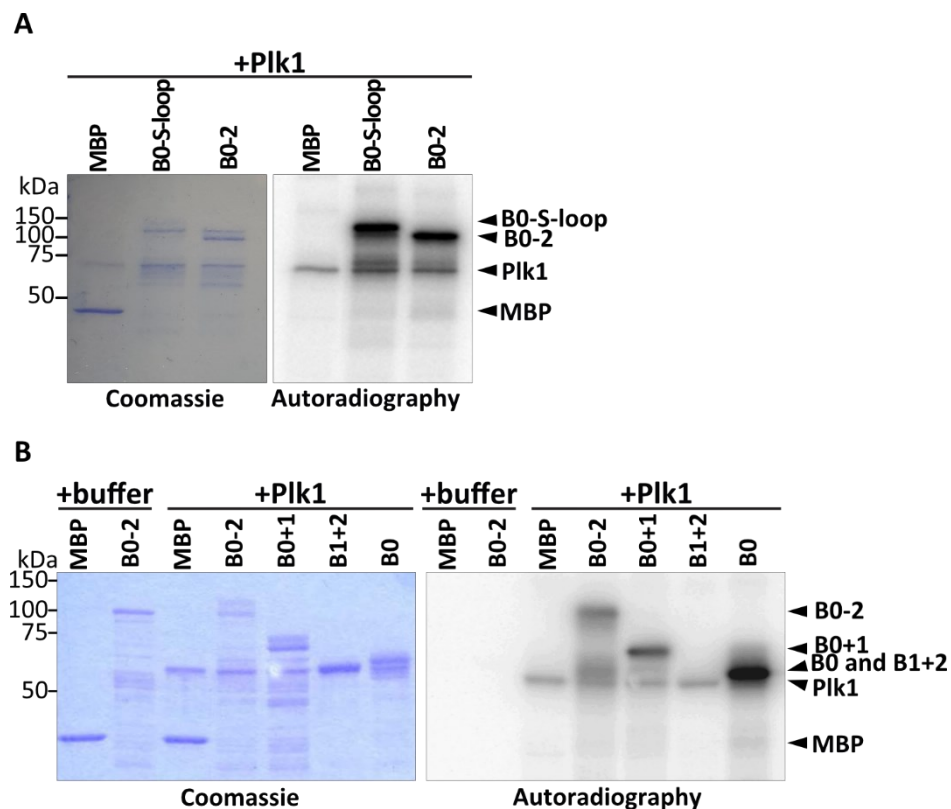


Figure 42: BRCT0 is phosphorylated by Plk1 *in vitro*. Purified MBP-tagged N-terminal Ect2 fragments with and without the S-loop (A) or different BRCT domains (B) (see Figure 36) were incubated with recombinant Plk1 in the presence of [γ -P32] ATP for 30 min at 30°C. Subsequently, proteins were separated by SDS-PAGE and the Coomassie blue stained gel was subjected to autoradiography. Coomassie stained gels are shown on the left and autoradiographs are shown on the right. Note the retarded bands of phosphorylated Ect2 on the gel and Plk1 autophosphorylation on autoradiographs. For all B=BRCT.

3.7 BRCT2-mediated inhibition acts in parallel to astral microtubules

The formation of the contractile ring is spatially and temporally controlled by signals emanating from the mitotic spindle. Stimulatory signals from midzone microtubules promote contractile ring formation at the equator and inhibitory signals from astral microtubules prevent cortical contractility at the cell poles (D'Avino et al., 2008; Green et al., 2012; Mishima, 2016; von Dassow, 2009). While perturbation of the inhibitory signals, by removing astral microtubules with low-doses of nocodazole, leads to RhoA accumulation in a broader equatorial zone (Murthy & Wadsworth, 2008; van Oostende Triplet et al., 2014a; Zanin et al., 2013), strengthening it by depleting the microtubule depolymerizing kinesin MCAK (Desai et al., 1999; Hedrick et al., 2008; Rankin & Wordeman, 2010b), results in a slimmer RhoA zone (van Oostende Triplet et al., 2014a; Zanin et al., 2013). Astral microtubules could limit the width of the zone by preventing binding of active RhoA to the membrane or RhoA activation. Latter seems to be the case since ectopic RhoA activation using light was followed by comparable furrow ingression at the cell equator and the poles, respectively (Wagner & Glotzer, 2016).

The BRCT2 domain inhibits Ect2 activity by direct interaction of its W307 residue with the DH-GEF domain (Chen et al., 2020) and we found that cells lacking this inhibition (Ect2^{ΔBRCT0-2}, Ect2^{ΔBRCT2}, and Ect2^{W307A}) frequently form large membrane blebs in meta- and anaphase due to increased RhoA activation (see chapters 3.5.1 and 3.5.4). Moreover, in these cells, the equatorial RhoA and anillin zone was broadened (data from Friederike Wolff summarized in Table 20). We speculated that astral microtubules exert their inhibitory action by stimulating the binding of BRCT2 to the GEF domain. To test this, astral microtubules were stabilized in Ect2^{ΔBRCT0-2} and Ect2^{ΔBRCT2} cells by depleting MCAK by RNAi. If astral microtubules promote BRCT2-DH-GEF binding outside the equatorial region, MCAK depletion in cells lacking BRCT2-mediated inhibition would be expected to not affect bleb formation and RhoA zone width. However, if astral microtubules use a mechanism independent of BRCT2, bleb formation, and RhoA zone width would be expected to be reduced. (Figure 43 B)

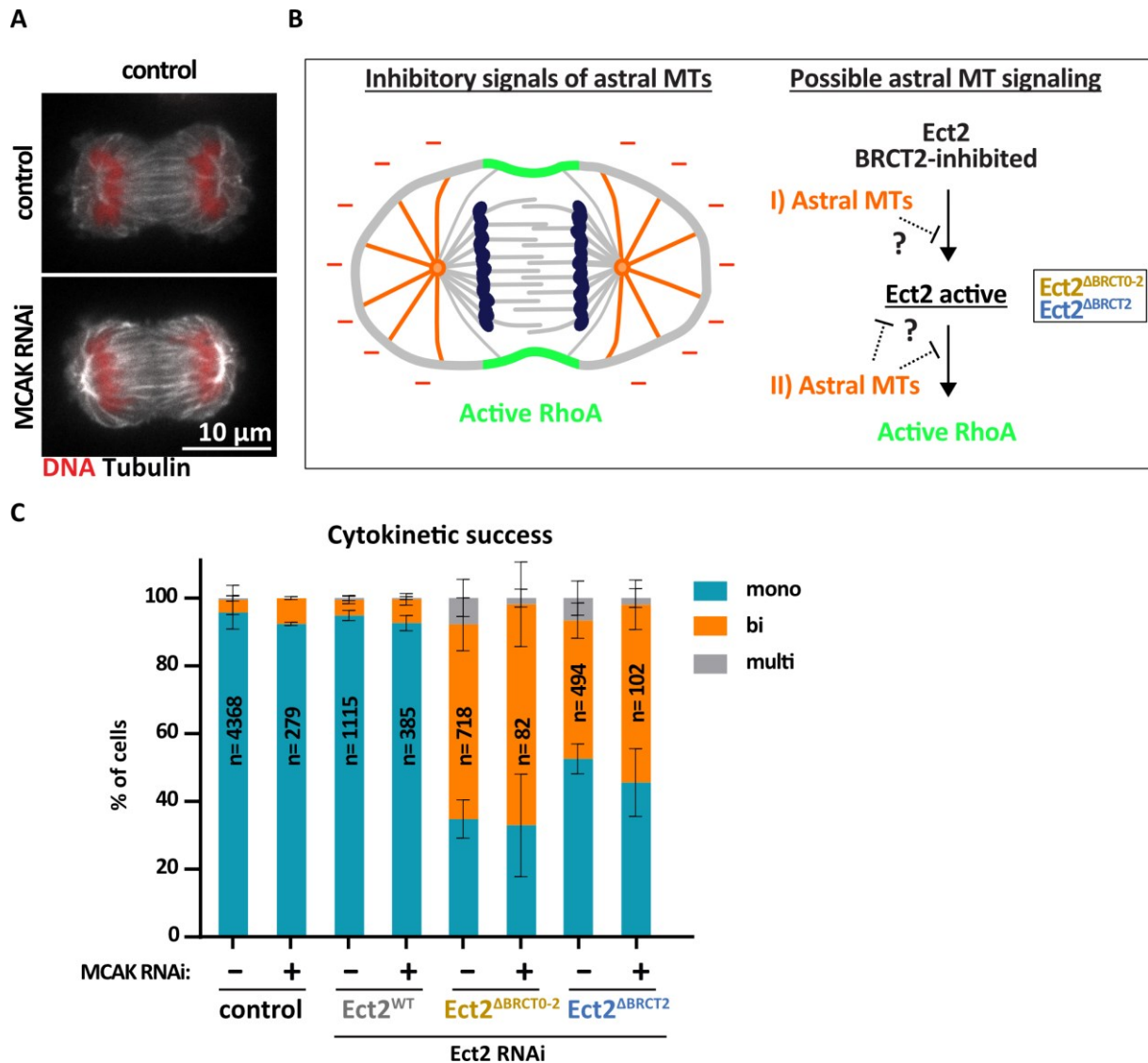


Figure 43: Stabilization of astral microtubules by depleting MCAK does not affect cytokinetic success in cells lacking BRCT2-mediated inhibition. (A) Immunofluorescence images of control and MCAK-depleted control cells in interphase stained with anti- α -tubulin (grey) and Hoechst (red). Images kindly provided by Friederike Wolff. (B) Schematic illustrations of the inhibitory signals emanating from astral microtubules (left) and of how they could contribute to RhoA activation in a narrow zone upstream or downstream of BRCT2-mediated GEF inhibition. (right). (C) Percentages of mono-, bi- and multinucleated cells in control, Ect2^{WT}, Ect2^{ΔBRCT0-2}, and Ect2^{ΔBRCT0-2} cells treated with or without MCAK RNAi. Endogenous Ect2 was depleted by RNAi as indicated. (n=number of cells, data from ≥ 2 independent experiments presented as mean \pm SD, data acquired by SS, KB, FW, EZ).

In principle, stabilizing microtubules could influence cytokinesis in many ways, which could interfere with the aforementioned experimental hypothesis. Thus, not only the effect of MCAK depletion on blebbing and RhoA accumulation was investigated, but also on several other aspects of cytokinesis such as cytokinetic success, furrow ingression, and Ect2 localization.

Moreover, my colleague Friederike Wolff analyzed RhoA accumulation. Her results will not be shown in the following but a summary can be found in Table 20.

MCAK RNAi led to the stabilization of microtubules in control cells (Figure 43 A) and did not influence the success of cytokinesis in control (92 % mononucleation) (% mononucleation not significant compared to control without MCAK RNAi, determined by Kruskal Wallis test), $Ect2^{WT}$ (93 % mononucleation) (% mononucleation not significant compared to $Ect2^{WT}$ without MCAK RNAi, determined by student's t-test), $Ect2^{\Delta BRCT0-2}$ (33 % mononucleation) (% mononucleation not significant compared to $Ect2^{\Delta BRCT0-2}$ without MCAK RNAi, determined by student's t-test), and $Ect2^{\Delta BRCT2}$ cells (46 % mononucleation) (% mononucleation not significant compared to $Ect2^{\Delta BRCT2}$ without MCAK RNAi, determined by student's t-test) (Figure 43 C). However, cells exhibited broad blebs ($\geq 67\%$ of cells after MCAK RNAi vs. 29 % \leq of cells after control RNAi), which are typical for MCAK depletion and generated by long astral microtubules pushing against the membrane (Rankin & Wordeman, 2010b) (Figure 44 A and B). These "medium" blebs with $>7 \mu m$ in width and length, were significantly bigger than small blebs, which had a width and length of around $5 \mu m$ (Figure 44 C). Nevertheless, medium blebs were distinct from large blebs, which are elicited by hyperactive Ect2, since these typically grew longer than $12 \mu m$ (see chapter 3.5.5.2). It is striking, that most cells, missing BRCT2-mediated inhibition, formed more than 3 medium blebs when treated with MCAK RNAi, whereas MCAK RNAi treated control and $Ect2^{WT}$ cells usually had 1-2 medium blebs. Probably, this difference can be explained by the already fragile cell shape of $Ect2^{\Delta BRCT0-2}$ and $Ect2^{\Delta BRCT2}$, which is more susceptible to additional perturbation by long microtubules.

Moreover, MCAK depletion had no impact on furrow ingression in $Ect2^{WT}$ ($8.5 \mu m$ after MCAK RNAi vs $6.4 \mu m$ in control RNAi), $Ect2^{\Delta BRCT0-2}$ ($15.3 \mu m$ after MCAK RNAi vs $13.0 \mu m$ in control RNAi), and $Ect2^{\Delta BRCT2}$ ($12.5 \mu m$ after MCAK RNAi vs $11.5 \mu m$ in control RNAi) cells, but led to a mild ingression delay in control cells ($11.8 \mu m$ after MCAK RNAi vs $6.3 \mu m$ in control RNAi) (Figure 44 E). Furthermore, quantification of large membrane blebs in these cell lines revealed no differences in the presence and absence of MCAK in meta- and anaphase, which was thought to hint towards astral microtubules stimulating BRCT2-mediated inhibition (Figure 44 D). However, given that MCAK depletion itself elicits elevated bleb formation, blebbing may not be a suitable readout to address whether astral microtubules promote BRCT2-mediated inhibition.

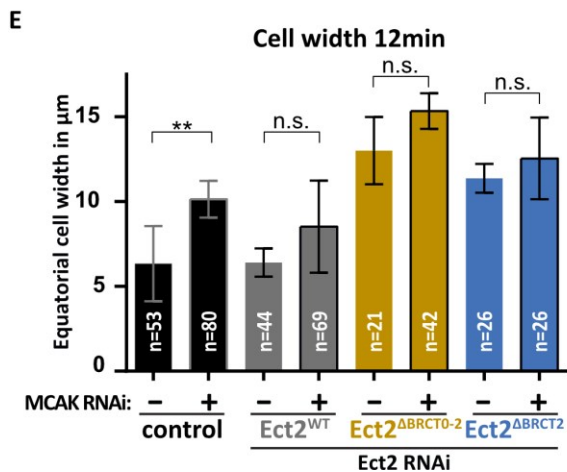
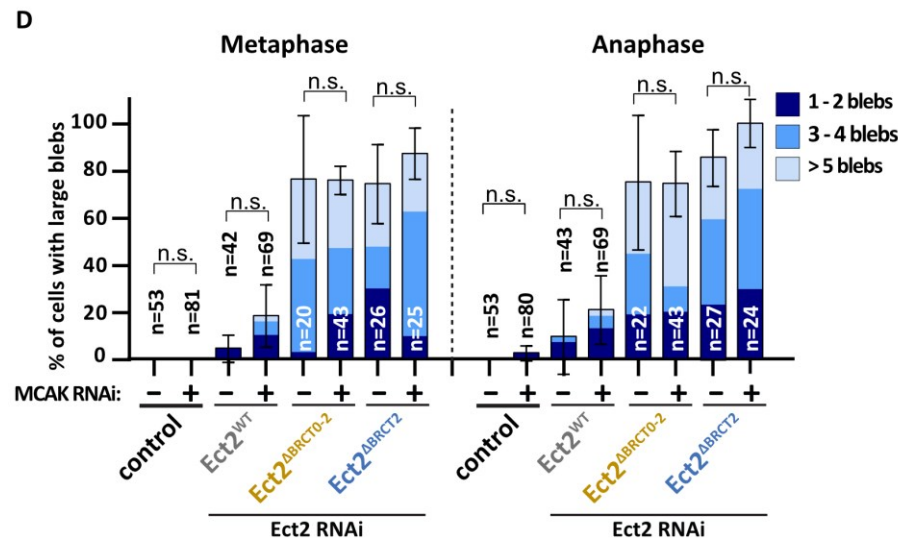
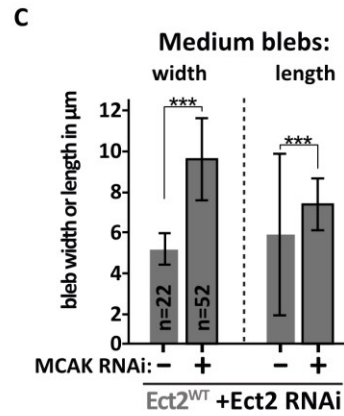
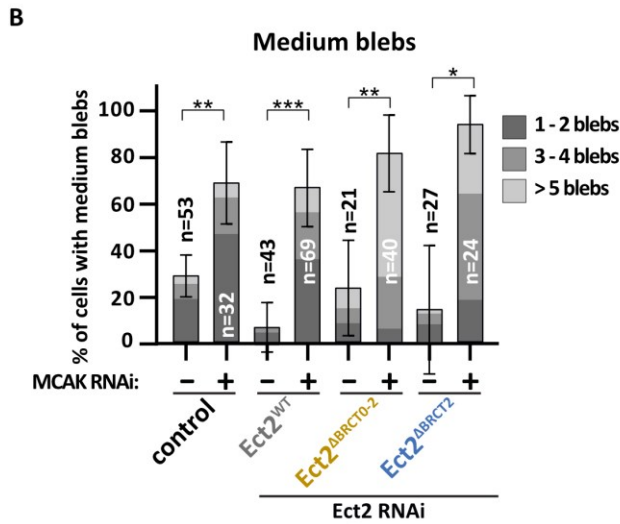
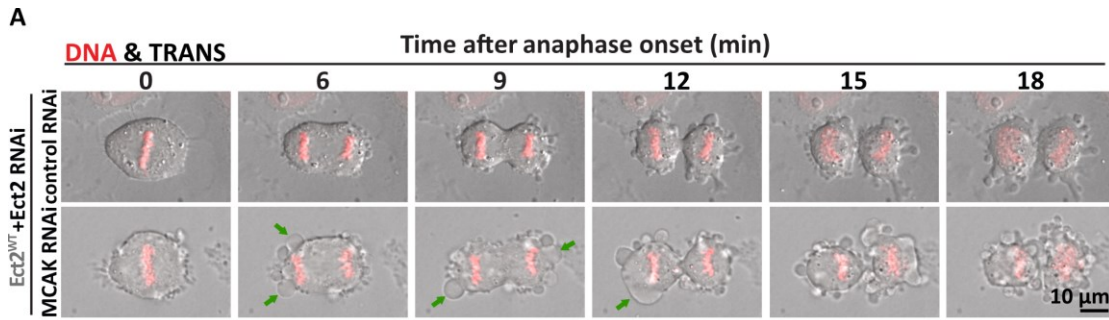


Figure 44: Stabilization of astral microtubules by depleting MCAK triggers the formation of medium blebs and does not influence the formation of large blebs and furrow ingression in cells lacking BRCT2-mediated inhibition. A) Representative live-cell image sequences of dividing Ect2^{WT} cells treated with control and MCAK RNAi. Endogenous Ect2 was depleted by RNAi. DNA was probed with SiR-DNA. Time in minutes after anaphase onset. Medium blebs are indicated with green arrows. (B) Percentages of control, Ect2^{WT}, Ect2^{ΔBRCT0-2}, and Ect2^{ΔBRCT2} cells, which formed 1-2, 3-4, and >5 medium blebs during meta- and anaphase. Endogenous Ect2 was depleted by RNAi as indicated. (n=number of cells, data from ≥4 independent experiments presented as mean, SD for total blebbing, ***p<0.001, **p<0.01, *p<0.05 and n.s.=not significant determined by Kruskal Wallis test except for Ect2^{ΔBRCT2}±MCAK RNAi which was determined by student's t-test). (C) Width and length (μm) of medium blebs in Ect2^{WT} cells treated with and without MCAK RNAi during anaphase. Endogenous Ect2 was depleted by RNAi. (n=number of blebs, ***p<0.001 determined by Kruskal Wallis test). (D) Percentages of control, Ect2^{WT}, Ect2^{ΔBRCT0-2}, and Ect2^{ΔBRCT2} cells, which formed 1-2, 3-4, and >5 large blebs during meta- and anaphase. Endogenous Ect2 was depleted by RNAi as indicated. (n=number of cells, data from ≥4 independent experiments presented as mean, SD for total blebbing, n.s.=not significant p>0.05 determined by Kruskal Wallis test and student's test according to normality). (E) Equatorial cell width in μm measured 12 min after anaphase onset for control, Ect2^{WT}, Ect2^{ΔBRCT0-2}, and Ect2^{ΔBRCT2} cells treated with or without MCAK RNAi. Endogenous Ect2 was depleted by RNAi as indicated. (n=number of cells, data from ≥5 independent experiments presented as mean ± SD, **p<0.01 and n.s.=not significant p>0.05 determined by student's t-test).

Further, MCAK depletion did not prevent Ect2 membrane localization in Ect2^{WT}, Ect2^{ΔBRCT0-2}, and Ect2^{ΔBRCT2} cells (Figure 45). While Ect2^{ΔBRCT0-2} and Ect2^{ΔBRCT2} levels at the equator, the poles, and the midzone were indistinguishable between MCAK RNAi-treated and untreated cells, Ect2^{WT} levels were reduced in the absence of MCAK (Figure 45 B and C). But importantly, the relative enrichment at the equator was not changed in all cell lines (Figure 45 D).

In summary, these results demonstrated that MCAK depletion does not greatly interfere with cytokinetic parameters such as cytokinetic success, furrow ingression, large bleb formation, and Ect2 localization either in control and Ect2^{WT} or in Ect2^{ΔBRCT0-2} and Ect2^{ΔBRCT2} expressing cells. However, MCAK depletion led to the formation of medium-sized blebs. As large bleb formation was supposed to be the main readout to assess whether astral microtubules stimulate BRCT2-dependent Ect2 autoinhibition, the formation of medium blebs upon MCAK depletion clashed with the experimental design. Thus, it was concluded that blebbing cannot be used to investigate this issue.

Contrary to that, RhoA intensity measurements (data from Friederike Wolff, Table 20) could show that astral microtubules actively regulate RhoA accumulation at the equatorial membrane in Ect2^{ΔBRCT0-2} and Ect2^{ΔBRCT2} cells. In Ect2^{ΔBRCT0-2} and Ect2^{ΔBRCT2} cells, MCAK

depletion resulted in a significantly reduced RhoA zone width (Schneid et al., 2021). Moreover, the total amount of RhoA at the equator was not altered (unpublished). Together, these findings argue for microtubules being important for the spatial restriction of active Ect2 to a certain area at the equator, rather than being directly involved in the negative regulation of Ect2 activity. Thus, astral microtubules and BRCT2-mediated inhibition act in parallel to control Ect2 activity. (also see chapter 4.8)

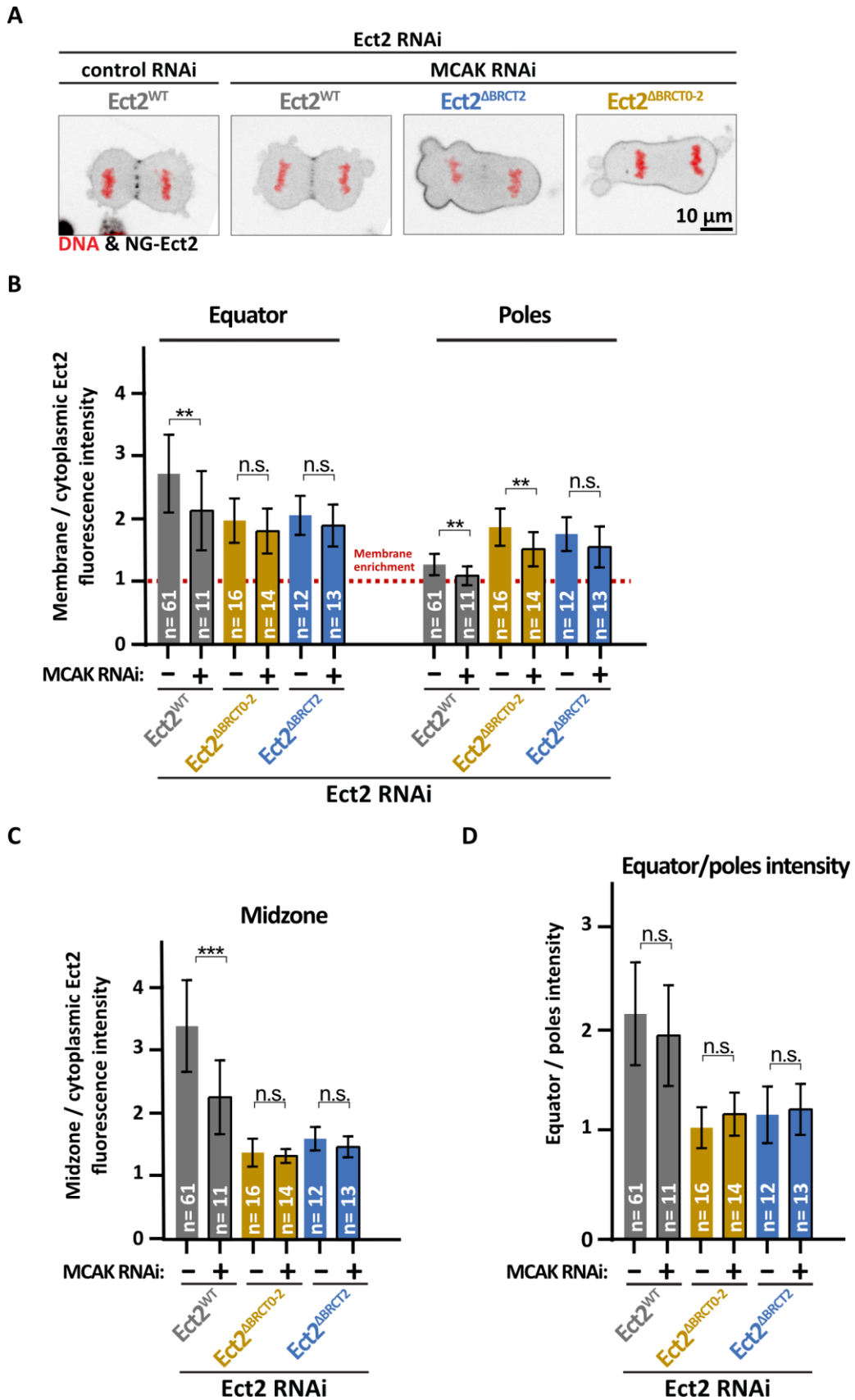


Figure 45: Stabilization of astral microtubules by depleting MCAK has no influence on Ect2 localization in cells lacking BRCT2-mediated inhibition. (A) Fluorescence live-cell images showing the localization of NG-Ect2^{WT}, NG-Ect2^{ΔBRCT0-2}, and NG-Ect2^{ΔBRCT2} in anaphase cells

treated with and without MCAK RNAi. Endogenous Ect2 was depleted by RNAi. DNA was probed with SiR-DNA. (B) Fluorescence intensities of NG-Ect2^{WT}, NG-Ect2^{ΔBRCT0-2}, and NG-Ect2^{ΔBRCT2} at the equatorial and polar membrane relative to cytoplasmic levels in cells treated with and without MCAK RNAi. Endogenous Ect2 was depleted by RNAi. (n= number of cells, data from ≥4 independent experiments presented as mean±SD, **p<0.01 and n.s.= not significant p>0.05 determined by Kruskal Wallis test and student's t-test according to normality). (C) Fluorescence intensities of NG-Ect2^{WT}, NG-Ect2^{ΔBRCT0-2}, and NG-Ect2^{ΔBRCT2} at the midzone relative to cytoplasmic levels in cells treated with and without MCAK RNAi. Endogenous Ect2 was depleted by RNAi. (n= number of cells, data from ≥4 independent experiments presented as mean±SD, ***p<0.001 and n.s.= not significant p>0.05 determined by Kruskal Wallis test and student's t-test according to normality) (D) Intensity ratio of the equatorial and the polar membrane of NG-Ect2^{WT}, NG-Ect2^{ΔBRCT0-2} and NG-Ect2^{ΔBRCT2} (n= number of cells, data from ≥4 independent experiments presented as mean±SD, n.s.= not significant p>0.05 determined by student's t-test).

3.8 Analyzing the contributions of the S-loop and the PH-domain to Ect2 function and regulation

In 2014, the crystal structure of the triple BRCT domain of Ect2 was solved, however, lacking the C-terminal domains (Zou et al., 2014). Recently, Chen et al. (2020) published the crystal structure of Ect2 including the DH-GEF domain and the PH-domain, which gives more insight into how Ect2 autoinhibition is structurally accomplished. Unlike the prevailing model that solely the BRCT domains are responsible for autoinhibition, they proposed that three structural domains of Ect2 seem to contribute to Ect2 regulation. The PH-domain folds back onto the DH-GEF domain and binds the catalytic center. Disruption of the DH-PH interaction by two point mutations (Ect2^{P703D} or Ect2^{C765K}) led to strongly increased GEF activity *in vitro*, which underlines the importance of this interaction. BRCT2 also directly interacts with the DH-GEF domain, but the loss of BRCT2 only resulted in mildly elevated GEF activity *in vitro*. Removing the S-loop also mildly increased GEF activity *in vitro* and it is assumed to inhibit Ect2 indirectly by blocking RhoA binding. Saito et al. (2004) could show that the loss of the linker region increased malignant transformation in cells and other groups have shown that several residues in the linker get phosphorylated, although the functional consequences of these phosphorylations for Ect2 are not clear yet (Hara et al., 2006; Justilien et al., 2011; Niiya et al., 2006; Yüce et al., 2005). Thus, Ect2 autoinhibition appears to be more complex than first thought.

That prompted us to further investigate whether PH-mediated inhibition plays a role in living cells and whether phosphorylation of the S-loop contributes to Ect2 regulation with the same assays described above for the BRCT domains (multinucleation assay, furrow ingression, bleb formation phenotype, localization, etc.).

3.8.1 The S-loop of Ect2 contributes to the negative regulation of Ect2 GEF activity during mitosis

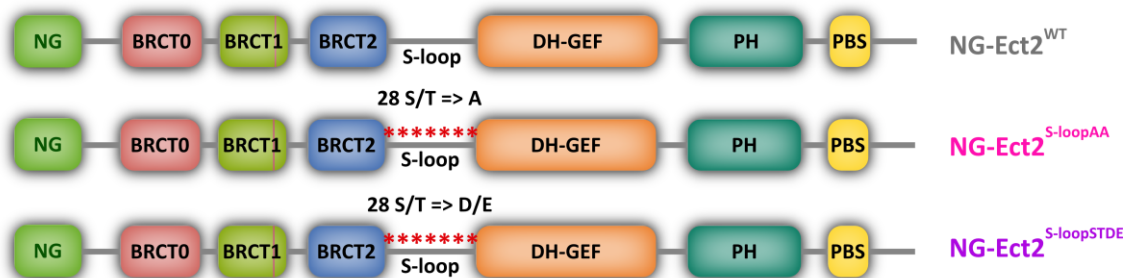
The S-loop of Ect2 is characterized by an unusually high amount of serines and threonines. Out of the 101 amino acids in the S-loop, 20 are serines (20 %) and 8 are threonines (8 %). As a result, the percentage of potential phosphorylation sites in the S-loop is almost twice as high as in the rest of the protein (28 % vs. 16 %, Figure 46 B). This makes the S-loop a likely target of phosphorylation events and a few specific sites have already been identified (Hara et al., 2006; Justilien et al., 2011; Niiya et al., 2006; Niiya et al., 2005; Suzuki et al., 2015; Tatsumoto et al., 1999). However, it is largely unclear what role phosphorylation plays in Ect2 function and regulation.

To test whether phosphorylation of residues in the S-loop is essential for Ect2 function and regulation in our replacement system, an Ect2 variant harboring a phospho-deficient S-loop (Ect2^{S-loopAA}) was used, that had been generated earlier in the laboratory by mutating all serines and threonines to alanines (Buchner, 2019) (Figure 46 A and B). Additionally, a phospho-mimetic S-loop (Ect2^{S-loopSTDE}) was generated by mutating all serines and threonines to aspartic acid and glutamic acid, respectively. (Figure 46 B). A description of which of the residues was mutated to aspartic acid and which to glutamic acid can be found in Figure 46 C.

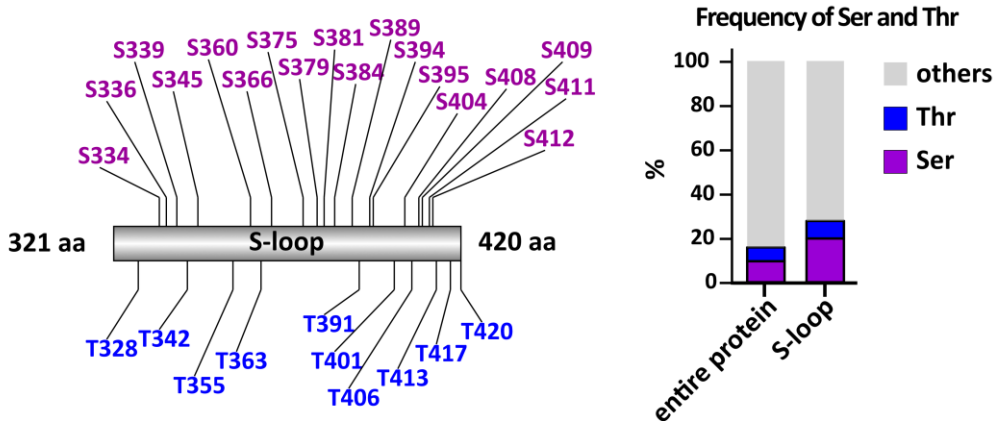
Dr. Kristina Buchner had generated and started the analysis of the Ect2^{S-loopAA} (Buchner, 2019). However, using immunoblot analysis and subsequent signal quantification, we found that Ect2^{S-loopAA} and Ect2^{S-loopSTDE} proteins were expressed above endogenous Ect2 levels when we induced their expression with 0.2 µg/ml of tetracycline (not shown). We tried to adjust expression levels by reducing the amount of tetracycline and found that induction with 0.01 µg/ml tetracycline resulted in mutant Ect2 proteins levels which were similar to endogenous Ect2 and Ect2^{WT} (Figure 47 A and Table 19). Thus, both S-loop mutants were analyzed using a reduced amount of tetracycline.

In the multinucleation assays, Ect2^{S-loopAA} and Ect2^{S-loopSTDE} supported successful cytokinesis, which resulted in 86.8 % and 75.1 %, respectively, mononucleated cells (Figure 47 B). Even though multinucleation was slightly increased in both mutants as compared to control and Ect2^{WT} (both >94 % mononucleated) (% mononucleation for Ect2^{S-loopAA} not significant and for Ect2^{S-loopSTDE} p<0.001 compared to control and Ect2^{WT}, determined by Tukey's test), they were considered functional as the increase was minor compared to the strong increase after the loss of endogenous Ect2 in control cells (~80 %).

A



B



C

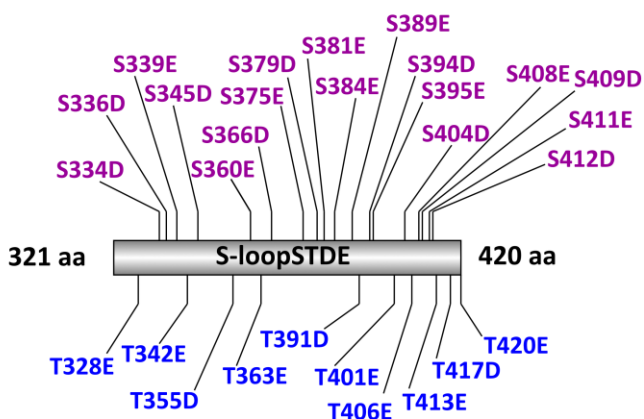


Figure 46: The S-loop encompasses about twice as many possible phosphorylation sites than the entire Ect2 protein. (A) Schematic representation showing the domain organization of the NG-tagged Ect2^{WT}, NG-Ect2^{S-loopAA}, and NG-Ect2^{S-loopSTDE} proteins. All serines and threonines were mutated to alanine (Ect2^{S-loopAA}) and aspartic and glutamic acid (Ect2^{S-loopSTDE}),

respectively. Point mutations are indicated by asterisks. (B) Schematic representation of the S-loop. The positions of serines (purple) and threonines (blue) within the S-loop are indicated and their frequency (20 % serines and 8 % threonines) is shown in comparison to the entire protein (10 % serines and 6 % threonines). (C) Schematic representation of the S-loopSTDE showing which of the alanine residues were mutated to aspartic acid and which to glutamic acid.

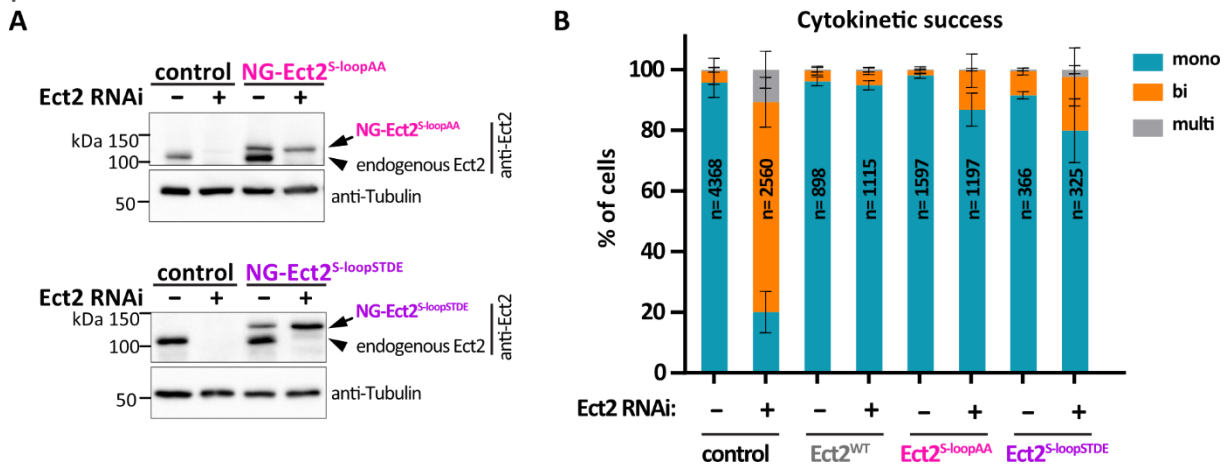


Figure 47: NG-Ect2^{S-loopAA} and NG-Ect2^{S-loopSTDE} proteins are expressed at endogenous levels and are functional during cytokinesis. (A) Western blot analysis of lysates from control, NG-Ect2^{S-loopAA}, and NG-Ect2^{S-loopSTDE} cells treated with and without Ect2 RNAi to knockdown endogenous Ect2. Blots were probed with anti-Ect2 and anti- α -tubulin (as loading control). Endogenous Ect2 has a molecular weight of 100.1 kDa, NG-Ect2^{S-loopAA} of 127.4 kDa, and NG-Ect2^{S-loopSTDE} of 127.9 kDa. (B) Percentages of mono-, bi- and multinucleated cells in control, Ect2^{WT}, Ect2^{S-loopAA}, and Ect2^{S-loopSTDE} cells treated with or without Ect2 RNAi to deplete endogenous Ect2. (n=number of cells, data from ≥ 3 independent experiments presented as mean \pm SD, data acquired by SS, KB, FW, EZ). For all experiments, Ect2^{S-loopAA} and Ect2^{S-loopSTDE} were induced with 0.01 μ g/ml of tetracycline. For all Ect2^{S-loopAA} and Ect2^{S-loopSTDE} were induced with 0.01 μ g/ml of tetracycline.

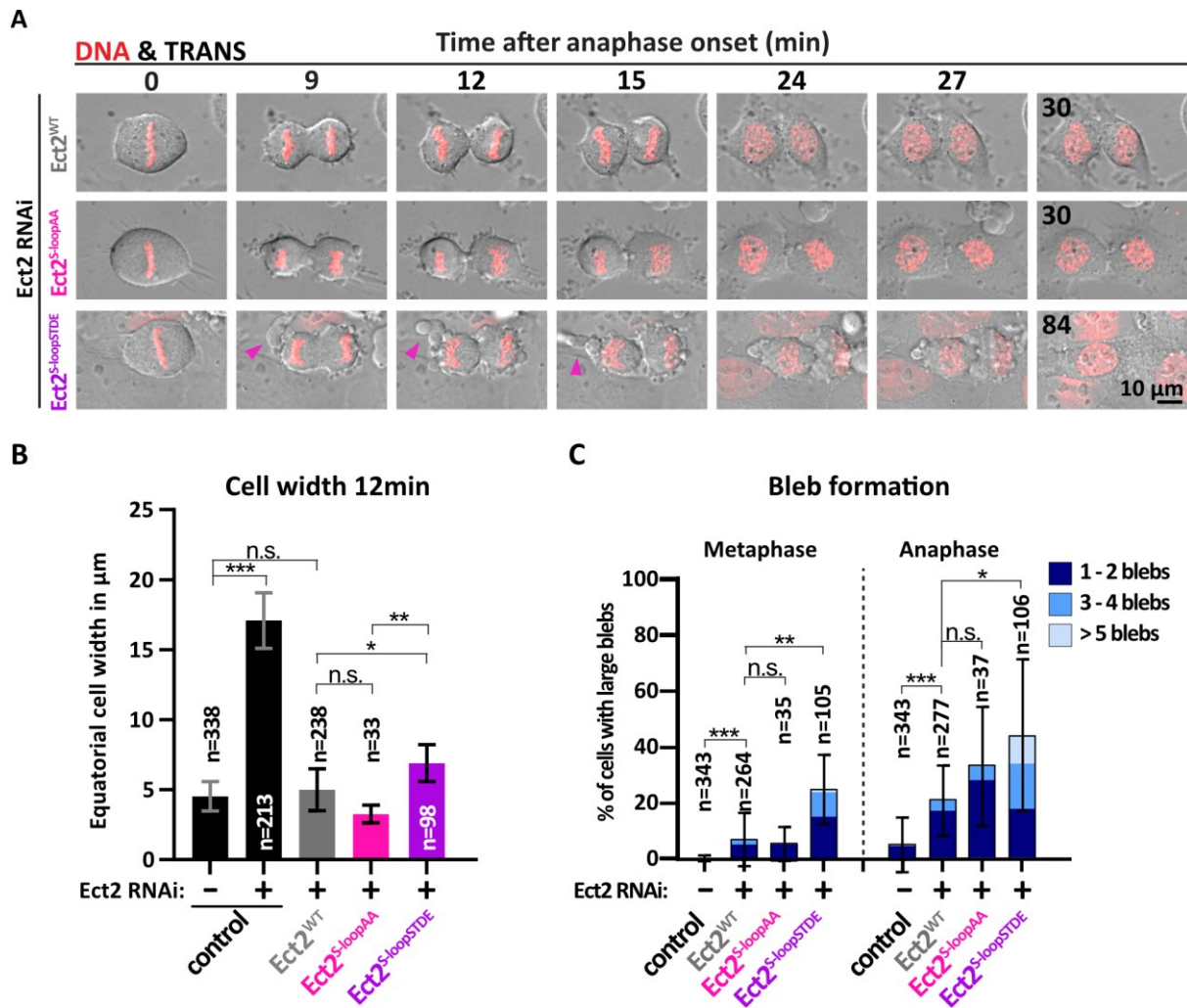


Figure 48: Phospho-deficient S-loop mutations slightly speed up furrow ingression and phospho-mimetic S-loop mutations slightly delay furrow ingression and elicit the formation of large membrane blebs. (A) Representative live-cell image sequences of dividing Ect2^{WT}, Ect2^{S-loopAA}, and Ect2^{S-loopSTDE} cells. Endogenous Ect2 was depleted by RNAi. DNA was probed with SiR-DNA. Time in minutes after anaphase onset. Large blebs are indicated with pink arrowheads. (B) Equatorial cell width in μ m measured 12 min after anaphase onset for control, Ect2^{WT}, Ect2^{S-loopAA}, and Ect2^{S-loopSTDE} cells. Endogenous Ect2 was depleted by RNAi as indicated. (n=number of cells, data from ≥ 4 independent experiments presented as mean \pm SD, *** $p < 0.001$, ** $p < 0.01$, * $p < 0.05$ and n.s.=not significant determined by Tukey's test) (C) Percentages of control, Ect2^{WT}, Ect2^{S-loopAA}, and Ect2^{S-loopSTDE} cells, which formed 1-2, 3-4 and >5 large blebs during meta- and anaphase. Endogenous Ect2 was depleted by RNAi as indicated. (n=number of cells, data from ≥ 4 independent experiments presented as mean, SD for total blebbing, ** $p < 0.01$, * $p < 0.05$ and n.s.=not significant determined by Kruskal Wallis test except for Ect2^{WT} and Ect2^{S-loopAA} in anaphase). For all Ect2^{S-loopAA} and Ect2^{S-loopSTDE} were induced with 0.01 μ g/ml of tetracycline.

Next, dividing Ect2^{S-loopAA} and Ect2^{S-loopSTDE} cells were filmed. Representative image sequences are shown in Figure 48 A. During time-lapse imaging Ect2^{S-loopAA} and Ect2^{S-loopSTDE} cells exhibited a phenotype very similar to control cells. Furrow ingression in Ect2^{S-loopAA} appeared slightly faster than in control cells, which was supported by the slightly smaller equatorial width of 3.27 μm 12 min after anaphase onset, as compared to control (4.5 μm) and Ect2^{WT} (5.0 μm) (Figure 48 B). Although this difference was not statistically significant, it was a clearly visible trend. Furrow ingression in Ect2^{S-loopSTDE} cells was a little bit slower than in control (4.5 μm) and Ect2^{WT} (5.0 μm) cells, given the equatorial cell width 12 min after anaphase onset of 6.9 μm (Figure 48 B). So it seems that timely furrow ingression is affected by the phosphorylation status of the S-loop.

The phospho-deficient S-loop (Ect2^{S-loopAA}) did not result in increased formation of membrane blebs. Similar to Ect2^{WT} (6.8 % and 20.4 %), 5.1 % and 32.7 % of Ect2^{S-loopAA} expressing cells exhibited membrane blebs in meta- and anaphase, respectively (Figure 48 C). Phospho-mimetic mutation of the S-loop had a more prominent effect on bleb formation. Expression of Ect2^{S-loopSTDE} led to blebbing in 24.5 % and 43.8 % of cells, respectively (numbers for meta- and anaphase, respectively) (Figure 48 C). While more than 1-2 blebs were rarely counted in Ect2^{S-loopAA} (0 % and 5.1 % of total cells in metaphase and anaphase, respectively), this was more likely in Ect2^{S-loopSTDE} cells (9.6 % and 26.4 % of total cells) (Figure 48 C). These results suggest that phosphorylation of the S-loop increases Ect2 GEF activity.

Taken together, we could show that mutating all serines and threonines in the S-loop to alanine or glutamic and aspartic acid does not affect the success of cytokinesis and only marginally influences timely furrow ingression. Moreover, Ect2^{S-loopSTDE} led to a medium increase in bleb formation, while Ect2^{S-loopAA} did not. These results suggested that phosphorylation of the S-loop results in a mild increase of Ect2 activity, however, its contribution is only minor.

3.8.2 The PH-domain negatively regulates Ect2 GEF activity during mitosis

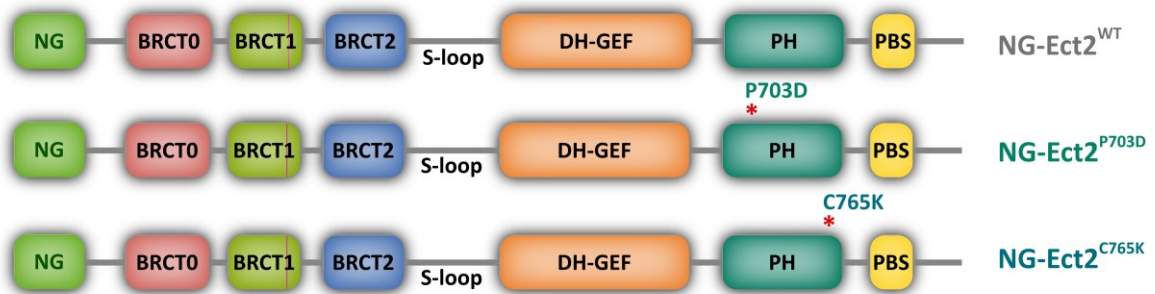
The PH domain of Ect2 is located directly behind the DH-GEF domain at the C-terminus (Schmidt & Hall, 2002; Zheng, 2001). It is required for cytokinesis and facilitates the localization to the plasma membrane by binding to phospholipids (Chalamalasetty et al., 2006; Frenette et al., 2012; Su et al., 2011). A common regulatory principle in DH-GEFs is that the PH domain regulates the activity of the adjacent DH-GEF domain (Zheng, 2001). Recent structural data (Chen et al., 2020) revealed that the PH domain in Ect2 folds back onto the DH-GEF domain and directly interacts with the catalytic center. The hydrophobic DH-PH interaction is mediated by two residues, P703 and C765, in the PH domain and can be disrupted by changing P703 to aspartic acid (P703D) and C765 to lysine (C765K), which highly increased GEF-activity *in vitro*. Additionally, overexpression of these mutants led to cell rounding and stress fiber formation in interphase cells (Chen et al., 2020). Together with the finding, that mutation of G707 (not conserved in human Ect2) in the PH domain to aspartic acid (G707D) boosted Ect2 activity in *C. elegans* (Zhang & Glotzer, 2015), these results strongly speak for an involvement of the PH domain in regulating Ect2 activity.

To determine whether the PH domain negatively regulates Ect2 activity during cell division, two transgenic cell lines, harboring the point mutations published by Chen et al. (2020) (Ect2^{P703D} and Ect2^{C765K}, Figure 49) were generated. Immunoblot analysis, revealed that the Ect2^{C765K} transgene was expressed similarly to control and Ect2^{WT} (Figure 50 A and Table 19). Protein levels of Ect2^{P703D}, however, were strongly increased when protein expression was induced with the standard tetracycline concentration of 0.2 µg/ml (data not shown). To achieve protein levels comparable to endogenous Ect2 and Ect2^{WT}, Ect2^{P703D} was induced with 0.02 µg/ml of tetracycline (Figure 50 A and Table 19).

Ect2^{P703D} fully rescued the cytokinetic failure phenotype after the depletion of Ect2 and cells showed similar percentages of mononucleated cells (91 %) as compared to control and Ect2^{WT} (96 % and 95 % respectively) (% mononucleation not significant compared to control and Ect2^{WT}, determined by Tukey's test) (Figure 50 B). Ect2^{C765K} exhibited slightly elevated levels of multinucleation (18 % bi- and 1 % multinucleated) (% mononucleation p<0.001 compared

to control and Ect2^{WT}, determined by Tukey's test), but given the light increase, was considered functional during cytokinesis (Figure 50 B).

A



B

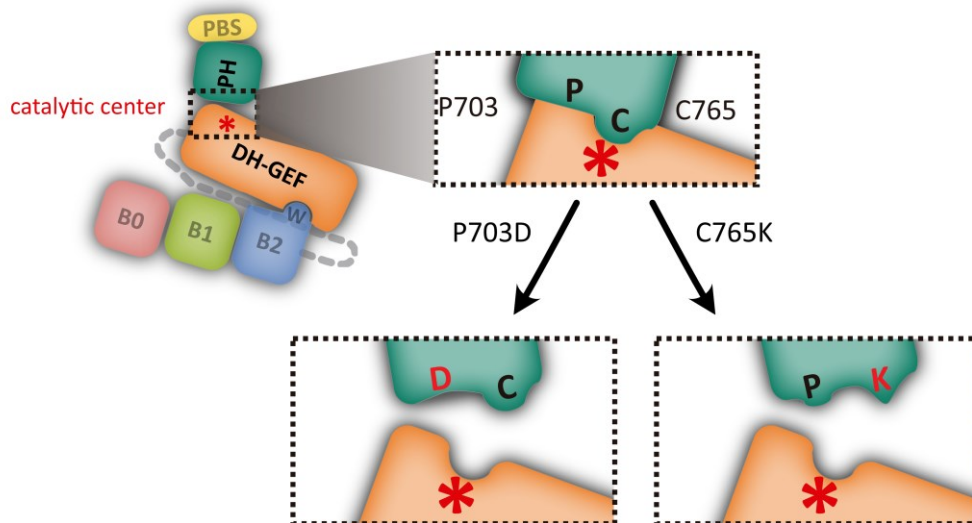


Figure 49: The PH domain folds back onto the DH-GEF domain and binds to the catalytic center. (A) Schematic representation showing the domain organization of the NG-tagged Ect2^{WT}, NG-Ect2^{P703D}, and NG-Ect2^{C765K} proteins. Point mutations are indicated by asterisks. (B) Schematic illustration of the interaction of the PH domain with the catalytic center in the DH-GEF domain, which depends on P703 and C765 located in the PH domain. P703D and C765K mutations abolish this interaction (Chen et al., 2020).

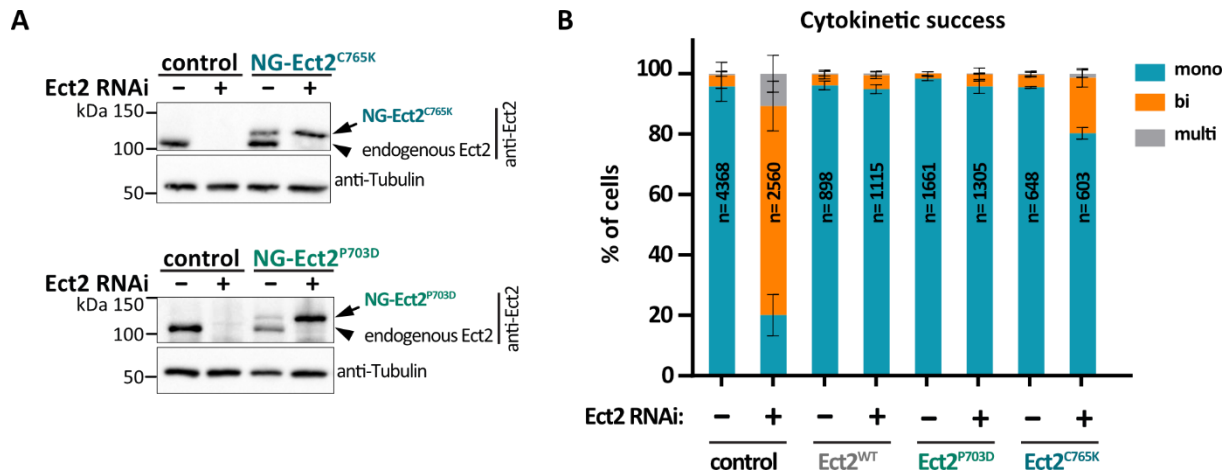


Figure 50: NG-Ect2^{P703D} and NG-Ect2^{C765K} proteins are expressed at endogenous levels and are functional during cytokinesis. (A) Western blot analysis of lysates from control, NG-Ect2^{P703D}, and NG-Ect2^{C765K} cells treated with and without Ect2 RNAi to knockdown endogenous Ect2. Blots were probed with anti-Ect2 and anti- α -tubulin (as loading control). Endogenous Ect2 has a molecular weight of 100.1 kDa, NG-Ect2^{P703D} of 127.0 kDa, and NG-Ect2^{C765K} of 127.0 kDa. (B) Percentages of mono-, bi- and multinucleated cells in control, Ect2^{WT}, Ect2^{P703D}, and Ect2^{C765K} cells treated with or without Ect2 RNAi to deplete endogenous Ect2. (n=number of cells, data from ≥ 3 independent experiments presented as mean \pm SD, data acquired by SS, KB, FW, EZ). For all Ect2^{P703D} was induced with 0.02 μ g/ml of tetracycline.

Next, time-lapse imaging of dividing Ect2^{P703D} and Ect2^{C765K} cells was performed. Exemplary image sequences for both cell lines are depicted in Figure 51 A. Live-cell imaging of Ect2^{P703D} cells showed no defect in furrow formation and Ect2 regulation (Figure 51 B and C). Measurement of the cell width 12 min after anaphase onset confirmed that there is no significant difference in furrow ingression compared to control and Ect2^{WT} (4.38 μ m versus 4.5 μ m and 5.0 μ m) (Figure 51 B). Moreover, mutation of P703 to aspartic acid (Ect2^{P703D}) did not trigger the formation of large membrane blebs in meta- and anaphase (3.5 % and 9.2 % versus 6.8 % and 20.4 % in Ect2^{WT}) (Figure 51 C). Therefore, Ect2^{P703D} fully supports timely furrow ingression and does not lead to hyperactive Ect2, and resembles the WT phenotype. Contrary to that, Ect2^{C765K} cells ingressed slightly slower compared to Ect2^{WT} and formed numerous large blebs in meta- and anaphase (Figure 51 B and C). Equatorial cell width 12 min after anaphase onset was 7.4 μ m as compared to 4.5 μ m in control and 5.0 μ m in Ect2^{WT} cells (Figure 51 B). Membrane blebbing in Ect2^{C765K} cells was the strongest observed among all mutants (including BRCT mutants), with 93.3 % and 86.7 % of cells forming large blebs in meta- and anaphase, respectively (Figure 51 C). Over 55 % of all blebbing cells in meta- and anaphase exhibited, more than 1-2 blebs. Ect2^{C765K} seems to lack proper regulation of Ect2 activity, which provokes excessive bleb formation.

In summary, the two point mutations P307D and C765K in the PH domain led to different effects on cytokinesis. Ect2^{P703D} did not elicit multinucleation, defects in furrow ingression, or the formation of large blebs and resembled Ect2^{WT}. Contrary to that, while not having a strong effect on the cytokinetic success and furrow ingression, Ect2^{C765K} strongly increased the formation of large blebs in meta- and anaphase. These findings clearly indicated a role of the PH domain in GEF activity regulation of Ect2.

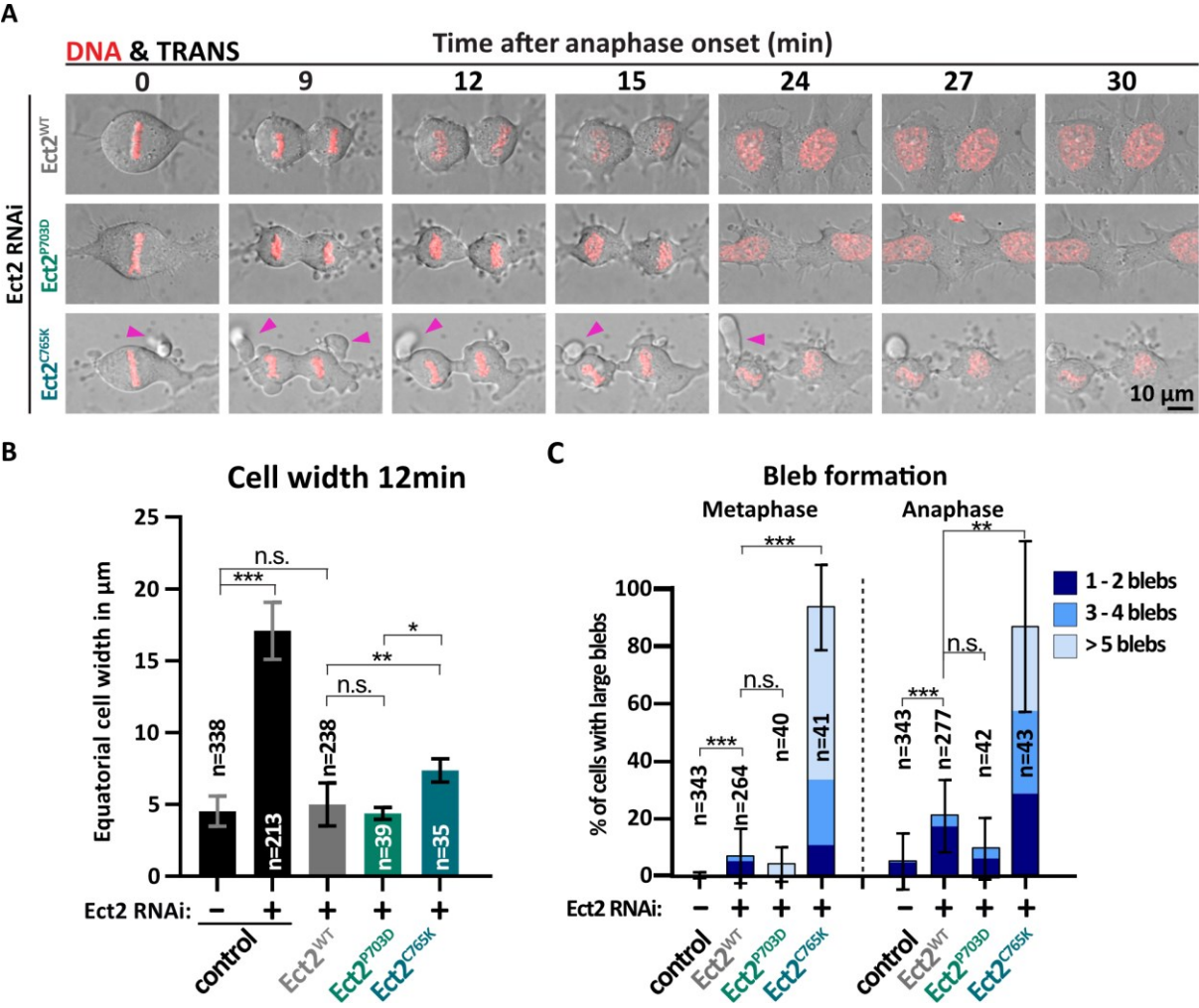


Figure 51: C765K mutation in the PH-domain slightly delays furrow ingression and triggers the formation of large membrane blebs, whereas mutation P703D shows none of these effects. (A) Representative live-cell image sequences of dividing Ect2^{WT}, Ect2^{P703D}, and Ect2^{C765K} cells. Endogenous Ect2 was depleted by RNAi. DNA was probed with SiR-DNA. Time in minutes after anaphase onset. Large blebs are indicated with pink arrowheads. (B) Equatorial cell width in μ m measured 12 min after anaphase onset for control, Ect2^{WT}, Ect2^{P703D}, and Ect2^{C765K} cells. Endogenous Ect2 was depleted by RNAi as indicated. (n=number of cells, data from ≥ 3 independent experiments presented as mean \pm SD, ***p<0.001, **p<0.01, *p<0.05 and n.s.=not significant determined by Tukey's test) (C) Percentages of control, Ect2^{WT}, Ect2^{P703D}, and Ect2^{C765K} cells, which formed 1-2, 3-4, and >5 large blebs during meta- and anaphase. Endogenous Ect2 was depleted by RNAi as indicated. (n=number of cells,

data from ≥ 3 independent experiments presented as mean, SD for total blebbing, *** $p < 0.001$, ** $p < 0.01$, * $p < 0.05$ and n.s.=not significant determined by Kruskal Wallis test except for Ect2^{WT} and Ect2^{P703D} in anaphase). For all Ect2^{P703D} was induced with 0.1 $\mu\text{g/ml}$ of tetracycline.

3.8.3 Increased intracellular pressure in strongly blebbing cells often results in cell shape oscillations and cytokinetic failure

As described in more detail in Chapter 3.5.5.3, increased RhoA signaling leads to elevated cortical contractility, which causes the formation of large blebs (Taneja et al., 2020; Zanin et al., 2013). Large membrane blebs can lead to internal pressure imbalances and trigger cell shape oscillations (Sedzinski et al., 2011). As we found that rendering the S-loop phosphomimetic (Ect2^{S-loopSTDE}) and mutating C765 to lysine (Ect2^{C765K}) triggers the formation of large blebs, we checked whether cells expressing these Ect2 mutants also exhibit cell shape oscillations.

Ect2^{S-loopSTDE} (8.9 %) and Ect2^{C765K} (32.6 %) both displayed more shape oscillation events during time-lapse imaging than Ect2^{WT} (1.3 %, n=78) (Figure 52 A). Again, the frequency of shape oscillations correlated with the intensity of the exhibited blebbing phenotype in anaphase (43.8 % and 86.7 % blebbing in Ect2^{S-loopSTDE} and Ect2^{C765K}, respectively). For comparison, cells expressing Ect2^{S-loopAA} (n=37) and Ect2^{P703D} (n=43), did not oscillate. Cell shape oscillations often lead to the failure of cytokinesis (Sedzinski et al., 2011; Taneja et al., 2020). As we have seen slightly increased levels of multinucleation in Ect2^{S-loopSTDE} and Ect2^{C765K}, we speculated that the reason for this could be their oscillation behavior. Indeed, 60.0 % and 92.9 % of oscillating cells in Ect2^{S-loopSTDE} and Ect2^{C765K}, respectively, were left binucleated. (Figure 52 B) These results further supported that in Ect2^{S-loopSTDE} and Ect2^{C765K} cells Ect2 activity is increased due to defects in inhibition.

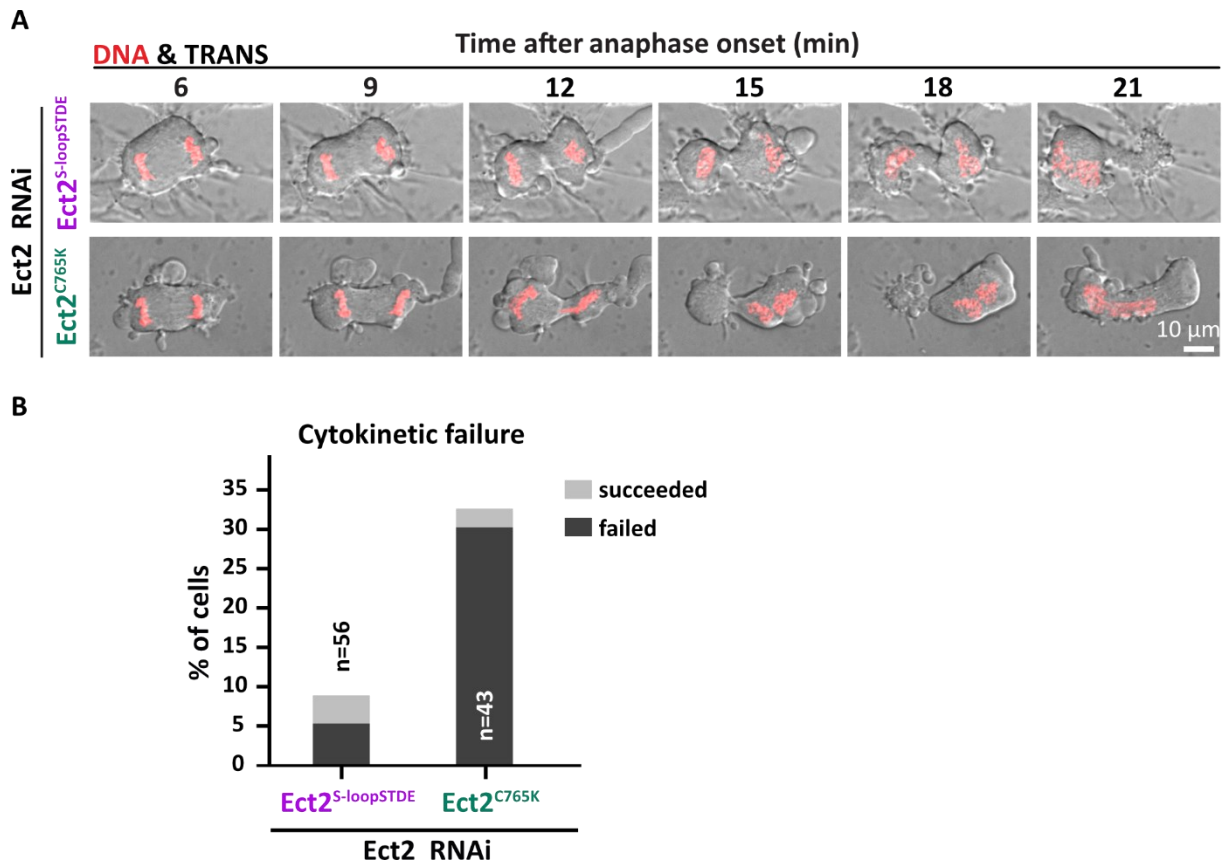


Figure 52: Hyperactive Ect2^{S-loopSTDE} and Ect2^{C765K} trigger cell shape oscillations during anaphase, which often result in cytokinesis failure. (A) Representative live-cell image sequences of dividing Ect2^{S-loopSTDE} and Ect2^{C765K} cells, which exhibit cell shape oscillations. Endogenous Ect2 was depleted by RNAi. DNA was probed with SiR-DNA. Time in minutes after anaphase onset. (B) Percentages of Ect2^{S-loopSTDE} and Ect2^{C765K} cells, which oscillated and managed to divide successfully (light grey) and failed cytokinesis (dark grey), respectively. (n=number of cells, data from ≥ 4 independent experiments presented as mean).

3.8.4 Analysis of the Ect2 localization in S-loop and PH-mutants

While being absent from the metaphase membrane Ect2 starts to localize to the equatorial membrane and the midzone at the onset of anaphase (Chalamalasetty et al., 2006; Tatsumoto et al., 1999). This characteristic accumulation of Ect2 is crucial for the equatorial recruitment and activation of RhoA and its downstream signaling (Su et al., 2011; Wolfe et al., 2009).

To test whether Ect2 localization during meta- and anaphase is altered in the S-loop and PH mutants, dividing cells were subjected to time-lapse imaging. Ect2 localization was assessed via the NG-fluorescence signal of the exogenous proteins.

3.8.4.1 Rendering the S-loop phospho-deficient and mutation C765K in the PH domain result in premature localization to the metaphase membrane

Two of the mutants analyzed displayed aberrant membrane localization during metaphase. *Ect2*^{C765K} and *Ect2*^{S-loopAA} both were visible at the membrane before the onset of anaphase where the latter seemed to exhibit the stronger signal. In Figure 53 representative images are shown. Along with images of whole metaphase cells, several membrane cutouts are displayed to get a better impression of the respective phenotype. For comparison *Ect2*^{WT}, *Ect2*^{P703D}, and *Ect2*^{ΔBRCT2} are shown, which all did not localize to the metaphase membrane.

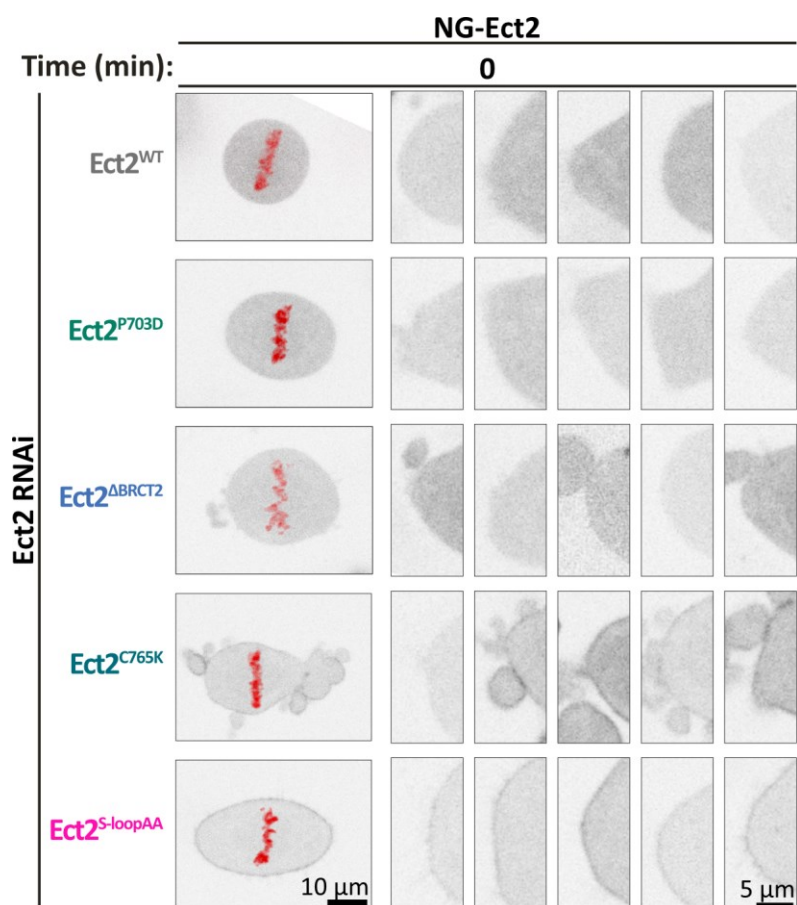


Figure 53: NG-Ect2 localization of different *Ect2* mutants during metaphase. Representative fluorescence images showing the localization (grey) of NG-Ect2^{WT}, NG-Ect2^{P703D}, NG-Ect2^{ΔBRCT2}, NG-Ect2^{C765K}, and NG-Ect2^{S-loopAA} at the last metaphase frame (0 min). Several cutouts showing the NG-Ect2 localization to the metaphase membrane (0 min) are presented behind each sequence. Endogenous *Ect2* was depleted by RNAi and DNA was probed with SiR-DNA.

To be able to distinguish the changes in localization, we analyzed NG-Ect2 localization quantitatively. For this, we measured NG-fluorescence intensity at the cortex by drawing two linescans, one horizontally (H) and one vertically (V), across metaphase cells as shown in Figure 54 A. An example of a resulting intensity plot is depicted in Figure 54 B. A detailed description of intensity measurement and analysis can be found in chapter 2.8.1.2. As values from horizontal and vertical linescans did not greatly differ, their values were combined (C) (Figure 54 C). Intensity measurements confirmed the results obtained by visual inspection of Ect2 localization. While Ect2^{P703D} (1.05-fold) and Ect2^{ΔBRCT2} (1.066-fold) showed no increase in membrane signal, both Ect2^{C765K} and Ect2^{S-loop} were enriched at the membrane. Ect2^{S-loop} (1.58-fold) accumulation, though, was stronger than that of Ect2^{C765K} (1.22-fold) (Figure 54 C). To summarize, both, rendering the S-loop phospho-deficient and mutation C765K in the PH domain allow premature Ect2 localization to the metaphase membrane. However, only C765K mutation results in strong membrane blebbing, which could indicate that Ect2 can bind the membrane while being inactive. Ect2^{S-loop^{STDE}} did not show a visible enrichment at the metaphase membrane, which is why it was not included in the presented analysis. However, in view of a future publication, the data would be helpful to illustrate the different effects of a phospho-mimetic (Ect2^{S-loop^{STDE}}) and phospho-deficient (Ect2^{S-loop^{AA}}) S-loop on Ect2 regulation and should be acquired in the future.

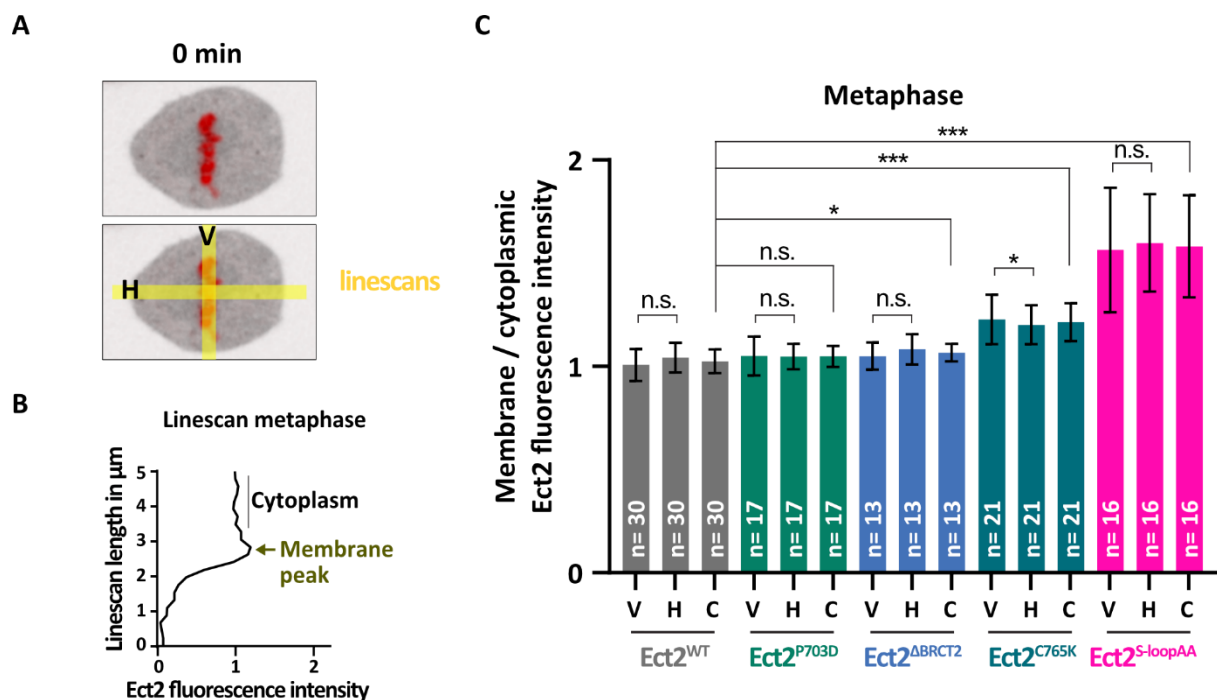


Figure 54: C765K mutation in the PH domain and phospho-deficient mutations in the S-loop result in premature Ect2 localization to the metaphase membrane. (A) Representative NG-

fluorescence images showing the cytoplasmic localization of Ect2^{WT} in a metaphase cell. As indicated in the bottom panel, two perpendicular linescans (V= vertical, H=horizontal, yellow) were used to measure NG-fluorescence intensity at the metaphase membrane. DNA was probed with SiR-DNA. (B) An exemplary intensity plot for the metaphase linescans is depicted and the equivalent membrane peak is marked. (C) Fluorescence intensities of NG-Ect2^{WT}, NG-Ect2^{P703D}, NG-Ect2^{ΔBRCT2}, and NG-Ect2^{S-loopAA} at the metaphase membrane relative to cytoplasmic levels. V= results from vertical linescan, H=results from horizontal linescan, and C=combination of both. (n= number of cells, data from ≥3 independent experiments presented as mean±SD, ***p<0.001, **p<0.01, *p<0.05, n.s.= not significant determined by Kruskal Wallis test and student's t-test according to data normality).

3.8.4.2 Rendering the S-loop phospho-mimetic and the C765K mutation in the PH domain increase Ect2 localization to the equatorial membrane and the midzone during anaphase

Among the S-loop and PH-mutants, one exhibited wild-type-like and the rest increased localization to the equatorial membrane and the midzone during anaphase. Serial images portraying their localization are shown in Figure 55. As above for the BRCT mutants, several representative midzone regions can be found behind each sequence. The P703D mutation in the PH-domain (Ect2^{P703D}) did not affect Ect2 localization, whereas C765K (Ect2^{C765K}), which also resides in the PH-domain, led to a very strong Ect2 association to the midzone as well as to the membrane. Unambiguously, the width of the Ect2 zone was enlarged in Ect2^{C765K}. Rendering the S-loop phospho-mimetic (Ect2^{S-loopSTDE}) led to an enhanced accumulation at the midzone. As shown in chapter 3.8.1 furrow ingression was slightly faster in Ect2^{S-loopAA} and many cells exhibited a very narrow equatorial width 9 min after anaphase onset. This led to a quite dense fluorescent signal at the midzone, which could lead to wrong conclusions. Hence, in addition, several midzones are shown 6 min after anaphase onset, where the furrow was similarly ingressed as in Ect2^{WT} (9 min) (Figure 55 B).

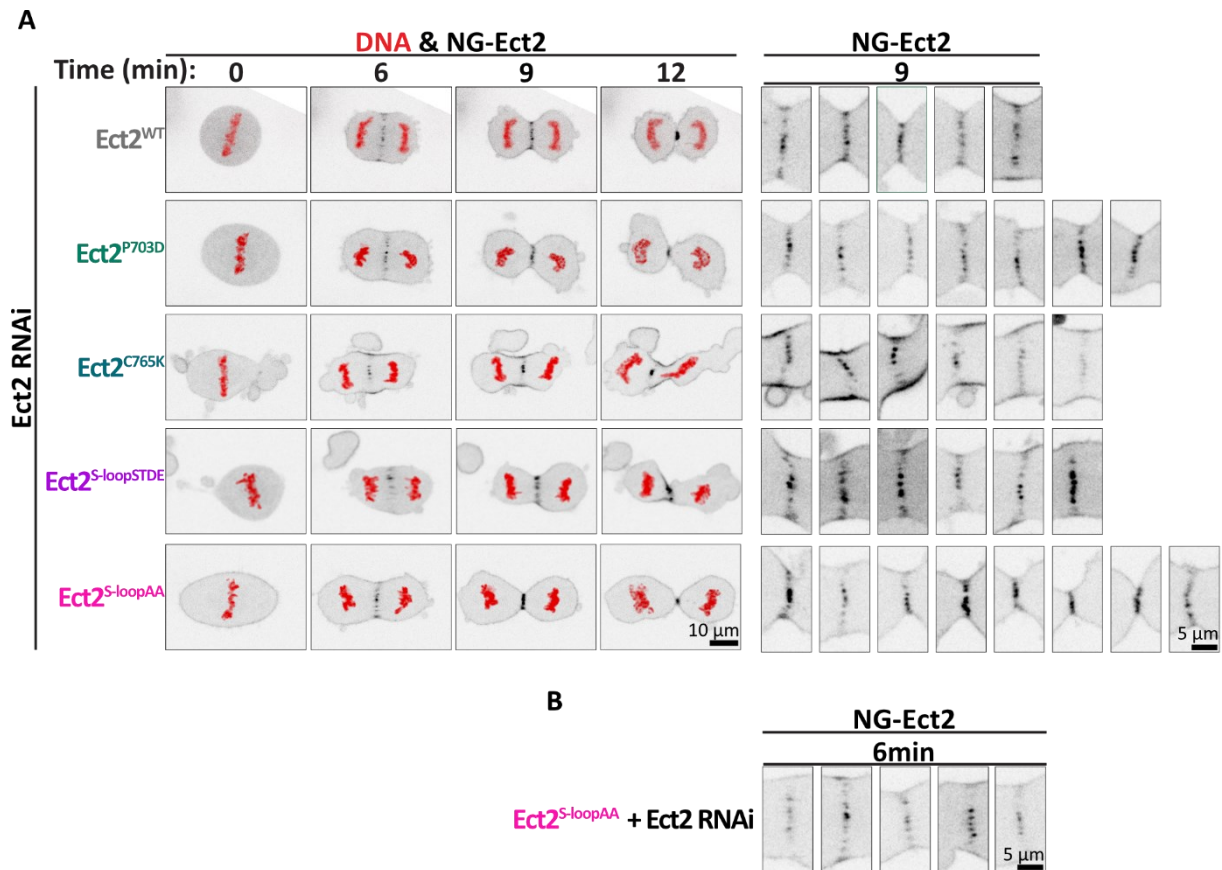


Figure 55: NG-Ect2 localization of different PH and S-loop mutants during meta- and anaphase. (A) Representative fluorescence image sequences showing the localization (grey) of NG-Ect2^{WT}, NG-Ect2^{P703D}, NG-Ect2^{C765K}, NG-Ect2^{S-loopSTDE}, and NG-Ect2^{S-loopAA} at consecutive timepoints during cell division. Several cutouts showing the NG-Ect2 localization to the equatorial region 9 min after anaphase onset are presented behind each sequence. Time in minutes after anaphase onset. DNA was probed with SiR-DNA. (B) Several cutouts showing NG-Ect2^{S-loopAA} localization to the equatorial region 6 min after anaphase onset. Endogenous Ect2 was depleted by RNAi and DNA was probed with SiR-DNA.

Again, quantitative analysis helped to highlight the subtle differences in localization seen between the different Ect2 mutants. As shown in Figure 34, fluorescence intensities were measured by drawing linescans across each pole and the equator. A detailed description of the measuring method and subsequent analysis can be found in chapter 2.8.1.2.

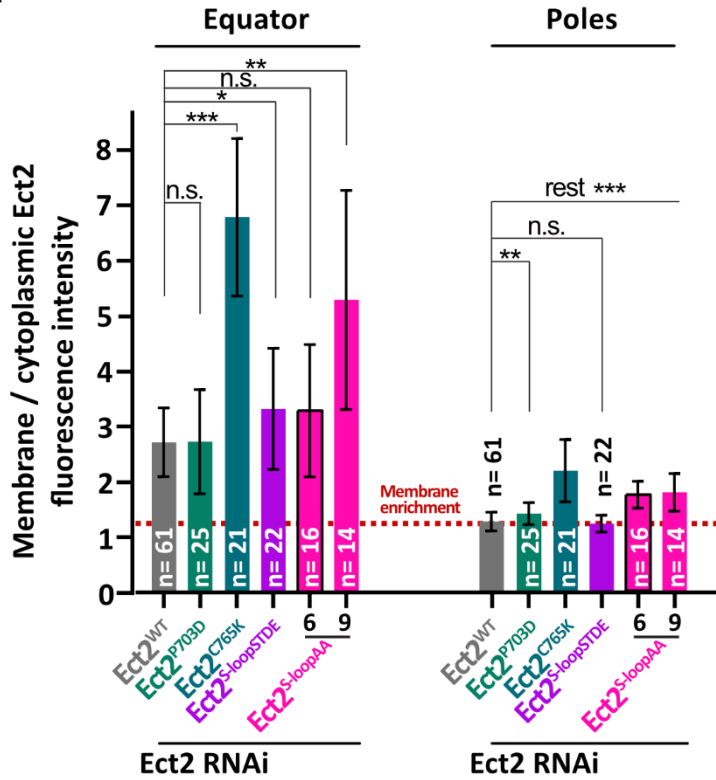
Mutation of P703 to alanine (Ect2^{P703D}) neither affected localization at the equatorial membrane nor at the midzone. However, slightly more signal was detected at the poles, but this did not alter the enrichment at the equator relative to the poles (Figure 56). Contrary to that, mutating C765 (Ect2^{C765K}) increased Ect2 accumulation at the equatorial membrane to 6.79-fold, which was even higher than in Ect2^{W307A} (Figure 56 A). Although recruitment to the midzone was elevated (4.39-fold) as compared to Ect2^{WT} (3.39-fold), the effect was less

prominent than in Ect2^{W307A} (Figure 56 B). Besides, the fluorescence signal at the polar membrane was almost twice as high in Ect2^{C765K} (2.17-fold) as it was in Ect2^{WT}, which led to a relative equatorial enrichment of 3.28-times. Although more Ect2^{S-loopSTDE} was found to accumulate at the equatorial membrane (3.30-fold) and the midzone (4.84-fold), polar intensity levels were indistinguishable from Ect2^{WT}. Thus, 2.71-times more Ect2^{S-loopSTDE} accumulated at the equatorial than at the polar membrane. Ect2^{S-loopAA} showed a small polar increase compared to Ect2^{WT} at 6 min and 9 min after anaphase onset. The effect, however, was weaker than in Ect2^{C765K}. While polar levels were the same, equatorial membrane and midzone levels differed strongly between both time points (3.27-fold versus 5.28-fold at the equatorial membrane and 4.42-fold versus 6.58-fold at the midzone). Consequently, equatorial membrane enrichment of Ect2^{S-loopAA} varied from 1.90- and 3.02-fold 6 min and 9 min after anaphase onset (Figure 56).

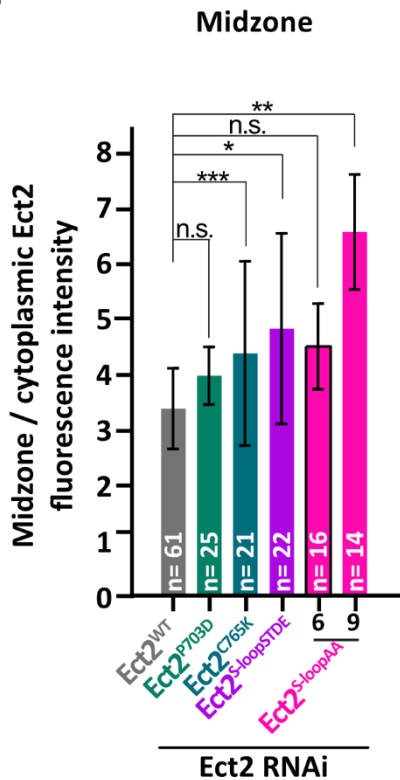
These results again indicate that only part of the entire Ect2 pool in a cell gets activated at anaphase onset (similarly to Ect2^{W307A} chapter 3.5.6.1). Consistently, perturbed autoinhibition in Ect2^{C765K} and Ect2^{S-loopSTDE} expressing cells results in a significant increase of Ect2 at the equator compared to Ect2^{WT}. Introducing P703D mutation in the PH domain, however, had no significant effect on Ect2 localization. Ect2^{S-loopAA} exhibited an increased localization to the midzone and the equatorial membrane at 9 min after anaphase onset, which would suggest that perturbed autoinhibition also allows more Ect2^{S-loopAA} to interact with RacGAP1 at the midzone and to localize to the membrane. However, as shown above, hyperactivity was not detected for Ect2^{S-loopAA}. But furrow ingression was slightly faster in Ect2^{S-loopAA} expressing cells, which resulted in a more compressed central spindle at 9 min compared to Ect2^{WT}. A higher compressed midzone means at the same time that Ect2 residing at the midzone gets more tightly packed. The result is a higher NG-fluorescence intensity in individual pixels. As the 10 highest pixels are averaged for the analysis, this would inevitably lead to increased fluorescence intensity. That is why Ect2^{S-loopAA} localization was also analyzed for 6 min after anaphase onset, a time point at which the furrow in Ect2^{S-loopAA} cells is similarly ingressed as in Ect2^{WT} cells. Contrary to the 9 min time point, NG-intensities at 6 min were not significantly different compared to Ect2^{WT}. In addition, Ect2^{S-loopAA} binding prematurely to the metaphase membrane is likely to contribute to increased membrane localization at 9 min after AOS, as Ect2^{S-loopAA} would have more time to accumulate at the equatorial membrane than Ect2^{WT}, which only starts to accumulate after anaphase onset. This in part is probably also true for

Ect2^{C765K}. To better grasp the localization phenotypes of Ect2^{S-loopAA} and Ect2^{C765K}, in the future higher temporal resolution might help as well as the analysis of Ect2^{WT} localization for several timepoints including 6 min AOS.

A



B



C

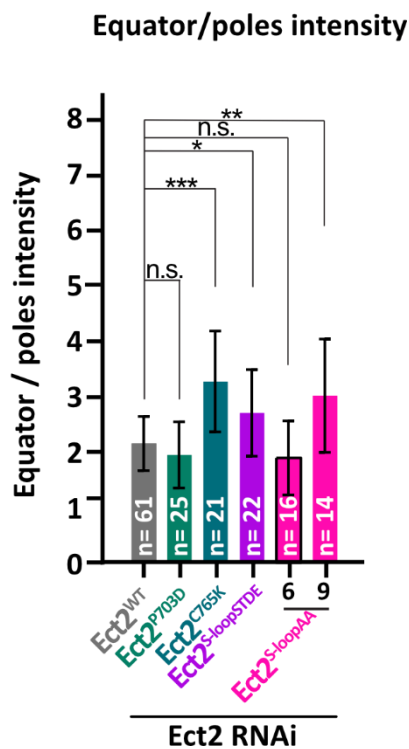


Figure 56: Mutations in the PH domain and the S-loop show different effects on Ect2 localization. (A) Fluorescence intensities of NG-Ect2^{WT}, NG-Ect2^{P703D}, NG-Ect2^{C765K}, NG-Ect2^{S-loopSTDE}, and NG-Ect2^{S-loopAA} at the equatorial and polar membrane during anaphase relative to cytoplasmic levels in cells depleted of endogenous Ect2 by RNAi. Standard analysis was done 9 min after anaphase onset. For NG-Ect2^{S-loopAA} two timepoints were analyzed 6 min (6) and 9 min (9) after anaphase onset. (n= number of cells, data from ≥ 3 independent experiments presented as mean \pm SD, ***p<0.001, **p<0.01, p*<0.05 and n.s.= not significant p>0.05 determined by Kruskal Wallis test and student's t-test according to normality). (B) Fluorescence intensities of NG-Ect2^{WT}, NG-Ect2^{P703D}, NG-Ect2^{C765K}, NG-Ect2^{S-loopSTDE}, and NG-Ect2^{S-loopAA} at the midzone relative to cytoplasmic levels in cells depleted of endogenous Ect2 by RNAi. Standard analysis was done 9 min after anaphase onset. For NG-Ect2^{S-loopAA} two timepoints were analyzed 6 min (6) and 9 min (9) after anaphase onset. (n= number of cells, data from ≥ 3 independent experiments presented as mean \pm SD, ***p<0.001, **p<0.01 and n.s.= not significant p>0.05 determined by Kruskal Wallis test and student's t-test according to normality). (C) The intensity ratio of the equatorial and the polar membrane for NG-Ect2^{WT}, NG-Ect2^{P703D}, NG-Ect2^{C765K}, NG-Ect2^{S-loopSTDE}, and NG-Ect2^{S-loopAA}. (n= number of cells, data from ≥ 3 independent experiments presented as mean \pm SD, ***p<0.001, **p<0.01, p*<0.05 and n.s.= not significant p>0.05 determined by Kruskal Wallis test and student's t-test according to normality).

4 Discussion

4.1 Overview and model of Ect2 regulation

At the beginning of cytokinesis, a contractile actomyosin ring physically separates a mother cell into two daughter cells. Although the basic principles of contractile ring assembly and positioning are well established and many key players (such as Ect2, RhoA) are identified, we still lack a deeper understanding of the exact processes, their coordination, and regulation. For example, it is known for years that Ect2 is essential for cytokinesis and that its activity is tightly regulated in time and space. However, how single structural domains are contributing to this is poorly understood. The presented thesis aimed to better understand Ect2 regulation during cytokinesis by deciphering how several structural domains contribute to its function and regulation in human cells. Here, the strategy was to eliminate individual functional contributions by either deleting entire protein domains or inserting mutations into specific domains of the protein. Key to the study was a genetic replacement system for Ect2 that was established earlier in the lab (Buchner, 2019), which allowed us to analyze Ect2 mutants at native expression levels in the absence of endogenous Ect2. We employed extensive confocal microscopy to track living cells expressing different Ect2 mutants after the depletion of endogenous Ect2 during cell division. Subsequently, it was analyzed how different mutations affect cytokinetic parameters such as cytokinetic success, furrow ingression, large bleb formation, and Ect2 localization. Together with the use of chemical inhibitors and genetic manipulations as well as biochemical techniques, this revealed, for the first time, that each of the N-terminal BRCT domains contributes differently to Ect2 functioning. Moreover, first evidence was found for a novel role of the PH domain and the S-loop in the regulation of Ect2 GEF activity in living cells. Based on the above-presented and previously published observations, we propose the following preliminary model of Ect2 regulation during cytokinesis (Figure 57):

During metaphase W307 of the BRCT2 domain and C765 of the PH domain each interact with the DH-GEF domain and inhibit GEF activity (Chen et al., 2020). At the onset of anaphase, the midzone forms and accumulates many proteins including Plk1 and RacGAP1 (through its binding partner MKLP1) (Mishima et al., 2002; Neef et al., 2007). There, Plk1 phosphorylates

RacGAP1 (Burkard et al., 2009; Wolfe et al., 2009) and binds to the BRCT domains via its PBD. Plk1 binding and phosphorylation of BRCT0 most likely lead to a partial opening of Ect2 autoinhibition, facilitating subsequent RacGAP1 binding. Then BRCT1, supported by BRCT0 and BRCT2, binds phosphorylated RacGAP1. This not only leads to the unbinding of the BRCT2 domain from the GEF domain, which allows Ect2 GEF activity but also anchors active Ect2 to the midzone and the equatorial membrane. We think, that at this point, GEF activity is still restrained by the PH domain. Upon membrane association, GTP-RhoA binds the PH domain and fully relieves autoinhibition. In regions outside the equator, Ect2 activity seems to be silenced by autoinhibition (probably by both BRCT2 and PH). Additionally, RhoA signaling is restricted to the equatorial region by astral microtubules of the mitotic spindle and this occurs independently of BRCT2-mediated inhibition.

The results that led to this proposed model are discussed in the following sections in more detail. These include results obtained by RhoA pattern analysis performed by Friederike Wolff. Her results are summarized in Table 20.

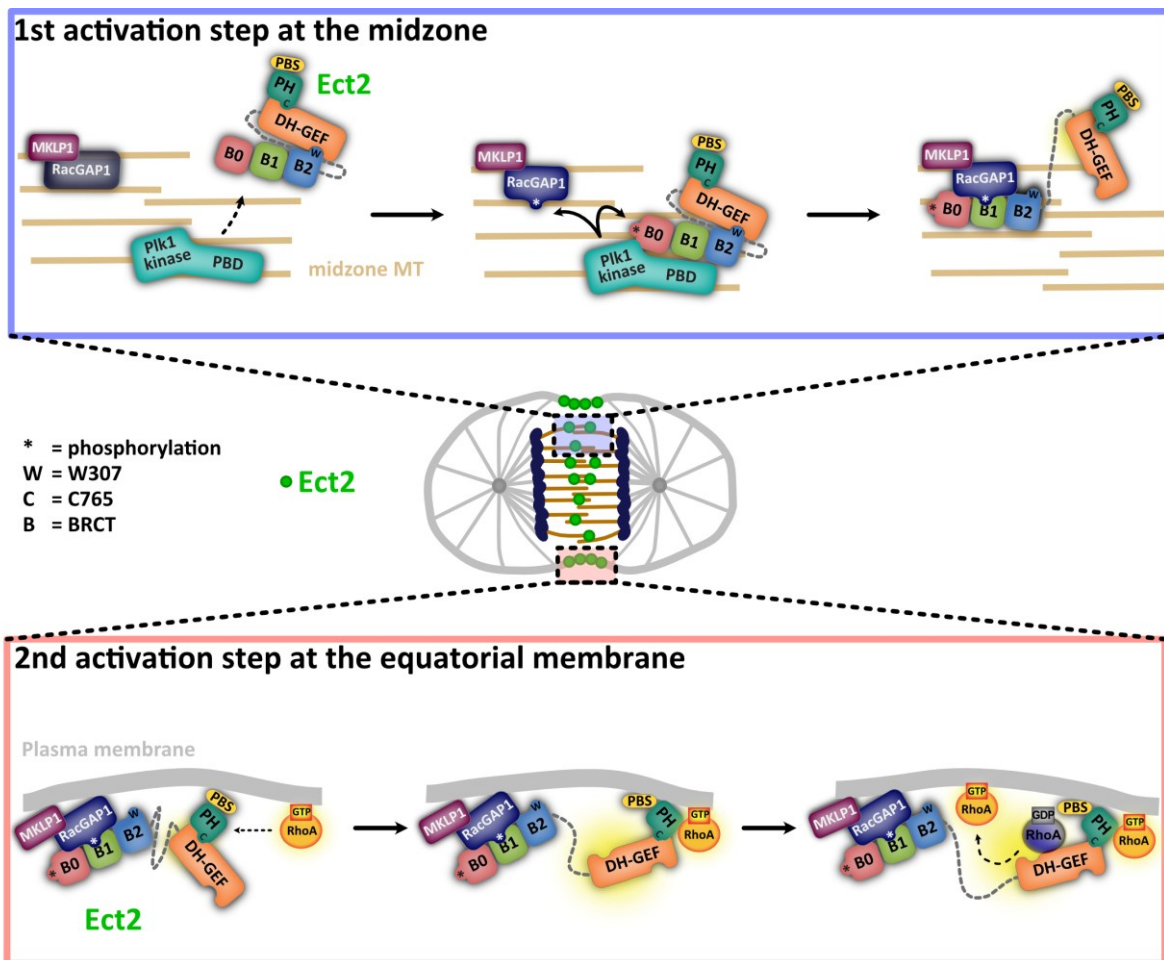


Figure 57: Schematic model of the 2-step activation of Ect2. (1) During metaphase Ect2 is kept inactive by BRCT2 and PH inhibition. At the onset of anaphase, the spindle is remodeled and the midzone forms. Many proteins are recruited to the midzone including the centralspindlin complex, formed by MKLP1 and RacGAP1, and Plk1 (Mishima et al., 2002; Neef et al., 2007). There Plk1 phosphorylates RacGAP1 (Burkard et al., 2009; Wolfe et al., 2009) and binds to all BRCT domains via its PBD. Plk1 binding and phosphorylation of BRCT0 likely triggers a conformational change that facilitates the subsequent interaction with RacGAP1. Responsible for this interaction is mainly BRCT1, but BRCT0 and BRCT2 also support the binding. Interaction with RacGAP1 not only leads to the unbinding of the BRCT2 from the DH-GEF domain, which allows Ect2 activity, but in addition tethers active Ect2 to the center of the cell (midzone and equatorial membrane), thereby supporting the formation of a narrow RhoA zone. We suggest that at this point PH inhibition is still intact and partially restrains Ect2 activity. (2) At the equatorial membrane, GTP-RhoA binds the PH domain and eventually releases it from the DH-GEF domain. This transfers Ect2 into a fully active state, which eventually activates RhoA and thereby induces contractile ring assembly.

Table 20: Summary of the results obtained by Friederike Wolff from analyzing the RhoA membrane localization during anaphase in Ect2 mutant cell lines (Schneid et al., 2021).

cell line	equatorial intensity	zone width	total amount in the zone
control + RNAi	strongly reduced to control (***)	no zone	no zone
Ect2^{WT}	n.s. to control	n.s. to control	n.s. to control
Ect2^{ΔBRCT0-2}	reduced to control (**)	broader than control (***)	n.s. to control
Ect2^{ΔBRCT0}	reduced to control (**)	n.s. to control	reduced to control (*)
Ect2^{ΔBRCT1}	strongly reduced to control (***)	no zone	no zone
Ect2^{T153A+K195M}	n.s. to control	n.s. to control	n.s. to control
Ect2^{ΔBRCT2}	reduced to control (*)	broader than control (***)	n.s. to control
Ect2^{W307A}	increased to control (**)	broader than control (***) but slimmer than Ect2^{ΔBRCT2}	n.s. to control /
control + BI	strongly reduced to control (***)	/	/
Ect2^{WT} + BI	strongly reduced to Ect2^{WT} (***)	/	/
Ect2^{ΔBRCT0-2} + BI	n.s. to Ect2^{ΔBRCT0-2}	n.s. to Ect2^{ΔBRCT0-2}	/
Ect2^{ΔBRCT2} + BI	n.s. to Ect2^{ΔBRCT2}	n.s. to Ect2^{ΔBRCT2}	/
control + MCAK RNAi	/	reduced to control (**)	/
Ect2^{WT} + MCAK RNAi	/	reduced to Ect2^{WT} (*)	/
Ect2^{ΔBRCT0-2} + MCAK RNAi	/	reduced to Ect2^{ΔBRCT0-2}	/
Ect2^{ΔBRCT2} + MCAK RNAi	/	reduced to Ect2^{ΔBRCT2}	/

4.2 RacGAP1 interaction with BRCT1 activates Ect2 in anaphase

Ect2 is activated by the release of the intramolecular interaction of the N-terminal BRCT domains with the catalytic DH-GEF domain. Previous interaction studies (Burkard et al., 2009; Kamijo et al., 2006; Kim et al., 2014; Nishimura & Yonemura, 2006; Somers & Saint, 2003; Wolfe et al., 2009; Yüce et al., 2005; Zhao & Fang, 2005; Zou et al., 2014) and experiments in living cells (Wolfe et al., 2009), have led to the canonical model of Ect2 activation, which suggests that the interaction of the BRCT1 domain with the centralspindlin component RacGAP1 releases autoinhibition. Contradictive findings by Kotýnková et al. (2016) however, have led to discrepancies in the field concerning the model of Ect2 activation. Because they have discovered that two mutations in BRCT1 (T153A+K195M), reported to abolish Ect2-

RacGAP1 interaction (Wolfe et al., 2009; Zou et al., 2014), do not negatively affect cytokinesis, the authors claimed that Ect2-RacGAP1 interaction is dispensable for Ect2 activation.

Unlike previous studies, instead of mutating individual residues, we deleted the entire BRCT1 domain to scrutinize the role of BRCT1 and its interaction with RacGAP1 during cytokinesis. This had the advantage that BRCT1-dependent RacGAP1 binding is certainly absent in the Ect2^{ΔBRCT1} mutant (Figure 23). Deletion of the entire BRCT1 domain led to high cytokinetic failure, comparable to the phenotype after depletion of endogenous Ect2 by RNAi. Live-cell recordings further revealed that Ect2^{ΔBRCT1} expressing cells were incapable of forming and ingressing a cleavage furrow (Figure 24). Analyses of RhoA and anillin levels at the membrane (done by Friederike Wolff), gave a rationale for these findings as removal of BRCT1 strongly reduced the ability of Ect2 to activate RhoA (Table 20). Strongly reduced RhoA recruitment was also found after losing Ect2 activity by RNAi-mediated gene knockdown (Table 20). This suggested that Ect2^{ΔBRCT1} expressing cells lack Ect2 activity. However, as RhoA activation and furrow ingression require Ect2 membrane association (Su et al., 2011), missing membrane localization could also explain our observations. During live-cell imaging, Ect2^{ΔBRCT1} efficiently translocated to the membrane in anaphase, which assured us that the observed cytokinetic defects are due to missing Ect2 activity (Figure 33). Earlier studies have suggested that Ect2-RacGAP1 interaction is required for successful cytokinesis (Yüce et al., 2005) and BRCT1 was thought to be key for this (Wolfe et al., 2009; Zou et al., 2014). Thus, we suspected that BRCT1 is required for cytokinesis because its interaction with RacGAP1 releases autoinhibition. It could be that residual binding of RacGAP1 and BRCT1 in Ect2^{T153A+K195M} is present, but could not be detected by previous immunofluorescence and binding studies. In their discussion, Kotýnková et al. (2016) mentioned that albeit Ect2^{T153A+K195M} midzone localization was strongly decreased, it was not completely abolished and the same was detected in our analysis (Figure 35). As we have seen for the BRCT0 deletion mutant (Ect2^{ΔBRCT0}) little midzone localization can allow successful cytokinesis (Figure 21 and Figure 33). Additionally, recent binding studies demonstrated that RacGAP1-Ect2 interaction is not abolished by the T153A+K195M mutations (Gomez-Cavazos et al., 2020). Thus, residual RacGAP1 interaction accounts for the observations made by us (Figure 23 C) and others (Kotýnková et al., 2016) that cytokinesis is unperturbed in Ect2^{T153A+K195M}. In strong contrast to that BRCT1 deletion completely abolished RacGAP1-dependent midzone localization and resulted in defective cytokinesis (Figure 23 C and Figure 33), which demonstrates that this interaction is indeed important for Ect2 activity.

In line with our observations, a different surface patch was recently identified on BRCT1 next to T153 and K195, which is essential for RacGAP1 binding and Ect2 function (Gomez-Cavazos et al., 2020).

The investigation of RacGAP1 binding was a long time shaped by the assumption that Ect2 features a canonical tandem BRCT repeat, in which BRCT1 provides the residues to bind phosphorylated RacGAP1 (T153 and K195 are the analogous residues to the ones in BRCA1 and MDC1) (Leung & Glover, 2011). However, structural data have revealed that Ect2 has three BRCT domains and that these are orientated very differently towards each other when compared to tandem BRCT repeats. This suggested a different functional principle of protein binding and brought up the question of whether BRCT0 and BRCT2 also interact with RacGAP1 and whether this could be important for Ect2 activation. Pull-down assays showed that all three BRCT domains can interact with RacGAP1 *in vitro*, but the strongest interaction was found for BRCT1 (Figure 37). As, Ect2^{ΔBRCT0} and Ect2^{ΔBRCT2} were both reduced at the midzone, but not completely gone (Figure 33 and Figure 35), BRCT0 and BRCT2 seem to be not essential for RacGAP1 binding. Further, albeit BRCT0 and BRCT2 can interact with RacGAP1, in the absence of BRCT1 they fail to recruit Ect2 to the midzone and release its autoinhibition (Figure 23, Figure 33 and Figure 35). This observation favors a sequential binding mode, in which an initial RacGAP1 binding to BRCT1 facilitates the subsequent binding of BRCT0 and BRCT2. From these observations, we conclude that specifically BRCT1-dependent interaction with RacGAP1 releases Ect2 autoinhibition and thereby stimulates GEF activity.

4.3 Mechanisms of Ect2 autoinhibition

Even though basal Ect2 activity is required in metaphase to trigger cortex modulations needed for cell rounding (Matthews et al., 2012), bulk activation in early anaphase is responsible for the formation of the contractile ring. The N-terminus of Ect2 interacts with the catalytic DH-GEF domain and this is thought to block GEF activity before the onset of anaphase. Previous work has established the critical role of the N-terminal BRCT domains for Ect2 autoinhibition (Kim et al., 2005; Saito et al., 2003; Tatsumoto et al., 1999), however, whether all three BRCT domains or only single BRCT domains are exerting the inhibitory function was not known. Thus, our approach of examining the contributions of each BRCT domain separately by

deleting each individually promised new insights into how Ect2 regulation is mechanistically achieved.

While BRCT1 is needed to activate Ect2 (discussed in 4.2), we found BRCT2 to be required to negatively regulate Ect2 activity. Deletion of the BRCT2 domain (Ect2^{ΔBRCT2}), but not of BRCT0 and BRCT1, elicited the formation of large blebs in living cells in meta- and anaphase (Figure 26 A and C). Normally, cells release internal pressure through small membrane blebs at the cell poles during anaphase, which ensures a stable cell shape during constriction of the contractile ring and buffers tension differences (Sedzinski et al., 2011). Increased cellular tension due to hyperactive RhoA results in the formation of larger membrane blebs (Taneja et al., 2020; Zanin et al., 2013). As Ect2 directly activates RhoA, large bleb formation serves as an indirect readout for increased GEF activity. Based on this analysis we reasoned that deleting BRCT2 interferes with the proper regulation of GEF-activity and thus renders Ect2 hyperactive. Consistent with enhanced Ect2 activity leading to increased RhoA activity, bleb formation was suppressed by the RhoA inhibitor C3 exoenzyme (Figure 27). Bleb formation allows cells to tolerate pressure imbalances and makes cytokinesis robust to perturbations (Sedzinski et al., 2011). However, when blebs grow too big, they can also introduce such imbalances in tension, which often lead to the destabilization of cell shape and oscillatory behavior (Tinevez et al., 2009). We observed that more than 12 % of cells expressing BRCT2-lacking Ect2 mutants (Ect2^{ΔBRCT0-2} and Ect2^{ΔBRCT2}) exhibited oscillatory behavior (Figure 32). This again hints at defective regulating of Ect2 activity when BRCT2 is missing. Further support for our conclusion comes from recent findings of *in vitro* GEF assays, which showed that removal of all BRCT domains but not BRCT0+BRCT1 results in increased GEF activity (Chen et al., 2020). In the same study, based on crystal structure analysis the authors identified a specific residue in the BRCT2 domain (W307) which directly contacts the DH-GEF domain. Its mutation to alanine (W307A) resulted in elevated GEF activity *in vitro*, which suggested that it releases Ect2 inhibition. Thus, we tested whether W307 is the critical residue for the inhibitory action of BRCT2 in living cells. Similar to the removal of the entire BRCT2 domain, mutation W307A resulted in the formation of large blebs during meta- and anaphase (Figure 26) and increased the occurrence of cell shape oscillations (Figure 32). From these observations, we conclude that BRCT2 inhibits Ect2 GEF activity via direct interaction of W307 with the DH-GEF domain in living cells. To further back up these conclusions one could directly test RhoA activation by applying a biosensor that specifically recognizes the active form of RhoA. This would allow the quantitative analysis of

RhoA activation and at the same time reveal its spatial and temporal dynamics in living cells. Another approach would be to analyze the recruitment of RhoA downstream effectors such as F-actin. The fluorescent probe SiR-actin or a fluorescently-tagged Lifeact peptide could be used to detect and quantitatively measure F-actin in living cells. Alternatively, active RhoA could be purified from cell lysates and its active amounts determined via western blot analysis. For active RhoA detection commercial kits are available.

During the course of the study, the crystal structure of Ect2 containing both the N- and C-terminus (Ect2^{ΔBRCT0}) was solved (Chen et al., 2020). This gave valuable insights into how domain interactions are structurally accomplished. Surprisingly it also proposed that Ect2 negative regulation, different from what was previously assumed, does not exclusively rely on the BRCT domains. Based on their structural analysis, Chen et al. (2020) reported the PH-domain to fold back onto the DH-GEF domain and to directly interact with it via two residues (P703 and C765). Mutation of both residues resulted in increased Ect2 GEF activity *in vitro*, which proposed that the PH domain contributes to Ect2 negative regulation. It has already been suggested that membrane binding of Ect2, which is mediated by the PH and PBS domain, represents a way to temporally control cytokinesis (Su et al., 2011). However, a direct role of the PH domain in GEF activity inhibition has so far only been described for other members of the Dbl family of GEFs (Han et al., 1998; Nimnual et al., 1998; Soisson et al., 1998), but not for Ect2. Our analysis in living cells elucidated that C765K mutation in the PH domain strongly increased Ect2 activity evaluated by means of large bleb formation (Figure 51). This is further supported by the increased occurrence of cell shape oscillations in Ect2^{C765K} expressing cells (Figure 52). Surprisingly, mutating P703 (P703D) in the PH domain did not influence Ect2 activity in any of the assessed cytokinetic parameters (chapters 3.8.2 and 3.8.4). These observations strongly suggest that the PH domain is involved in Ect2 activity regulation in living cells and that mutation of C765, but not of P703, releases the PH-mediated inhibition. Why P703D does not show the same effect on Ect2 activity as seen *in vitro* is questionable. However, one has to keep in mind that *in vitro* GEF assays are carried out in a controlled and isolated environment, which may differ greatly from the situation in living cells. As so, macromolecular crowding and the presence of other factors such as binding partners could affect the consequences of P703D mutation on Ect2 activity in living cells. Moreover, why earlier studies could not detect increased *in vitro* GEF activity of C-terminal Ect2 after the removal of the entire PH domain remains puzzling (Solski et al., 2004; Su et al., 2011). Although

PH-mediated membrane localization is required for Ect2 function and RhoA activation (Su et al., 2011), this would only be relevant for functional studies in living cells and not *in vitro*. Further, Su et al., 2011 detected an increase in GEF activity after the removal of the entire C-terminal part following the DH domain (PH and the PBS domain), but not after the removal of the PH domain alone. This could mean that the remaining PBS domain is partially capable of inhibiting GEF activity and could explain the different results observed in later studies (Chen et al., 2020 and the data presented in this thesis). Strangely, similar GEF assays performed by Solski et al. (2004) led to the exact opposite results. When they deleted the entire C-terminal part following the DH domain, GEF activity was reduced. This would rather suggest that the catalytic DH-GEF domain requires the PH domain to function normally. More work is needed in the future to clarify the discrepancy between these results. Suitable experiments would include the analysis of the RhoA pattern in Ect2^{C765K} expressing cells, either by immunostainings or via a biosensor for active RhoA. Moreover, the effect of C765K on RhoA effectors such as F-actin should be determined. As GTP-RhoA binding is thought to release PH-mediated autoinhibition, in addition, the effect of the PH release-deficient Ect2 mutants (Ect2^{Y625A}, Ect2^{F621A}) (Chen et al., 2020) on Ect2 activity during cytokinesis should be analyzed in detail. Moreover, direct interaction between the DH-GEF and the PH domain could be probed by interaction studies.

The S-loop connects the N- and the C-terminus and harbors many potential phosphorylation sites. For some sites phosphorylation has already been reported (Hara et al., 2006; Justilien et al., 2011; Niiya et al., 2006; Yüce et al., 2005) and it was suggested that phosphorylation regulates Ect2 activity (Hara et al., 2006). Rendering the S-loop phospho-mimetic led to increased formation of large membrane blebs in meta- and anaphase, while the phospho-deficient S-loop did not (Figure 48 A and C). In earlier experiments of our group, Ect2^{S-loopAA} expressing cells formed large blebs in meta- and anaphase in the presence of endogenous Ect2 (Buchner, 2019). This inconsistency, is likely a result of increased amounts of Ect2 being present in the cell in earlier studies as (1) endogenous Ect2 was present and (2) Ect2^{S-loopAA} expression was induced with a higher concentration (0.2 µg/ml) of tetracycline, which we found to result in increased protein levels (not shown). Furthermore, oscillation events were only increased in Ect2^{S-loopSTDE} but not Ect2^{S-loopAA} expressing cells (Figure 52). Although these results suggest that phosphorylation of the S-loop positively regulates Ect2 activity, one has to keep in mind that one third of the residues (28/100aa) in the S-loop is mutated in Ect2^S

loop^{STDE} and that glutamic and aspartic acid have longer side chains compared to serines. This alone could lead to the observed phenotypes. Recent observations by Chen et al. (2020), suggest that the S-loop regulates Ect2 activity by physically interfering with RhoA binding. The authors observed that Ect2 missing the S-loop and the BRCT domains exhibited higher RhoA binding affinity and further increased GEF activity than Ect2 solely missing the BRCT domains. Thus, it could be that the bulkier structure of the phospho-mimetic S-loop interferes with the occlusion of the RhoA binding site and thereby allows abnormal RhoA interaction and activation. While this would still speak for an involvement of the S-loop in GEF activity regulation, it would argue against phosphorylation playing a role. These results, therefore, need to be interpreted with caution, and further work is required to clarify the significance of the presented findings. Future research must try to identify which of the 28 sites are responsible for the phenotypes observed. To identify the phosphorylated sites in the S-loop Ect2 should be immunoprecipitated from meta- and anaphase lysates and analyzed by mass spectrometry. Prior targeted inhibition of mitotic kinases through the use of inhibitors or ATP-analogues, further, could reveal which of them is/are responsible for the phosphorylations. Likely candidates are Cdk1 and Plk1, however, Aurora A and B could also be involved. After specific sites were identified one could repeat the structure-function studies with the respective phospho-mimetic and phospho-deficient Ect2 variants to check, whether these lead to similar phenotypes as described above. Moreover, RhoA and anillin pattern analysis could help to understand the observed phenotypes.

4.4 RacGAP1 exerts spatial control upon active Ect2

In 4.2 we demonstrate that RacGAP1 interaction is crucial for Ect2 activation. However, our data further suggest that RacGAP1-Ect2 interaction helps to specify a narrow zone for contractile ring formation. Ect2 missing the entire BRCT2 domain is hyperactive and according to its midzone recruitment most likely displays reduced RacGAP1 binding. We found that an equatorial RhoA zone can form, however, the same amount of RhoA is spread over a larger equatorial area (Table 20). Interestingly, retaining RacGAP1 binding, while losing BRCT2-mediated GEF inhibition by mutation W307A resulted in a slimmer zone in comparison to the full BRCT2 deletion (Table 20). Hence, in the absence of autoinhibition, by binding to BRCT2, RacGAP1 can keep active Ect2 from spreading across the membrane and thereby ensure a

tight RhoA zone. Therefore, we suggest that RacGAP1 binding to BRCT2, after Ect2 activation, represents another facet of the regulatory mechanisms employed by the cell to tightly control the spatial dimension of contractile ring formation. In order to test the stated suggestions, in the future, it would be important to examine the ability of Ect2^{ΔBRCT2} and Ect2^{W307A} to bind RacGAP1 in more detail. Suitable experiments are discussed in the next section.

4.5 Autoinhibition keeps part of Ect2 pool inactive during anaphase

We found increased Ect2 midzone localization in Ect2^{W307A}, which lacks the binding between BRCT2 and the DH-GEF domain but still allows RacGAP1 binding (Figure 33 and Figure 35). This indicates that in the absence of W307-dependent inhibition the amount of open Ect2, which is capable of RacGAP1 binding, is increased. From this, we reasoned that not the entire Ect2 pool gets activated during anaphase in wild-type cells, but a significant amount is held inactive by autoinhibition. Autoinhibition, therefore, represents a fundamental tool to control Ect2 activity and thereby also of RhoA-dependent signaling. It may help cells to adapt to perturbations and to quickly shut down Ect2 activity in regions where it normally should be inactive such as at the cell poles. Further, autoinhibition could contribute to a defined equatorial zone of active Ect2. Rapid cycles of activation and deactivation of RhoA at the cell equator were proposed to contribute to narrow RhoA zone formation (Bement et al., 2006; Miller & Bement, 2009) and such a mechanism could also exist for Ect2. To confirm that Ect2^{W307A} is still able to bind RacGAP1, co-immunoprecipitation or pull-down assays should be carried out in the future. This could also shed light on whether more Ect2 is capable to interact with RacGAP1. Here, the positive control could be N-terminal Ect2 (Ect2^{BRCT0-2}), which should in principle exhibit unrestrained RacGAP1 interaction and thus increased midzone localization. Especially, quantitative co-immunoprecipitation technologies such as those based on luminescence, would be suitable for that. Optical techniques such as dual-polarization interferometry could also be used for even more accurate binding affinities.

4.6 BRCT2-mediated inhibition vs PH-mediated inhibition- which one is released first?

We found strong evidence that Ect2 autoinhibition in living cells is accomplished by several structural domains (see 4.3). In our study, especially the N-terminal BRCT2 domain and the membrane binding PH domain could suppress Ect2-mediated RhoA activation (Figure 26 and Figure 51). Our findings are supported by recent crystal structure studies, which found specific contact sites between the DH-GEF domain and the BRCT2 and PH domain, respectively (Chen et al., 2020). Nevertheless, we lack a detailed understanding of how both inhibitions collaborate to facilitate efficient control over Ect2 activity. One important question is whether both inhibitions are released simultaneously or sequentially. Recently, Gomez-Cavazos et al. (2020) proposed a sequential activation model in which Ect2 initially associates to the plasma membrane via its membrane binding domains in anaphase (Figure 58 left). Here GTP-RhoA can bind and release the PH mediated block of Ect2 activity (Chen et al., 2020), which partially opens up Ect2 autoinhibition. Subsequent binding of phosphorylated RacGAP1 releases the residual BRCT2 constraint, which unleashes full RhoA activation capacity. However, their model is mainly based on observations made in *C. elegans*, in which, in contrast to human cells, Ect2 does not localize to the midzone due to stronger autoinhibition (Gomez-Cavazos et al., 2020). Our findings in human cells also support a stepwise release, but they rather favor a reverse activation mode in which first BRCT2-DH-GEF interaction is relieved at the midzone and the plasma membrane through the interaction with RacGAP1 (Figure 58 right). Several findings support this alternative activation mode:

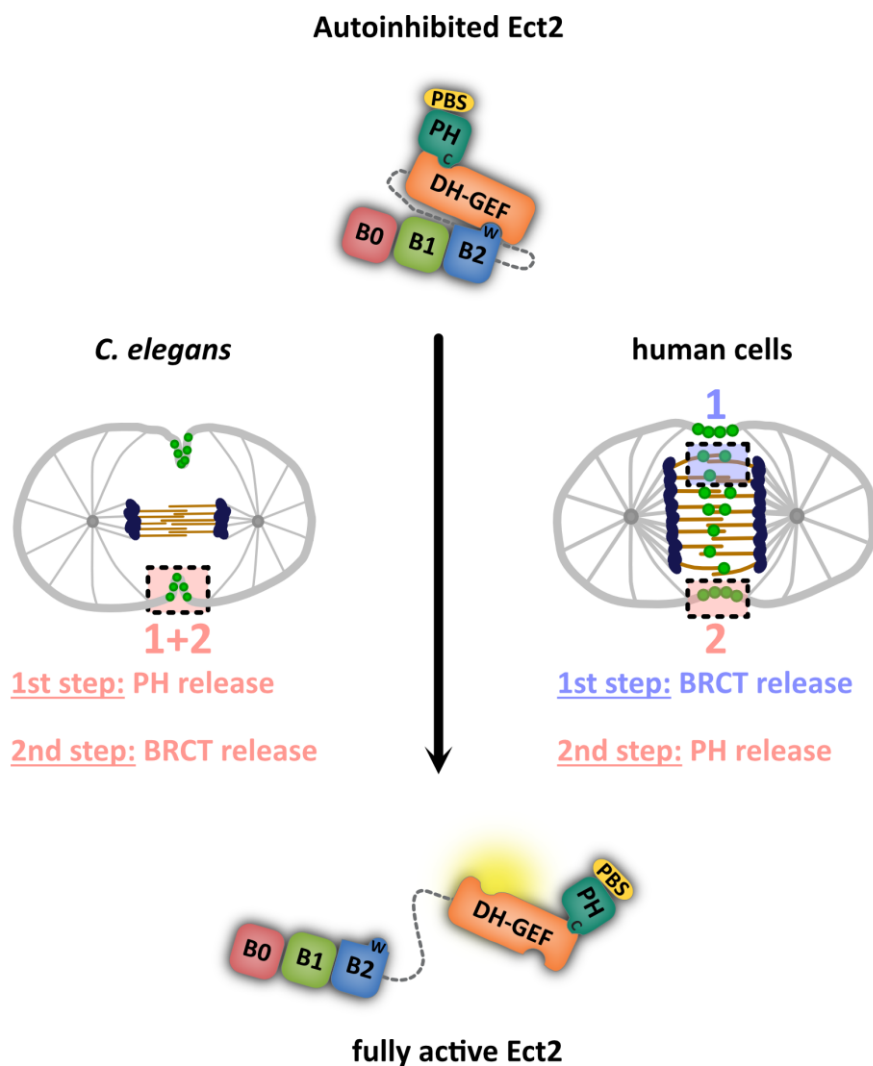


Figure 58: Models of releasing autoinhibition in *C. elegans* and human cells. In *C. elegans* it was suggested that both inhibitory interactions are released at the plasma membrane (Gomez-Cavazos et al., 2020). First GTP-RhoA releases the PH inhibition as Ect2 binds the membrane and subsequently RacGAP1 binding releases the BRCT autoinhibition and fully activates Ect2. Based on our results, we propose a reversed sequence of activation in human cells. We think that first BRCT inhibition is relieved at the midzone by binding to RacGAP1 and then the PH inhibition is released at the plasma membrane by GTP-RhoA. B= BRCT, W= W307 and C= C765.

We found that releasing PH-mediated inhibition by mutation C765K leads to precocious membrane localization while releasing BRCT2-mediated inhibition, either by point mutation W307A or removal of the entire domain, showed correct temporal membrane recruitment upon the entry into anaphase (Figure 33, Figure 53, Figure 54 and Figure 55). This demonstrates that relieving BRCT2 inhibition does not automatically increase membrane binding and would suggest that unbinding of BRCT2 does not directly trigger the PH release, as we would otherwise expect metaphase recruitment of Ect2^{ΔBRCT2} and Ect2^{W307A}. Reversely, whether preventing the DH-PH binding loosens up the BRCT2 binding cannot be assessed

based on our data, but it could explain why mutation C765K resulted in higher GEF activity *in vitro* than the removal of the BRCT domains in earlier studies (Chen et al., 2020). C765K mutation seems to override the blockade, which prevents Ect2 membrane translocation before anaphase (Su et al., 2011). This could be an effect of the removal of PH-mediated inhibition or a nonspecific effect caused by the mutation itself. To begin with, premature membrane localization of Ect2^{C765K} could simply be an artifact due to the introduction of another positive charge into the PH domain, which may influence its ability to bind the membrane. To exclude this option, a negative charge could be introduced for example by mutating C765 to aspartic acid or glutamic acid and analyzing whether premature membrane localization is possible. However, one has to ensure that this does not introduce artifacts itself such as residual autoinhibition or perturbed membrane binding. Another possibility would be that C765K allows the premature interaction between the PH domain and anillin, which homogeneously localizes to the cell periphery throughout metaphase (Field & Alberts, 1995; Frenette et al., 2012; Oegema et al., 2000). However, one has to consider that C765K mutation, and not the disrupted PH inhibition per se, could lead to membrane localization in metaphase. The unique accumulation of Ect2^{C765K} in an abnormally wide equatorial zone during anaphase could indicate that Ect2^{C765K} has an enhanced binding affinity towards anillin, which would hint at a specific effect of C765K mutation rather than a general consequence of the PH release. To test this hypothesis one should prevent the interaction between anillin and Ect2 by depleting anillin by RNAi and simultaneously inhibit contractility by the myosin II inhibitor blebbistatin as anillin RNAi destabilizes the contractile ring and triggers cell shape oscillations (Piekny & Glotzer, 2008). Alternatively, one could try to explicitly inhibit Ect2 interaction by expressing an anillin variant lacking the C-terminal part of its anillin homology domain (AHD), which is required for Ect2 binding (Frenette et al., 2012), after depletion of endogenous anillin. The broad Ect2 zone could, however, also be a consequence of an enhanced binding to phosphoinositides, which are typically bound by PH domains and enriched at the cleavage furrow (Emoto et al., 2005; Lemmon, 2008). Towards this direction, it could be tested by lipid binding assays whether Ect2^{C765K} can interact more strongly with phosphoinositides than Ect2^{WT}. The contact between the PH and the DH-GEF domain was proposed to be relieved by GTP-RhoA binding to the PH domain upon membrane binding (Chen et al., 2020). We found Ect2^{ΔBRCT0}, Ect2^{T153A+K195M}, and Ect2^{S-loopAA} to localize to the polar membrane and Ect2^{S-loopAA} even to the metaphase membrane, however, we did not see signs

of Ect2 hyperactivity. This implies that, despite being attached to the membrane, Ect2 is kept inactive by BRCT2- and/or PH-mediated autoinhibition. Moreover, we observed Ect2^{ΔBRCT1} localizing to the membrane in anaphase, yet it remains inactive due to its inability to interact with RacGAP1. This suggests that there is more to the release of the PH mediated inhibition than simply binding to the membrane. One possible explanation could be that, first, BRCT2 inhibition must be removed to allow the subsequent PH release. The release of BRCT2 requires the interaction with RacGAP1, consequently, Ect2 activation can only occur at the cell equator and only in anaphase. However, it could also be that another, yet unknown factor is required to release PH-mediated inhibition and this factor, most probably, resides at the equatorial plane. Further, it cannot be excluded that BRCT1 function is required in a different manner than releasing BRCT2 inhibition. For example, it could also mediate the release of the PH inhibition.

Moreover, the simple fact that Ect2 gets strongly recruited to the midzone by RacGAP1 and only mildly accumulates at the plasma membrane speaks in favor of the reverse model. The interaction of Ect2 and RacGAP1 liberates the GEF domain from its intramolecular autoinhibition by the BRCT2 domain. Thus, in the majority of the Ect2 molecules BRCT2 is inevitably released at the midzone before Ect2 translocates to the membrane. However, as explained above, releasing BRCT2-mediated inhibition does not seem to be a prerequisite for membrane association. Furthermore, all of this does not necessarily exclude that the Ect2-RacGAP1 interaction at the membrane also contributes to Ect2 activation, but merely suggests that the bulk release of Ect2 inhibition occurs at the midzone. Since we have revealed that BRCT0 gets phosphorylated by Plk1, which is required for efficient Ect2 activity, this would again speak for the alternative model, as Plk1 also resides at the midzone (Petronczki et al., 2007).

Further, placing the autocatalytic GTP-RhoA step after the unbinding of BRCT2 has one big advantage. Partially open Ect2 is held in the equatorial zone by RacGAP1 binding to BRCT2. This allows rapid Ect2 activation by GTP-RhoA in a restricted zone, which can thereby help to control RhoA zone dimensions.

In the future, the analysis of Ect2 mutants that are unable to relieve the PH-mediated inhibition (Ect2^{F621A}, Ect2^{Y625A}) (Chen et al., 2020), could further clarify whether the inhibitory actions of the PH and BRCT2 domain are released sequentially and whether they are

interdependent or one dominates the other. Examining the consequences of combined mutations/modifications in Ect2 such as C765K along with the BRCT1 deletion or W307A plus F621A/Y625A could provide further hints regarding this matter. One limitation of our study is that we can only assess Ect2 activity based on morphological hallmarks (bleb formation, furrow formation) or the recruitment of contractile ring components to the cell membrane (anillin, RhoA). This makes it hard to scrutinize the chronological order of releasing different inhibitory interactions and their overall effect on Ect2 activation in living cells. Recently, Azoitei et al. (2019) developed an activation biosensor to track the activation of GEF-H1. GEF-H1 is another RhoA activator, which is, among others, involved in cell migration (Birkenfeld et al., 2008). The development of such a biosensor for Ect2 could help to answer open questions regarding the spatial and temporal aspects of releasing inhibitory contributions.

4.7 The role of BRCT0 and Plk1 in releasing Ect2 autoinhibition

Plk1-dependent phosphorylation of RacGAP1 is required for its interaction with Ect2 and this is thought to trigger the release of Ect2 autoinhibition in anaphase. However, although phospho-mimetic RacGAP1 was able to rescue the interaction with N-terminal Ect2 *in vitro* in the absence of Plk1 activity, it failed to rescue cytokinesis in the absence of Plk1 activity and endogenous RacGAP1 in living cells (Wolfe et al., 2009). Together with the finding that N-terminal Ect2, but not full-length Ect2 could be recruited to the midzone by phospho-mimetic RacGAP1, this suggests an additional, yet unknown, step of releasing Ect2 inhibition requires Plk1 activity. Plk1 directly interacts with Ect2 via its PBD and also phosphorylates Ect2 *in vitro* (Niiya et al., 2006). Thus, it was tempting to speculate that Plk1-mediated phosphorylation of Ect2 helps to release Ect2 autoinhibition. Interestingly we found that when the BRCT2 mediated inhibition is absent (Ect2^{ΔBRCT0-2} and Ect2^{ΔBRCT2}) Ect2 activity does not depend on Plk1 activity anymore. Neither bleb formation nor RhoA intensity or RhoA zone width at the equator were affected by Plk1 inhibition in these cells (performed by EZ and FW respectively) (Figure 40 and Table 20). Thus, the additional step requiring Plk1 activity must occur upstream of releasing BRCT2-mediated inhibition and probably primes the latter. Further, we were interested in whether this step involves Plk1 targeting of one or more of the BRCT domains. In binding assays using purified N-terminal Ect2 fragments and GST-PBD, we found that all

BRCT domains could interact with the PBD of Plk1, but the strongest interaction was seen with BRCT0 (Figure 41). Moreover, Plk1 could phosphorylate BRCT0, but not BRCT1 or BRCT2, *in vitro* (Figure 42). Plk1 often targets its substrates by binding to Cdk1-phosphorylated sites with the consensus sequence of Ser-(pSer/pThr)-Pro (Elia, Cantley, et al., 2003; Elia, Rellos, et al., 2003). However, phospho-independent interactions have also been reported in the past (Almawi et al., 2020; Archambault et al., 2008; Hanisch et al., 2006). Earlier studies have identified a Cdk1-phosphorylation site in the S-loop of Ect2 (T412), which enhances Plk1 interaction *in vitro* and supports RhoA activation (Niiya et al., 2006). Together with the fact that Plk1 still interacted with Ect2^{T412A} (Niiya et al., 2006), our results suggest that T412 in the S-loop is supported by the BRCT domains in Plk1 binding. Once bound, Plk1 phosphorylates BRCT0 and we propose that this represents a key step in the release of Ect2 autoinhibition. For example, it could introduce a conformational change, which partially opens up Ect2 and allows the binding of phosphorylated RacGAP1. It could also keep Plk1 close to RacGAP1 and thereby promote efficient Ect2-RacGAP1 complex formation. Both scenarios would explain the observed lower equatorial RhoA levels, slower furrow ingression, and reduced Ect2 midzone localization in Ect2^{ΔBRCT0}. One could argue that these observations are simply the results of reduced Ect2^{ΔBRCT0} localization to the equatorial membrane. However, our findings that Ect2^{T153A+K195M}, which showed a similar reduction at the equatorial membrane, exhibited normal RhoA enrichment and furrow ingression, however, support the previously proposed model of BRCT0 functioning. Further work in the future will be required to establish the exact mode of action of BRCT0, to identify the specific Plk1 target sites in BRCT0, and to clarify whether Plk1 binds all the domains at once or if they are bound in a sequential manner.

4.8 RhoA zone formation in Ect2 missing the BRCT domains

Ect2^{ΔBRCT0-2} was absent from the midzone and showed similar localization to the equatorial and polar membrane (Figure 35), yet a defined equatorial RhoA zone was formed (Table 20). Ect2 midzone accumulation relies on its BRCT domain-mediated interaction with RacGAP1 (Yüce et al., 2005, our data) and is thought to be an important spatial cue that directs contractile ring formation to the cell equator (midzone stimulation, Eggert et al., 2006; Mishima, 2016; Verma et al., 2019). So, when there is no midzone anchored Ect2 due to the deletion of all three BRCT domains, where does the cue for contractile ring formation come

from? As signals from both midzone and astral microtubules contribute to contractile ring formation at the equator (D'Avino et al., 2015; Green et al., 2012; Mishima, 2016; von Dassow, 2009), we speculated that signals from astral microtubules could be responsible for RhoA zone formation in $Ect2^{\Delta BRCT0-2}$.

Astral microtubules prevent the accumulation of contractile ring components at the cell poles (D'Avino et al., 2015; Green et al., 2012; Mishima, 2016; von Dassow, 2009). Since we have shown that Ect2 activity is inhibited by BRCT2, Ect2 inactivation by stimulating the BRCT2-DH-GEF interaction could represent a way for astral microtubules to prevent cortical contractility at the poles. Strengthening the aster-based signal should then have no influence on Ect2 activity in cells that lack BRCT2-dependent inhibition. In $Ect2^{\Delta BRCT0-2}$ and $Ect2^{\Delta BRCT2}$ cells, the reinforcement of the inhibitory signal by the stabilization of microtubules (Desai et al., 1999; Hedrick et al., 2008; Rankin & Wordeman, 2010a) could not reduce cortical contractility (evaluated by the means of large bleb formation, Figure 44). Moreover, stabilized microtubules pushed against the membrane and led to the formation of medium-sized membrane blebs in $Ect2^{\Delta BRCT0-2}$ and $Ect2^{\Delta BRCT2}$, but also in control and $Ect2^{WT}$ cells (Figure 44, Rankin & Wordeman, 2010a). We had hoped that examining large bleb formation would give insights into whether astral microtubules exert their inhibitory actions by keeping Ect2 inactive. However, given that stabilized microtubules themselves introduce bleb formation, this may not be a suitable readout to assess this question.

Another way to test astral microtubule contribution to RhoA zone formation in $Ect2^{\Delta BRCT0-2}$ is to check whether their stabilization can decrease the width of the RhoA zone similar to earlier observations in control cells (van Oostende Triplet et al., 2014a; Zanin et al., 2013). Stabilized astral microtubules led to a slimmer RhoA zone in $Ect2^{\Delta BRCT0-2}$ expressing cells (Table 20), which implies that astral microtubules negatively control spatial RhoA signaling in $Ect2^{\Delta BRCT0-2}$, this, however, is not achieved by shutting off Ect2 activity. Astral microtubules, therefore, depict an independent control mechanism of RhoA signaling in addition to Ect2 autoinhibition. Nevertheless, when Ect2 autoinhibition is absent for example in $Ect2^{\Delta BRCT0-2}$, astral microtubules cannot completely compensate for the increase in GEF activity, which results in the broadening of the RhoA zone. Cortical polarization during anaphase is moreover influenced by direct RhoA inactivation through the actions of MP-GAP and chromosome-based signals, which lead to the relaxation of the polar cortex (Rodrigues et al., 2015; Zanin et

al., 2013). Thus, when Ect2 autoinhibition is lost, the remaining inhibitory mechanisms prevent homogenous RhoA activation and allow the generation of a discrete, yet broader, RhoA zone. In Ect2^{ΔBRCT0-2} expressing cells, we would expect that active RhoA accumulates less efficiently to the equatorial membrane, as a focused pool of its activator Ect2 at the center of the cell is missing. This is why our observation that wildtype amounts of RhoA are present at the cell equator of Ect2^{ΔBRCT0-2} expressing cells, suggests the existence of other positive signals, which are independent of midzone-tethered Ect2 and boost RhoA accumulation. Ect2 can interact with anillin and RacGAP1 via its PH and DH-PH domains, respectively, and both interactions were proposed to support Ect2 functioning during cytokinesis (Frenette et al., 2012; Zhang & Glotzer, 2015). These interactions might provide positive feedback loops that together with the mentioned negative control mechanisms, direct RhoA accumulation to the cell equator in Ect2^{ΔBRCT0-2} cells. Experimentally this could be tested by preventing these interactions and analyzing the effect on RhoA zone formation. Anillin binds Ect2 via the C-terminal part of its AHD (Frenette et al., 2012), thus expressing a truncated version of anillin after the depletion of endogenous anillin might clarify whether this positively contributes to RhoA zone formation in Ect2^{ΔBRCT0-2}. Furthermore, one could try to replace the PH domain of Ect2 with another membrane interaction domain, which allows membrane binding but no anillin interaction. Testing the role of the interaction between the catalytic domains of Ect2 and RacGAP1 is more challenging, as apart from Ect2 activity, also RacGAP1 activity seems to be required for RhoA activation (Zhang & Glotzer, 2015); thus one cannot simply deplete one of them. As the interaction was demonstrated for a DH-PH fragment of Ect2 and the GAP domain of RacGAP1 (Zhang & Glotzer, 2015), the PH domain could in principle be the interacting domain. Thus, one should first decipher which part of the DH-PH domains is required for the interaction. This might reveal a possibility to prevent the interaction without jeopardizing the normal function of the catalytic domains.

4.9 Closing remarks and future perspective

The presented study reports on the contributions made by several structural domains of the GEF Ect2 regarding its function and regulation during cytokinesis in human cells. By analyzing the functional impact of structural modifications this study provides detailed mechanistic insights into how Ect2 function and regulation is accomplished by the interplay of different domain contributions in space and time. Furthermore, the study highlights that several cooperating regulatory strategies restrict contractile ring formation to the cell equator. Our results underpin the essential role of RacGAP1 in releasing Ect2 autoinhibition, an issue that has been highly debated in the field over the past years. Moreover, it was revealed that the N-terminal BRCT domains, unlike earlier assumptions, do not operate as a functional unit, but each holds different functionalities. BRCT1, together with BRCT0, facilitates Ect2 activation, whereas BRCT2 suppresses Ect2 GEF activity. Moreover, it seems that Ect2 autoinhibition is more complex than previously assumed. First evidence obtained in living cells, supports an involvement of the membrane binding domain PH and the S-loop in GEF inhibition during cytokinesis. Thus, the prevailing model of Ect2 regulation has to be revised and extended to incorporate novel findings. Given that cytokinesis is a crucial process of cell division, it is not astonishing that several, partially overlapping mechanisms ensure the correct positioning and timely ingression of the contractile ring. The redundancy of regulatory processes makes cytokinesis more robust and allows it to tolerate small perturbations without sabotaging its overall success. Even though we contributed valuable insights, further research will be needed to understand the exact mechanisms of cytokinetic regulation. One main question is how RacGAP1 releases BRCT2-GEF interaction by binding to the BRCT domains. Further, the detailed characterization of the PH-inhibition in living cells would allow comments on (1) how it is mechanistically achieved, (2) how significant this interaction is compared to BRCT2 inhibition, and (3) how it is coordinated with for example BRCT2-inhibition in space and time. Over the past twenty years, more and more evidence has accumulated that links defects in Ect2 regulation to the development of cancer and poor prognosis (Cook et al., 2022; Guo et al., 2017; Li et al., 2021). Therefore, it is crucial to gain a full understanding of how Ect2 activity is temporally and spatially regulated, which may allow the development of new therapeutic strategies.

Bibliography

- Adams, R. R., Tavares, A. A., Salzberg, A., Bellen, H. J., & Glover, D. M. (1998). pavarotti encodes a kinesin-like protein required to organize the central spindle and contractile ring for cytokinesis. *Genes Dev*, *12*(10), 1483-1494. doi:10.1101/gad.12.10.1483
- Almawi, A. W., Langlois-Lemay, L., Boulton, S., Rodriguez Gonzalez, J., Melacini, G., D'Amours, D., & Guarne, A. (2020). Distinct surfaces on Cdc5/PLK Polo-box domain orchestrate combinatorial substrate recognition during cell division. *Sci Rep*, *10*(1), 3379. doi:10.1038/s41598-020-60344-4
- Archambault, V., D'Avino, P. P., Deery, M. J., Lilley, K. S., & Glover, D. M. (2008). Sequestration of Polo kinase to microtubules by phosphopriming-independent binding to Map205 is relieved by phosphorylation at a CDK site in mitosis. *Genes Dev*, *22*(19), 2707-2720. doi:10.1101/gad.486808
- Azoitei, M. L., Noh, J., Marston, D. J., Roudot, P., Marshall, C. B., Daugird, T. A., Lianza, S. L., Sandi, M. J., Ikura, M., Sondek, J., Rottapel, R., Hahn, K. M., & Danuser, G. (2019). Spatiotemporal dynamics of GEF-H1 activation controlled by microtubule- and Src-mediated pathways. *J Cell Biol*, *218*(9), 3077-3097. doi:10.1083/jcb.201812073
- Bagge, J., Oestergaard, V. H., & Lisby, M. (2021). Functions of TopBP1 in preserving genome integrity during mitosis. *Semin Cell Dev Biol*, *113*, 57-64. doi:10.1016/j.semcdb.2020.08.009
- Baruni, J. K., Munro, E. M., & von Dassow, G. (2008). Cytokinetic furrowing in toroidal, binucleate and anucleate cells in *C. elegans* embryos. *J Cell Sci*, *121*(Pt 3), 306-316. doi:10.1242/jcs.022897
- Basant, A., & Glotzer, M. (2018). Spatiotemporal Regulation of RhoA during Cytokinesis. *Current Biology*, *28*(9), R570-R580. doi:<https://doi.org/10.1016/j.cub.2018.03.045>
- Bement, W. M., Benink, H. A., & von Dassow, G. (2005). A microtubule-dependent zone of active RhoA during cleavage plane specification. *J Cell Biol*, *170*(1), 91-101. doi:10.1083/jcb.200501131
- Bement, W. M., Leda, M., Moe, A. M., Kita, A. M., Larson, M. E., Golding, A. E., Pfeuti, C., Su, K. C., Miller, A. L., Goryachev, A. B., & von Dassow, G. (2015). Activator-inhibitor coupling between Rho signalling and actin assembly makes the cell cortex an excitable medium. *Nat Cell Biol*, *17*(11), 1471-1483. doi:10.1038/ncb3251
- Bement, W. M., Miller, A. L., & von Dassow, G. (2006). Rho GTPase activity zones and transient contractile arrays. *Bioessays*, *28*(10), 983-993. doi:10.1002/bies.20477
- Berman, H. M., Westbrook, J., Feng, Z., Gilliland, G., Bhat, T. N., Weissig, H., Shindyalov, I. N., & Bourne, P. E. (2000). The Protein Data Bank. *Nucleic Acids Research*, *28*(1), 235-242. doi:10.1093/nar/28.1.235

- Bettencourt-Dias, M., Hildebrandt, F., Pellman, D., Woods, G., & Godinho, S. A. (2011). Centrosomes and cilia in human disease. *Trends Genet*, 27(8), 307-315. doi:10.1016/j.tig.2011.05.004
- Birkenfeld, J., Nalbant, P., Yoon, S. H., & Bokoch, G. M. (2008). Cellular functions of GEF-H1, a microtubule-regulated Rho-GEF: is altered GEF-H1 activity a crucial determinant of disease pathogenesis? *Trends Cell Biol*, 18(5), 210-219. doi:10.1016/j.tcb.2008.02.006
- Blomberg, N., & Nilges, M. (1997). Functional diversity of PH domains: an exhaustive modelling study. *Fold Des*, 2(6), 343-355. doi:10.1016/S1359-0278(97)00048-5
- Bonaccorsi, S., Giansanti, M. G., & Gatti, M. (1998). Spindle self-organization and cytokinesis during male meiosis in asterless mutants of *Drosophila melanogaster*. *J Cell Biol*, 142(3), 751-761. doi:10.1083/jcb.142.3.751
- Brennan, I. M., Peters, U., Kapoor, T. M., & Straight, A. F. (2007). Polo-like kinase controls vertebrate spindle elongation and cytokinesis. *PLoS One*, 2(5), e409. doi:10.1371/journal.pone.0000409
- Bretz, F., Hothorn, T., & Westfall, P. H. (2011). *Multiple comparisons using R*. Boca Raton, FL: CRC Press.
- Breznau, E. B., Murt, M., Blasius, T. L., Verhey, K. J., & Miller, A. L. (2017). The MgcRacGAP SxIP motif tethers Centralspindlin to microtubule plus ends in *Xenopus laevis*. *J Cell Sci*, 130(10), 1809-1821. doi:10.1242/jcs.195891
- Bringmann, H., & Hyman, A. A. (2005). A cytokinesis furrow is positioned by two consecutive signals. *Nature*, 436(7051), 731-734. doi:10.1038/nature03823
- Buchner, K. (2019). *Functional characterization of the BRCT domains of the RhoA GEF Ect2 during cell division*. Dissertation, LMU München, Retrieved from <http://nbn-resolving.de/urn:nbn:de:bvb:19-244595> (ediss:24459)
- Budnar, S., Husain, K. B., Gomez, G. A., Naghibosadat, M., Varma, A., Verma, S., Hamilton, N. A., Morris, R. G., & Yap, A. S. (2019). Anillin Promotes Cell Contractility by Cyclic Resetting of RhoA Residence Kinetics. *Dev Cell*, 49(6), 894-906 e812. doi:10.1016/j.devcel.2019.04.031
- Burkard, M. E., Maciejowski, J., Rodriguez-Bravo, V., Repka, M., Lowery, D. M., Clauser, K. R., Zhang, C., Shokat, K. M., Carr, S. A., Yaffe, M. B., & Jallepalli, P. V. (2009). Plk1 self-organization and priming phosphorylation of HsCYK-4 at the spindle midzone regulate the onset of division in human cells. *PLoS Biol*, 7(5), e1000111. doi:10.1371/journal.pbio.1000111
- Burkard, M. E., Randall, C. L., Laroche, S., Zhang, C., Shokat, K. M., Fisher, R. P., & Jallepalli, P. V. (2007). Chemical genetics reveals the requirement for Polo-like kinase 1 activity in positioning RhoA and triggering cytokinesis in human cells. *Proc Natl Acad Sci U S A*, 104(11), 4383-4388. doi:10.1073/pnas.0701140104

- Cabernard, C., Prehoda, K. E., & Doe, C. Q. (2010). A spindle-independent cleavage furrow positioning pathway. *Nature*, *467*(7311), 91-94. doi:10.1038/nature09334
- Calvert, M. E., Wright, G. D., Leong, F. Y., Chiam, K. H., Chen, Y., Jedd, G., & Balasubramanian, M. K. (2011). Myosin concentration underlies cell size-dependent scalability of actomyosin ring constriction. *J Cell Biol*, *195*(5), 799-813. doi:10.1083/jcb.201101055
- Canman, J. C., Cameron, L. A., Maddox, P. S., Straight, A., Tirnauer, J. S., Mitchison, T. J., Fang, G., Kapoor, T. M., & Salmon, E. D. (2003). Determining the position of the cell division plane. *Nature*, *424*(6952), 1074-1078. doi:10.1038/nature01860
- Cao, L. G., & Wang, Y. L. (1996). Signals from the spindle midzone are required for the stimulation of cytokinesis in cultured epithelial cells. *Mol Biol Cell*, *7*(2), 225-232. doi:10.1091/mbc.7.2.225
- Carmena, M., & Earnshaw, W. C. (2003). The cellular geography of aurora kinases. *Nat Rev Mol Cell Biol*, *4*(11), 842-854. doi:10.1038/nrm1245
- Carvalho, A., Desai, A., & Oegema, K. (2009). Structural memory in the contractile ring makes the duration of cytokinesis independent of cell size. *Cell*, *137*(5), 926-937. doi:10.1016/j.cell.2009.03.021
- Castrillon, D. H., & Wasserman, S. A. (1994). Diaphanous is required for cytokinesis in *Drosophila* and shares domains of similarity with the products of the limb deformity gene. *Development*, *120*(12), 3367-3377. Retrieved from <https://www.ncbi.nlm.nih.gov/pubmed/7821209>
- Chalamalasetty, R. B., Hummer, S., Nigg, E. A., & Sillje, H. H. (2006). Influence of human Ect2 depletion and overexpression on cleavage furrow formation and abscission. *J Cell Sci*, *119*(Pt 14), 3008-3019. doi:10.1242/jcs.03032
- Chan, E., & Nance, J. (2013). Mechanisms of CDC-42 activation during contact-induced cell polarization. *J Cell Sci*, *126*(Pt 7), 1692-1702. doi:10.1242/jcs.124594
- Chapa, Y. L. B., Hamanaka, M., Wray, A., Balasubramanian, M. K., & Mishima, M. (2020). Polar relaxation by dynein-mediated removal of cortical myosin II. *J Cell Biol*, *219*(8). doi:10.1083/jcb.201903080
- Charras, G. T., Coughlin, M., Mitchison, T. J., & Mahadevan, L. (2008). Life and times of a cellular bleb. *Biophys J*, *94*(5), 1836-1853. doi:10.1529/biophysj.107.113605
- Chen, A., Ulloa Severino, L., Panagiotou, T. C., Moraes, T. F., Yuen, D. A., Lavoie, B. D., & Wilde, A. (2021). Inhibition of polar actin assembly by astral microtubules is required for cytokinesis. *Nat Commun*, *12*(1), 2409. doi:10.1038/s41467-021-22677-0
- Chen, M., Pan, H., Sun, L., Shi, P., Zhang, Y., Li, L., Huang, Y., Chen, J., Jiang, P., Fang, X., Wu, C., & Chen, Z. (2020). Structure and regulation of human epithelial cell transforming 2 protein. *Proc Natl Acad Sci U S A*, *117*(2), 1027-1035. doi:10.1073/pnas.1913054117

- Chen, W., Foss, M., Tseng, K. F., & Zhang, D. (2008). Redundant mechanisms recruit actin into the contractile ring in silkworm spermatocytes. *PLoS Biol*, 6(9), e209. doi:10.1371/journal.pbio.0060209
- Colicino, E. G., & Hehnlly, H. (2018). Regulating a key mitotic regulator, polo-like kinase 1 (PLK1). *Cytoskeleton (Hoboken)*, 75(11), 481-494. doi:10.1002/cm.21504
- Combes, G., Alharbi, I., Braga, L. G., & Elowe, S. (2017). Playing polo during mitosis: PLK1 takes the lead. *Oncogene*, 36(34), 4819-4827. doi:10.1038/onc.2017.113
- Cook, D. R., Kang, M., Martin, T. D., Galanko, J. A., Loeza, G. H., Trembath, D. G., Justilien, V., Pickering, K. A., Vincent, D. F., Jarosch, A., Jurmeister, P., Waters, A. M., Hibshman, P. S., Campbell, A. D., Ford, C. A., Keku, T. O., Yeh, J. J., Lee, M. S., Cox, A. D., Fields, A. P., Sandler, R. S., Sansom, O. J., Sers, C., Schaefer, A., & Der, C. J. (2022). Aberrant Expression and Subcellular Localization of ECT2 Drives Colorectal Cancer Progression and Growth. *Cancer Res*, 82(1), 90-104. doi:10.1158/0008-5472.CAN-20-4218
- D'Avino, P. P., & Capalbo, L. (2016). Regulation of midbody formation and function by mitotic kinases. *Semin Cell Dev Biol*, 53, 57-63. doi:10.1016/j.semcdb.2016.01.018
- D'Avino, P. P., Giansanti, M. G., & Petronczki, M. (2015). Cytokinesis in animal cells. *Cold Spring Harb Perspect Biol*, 7(4), a015834. doi:10.1101/cshperspect.a015834
- D'Avino, P. P., Takeda, T., Capalbo, L., Zhang, W., Lilley, K. S., Laue, E. D., & Glover, D. M. (2008). Interaction between Anillin and RacGAP50C connects the actomyosin contractile ring with spindle microtubules at the cell division site. *J Cell Sci*, 121(Pt 8), 1151-1158. doi:10.1242/jcs.026716
- Dechant, R., & Glotzer, M. (2003). Centrosome separation and central spindle assembly act in redundant pathways that regulate microtubule density and trigger cleavage furrow formation. *Dev Cell*, 4(3), 333-344. doi:10.1016/s1534-5807(03)00057-1
- Desai, A., Verma, S., Mitchison, T. J., & Walczak, C. E. (1999). Kin I kinesins are microtubule-destabilizing enzymes. *Cell*, 96(1), 69-78. doi:10.1016/s0092-8674(00)80960-5
- Drechsel, D. N., Hyman, A. A., Hall, A., & Glotzer, M. (1997). A requirement for Rho and Cdc42 during cytokinesis in *Xenopus* embryos. *Curr Biol*, 7(1), 12-23. doi:10.1016/s0960-9822(06)00023-6
- Eggert, U. S., Mitchison, T. J., & Field, C. M. (2006). Animal cytokinesis: from parts list to mechanisms. *Annu Rev Biochem*, 75, 543-566. doi:10.1146/annurev.biochem.74.082803.133425
- Elia, A. E., Cantley, L. C., & Yaffe, M. B. (2003). Proteomic screen finds pSer/pThr-binding domain localizing Plk1 to mitotic substrates. *Science*, 299(5610), 1228-1231. doi:10.1126/science.1079079
- Elia, A. E., Rellos, P., Haire, L. F., Chao, J. W., Ivins, F. J., Hoepker, K., Mohammad, D., Cantley, L. C., Smerdon, S. J., & Yaffe, M. B. (2003). The molecular basis for phosphodependent

- substrate targeting and regulation of Plks by the Polo-box domain. *Cell*, 115(1), 83-95. doi:10.1016/s0092-8674(03)00725-6
- Emoto, K., Inadome, H., Kanaho, Y., Narumiya, S., & Umeda, M. (2005). Local change in phospholipid composition at the cleavage furrow is essential for completion of cytokinesis. *J Biol Chem*, 280(45), 37901-37907. doi:10.1074/jbc.M504282200
- Etienne-Manneville, S., & Hall, A. (2002). Rho GTPases in cell biology. *Nature*, 420(6916), 629-635. doi:10.1038/nature01148
- Evangelista, M., Pruyne, D., Amberg, D. C., Boone, C., & Bretscher, A. (2002). Formins direct Arp2/3-independent actin filament assembly to polarize cell growth in yeast. *Nat Cell Biol*, 4(3), 260-269. doi:10.1038/ncb770
- Fededa, J. P., & Gerlich, D. W. (2012). Molecular control of animal cell cytokinesis. *Nat Cell Biol*, 14(5), 440-447. doi:10.1038/ncb2482
- Field, C. M., & Alberts, B. M. (1995). Anillin, a contractile ring protein that cycles from the nucleus to the cell cortex. *J Cell Biol*, 131(1), 165-178. doi:10.1083/jcb.131.1.165
- Field, C. M., Coughlin, M., Doberstein, S., Marty, T., & Sullivan, W. (2005). Characterization of anillin mutants reveals essential roles in septin localization and plasma membrane integrity. *Development*, 132(12), 2849-2860. doi:10.1242/dev.01843
- Fields, A. P., & Justilien, V. (2010). The guanine nucleotide exchange factor (GEF) Ect2 is an oncogene in human cancer. *Adv Enzyme Regul*, 50(1), 190-200. doi:10.1016/j.advenzreg.2009.10.010
- Foe, V. E., & von Dassow, G. (2008). Stable and dynamic microtubules coordinately shape the myosin activation zone during cytokinetic furrow formation. *J Cell Biol*, 183(3), 457-470. doi:10.1083/jcb.200807128
- Frenette, P., Haines, E., Loloian, M., Kinal, M., Pakarian, P., & Piekny, A. (2012). An anillin-Ect2 complex stabilizes central spindle microtubules at the cortex during cytokinesis. *PLoS One*, 7(4), e34888. doi:10.1371/journal.pone.0034888
- Gadde, S., & Heald, R. (2004). Mechanisms and molecules of the mitotic spindle. *Curr Biol*, 14(18), R797-805. doi:10.1016/j.cub.2004.09.021
- Gai, M., Camera, P., Dema, A., Bianchi, F., Berto, G., Scarpa, E., Germena, G., & Di Cunto, F. (2011). Citron kinase controls abscission through RhoA and anillin. *Mol Biol Cell*, 22(20), 3768-3778. doi:10.1091/mbc.E10-12-0952
- Garcia-Mata, R., Boulter, E., & Burridge, K. (2011). The 'invisible hand': regulation of RHO GTPases by RHO GDI. *Nature Reviews Molecular Cell Biology*, 12(8), 493-504. doi:10.1038/nrm3153
- Giansanti, M. G., Gatti, M., & Bonaccorsi, S. (2001). The role of centrosomes and astral microtubules during asymmetric division of *Drosophila* neuroblasts. *Development*, 128(7), 1137-1145. doi:10.1242/dev.128.7.1137

- Glotzer, M. (2009). The 3Ms of central spindle assembly: microtubules, motors and MAPs. *Nat Rev Mol Cell Biol*, *10*(1), 9-20. doi:10.1038/nrm2609
- Goldschmidt-Clermont, P. J., Furman, M. I., Wachsstock, D., Safer, D., Nachmias, V. T., & Pollard, T. D. (1992). The control of actin nucleotide exchange by thymosin beta 4 and profilin. A potential regulatory mechanism for actin polymerization in cells. *Mol Biol Cell*, *3*(9), 1015-1024. doi:10.1091/mbc.3.9.1015
- Golsteyn, R. M., Mundt, K. E., Fry, A. M., & Nigg, E. A. (1995). Cell cycle regulation of the activity and subcellular localization of Plk1, a human protein kinase implicated in mitotic spindle function. *J Cell Biol*, *129*(6), 1617-1628. doi:10.1083/jcb.129.6.1617
- Gomez-Cavazos, J. S., Lee, K. Y., Lara-Gonzalez, P., Li, Y., Desai, A., Shiau, A. K., & Oegema, K. (2020). A Non-canonical BRCT-Phosphopeptide Recognition Mechanism Underlies RhoA Activation in Cytokinesis. *Curr Biol*, *30*(16), 3101-3115 e3111. doi:10.1016/j.cub.2020.05.090
- Green, R. A., Paluch, E., & Oegema, K. (2012). Cytokinesis in animal cells. *Annu Rev Cell Dev Biol*, *28*, 29-58. doi:10.1146/annurev-cellbio-101011-155718
- Gruneberg, U., Neef, R., Honda, R., Nigg, E. A., & Barr, F. A. (2004). Relocation of Aurora B from centromeres to the central spindle at the metaphase to anaphase transition requires MKlp2. *J Cell Biol*, *166*(2), 167-172. doi:10.1083/jcb.200403084
- Guo, Z., Chen, X., Du, T., Zhu, D., Lai, Y., Dong, W., Wu, W., Lin, C., Liu, L., & Huang, H. (2017). Elevated levels of epithelial cell transforming sequence 2 predicts poor prognosis for prostate cancer. *Med Oncol*, *34*(1), 13. doi:10.1007/s12032-016-0872-3
- Haga, R. B., & Ridley, A. J. (2016). Rho GTPases: Regulation and roles in cancer cell biology. *Small GTPases*, *7*(4), 207-221. doi:10.1080/21541248.2016.1232583
- Hammel, M., Rashid, I., Sverzhinsky, A., Pourfarjam, Y., Tsai, M. S., Ellenberger, T., Pascal, J. M., Kim, I. K., Tainer, J. A., & Tomkinson, A. E. (2021). An atypical BRCT-BRCT interaction with the XRCC1 scaffold protein compacts human DNA Ligase IIIalpha within a flexible DNA repair complex. *Nucleic Acids Res*, *49*(1), 306-321. doi:10.1093/nar/gkaa1188
- Han, J., Luby-Phelps, K., Das, B., Shu, X., Xia, Y., Mosteller, R. D., Krishna, U. M., Falck, J. R., White, M. A., & Broek, D. (1998). Role of substrates and products of PI 3-kinase in regulating activation of Rac-related guanosine triphosphatases by Vav. *Science*, *279*(5350), 558-560. doi:10.1126/science.279.5350.558
- Hanisch, A., Wehner, A., Nigg, E. A., & Sillje, H. H. (2006). Different Plk1 functions show distinct dependencies on Polo-Box domain-mediated targeting. *Mol Biol Cell*, *17*(1), 448-459. doi:10.1091/mbc.e05-08-0801
- Hara, T., Abe, M., Inoue, H., Yu, L. R., Veenstra, T. D., Kang, Y. H., Lee, K. S., & Miki, T. (2006). Cytokinesis regulator ECT2 changes its conformation through phosphorylation at Thr-341 in G2/M phase. *Oncogene*, *25*(4), 566-578. doi:10.1038/sj.onc.1209078

- He, D., Xiang, J., Li, B., & Liu, H. (2016). The dynamic behavior of Ect2 in response to DNA damage. *Sci Rep*, *6*, 24504. doi:10.1038/srep24504
- Heasman, S. J., & Ridley, A. J. (2008). Mammalian Rho GTPases: new insights into their functions from in vivo studies. *Nature Reviews Molecular Cell Biology*, *9*(9), 690-701. doi:10.1038/nrm2476
- Hedrick, D. G., Stout, J. R., & Walczak, C. E. (2008). Effects of anti-microtubule agents on microtubule organization in cells lacking the kinesin-13 MCAK. *Cell Cycle*, *7*(14), 2146-2156. doi:10.4161/cc.7.14.6239
- Hickson, G. R., Echard, A., & O'Farrell, P. H. (2006). Rho-kinase controls cell shape changes during cytokinesis. *Curr Biol*, *16*(4), 359-370. doi:10.1016/j.cub.2005.12.043
- Hillen, W., & Berens, C. (1994). Mechanisms underlying expression of Tn10 encoded tetracycline resistance. *Annu Rev Microbiol*, *48*, 345-369. doi:10.1146/annurev.mi.48.100194.002021
- Hillen, W., Gatz, C., Altschmied, L., Schollmeier, K., & Meier, I. (1983). Control of expression of the Tn10-encoded tetracycline resistance genes. Equilibrium and kinetic investigation of the regulatory reactions. *J Mol Biol*, *169*(3), 707-721. doi:10.1016/s0022-2836(83)80166-1
- Hime, G., & Saint, R. (1992). Zygotic expression of the pebble locus is required for cytokinesis during the postblastoderm mitoses of *Drosophila*. *Development*, *114*(1), 165-171. doi:10.1242/dev.114.1.165
- Hofweber, M., Hutten, S., Bourgeois, B., Spreitzer, E., Niedner-Boblenz, A., Schifferer, M., Ruepp, M. D., Simons, M., Niessing, D., Madl, T., & Dormann, D. (2018). Phase Separation of FUS Is Suppressed by Its Nuclear Import Receptor and Arginine Methylation. *Cell*, *173*(3), 706-719 e713. doi:10.1016/j.cell.2018.03.004
- Holder, J., Poser, E., & Barr, F. A. (2019). Getting out of mitosis: spatial and temporal control of mitotic exit and cytokinesis by PP1 and PP2A. *FEBS Lett*, *593*(20), 2908-2924. doi:10.1002/1873-3468.13595
- Hu, C. K., Coughlin, M., Field, C. M., & Mitchison, T. J. (2011). KIF4 regulates midzone length during cytokinesis. *Curr Biol*, *21*(10), 815-824. doi:10.1016/j.cub.2011.04.019
- Hu, C. K., Coughlin, M., & Mitchison, T. J. (2012). Midbody assembly and its regulation during cytokinesis. *Mol Biol Cell*, *23*(6), 1024-1034. doi:10.1091/mbc.E11-08-0721
- Jantsch-Plunger, V., Gonczy, P., Romano, A., Schnabel, H., Hamill, D., Schnabel, R., Hyman, A. A., & Glotzer, M. (2000). CYK-4: A Rho family gtpase activating protein (GAP) required for central spindle formation and cytokinesis. *J Cell Biol*, *149*(7), 1391-1404. doi:10.1083/jcb.149.7.1391
- Joo, E., Surka, M. C., & Trimble, W. S. (2007). Mammalian SEPT2 is required for scaffolding nonmuscle myosin II and its kinases. *Dev Cell*, *13*(5), 677-690. doi:10.1016/j.devcel.2007.09.001

- Jordan, S. N., & Canman, J. C. (2012). Rho GTPases in animal cell cytokinesis: an occupation by the one percent. *Cytoskeleton (Hoboken)*, *69*(11), 919-930. doi:10.1002/cm.21071
- Jordan, S. N., Davies, T., Zhuravlev, Y., Dumont, J., Shirasu-Hiza, M., & Canman, J. C. (2016). Cortical PAR polarity proteins promote robust cytokinesis during asymmetric cell division. *J Cell Biol*, *212*(1), 39-49. doi:10.1083/jcb.201510063
- Justilien, V., Jameison, L., Der, C. J., Rossman, K. L., & Fields, A. P. (2011). Oncogenic activity of Ect2 is regulated through protein kinase C ι -mediated phosphorylation. *J Biol Chem*, *286*(10), 8149-8157. doi:10.1074/jbc.M110.196113
- Kamasaki, T., O'Toole, E., Kita, S., Osumi, M., Usukura, J., McIntosh, J. R., & Goshima, G. (2013). Augmin-dependent microtubule nucleation at microtubule walls in the spindle. *J Cell Biol*, *202*(1), 25-33. doi:10.1083/jcb.201304031
- Kamijo, K., Ohara, N., Abe, M., Uchimura, T., Hosoya, H., Lee, J. S., & Miki, T. (2006). Dissecting the role of Rho-mediated signaling in contractile ring formation. *Mol Biol Cell*, *17*(1), 43-55. doi:10.1091/mbc.e05-06-0569
- Kawamura, K. (1977). Microdissection studies on the dividing neuroblast of the grasshopper, with special reference to the mechanism of unequal cytokinesis. *Exp Cell Res*, *106*(1), 127-137. doi:10.1016/0014-4827(77)90249-x
- Kechad, A., Jananji, S., Ruella, Y., & Hickson, G. R. (2012). Anillin acts as a bifunctional linker coordinating midbody ring biogenesis during cytokinesis. *Curr Biol*, *22*(3), 197-203. doi:10.1016/j.cub.2011.11.062
- Kim, H., Guo, F., Brahma, S., Xing, Y., & Burkard, M. E. (2014). Centralspindlin assembly and 2 phosphorylations on MgcRacGAP by Polo-like kinase 1 initiate Ect2 binding in early cytokinesis. *Cell Cycle*, *13*(18), 2952-2961. doi:10.4161/15384101.2014.947201
- Kim, J. E., Billadeau, D. D., & Chen, J. (2005). The tandem BRCT domains of Ect2 are required for both negative and positive regulation of Ect2 in cytokinesis. *J Biol Chem*, *280*(7), 5733-5739. doi:10.1074/jbc.M409298200
- Kimura, K., Tsuji, T., Takada, Y., Miki, T., & Narumiya, S. (2000). Accumulation of GTP-bound RhoA during cytokinesis and a critical role of ECT2 in this accumulation. *J Biol Chem*, *275*(23), 17233-17236. doi:10.1074/jbc.C000212200
- Kishi, K., Sasaki, T., Kuroda, S., Itoh, T., & Takai, Y. (1993). Regulation of cytoplasmic division of *Xenopus* embryo by rho p21 and its inhibitory GDP/GTP exchange protein (rho GDI). *J Cell Biol*, *120*(5), 1187-1195. doi:10.1083/jcb.120.5.1187
- Kosako, H., Yoshida, T., Matsumura, F., Ishizaki, T., Narumiya, S., & Inagaki, M. (2000). Rho-kinase/ROCK is involved in cytokinesis through the phosphorylation of myosin light chain and not ezrin/radixin/moesin proteins at the cleavage furrow. *Oncogene*, *19*(52), 6059-6064. doi:10.1038/sj.onc.1203987

- Kotýnková, K., Su, K.-C., West, S. C., & Petronczki, M. (2016). Plasma Membrane Association but Not Midzone Recruitment of RhoGEF ECT2 Is Essential for Cytokinesis. *Cell Reports*, 17(10), 2672-2686. doi:10.1016/j.celrep.2016.11.029
- Kusumi, A., Fujiwara, T. K., Chadda, R., Xie, M., Tsunoyama, T. A., Kalay, Z., Kasai, R. S., & Suzuki, K. G. (2012). Dynamic organizing principles of the plasma membrane that regulate signal transduction: commemorating the fortieth anniversary of Singer and Nicolson's fluid-mosaic model. *Annu Rev Cell Dev Biol*, 28, 215-250. doi:10.1146/annurev-cellbio-100809-151736
- Lacroix, B., & Maddox, A. S. (2012). Cytokinesis, ploidy and aneuploidy. *J Pathol*, 226(2), 338-351. doi:10.1002/path.3013
- Lai, S. L., Chang, C. N., Wang, P. J., & Lee, S. J. (2005). Rho mediates cytokinesis and epiboly via ROCK in zebrafish. *Mol Reprod Dev*, 71(2), 186-196. doi:10.1002/mrd.20290
- Lane, H. A., & Nigg, E. A. (1996). Antibody microinjection reveals an essential role for human polo-like kinase 1 (Plk1) in the functional maturation of mitotic centrosomes. *J Cell Biol*, 135(6 Pt 2), 1701-1713. doi:10.1083/jcb.135.6.1701
- Lara-Gonzalez, P., Westhorpe, F. G., & Taylor, S. S. (2012). The spindle assembly checkpoint. *Curr Biol*, 22(22), R966-980. doi:10.1016/j.cub.2012.10.006
- Lehner, C. F. (1992). The pebble gene is required for cytokinesis in *Drosophila*. *J Cell Sci*, 103 (Pt 4), 1021-1030. Retrieved from <https://www.ncbi.nlm.nih.gov/pubmed/1487486>
- Lekomtsev, S., Su, K. C., Pye, V. E., Blight, K., Sundaramoorthy, S., Takaki, T., Collinson, L. M., Cherepanov, P., Divecha, N., & Petronczki, M. (2012). Centralspindlin links the mitotic spindle to the plasma membrane during cytokinesis. *Nature*, 492(7428), 276-279. doi:10.1038/nature11773
- Lemmon, M. A. (2007). Pleckstrin homology (PH) domains and phosphoinositides. *Biochem Soc Symp*(74), 81-93. doi:10.1042/BSS0740081
- Lemmon, M. A. (2008). Membrane recognition by phospholipid-binding domains. *Nat Rev Mol Cell Biol*, 9(2), 99-111. doi:10.1038/nrm2328
- Lenoir, M., Kufareva, I., Abagyan, R., & Overduin, M. (2015). Membrane and Protein Interactions of the Pleckstrin Homology Domain Superfamily. *Membranes (Basel)*, 5(4), 646-663. doi:10.3390/membranes5040646
- Lens, S. M. A., & Medema, R. H. (2019). Cytokinesis defects and cancer. *Nat Rev Cancer*, 19(1), 32-45. doi:10.1038/s41568-018-0084-6
- Leung, C. C., & Glover, J. N. (2011). BRCT domains: easy as one, two, three. *Cell Cycle*, 10(15), 2461-2470. doi:10.4161/cc.10.15.16312
- Lewellyn, L., Carvalho, A., Desai, A., Maddox, A. S., & Oegema, K. (2011). The chromosomal passenger complex and centralspindlin independently contribute to contractile ring assembly. *J Cell Biol*, 193(1), 155-169. doi:10.1083/jcb.201008138

- Li, C., Peng, Z., Wang, Y., Lam, G., Nissen, N., Tang, J., Yuan, X., Lewis, M., Greene, M. I., Pandol, S. J., & Wang, Q. (2021). Epithelial cell transforming 2 is regulated by Yes-associated protein 1 and mediates pancreatic cancer progression and metastasis. *Am J Physiol Gastrointest Liver Physiol*, *320*(3), G380-g395. doi:10.1152/ajpgi.00185.2020
- Life Technologies Corporation. (2012). *Flp-In™ T-REx™ Core Kit* [Manual]. Retrieved from https://www.thermofisher.com/document-connect/document-connect.html?url=https%3A%2F%2Fassets.thermofisher.com%2FTFS-Assets%2FSLG%2Fmanuals%2Fflpintrex_man.pdf
- Lim, S., & Ganem, N. J. (2014). Tetraploidy and tumor development. *Oncotarget*, *5*(22), 10959-10960. doi:10.18632/oncotarget.2790
- Limzerwala, J. F., Jeganathan, K. B., Kloeber, J. A., Davies, B. A., Zhang, C., Sturmlechner, I., Zhong, J., Fierro Velasco, R., Fields, A. P., Yuan, Y., Baker, D. J., Zhou, D., Li, H., Katzmann, D. J., & van Deursen, J. M. (2020). FoxM1 insufficiency hyperactivates Ect2-RhoA-mDia1 signaling to drive cancer. *Nat Cancer*, *1*(10), 1010-1024. doi:10.1038/s43018-020-00116-1
- Liot, C., Seguin, L., Siret, A., Crouin, C., Schmidt, S., & Bertoglio, J. (2011). APC(cdh1) mediates degradation of the oncogenic Rho-GEF Ect2 after mitosis. *PLoS One*, *6*(8), e23676. doi:10.1371/journal.pone.0023676
- Liu, J., Fairn, G. D., Ceccarelli, D. F., Sicheri, F., & Wilde, A. (2012). Cleavage furrow organization requires PIP(2)-mediated recruitment of anillin. *Curr Biol*, *22*(1), 64-69. doi:10.1016/j.cub.2011.11.040
- Liu, X. F., Ishida, H., Raziuddin, R., & Miki, T. (2004). Nucleotide exchange factor ECT2 interacts with the polarity protein complex Par6/Par3/protein kinase Czeta (PKCzeta) and regulates PKCzeta activity. *Mol Cell Biol*, *24*(15), 6665-6675. doi:10.1128/MCB.24.15.6665-6675.2004
- Loria, A., Longhini, K. M., & Glotzer, M. (2012). The RhoGAP domain of CYK-4 has an essential role in RhoA activation. *Curr Biol*, *22*(3), 213-219. doi:10.1016/j.cub.2011.12.019
- Mabuchi, I. (1994). Cleavage furrow: timing of emergence of contractile ring actin filaments and establishment of the contractile ring by filament bundling in sea urchin eggs. *J Cell Sci*, *107* (Pt 7), 1853-1862. Retrieved from <https://www.ncbi.nlm.nih.gov/pubmed/7983152>
- Mabuchi, I., Hamaguchi, Y., Fujimoto, H., Morii, N., Mishima, M., & Narumiya, S. (1993). A rho-like protein is involved in the organisation of the contractile ring in dividing sand dollar eggs. *Zygote*, *1*(4), 325-331. doi:10.1017/s0967199400001659
- Makyio, H., Ohgi, M., Takei, T., Takahashi, S., Takatsu, H., Katoh, Y., Hanai, A., Ueda, T., Kanaho, Y., Xie, Y., Shin, H. W., Kamikubo, H., Kataoka, M., Kawasaki, M., Kato, R., Wakatsuki, S., & Nakayama, K. (2012). Structural basis for Arf6-MKLP1 complex formation on the Flemming body responsible for cytokinesis. *EMBO J*, *31*(11), 2590-2603. doi:10.1038/emboj.2012.89

- Malumbres, M. (2014). Cyclin-dependent kinases. *Genome Biol*, 15(6), 122. doi:10.1186/gb4184
- Mangal, S., Sacher, J., Kim, T., Osorio, D. S., Motegi, F., Carvalho, A. X., Oegema, K., & Zanin, E. (2018). TPXL-1 activates Aurora A to clear contractile ring components from the polar cortex during cytokinesis. *J Cell Biol*, 217(3), 837-848. doi:10.1083/jcb.201706021
- Martino, L., Morchoisne-Bolhy, S., Cheerambathur, D. K., Van Hove, L., Dumont, J., Joly, N., Desai, A., Doye, V., & Pintard, L. (2017). Channel Nucleoporins Recruit PLK-1 to Nuclear Pore Complexes to Direct Nuclear Envelope Breakdown in *C. elegans*. *Dev Cell*, 43(2), 157-171 e157. doi:10.1016/j.devcel.2017.09.019
- Mastrorarde, D. N., McDonald, K. L., Ding, R., & McIntosh, J. R. (1993). Interpolar spindle microtubules in PTK cells. *J Cell Biol*, 123(6 Pt 1), 1475-1489. doi:10.1083/jcb.123.6.1475
- Matthews, Helen K., Delabre, U., Rohn, Jennifer L., Guck, J., Kunda, P., & Baum, B. (2012). Changes in Ect2 Localization Couple Actomyosin-Dependent Cell Shape Changes to Mitotic Progression. *Developmental Cell*, 23(2), 371-383. doi:10.1016/j.devcel.2012.06.003
- Mazzarello, P. (1999). A unifying concept: the history of cell theory. *Nat Cell Biol*, 1(1), E13-15. doi:10.1038/8964
- McDonald, K. L., Edwards, M. K., & McIntosh, J. R. (1979). Cross-sectional structure of the central mitotic spindle of *Diatoma vulgare*. Evidence for specific interactions between antiparallel microtubules. *J Cell Biol*, 83(2 Pt 1), 443-461. doi:10.1083/jcb.83.2.443
- McIntosh, J. R., McDonald, K. L., Edwards, M. K., & Ross, B. M. (1979). Three-dimensional structure of the central mitotic spindle of *Diatoma vulgare*. *J Cell Biol*, 83(2 Pt 1), 428-442. doi:10.1083/jcb.83.2.428
- McIntosh, J. R., Molodtsov, M. I., & Ataullakhanov, F. I. (2012). Biophysics of mitosis. *Q Rev Biophys*, 45(2), 147-207. doi:10.1017/S0033583512000017
- Melendez, J., Stengel, K., Zhou, X., Chauhan, B. K., Debidda, M., Andreassen, P., Lang, R. A., & Zheng, Y. (2011). RhoA GTPase is dispensable for actomyosin regulation but is essential for mitosis in primary mouse embryonic fibroblasts. *J Biol Chem*, 286(17), 15132-15137. doi:10.1074/jbc.C111.229336
- Michaelson, D., Silletti, J., Murphy, G., D'Eustachio, P., Rush, M., & Philips, M. R. (2001). Differential localization of Rho GTPases in live cells: regulation by hypervariable regions and RhoGDI binding. *J Cell Biol*, 152(1), 111-126. doi:10.1083/jcb.152.1.111
- Mierzwa, B., & Gerlich, D. W. (2014). Cytokinetic abscission: molecular mechanisms and temporal control. *Dev Cell*, 31(5), 525-538. doi:10.1016/j.devcel.2014.11.006
- Miki, T., Fleming, T. P., Bottaro, D. P., Rubin, J. S., Ron, D., & Aaronson, S. A. (1991). Expression cDNA cloning of the KGF receptor by creation of a transforming autocrine loop. *Science*, 251(4989), 72-75. doi:10.1126/science.1846048

- Miki, T., Smith, C. L., Long, J. E., Eva, A., & Fleming, T. P. (1993). Oncogene *ect2* is related to regulators of small GTP-binding proteins. *Nature*, *362*(6419), 462-465. doi:10.1038/362462a0
- Miller, A. L., & Bement, W. M. (2009). Regulation of cytokinesis by Rho GTPase flux. *Nat Cell Biol*, *11*(1), 71-77. doi:10.1038/ncb1814
- Mishima, M. (2016). Centralspindlin in Rappaport's cleavage signaling. *Semin Cell Dev Biol*, *53*, 45-56. doi:10.1016/j.semcdb.2016.03.006
- Mishima, M., Kaitna, S., & Glotzer, M. (2002). Central spindle assembly and cytokinesis require a kinesin-like protein/RhoGAP complex with microtubule bundling activity. *Dev Cell*, *2*(1), 41-54. doi:10.1016/s1534-5807(01)00110-1
- Moorman, J. P., Bobak, D. A., & Hahn, C. S. (1996). Inactivation of the small GTP binding protein Rho induces multinucleate cell formation and apoptosis in murine T lymphoma EL4. *J Immunol*, *156*(11), 4146-4153. Retrieved from <https://www.ncbi.nlm.nih.gov/pubmed/8666781>
- Morgan, D. (2006). *The cell cycle : principles of control*. Oxford: Oxford University Press.
- Motegi, F., Velarde, N. V., Piano, F., & Sugimoto, A. (2006). Two phases of astral microtubule activity during cytokinesis in *C. elegans* embryos. *Dev Cell*, *10*(4), 509-520. doi:10.1016/j.devcel.2006.03.001
- Murrell, M., Oakes, P. W., Lenz, M., & Gardel, M. L. (2015). Forcing cells into shape: the mechanics of actomyosin contractility. *Nat Rev Mol Cell Biol*, *16*(8), 486-498. doi:10.1038/nrm4012
- Murthy, K., & Wadsworth, P. (2008). Dual role for microtubules in regulating cortical contractility during cytokinesis. *J Cell Sci*, *121*(Pt 14), 2350-2359. doi:10.1242/jcs.027052
- Nazockdast, E., & Redemann, S. (2020). Mechanics of the spindle apparatus. *Semin Cell Dev Biol*, *107*, 91-102. doi:10.1016/j.semcdb.2020.06.018
- Neef, R., Gruneberg, U., Kopajtich, R., Li, X., Nigg, E. A., Sillje, H., & Barr, F. A. (2007). Choice of Plk1 docking partners during mitosis and cytokinesis is controlled by the activation state of Cdk1. *Nat Cell Biol*, *9*(4), 436-444. doi:10.1038/ncb1557
- Niiya, F., Tatsumoto, T., Lee, K. S., & Miki, T. (2006). Phosphorylation of the cytokinesis regulator ECT2 at G2/M phase stimulates association of the mitotic kinase Plk1 and accumulation of GTP-bound RhoA. *Oncogene*, *25*(6), 827-837. doi:10.1038/sj.onc.1209124
- Niiya, F., Xie, X., Lee, K. S., Inoue, H., & Miki, T. (2005). Inhibition of cyclin-dependent kinase 1 induces cytokinesis without chromosome segregation in an ECT2 and MgcRacGAP-dependent manner. *J Biol Chem*, *280*(43), 36502-36509. doi:10.1074/jbc.M508007200

- Nimnual, A. S., Yatsula, B. A., & Bar-Sagi, D. (1998). Coupling of Ras and Rac guanosine triphosphatases through the Ras exchanger Sos. *Science*, *279*(5350), 560-563. doi:10.1126/science.279.5350.560
- Nishimura, Y., & Yonemura, S. (2006). Centralspindlin regulates ECT2 and RhoA accumulation at the equatorial cortex during cytokinesis. *J Cell Sci*, *119*(Pt 1), 104-114. doi:10.1242/jcs.02737
- O'Gorman, S., Fox, D. T., & Wahl, G. M. (1991). Recombinase-mediated gene activation and site-specific integration in mammalian cells. *Science*, *251*(4999), 1351-1355. doi:10.1126/science.1900642
- O'Shaughnessy, B., & Thiyagarajan, S. (2018). Mechanisms of contractile ring tension production and constriction. *Biophys Rev*, *10*(6), 1667-1681. doi:10.1007/s12551-018-0476-6
- Oegema, K., Savoian, M. S., Mitchison, T. J., & Field, C. M. (2000). Functional analysis of a human homologue of the Drosophila actin binding protein anillin suggests a role in cytokinesis. *J Cell Biol*, *150*(3), 539-552. doi:10.1083/jcb.150.3.539
- Pavin, N., & Tolic, I. M. (2021). Mechanobiology of the Mitotic Spindle. *Dev Cell*, *56*(2), 192-201. doi:10.1016/j.devcel.2020.11.003
- Petronczki, M., Glotzer, M., Kraut, N., & Peters, J. M. (2007). Polo-like kinase 1 triggers the initiation of cytokinesis in human cells by promoting recruitment of the RhoGEF Ect2 to the central spindle. *Dev Cell*, *12*(5), 713-725. doi:10.1016/j.devcel.2007.03.013
- Petronczki, M., Lenart, P., & Peters, J. M. (2008). Polo on the Rise-from Mitotic Entry to Cytokinesis with Plk1. *Dev Cell*, *14*(5), 646-659. doi:10.1016/j.devcel.2008.04.014
- Piekny, A., Werner, M., & Glotzer, M. (2005). Cytokinesis: welcome to the Rho zone. *Trends Cell Biol*, *15*(12), 651-658. doi:10.1016/j.tcb.2005.10.006
- Piekny, A. J., & Glotzer, M. (2008). Anillin is a scaffold protein that links RhoA, actin, and myosin during cytokinesis. *Curr Biol*, *18*(1), 30-36. doi:10.1016/j.cub.2007.11.068
- Pines, J. (2011). Cubism and the cell cycle: the many faces of the APC/C. *Nat Rev Mol Cell Biol*, *12*(7), 427-438. doi:10.1038/nrm3132
- Poon, R. Y. (2016). Cell Cycle Control: A System of Interlinking Oscillators. *Methods Mol Biol*, *1342*, 3-19. doi:10.1007/978-1-4939-2957-3_1
- Pourfarjam, Y., Ellenberger, T., Tainer, J.A., Tomkinson, A.E., Kim, I.K. (2020). Structure of the C-terminal BRCT domain of human XRCC1. doi:10.2210/pdb6wh2/pdb
- Prokopenko, S. N., Brumby, A., O'Keefe, L., Prior, L., He, Y., Saint, R., & Bellen, H. J. (1999). A putative exchange factor for Rho1 GTPase is required for initiation of cytokinesis in Drosophila. *Genes Dev*, *13*(17), 2301-2314.

- R Core Team. (2021). R: A Language and Environment for Statistical Computing. Vienna, Austria: R Foundation for Statistical Computing. Retrieved from <https://www.R-project.org/>
- Ramkumar, N., Patel, J. V., Anstatt, J., & Baum, B. (2021). Aurora B-dependent polarization of the cortical actomyosin network during mitotic exit. *EMBO Rep*, 22(10), e52387. doi:10.15252/embr.202152387
- Rankin, K. E., & Wordeman, L. (2010a). Long astral microtubules uncouple mitotic spindles from the cytokinetic furrow. *Journal of Cell Biology*, 190(1), 35-43. doi:10.1083/jcb.201004017
- Rankin, K. E., & Wordeman, L. (2010b). Long astral microtubules uncouple mitotic spindles from the cytokinetic furrow. *J Cell Biol*, 190(1), 35-43. doi:10.1083/jcb.201004017
- Rappaport, R. (1961). Experiments concerning the cleavage stimulus in sand dollar eggs. *Journal of Experimental Zoology*, 148(1), 81-89. doi:<https://doi.org/10.1002/jez.1401480107>
- Rappaport, R. (1985). Repeated furrow formation from a single mitotic apparatus in cylindrical sand dollar eggs. *J Exp Zool*, 234(1), 167-171. doi:10.1002/jez.1402340120
- Rappas, M., Oliver, A. W., & Pearl, L. H. (2011). Structure and function of the Rad9-binding region of the DNA-damage checkpoint adaptor TopBP1. *Nucleic Acids Res*, 39(1), 313-324. doi:10.1093/nar/gkq743
- Rhind, N., & Russell, P. (2012). Signaling pathways that regulate cell division. *Cold Spring Harb Perspect Biol*, 4(10). doi:10.1101/cshperspect.a005942
- Rodrigues, N. T., Lekomtsev, S., Jananji, S., Kriston-Vizi, J., Hickson, G. R., & Baum, B. (2015). Kinetochores-localized PP1-Sds22 couples chromosome segregation to polar relaxation. *Nature*, 524(7566), 489-492. doi:10.1038/nature14496
- Rossmann, K. L., Der, C. J., & Sondek, J. (2005). GEF means go: turning on RHO GTPases with guanine nucleotide-exchange factors. *Nat Rev Mol Cell Biol*, 6(2), 167-180. doi:10.1038/nrm1587
- Saito, S., Liu, X. F., Kamijo, K., Raziuddin, R., Tatsumoto, T., Okamoto, I., Chen, X., Lee, C. C., Lorenzi, M. V., Ohara, N., & Miki, T. (2004). Deregulation and mislocalization of the cytokinesis regulator ECT2 activate the Rho signaling pathways leading to malignant transformation. *J Biol Chem*, 279(8), 7169-7179. doi:10.1074/jbc.M306725200
- Saito, S., Tatsumoto, T., Lorenzi, M. V., Chedid, M., Kapoor, V., Sakata, H., Rubin, J., & Miki, T. (2003). Rho exchange factor ECT2 is induced by growth factors and regulates cytokinesis through the N-terminal cell cycle regulator-related domains. *J Cell Biochem*, 90(4), 819-836. doi:10.1002/jcb.10688
- Salaun, P., Rannou, Y., & Prigent, C. (2008). Cdk1, Plks, Auroras, and Neks: the mitotic bodyguards. *Adv Exp Med Biol*, 617, 41-56. doi:10.1007/978-0-387-69080-3_4

- Santamaria, A., Neef, R., Eberspacher, U., Eis, K., Husemann, M., Mumberg, D., Prectl, S., Schulze, V., Siemeister, G., Wortmann, L., Barr, F. A., & Nigg, E. A. (2007). Use of the novel Plk1 inhibitor ZK-thiazolidinone to elucidate functions of Plk1 in early and late stages of mitosis. *Mol Biol Cell*, *18*(10), 4024-4036. doi:10.1091/mbc.e07-05-0517
- Scheffzek, K., & Welti, S. (2012). Pleckstrin homology (PH) like domains - versatile modules in protein-protein interaction platforms. *FEBS Lett*, *586*(17), 2662-2673. doi:10.1016/j.febslet.2012.06.006
- Schiel, J. A., & Prekeris, R. (2013). Membrane dynamics during cytokinesis. *Curr Opin Cell Biol*, *25*(1), 92-98. doi:10.1016/j.ceb.2012.10.012
- Schmidt, A., & Hall, A. (2002). Guanine nucleotide exchange factors for Rho GTPases: turning on the switch. *Genes Dev*, *16*(13), 1587-1609. doi:10.1101/gad.1003302
- Schmucker, S., & Sumara, I. (2014). Molecular dynamics of PLK1 during mitosis. *Mol Cell Oncol*, *1*(2), e954507. doi:10.1080/23723548.2014.954507
- Schneid, S., Wolff, F., Buchner, K., Bertram, N., Baygun, S., Barbosa, P., Mangal, S., & Zanin, E. (2021). The BRCT domains of ECT2 have distinct functions during cytokinesis. *Cell Rep*, *34*(9), 108805. doi:10.1016/j.celrep.2021.108805
- Schroeder, T. E. (1968). Cytokinesis: filaments in the cleavage furrow. *Exp Cell Res*, *53*(1), 272-276. doi:10.1016/0014-4827(68)90373-x
- Schroeder, T. E. (1972). The contractile ring. II. Determining its brief existence, volumetric changes, and vital role in cleaving *Arbacia* eggs. *J Cell Biol*, *53*(2), 419-434. doi:10.1083/jcb.53.2.419
- Schroeder, T. E. (1990). The contractile ring and furrowing in dividing cells. *Ann N Y Acad Sci*, *582*, 78-87. doi:10.1111/j.1749-6632.1990.tb21669.x
- Sedzinski, J., Biro, M., Oswald, A., Tinevez, J. Y., Salbreux, G., & Paluch, E. (2011). Polar actomyosin contractility destabilizes the position of the cytokinetic furrow. *Nature*, *476*(7361), 462-466. doi:10.1038/nature10286
- Seguin, L., Liot, C., Mzali, R., Harada, R., Siret, A., Nepveu, A., & Bertoglio, J. (2009). CUX1 and E2F1 regulate coordinated expression of the mitotic complex genes Ect2, MgcRacGAP, and MKLP1 in S phase. *Mol Cell Biol*, *29*(2), 570-581. doi:10.1128/MCB.01275-08
- Sehnal, D., Bittrich, S., Deshpande, M., Svobodová, R., Berka, K., Bazgier, V., Velankar, S., Burley, S. K., Koča, J., & Rose, A. S. (2021). Mol* Viewer: modern web app for 3D visualization and analysis of large biomolecular structures. *Nucleic Acids Research*, *49*(W1), W431-W437. doi:10.1093/nar/gkab314
- Sheng, Z. Z., Zhao, Y. Q., & Huang, J. F. (2011). Functional Evolution of BRCT Domains from Binding DNA to Protein. *Evol Bioinform Online*, *7*, 87-97. doi:10.4137/EBO.S7084

- Soisson, S. M., Nimnual, A. S., Uy, M., Bar-Sagi, D., & Kuriyan, J. (1998). Crystal structure of the Dbl and pleckstrin homology domains from the human Son of sevenless protein. *Cell*, *95*(2), 259-268. doi:10.1016/s0092-8674(00)81756-0
- Solski, P. A., Wilder, R. S., Rossman, K. L., Sondek, J., Cox, A. D., Campbell, S. L., & Der, C. J. (2004). Requirement for C-terminal sequences in regulation of Ect2 guanine nucleotide exchange specificity and transformation. *J Biol Chem*, *279*(24), 25226-25233. doi:10.1074/jbc.M313792200
- Somers, W. G., & Saint, R. (2003). A RhoGEF and Rho family GTPase-activating protein complex links the contractile ring to cortical microtubules at the onset of cytokinesis. *Dev Cell*, *4*(1), 29-39. doi:10.1016/s1534-5807(02)00402-1
- Spira, F., Cuylen-Haering, S., Mehta, S., Samwer, M., Reversat, A., Verma, A., Oldenbourg, R., Sixt, M., & Gerlich, D. W. (2017). Cytokinesis in vertebrate cells initiates by contraction of an equatorial actomyosin network composed of randomly oriented filaments. *Elife*, *6*. doi:10.7554/eLife.30867
- Steegmaier, M., Hoffmann, M., Baum, A., Lenart, P., Petronczki, M., Krssak, M., Gurtler, U., Garin-Chesa, P., Lieb, S., Quant, J., Grauert, M., Adolf, G. R., Kraut, N., Peters, J. M., & Rettig, W. J. (2007). BI 2536, a potent and selective inhibitor of polo-like kinase 1, inhibits tumor growth in vivo. *Curr Biol*, *17*(4), 316-322. doi:10.1016/j.cub.2006.12.037
- Storchova, Z., & Kuffer, C. (2008). The consequences of tetraploidy and aneuploidy. *J Cell Sci*, *121*(Pt 23), 3859-3866. doi:10.1242/jcs.039537
- Straight, A. F., Field, C. M., & Mitchison, T. J. (2005). Anillin binds nonmuscle myosin II and regulates the contractile ring. *Mol Biol Cell*, *16*(1), 193-201. doi:10.1091/mbc.e04-08-0758
- Su, K. C., Bement, W. M., Petronczki, M., & von Dassow, G. (2014). An astral simulacrum of the central spindle accounts for normal, spindle-less, and anucleate cytokinesis in echinoderm embryos. *Mol Biol Cell*, *25*(25), 4049-4062. doi:10.1091/mbc.E14-04-0859
- Su, K. C., Takaki, T., & Petronczki, M. (2011). Targeting of the RhoGEF Ect2 to the equatorial membrane controls cleavage furrow formation during cytokinesis. *Dev Cell*, *21*(6), 1104-1115. doi:10.1016/j.devcel.2011.11.003
- Subramanian, R., Wilson-Kubalek, E. M., Arthur, C. P., Bick, M. J., Campbell, E. A., Darst, S. A., Milligan, R. A., & Kapoor, T. M. (2010). Insights into antiparallel microtubule crosslinking by PRC1, a conserved nonmotor microtubule binding protein. *Cell*, *142*(3), 433-443. doi:10.1016/j.cell.2010.07.012
- Sugioka, K. (2021). Symmetry-breaking of animal cytokinesis. *Semin Cell Dev Biol*. doi:10.1016/j.semcdb.2021.12.008
- Sumara, I., Gimenez-Abian, J. F., Gerlich, D., Hirota, T., Kraft, C., de la Torre, C., Ellenberg, J., & Peters, J. M. (2004). Roles of polo-like kinase 1 in the assembly of functional mitotic spindles. *Curr Biol*, *14*(19), 1712-1722. doi:10.1016/j.cub.2004.09.049

- Suzuki, K., Sako, K., Akiyama, K., Isoda, M., Senoo, C., Nakajo, N., & Sagata, N. (2015). Identification of non-Ser/Thr-Pro consensus motifs for Cdk1 and their roles in mitotic regulation of C2H2 zinc finger proteins and Ect2. *Sci Rep*, *5*, 7929. doi:10.1038/srep07929
- Szafer-Glusman, E., Fuller, M. T., & Giansanti, M. G. (2011). Role of Survivin in cytokinesis revealed by a separation-of-function allele. *Mol Biol Cell*, *22*(20), 3779-3790. doi:10.1091/mbc.E11-06-0569
- Takaishi, K., Sasaki, T., Kameyama, T., Tsukita, S., Tsukita, S., & Takai, Y. (1995). Translocation of activated Rho from the cytoplasm to membrane ruffling area, cell-cell adhesion sites and cleavage furrows. *Oncogene*, *11*(1), 39-48. Retrieved from <https://www.ncbi.nlm.nih.gov/pubmed/7624130>
- Taneja, N., Bersi, M. R., Baillargeon, S. M., Fenix, A. M., Cooper, J. A., Ohi, R., Gama, V., Merryman, W. D., & Burnette, D. T. (2020). Precise Tuning of Cortical Contractility Regulates Cell Shape during Cytokinesis. *Cell Rep*, *31*(1), 107477. doi:10.1016/j.celrep.2020.03.041
- Tatsumoto, T., Xie, X., Blumenthal, R., Okamoto, I., & Miki, T. (1999). Human ECT2 is an exchange factor for Rho GTPases, phosphorylated in G2/M phases, and involved in cytokinesis. *J Cell Biol*, *147*(5), 921-928. Retrieved from <https://www.ncbi.nlm.nih.gov/pubmed/10579713>
- Tighe, A., Johnson, V. L., & Taylor, S. S. (2004). Truncating APC mutations have dominant effects on proliferation, spindle checkpoint control, survival and chromosome stability. *J Cell Sci*, *117*(Pt 26), 6339-6353. doi:10.1242/jcs.01556
- Tinevez, J. Y., Schulze, U., Salbreux, G., Roensch, J., Joanny, J. F., & Paluch, E. (2009). Role of cortical tension in bleb growth. *Proc Natl Acad Sci U S A*, *106*(44), 18581-18586. doi:10.1073/pnas.0903353106
- Tokumitsu, T., & Maramorosch, K. (1967). Cytoplasmic protrusions in insect cells during mitosis in vitro. *J Cell Biol*, *34*(2), 677-683. doi:10.1083/jcb.34.2.677
- Turlier, H., Audoly, B., Prost, J., & Joanny, J. F. (2014). Furrow constriction in animal cell cytokinesis. *Biophys J*, *106*(1), 114-123. doi:10.1016/j.bpj.2013.11.014
- Tyers, M., Rachubinski, R. A., Stewart, M. I., Varrichio, A. M., Shorr, R. G., Haslam, R. J., & Harley, C. B. (1988). Molecular cloning and expression of the major protein kinase C substrate of platelets. *Nature*, *333*(6172), 470-473. doi:10.1038/333470a0
- Uehara, R., & Goshima, G. (2010). Functional central spindle assembly requires de novo microtubule generation in the interchromosomal region during anaphase. *J Cell Biol*, *191*(2), 259-267. doi:10.1083/jcb.201004150
- Uehara, R., Nozawa, R. S., Tomioka, A., Petry, S., Vale, R. D., Obuse, C., & Goshima, G. (2009). The augmin complex plays a critical role in spindle microtubule generation for mitotic progression and cytokinesis in human cells. *Proc Natl Acad Sci U S A*, *106*(17), 6998-7003. doi:10.1073/pnas.0901587106

- Uehata, M., Ishizaki, T., Satoh, H., Ono, T., Kawahara, T., Morishita, T., Tamakawa, H., Yamagami, K., Inui, J., Maekawa, M., & Narumiya, S. (1997). Calcium sensitization of smooth muscle mediated by a Rho-associated protein kinase in hypertension. *Nature*, *389*(6654), 990-994. doi:10.1038/40187
- van Oostende Triplet, C., Jaramillo Garcia, M., Haji Bik, H., Beaudet, D., & Piekny, A. (2014a). Anillin interacts with microtubules and is part of the astral pathway that defines cortical domains. *Journal of Cell Science*, *127*(17), 3699-3710. doi:10.1242/jcs.147504
- van Oostende Triplet, C., Jaramillo Garcia, M., Haji Bik, H., Beaudet, D., & Piekny, A. (2014b). Anillin interacts with microtubules and is part of the astral pathway that defines cortical domains. *J Cell Sci*, *127*(Pt 17), 3699-3710. doi:10.1242/jcs.147504
- Verma, V., & Maresca, T. J. (2019). Microtubule plus-ends act as physical signaling hubs to activate RhoA during cytokinesis. *Elife*, *8*. doi:10.7554/eLife.38968
- Verma, V., Mogilner, A., & Maresca, T. J. (2019). Classical and Emerging Regulatory Mechanisms of Cytokinesis in Animal Cells. *Biology (Basel)*, *8*(3). doi:10.3390/biology8030055
- Vietri, M., Radulovic, M., & Stenmark, H. (2020). The many functions of ESCRTs. *Nat Rev Mol Cell Biol*, *21*(1), 25-42. doi:10.1038/s41580-019-0177-4
- von Dassow, G. (2009). Concurrent cues for cytokinetic furrow induction in animal cells. *Trends Cell Biol*, *19*(4), 165-173. doi:10.1016/j.tcb.2009.01.008
- von Dassow, G., Verbrugghe, K. J., Miller, A. L., Sider, J. R., & Bement, W. M. (2009). Action at a distance during cytokinesis. *J Cell Biol*, *187*(6), 831-845. doi:10.1083/jcb.200907090
- Wadsworth, P. (2021). The multifunctional spindle midzone in vertebrate cells at a glance. *J Cell Sci*, *134*(10). doi:10.1242/jcs.250001
- Wagner, E., & Glotzer, M. (2016). Local RhoA activation induces cytokinetic furrows independent of spindle position and cell cycle stage. *Journal of Cell Biology*, *213*(6), 641-649. doi:10.1083/jcb.201603025
- Watanabe, S., Ando, Y., Yasuda, S., Hosoya, H., Watanabe, N., Ishizaki, T., & Narumiya, S. (2008). mDia2 induces the actin scaffold for the contractile ring and stabilizes its position during cytokinesis in NIH 3T3 cells. *Mol Biol Cell*, *19*(5), 2328-2338. doi:10.1091/mbc.E07-10-1086
- Werner, M., Munro, E., & Glotzer, M. (2007). Astral signals spatially bias cortical myosin recruitment to break symmetry and promote cytokinesis. *Curr Biol*, *17*(15), 1286-1297. doi:10.1016/j.cub.2007.06.070
- Wolfe, B. A., Takaki, T., Petronczki, M., & Glotzer, M. (2009). Polo-like kinase 1 directs assembly of the HsCyk-4 RhoGAP/Ect2 RhoGEF complex to initiate cleavage furrow formation. *PLoS Biol*, *7*(5), e1000110. doi:10.1371/journal.pbio.1000110

- Yamamoto, K., Miura, H., Ishida, M., Mii, Y., Kinoshita, N., Takada, S., Ueno, N., Sawai, S., Kondo, Y., & Aoki, K. (2021). Optogenetic relaxation of actomyosin contractility uncovers mechanistic roles of cortical tension during cytokinesis. *Nat Commun*, *12*(1), 7145. doi:10.1038/s41467-021-27458-3
- Yao, F., Svensjo, T., Winkler, T., Lu, M., Eriksson, C., & Eriksson, E. (1998). Tetracycline repressor, tetR, rather than the tetR-mammalian cell transcription factor fusion derivatives, regulates inducible gene expression in mammalian cells. *Hum Gene Ther*, *9*(13), 1939-1950. doi:10.1089/hum.1998.9.13-1939
- Yen, T. J., Compton, D. A., Wise, D., Zinkowski, R. P., Brinkley, B. R., Earnshaw, W. C., & Cleveland, D. W. (1991). CENP-E, a novel human centromere-associated protein required for progression from metaphase to anaphase. *EMBO J*, *10*(5), 1245-1254. Retrieved from <https://www.ncbi.nlm.nih.gov/pubmed/2022189>
- Yonemura, S., Hirao-Minakuchi, K., & Nishimura, Y. (2004). Rho localization in cells and tissues. *Exp Cell Res*, *295*(2), 300-314. doi:10.1016/j.yexcr.2004.01.005
- Yüce, Ö., Piekny, A., & Glotzer, M. (2005). An ECT2–centralspindlin complex regulates the localization and function of RhoA. *The Journal of Cell Biology*, *170*(4), 571-582. doi:10.1083/jcb.200501097
- Zanin, E., Desai, A., Poser, I., Toyoda, Y., Andree, C., Moebius, C., Bickle, M., Conradt, B., Piekny, A., & Oegema, K. (2013). A conserved RhoGAP limits M phase contractility and coordinates with microtubule asters to confine RhoA during cytokinesis. *Dev Cell*, *26*(5), 496-510. doi:10.1016/j.devcel.2013.08.005
- Zhang, D., & Glotzer, M. (2015). The RhoGAP activity of CYK-4/MgcRacGAP functions non-canonically by promoting RhoA activation during cytokinesis. *Elife*, *4*. doi:10.7554/eLife.08898
- Zhao, W. M., & Fang, G. (2005). MgcRacGAP controls the assembly of the contractile ring and the initiation of cytokinesis. *Proc Natl Acad Sci U S A*, *102*(37), 13158-13163. doi:10.1073/pnas.0504145102
- Zheng, Y. (2001). Dbl family guanine nucleotide exchange factors. *Trends Biochem Sci*, *26*(12), 724-732. doi:10.1016/s0968-0004(01)01973-9
- Zou, Y., Shao, Z., Peng, J., Li, F., Gong, D., Wang, C., Zuo, X., Zhang, Z., Wu, J., Shi, Y., & Gong, Q. (2014). Crystal structure of triple-BRCT-domain of ECT2 and insights into the binding characteristics to CYK-4. *FEBS Lett*, *588*(17), 2911-2920. doi:10.1016/j.febslet.2014.07.019